Synthesis & Characterization of Modified Barium Titanate Ferroelectrics by Modified Solid State Reaction and Microwave Sintering Routes

Submitted

in fulfillment of the requirement of the degree of

DOCTOR OF PHILOSOPHY

by

Sonia

to the

Department of Chemistry

National Institute of Technology, Rourkela

Rourkela -769008, India

March 2011

This thesis is dedicated
to my father
(late Sh. Ram Kumar) &
my mother

CERTIFICATE

This is to certify that the thesis entitled '**Synthesis & Characterization of Modified Barium Titanate Ferroelectrics by Modified Solid State Reaction and Microwave Sintering Routes"** being submitted by Ms. Sonia to the Department of Chemistry, National Institute of Technology, Rourkela, for the award of the Doctor of Philosophy, is a record of bonafide research carried out by her. She has worked under our guidance and supervision, and has fulfilled the requirements for the submission of this thesis, which to our knowledge has reached the requisite standard.

The results contained herein have not been submitted in part or full to any other university or institution for award of any degree or diploma.

(Prof. R. K. Patel)
Associate Prof.
NIT Rourkela
Rourkela-769008, India

(Dr. Chandra Prakash)
Additional Director
Directorate of IE & IPR, DRDO,
New Delhi-110011

ACKNOWLEDGEMENTS

I am deeply indebted to my thesis supervisors, Prof. R. K. Patel and Dr. C. Prakash for their constant encouragements during the tenure of this work. They were always available for helping me and provided me all kinds of facilities for carrying out my research work. I am grateful to them for being a constant source of motivation and guiding me throughout my research work. I express my obligations and gratitude towards Dr. B. Ganguli for allowing me to use experimental facilities available at electro-ceramic lab. I am also grateful to Dr. Jyoti Juneja, Principal GVM Sonepat & Prof. R. Chatterjee (IIT Delhi) for helping and providing me the characterization facilities. Thanks are also due to Prof. D. K. Agrawal (Penn State, USA) and Dr. J.K Juneja (Hindu College, Sonepat) for their constructive discussions and suggestions. Thanks are also due to Dr. B.G. Mishra, Dr. N. Panda and Dr. A Sahoo, my DSC members, for their valuable criticism and suggestions.

I am sincerely thankful to Dr. K.M. Purohit, Dr. G. D. Hota, Dr. S. Chatterjee, Dr. R. Dinda, Dr. A. Mondal, Dr. S. Mohapatra, Dr. U. Subuddhi and Dr. S. Patel (Dept. of Chemistry, NIT Rourkela) for their constructive suggestions and helpful advice during the research period.

I acknowledge with thanks the financial assistance provided by DRDO during the research work. I am thankful to Mr. A. Pathak, Ms. A. Singh, Dr. A. Singh (IIT Delhi), Mr. P. Palei, Mr. S.N. Naresh, Ms. M. Patnaik, Ms. P. Mishra, Mr. S.K. Kar, Ms. S. Swain (NIT Rourkela), Mr. P. Paliwal and Ms. P. Singh (GVM Sonepat) for helping me in my experimental and characterization work. I am personally grateful to my family members for their constant inspiration and moral support. Last but not the least I am thankful to my husband Dr. Pawan Kumar for his valuable criticism and

suggestions during the course of my work. I am also thankful to my daughter, Premamanjari for co-operating with me in my thesis writing.

Above all, I am specially thankful to the Supereme Personality of Godhead from whom I gathered the strength and perseverance during the course of my work.

(Sonia)

ABSTRACT

These following five series have been synthesized by modified solid state reaction (MSSR) route:

(i) $Ba_{1-x}Ca_xTiO_3$/BCT (ii) $Ba_{1-x}Mg_xTiO_3$/BMT

(iii) $Ba_{1-x}Sr_xTiO_3$ /BST (iv) $Ba_{1-x}Sm_xTi_{(1-x/4)}O_3$ /BSmT

(v) $Ba_{1-x}La_xTi_{(1-x/4)}O_3$ /BLT where x=0.02, 0.04, 0.06 & 0.08.

(In the present work for x=0.02, 0.04. 0.06 & 0.08, we have used BCT1, BCT2, BCT3, BCT4, BMT1, BMT2, BMT3, BMT4, BST1, BST2, BST3, BST4, BSmT1, BSmT2, BSmT3, BSmT4 & BLT1, BLT2, BLT3, BLT4 notations).

In the modified solid state reaction route (MSSR) barium acetate trihydate, calcium acetate/strontium acetate/magnesium acetate/lanthanum acetate/samarium acetate (all from Aldrich, USA with 99.8% purity) and fumed TiO_2 (Degussa) were used as starting precursors. Calcination temperature for single perovskite phase formation of iso-valent modified BT ceramic samples was optimized at 900°C for 4 hrs whereas for higher% of off-valent substituted BT samples, calcination temperature is little higher (950°C for 4 hrs). For better density and morphology, iso-valent & off-valent substituted BT systems pellets were sintered at 1300^oC for 4 hrs. Calcination and sintering temperature of the iso-valent and off-valent substituted BT systems synthesized by MSSR route is significantly lower than the same systems processed through SSR route (calcination ~1200^0C & sintering temperature ~1450^oC). Lowering of sintering temperature is attributed to the fine particle size of the precursors. In BMT and BST systems a tetragonal structure is found. The tetragonality (c/a ratio) decreases with the increase in Mg & Sr substitution% in BMT & BST systems. In BCT ceramic samples

tetragonality increases with the increase of Ca substitution% . In BLT ceramics, the tetragonality (c/a ratio) decreases with the increase of La substitution% and in BLT2, BLT3 & BLT4 systems the structure is found to be cubic. In BSmT ceramic samples the tetragonality (c/a ratio) decreases with the increase of Sm substitution fraction and in BSmT4 system the structure is found to be cubic.

Surface micrographs (SEM) of all the iso-valent and off-valent substituted BT systems showed well developed grains. Presences of nearly pore free uniform grains in these ceramic samples suggest the advantage of using MSSR route over conventional SSR route. Grain size increases with the increase of Ca and decreases with the increase of Mg, Sr, La & Sm substitution% in modified BT systems. Densities of iso-valent and off-valent modified BT samples synthesized by MSSR route at significantly lower processing temperature is better than the same samples synthesized by SSR route.

Variation of ε_r and tanδ at different frequencies (1kHz-1MHz) as a function of temperature of all the iso-valent and off-valent substituted BT system synthesized by MSSR route have been studied. Room temperature (RT) variation of ε_r and tanδ as a function of frequency of the modified BT system has also been studied. Variation of dielectric properties with frequency shows the usual behaviour of dielectric materials i.e decrease of the value of ε_r with the increase of frequency. With the increase of substitutions% of Ca in BCT system, position of T_c increases slightly. With the increase in Sr & Mg substitution% in BST & BMT systems, the position of T_c decreases but remains above RT. Temperature coefficient of capacitance from RT to 70^oC in BCT1, BCT2 & BCT3 samples is almost negligible compare to unmodified BT samples, which signifies the importance of Ca modification in BT system for its use in multilayer

capacitors. Whereas, with the increase of La and Sm substitution% in BLT & BSmT systems, the position of T_c decreases drastically giving rise to high value of ε_r at RT. High value of ε_r at RT in BLT1 system suggested it as a useful material for MLC applications. Diffusivity factor (γ) is increasing slightly with the increase of Ca substitution concentration in BCT ceramic samples but remains near to 1, which represents normal phase transition. This establishes the good solubility of Ca in BT system and as a result less compositional fluctuations. Whereas with the increase of Mg and Sr substitution concentration in modified BT systems the value of γ factor increases, indicating the increase in diffusive nature of phase transition. Similarly, in BSmT & BLT series the value of γ factor is more than 1 and indicates the diffuse phase transition nature of these modified BT systems. Existence of good dielectric properties in the modified BT ceramic samples synthesized by MSSR route at comparably lower processing temperature than SSR route & using cheap chemicals comparable to chemical routes suggested the advantage of using MSSR route in the present study.

P-E hysteresis loops of all the iso-valent and off-valent substituted BT systems synthesized by MSSR route have been studied. Value of coercive field (E_c) and remnant polarization (P_r) is decreasing with the increase of Ca and Sm substitution% in BCT & BSmT systems. Whereas, with the increase of La substitution % in BLT system, the P-E hysteresis loops shows the disappearance of ferroelectric nature of the samples. With the increase of Mg substitution% in BMT ceramic samples the ferroelectric nature decreases. With the increase of Sr substitution% in BST ceramic samples the value of P_r increases. The value of remnant polarization (P_r) of modified BT ceramic samples synthesized by

MSSR route is comparable to the same systems synthesized by other routes. This again hints towards the advantage of using MSSR route in the present study.

Longitudinal strain versus bipolar electric field (S-E) behavior of iso-valent and off-valent modified BT ceramic samples have also been studied. The appearance of a butterfly shape loop confirms the piezoelectric nature. Strain as high as ~0.13% has been observed in unmodified BT ceramic samples synthesized by MSSR route.

BLT & BCT SAMPLES SYNTHESIZED BY MW PROCESSING TECHNIQUE

The pellets of polycrystalline calcined ceramic samples of BCT and BLT systems obtained from carbonate and oxide powders were sintered by microwave processing technique. The microwave sintering of the BCT & BLT ceramic samples was carried out at 1100^0C for 1 h with a heating rate of 25^0C/min by placing the pellets in the centre of a 4.4 kW, 2.45-GHz multi mode microwave cavity. The microwave furnace temperature was recorded by using a Raytek non-contact sensor (XRTG5).

In the MW processed BCT samples, with the increase in Ca concentration the splitting at (200) plane decreases indicating the decrease in tetragonality. Whereas in the MW processed BLT samples with the increase in La concentration the splitting near $2\theta=45^o$ merges into singlet indicating the structure changes from tetragonal to cubic. The MW processed BLT1 samples were indexed with tetragonal structure, whereas BLT2, BLT3 & BLT4 samples were indexed with cubic structure.

Densities of the microwave sintered BCT and BLT ceramics were measured using Archimedes' principle. The density measurements showed a better densified and less porous product of the microwave processed BCT and BLT samples at significantly lower sintering temperature and time. The obtained densities of MW sintered modified BT

samples sintered at significantly lower sintering temperature and time are higher than the earlier reports on modified and unmodified BT ceramic samples processed through other processes including MW technique. It is evident that the microwave processing technique takes only a fraction of the time required in the conventional processing to achieve single-phase dense material. Grain size of microwave sintered Ca & La modified BT ceramic samples is lower than the same systems processed by SSR route. Better densification with the formation of finer and uniform grains in the case of microwave sintered samples hints towards the advantage of using this technique.

Temperature variation of ε_r and tanδ at different frequencies of microwave sintered BCT and BLT ceramic samples were studied. For various substitutions of Ca in BCT system, position of T_c decreases slightly, whereas with the increase of La substitution% in BLT system, the position of T_c decreases drastically giving rise to high value of ε_r at RT. In BLT1 and BLT2 systems, the temperature coefficient of capacitance is very small. In BLT1 system, the capacitance variation with temperature at different frequencies is almost negligible from RT to 70^oC. Temperature coefficient of ε_r from RT to 80^oC is almost zero for BCT2 and BCT3 systems.

P-E hysteresis loops of microwave sintered BCT and BLT systems were studied. Value of coercive field (E_c) and remnant polarization (P_r) is decreasing with the increase of Ca substitution% whereas, with the increase of La substitution % in BT systems, the P-E hysteresis loop study shows the disappearance of ferroelectric nature in the BLT2, BLT3 & BLT4 ceramic samples.

Longitudinal strain versus bipolar electric field (S-E) behavior of MW processed modified BT ceramic samples has also been studied. The appearance of a butterfly shape

loop confirms hints towards the piezoelectric nature of the samples. Strain as high as ~0.15% has been observed in BCT3 & BLT1 ceramic samples.

Finally, in the present study, MSSR and microwave processing have decreased the processing temperatures and time. High value of ε_r and low value of tanδ have been obtained at RT in Ca & La modified BT systems synthesized by MSSR route. MSSR route promises desired dielectric properties at lower processing temperatures. High density with the presence of pore free uniform grains at lower sintering temperature & time suggested the advantage of using MW processing technique. Temperature coefficient of ε_r from RT to 80^{o}C was almost zero for MW processed BCT2 and BCT3 systems indicating increase in temperature stability of these compounds and their usefulness in MLC applications.

This work is reported in eight chapters. First chapter describes a short review of the historical developments of ferroelectricity. This chapter also describes different structures of ferroelectric materials and establishes the motivation and aim of the present work.

Chapter II describes a detailed review about the investigated parameters.

Chapter III describes about the methodology of sample preparation and characterization techniques used for studying structural, micro-structural, dielectric, ferroelectric, piezoelectric properties and strain induced by electric field behaviors.

Chapter IV discusses about the perovskite phase evolution, structural, micro-structural and density properties.

Chapter V discusses about the dielectric properties.

Chapter VI discusses about the ferroelectric & piezoelectric properties and strain induced by electric field behaviors.

Chapter VII discusses about the synthesis & characterization of modified BT ceramics synthesized by MW process.

Chapter VIII presents the conclusions of the present work and recommendations for future work in this field.

This work has resulted in the following publications:

1. Low Temperature Perovskite Phase Formation in PCT 90/10 System, Sonia *et.al*, Applied Surface Science, 255 (2009) 5686–5689.

2. Synthesis and characterization of calcium modified barium titanate ceramics by partial precipitation route, Sonia *et.al*, Materials Science: An Indian Journal, 5 [3] (2009) 1.

3. Synthesis and Characterization of Isovalent Substituted BaTiO3 Ceramics by Modified Chemical Route, Sonia *et.al*, Integrated Ferroelectrics, 118:1 (2010) 106.

4. Structural, Dielectric & Ferroelectric Study of Microwave Sintered Lanthanum Substituted $BaTiO_3$ Ceramics, Sonia *et.al*, Materials Chemistry & Physics, 130 (2011) 191– 195.

5. Effect of Sm and La off-valent Ion Substitution in BT Ceramics Synthesized by Modified Solid State Route, Sonia *et.al*, International J Mat. Sci. 6 [2] (2011) 133–140.

6. Effect of Microwave Processing on Structural, Dielectric and Ferroelectric Properties of Calcium Doped $BaTiO_3$ Ceramics, Sonia *et.al*, J. Ceramic Progress & Research (In Press).

7. Characterizations of BT ceramics synthesized by modified solid state route, Sonia *et.al*, AIP Conf. Proc. **1372**, (2011) 116.

8. Phase, dielectric and ferroelectric properties of microwave sintered la & ca modified batio$_3$ ceramics, Sonia *et.al*, AIP Conf. Proc. **1372**, (2011) 57.

9. Low temperature synthesis and dielectric, ferroelectric and piezoelectric study of microwave sintered of $BaTiO_3$ ceramics, Sonia *et.al*, Ceramic International, 38 (2012) 1585–1589.

Keywords: Lead Free; Barium Titanate Ceramics; Solid State Reaction Route; Modified Solid State Reaction Route; Microwave Route; Iso-valent & Off-Valent Modified Barium Titanate Ceramics; X-ray Diffraction; Scanning Electron Microscope; Perovskite Phase; Multilayer Capactior Applications; Dielectric Properties; Ferroelectric Properties; Strain vs. Electric Field Study.

TABLE OF CONTENTS

List of Figures

Chapter I

Chapter II

Chapter III

Chapter IV

Chapter V

Chapter VI

Chapter VII

List of Tables

Chapter I

Chapter IV

Chapter V

Chapter VI

Chapter VII

CHAPTER I

INTRODUCTION

1.1 Introduction

Thousands of years ago, the conversion of molded, naturally occurring clay into fired, insoluble ceramic pottery began mankind's technical mastery over nature. 'Ceramic' word is derived from Greek word 'keramos', which literally means burnt earth. Although, there is no particular definition of ceramics, one can vaguely define ceramics as those materials, which are inorganic, non-metallic, polycrystalline and acquire its mechanical strength through a sintering/firing type of processes. Table 1.1 gives the brief description of various classes of ceramics and fields of application [1]. In other words, these are the materials, which are first shaped and subsequently hardened by heat treatment. During the present millennia, an ever-increasing ability to manipulate and control the properties of ceramic materials is achieved. Generally, ceramics are admired for their mechanical, chemical and thermal stability. The key feature that generally describe ceramics and consequently electro-ceramics are:

- Presence of ionic-covalent bonding
- Microstructure comprising inorganic crystal compounds and or/ amorphous glass in varying proportions
- Thermal process conducted at elevated temperature

Presently, the field of electroceramics is application driven and technology focused [2]. Unique properties of ceramics like: electrical, optical and magnetic have made them important in many key technologies including communications, energy conversion and storage, electronics, automation etc. Here, the combination of traditional ruggedness of conventional ceramics and the exceptional functionality of some electroceramic materials make the electroceramics particularly attractive as

smart materials [3-5]. Fig. 1.1 shows the historical development of the relative importance of materials [1-5].

Table - 1.1 Classes of Ceramics and Fields of Application

Materials Group	Property	Application
Traditional Ceramics	Compressive Strength	Bricks
	Density + Strength	Ceramic Hollow Ware
	Density + Wear Resistance	Structural Clay Products
	Heat and Corrosion Resistance	Refractories
Structural Ceramics	Hardness	Grinding Grits and Disks
	Strength + Toughness	Engineering Ceramics
	Biocompatibility, Bioactivity	Bioceramics
	Nuclear Properties	Nuclear Ceramics
	Corrosion Resistance, Catalytic Properties	Chemocermics
Functional Ceramics	Electric Resistivity, Dielectric Properties	Electroceramics
	Magnetic Susceptibility	Magnetoceramics
	Anisotropic Optical properties	Optoceramics

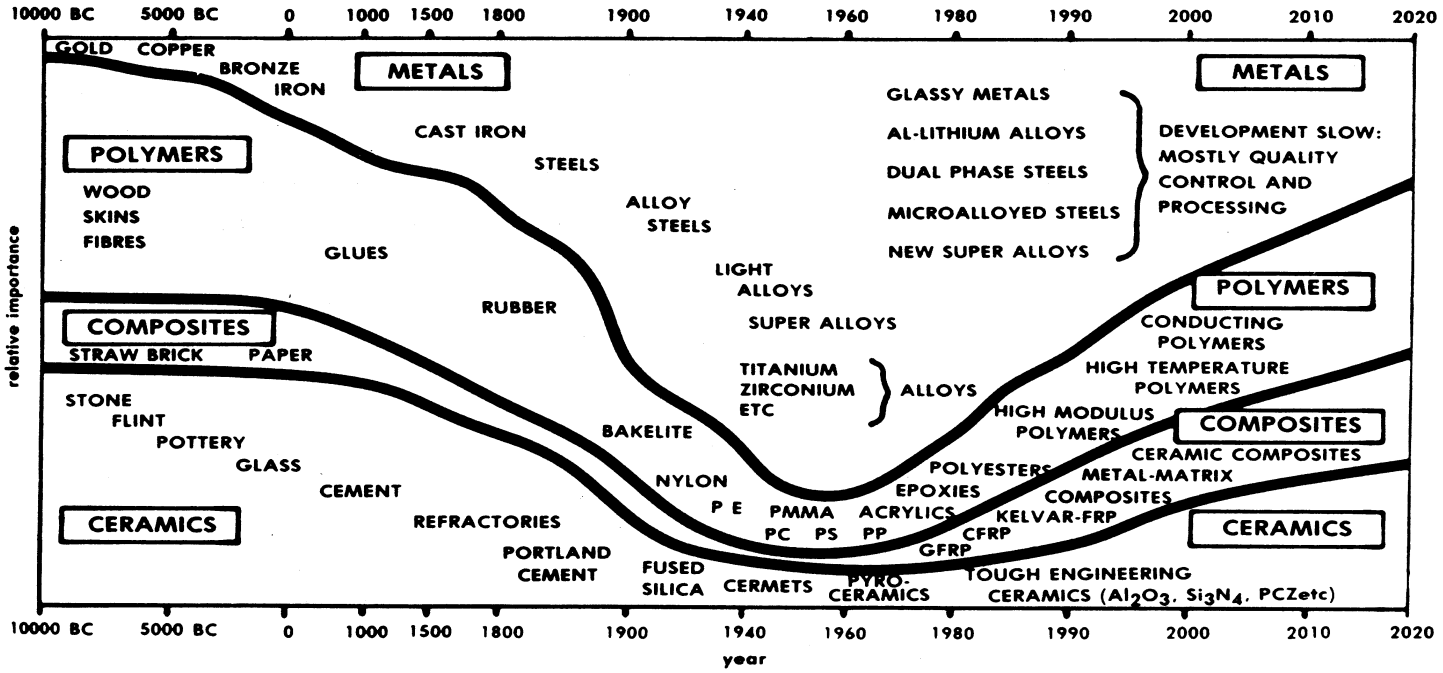

Fig. 1.1 Historical development of the relative importance of materials.

1.2 Historical Background

The phenomenon of temperature dependent spontaneous electric dipole moment (pyroelectric) in some materials has been known since ancient times. In 1880, J. and P. Curie discovered that certain crystalline materials can develop an electric charge proportional to a mechanical stress, known as piezoelectric effect. Reversal of polarization by an electric field, the ferroelectric phenomenon, was first discovered by Valasek [6] in 1921 in rochelle salt (potassium sodium tartrate).

Before 1940, only two types of ferroelectrics were known, rochelle salt and potassium dihydrogen phosphate and its isomorphous [7]. In the early of 1940's, the discovery of barium titanate ($BaTiO_3$) ceramic, the first ferroelectric ceramic without hydrogen bonds, has lead to the discovery of a large number of similar type of perovskite ceramics viz. $KNbO_3$, $LiNbO_3$, $PbTiO_3$ etc. [8]. Polycrystalline ceramics have advantage over single crystals, because polycrystalline ceramics can be formed into any desired shape, the orientation of polar axis can be chosen and synthesis process is cheaper than the single crystal growth process [9]. A major breakthrough in the applications of ferroelectric ceramics came during the 2nd world war with the discovery that polycrystalline ceramics, though macroscopically isotropic, can be made to show pyroelectric, piezoelectric and electro-optic effects by inducing a polar axis using a process, called poling. This poling process is realized with the application of a very high electric field at an elevated temperature (below T_c), sufficient to reverse the electric moments of spontaneously polarized regions in the ceramics as near to the field direction as the local environment and what the ceramic structure allows [10]. The major breakthrough in the research on ferroelectric materials came in the early 1950's with the widespread use of $BaTiO_3$ based ceramics in capacitor applications and piezoelectric transducer devices [11]. After 1950, many other ferroelectric

ceramics including lead titanate (PT), lead zirconate titanate (PZT), lead lanthanum zirconate titanate (PLZT) etc. (particularly lead oxide based) have been developed, which find their use in various applications and devices. These lead oxide based systems are the most widely used materials for piezoelectric transducers, actuators and transformers due to their excellent piezoelectric properties close to the morphotropic phase boundary (MPB) [10, 12, 13] compositions. However, because of the lead oxide toxicity, there is a raising concern about the recycling and disposal of devices containing lead [14-20]. The facts that lead oxide vaporize during processing and that it causes harm to the environment have led to legislation in many countries. In addition, the volatilization of toxic PbO during high-temperature sintering requires an appropriate treatment of lead-contained wastes to avoid environmental problems. Hence, again the research in ferroelectric ceramics is being focused on lead free ferroelectric system [21].

1.3 Structure of Ferroelectrics

All the crystals can be grouped into seven crystal systems as shown in Fig. 1.2. Depending on the symmetry elements, these seven crystal systems can be subdivided into 32 point groups, where a point group is a combination of symmetry elements. Out of these, only 21 belong to non-centrosymmetric classes. All except one are piezoelectric, means they exhibit electrical polarity when subjected to stress. Again, out of 20 piezoelectric crystal classes, 10 possess a spontaneous polarization, which is temperature dependent and these are known as pyroelectric materials. There exists a subclass of pyroelectric materials, which have two or more orientation states of polarization in the absence of an electric field. The polarization in these materials can be switched from one state to other with the application of an electric field and are

known as ferroelectric materials. As shown in Fig.1.3, according to the nature of chemical bonds, crystalline ferroelectrics may be classified into four types [12]:

(i) Tungsten bronze eg: ($PbNb_2O_6$) (ii) Pyrochlore eg: ($Cd_2Nb_2O_7$)

(iii) Layer structure eg: ($Bi_4Ti_3O_{12}$) (iv) Oxygen octahedral eg: ($BaTiO_3$, PZT)

}

Out of these, oxygen octahedral (perovskite) structure is easy to understand, easy to modify and the process of perovskite phase formation of these materials is cheaper than other classes of ferroelectric materials [12]. Therefore, materials of perovskite

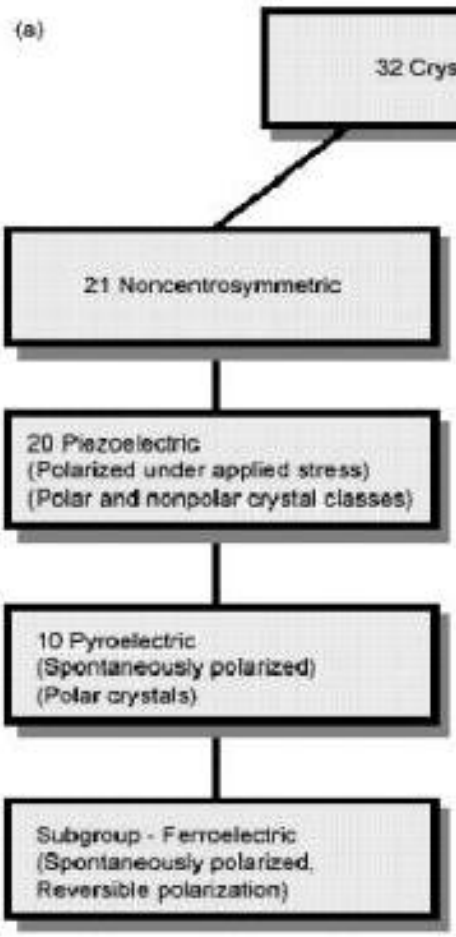

(b)

Crystal System	Noncentrosymmetric Crystal Classes					Optic Axes
	Nonpolar			Polar		
Cubic	432	$\bar{3}$m	23	None		Isotropic
Hexagonal	$\bar{6}$	$\bar{6}$m2	622	6	6mm	Uniaxial
Rhombohedral	32			3	3m	
Tetragonal	$\bar{4}$	$\bar{4}$2m	22	4	4mm	
Orthorhombic	222			mm2		Biaxial
Monoclinic	None			2	m	
Triclinic	None			1		

Fig. 1.2 (a) Relationship between crystal classes and piezoelectric, pyroelectric and ferroelectric properties. (b) Specific crystal classes for piezoelectric and pyroelectric materials together with their general optical response (432 is not piezoelectric).

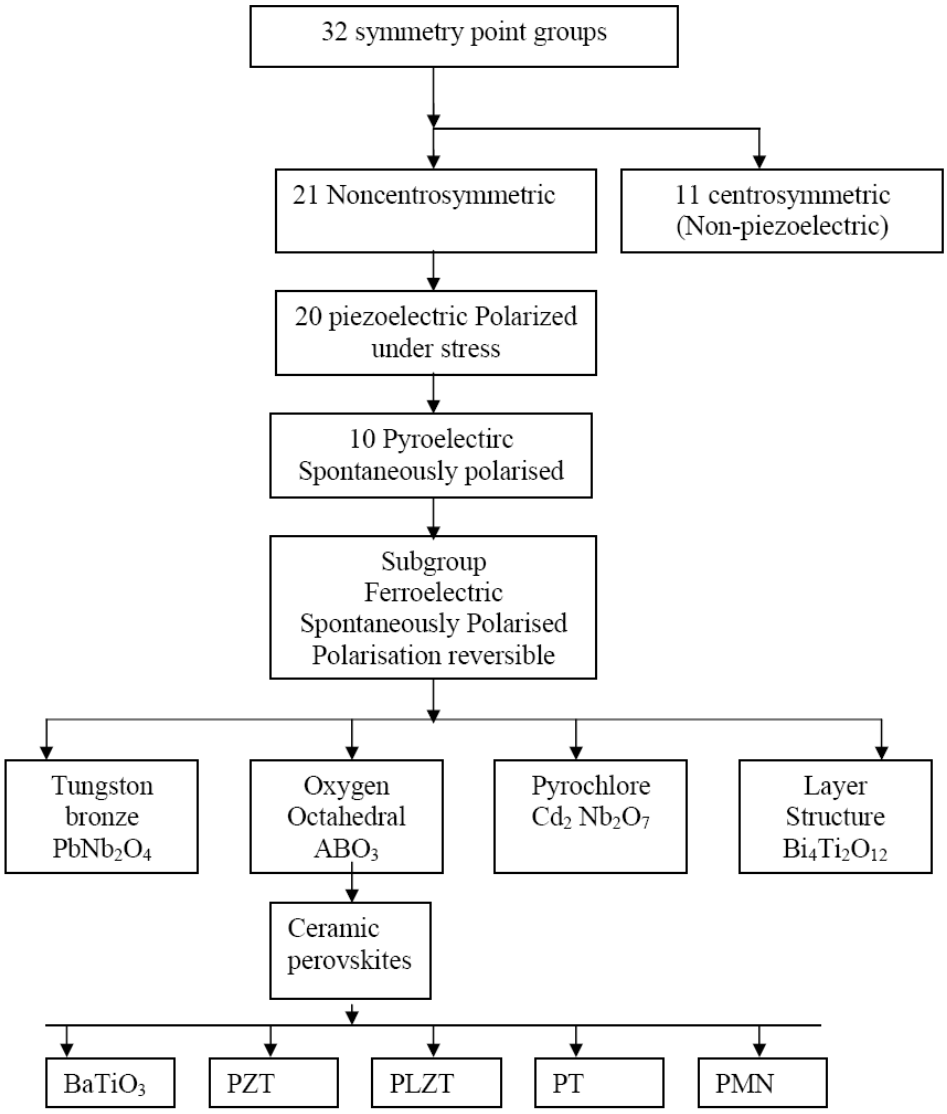

(Where PZT:Lead Zirconate Titanate; PT:Lead Titanate; PLZT: Lead Lanthanum Zirconate Titanate, PMN: Lead Magnesium Niobate)

Fig. 1.3 Crystallographic Symmetry and Ferroelectric Materials

structure are finding great attention. Generally, the perovskite structure is adopted by ABO_3 type compounds, as shown in Fig 1.4 where A is a large radius cation, which occupies the empty sites between O_2 octahedra, while B is a small radius cation, which occupies the center of the octahedron, formed by O_2^- ions. Ferroelectricity is the characteristics of a compound with distorted perovskite structure. The distortion of cations, leading to ferroelectricity is shown in Fig. 1.4. In these ferroelectric materials

there exits a characteristic temperature, known as Curie temperature (T_c), below which the perovskite unit cell is non centrosymmetric and for $T > T_c$, perovskite unit cell becomes symmetric and the state of material is known as paraelectric [10].

This perovskite structure adopted by many oxides is very versatile and has been a subject of numerous studies due to its interesting dielectric, piezoelectric, pyroelectric, electro-optic and superconducting properties. A wide variety of cations can be substituted in the ABO_3 perovskite. Gold Schmidt [10] has given a criteria for this substitution

$$t = (R_A+R_0)/\sqrt{2}\,(R_B+R_0) \qquad \text{---------1.1}$$

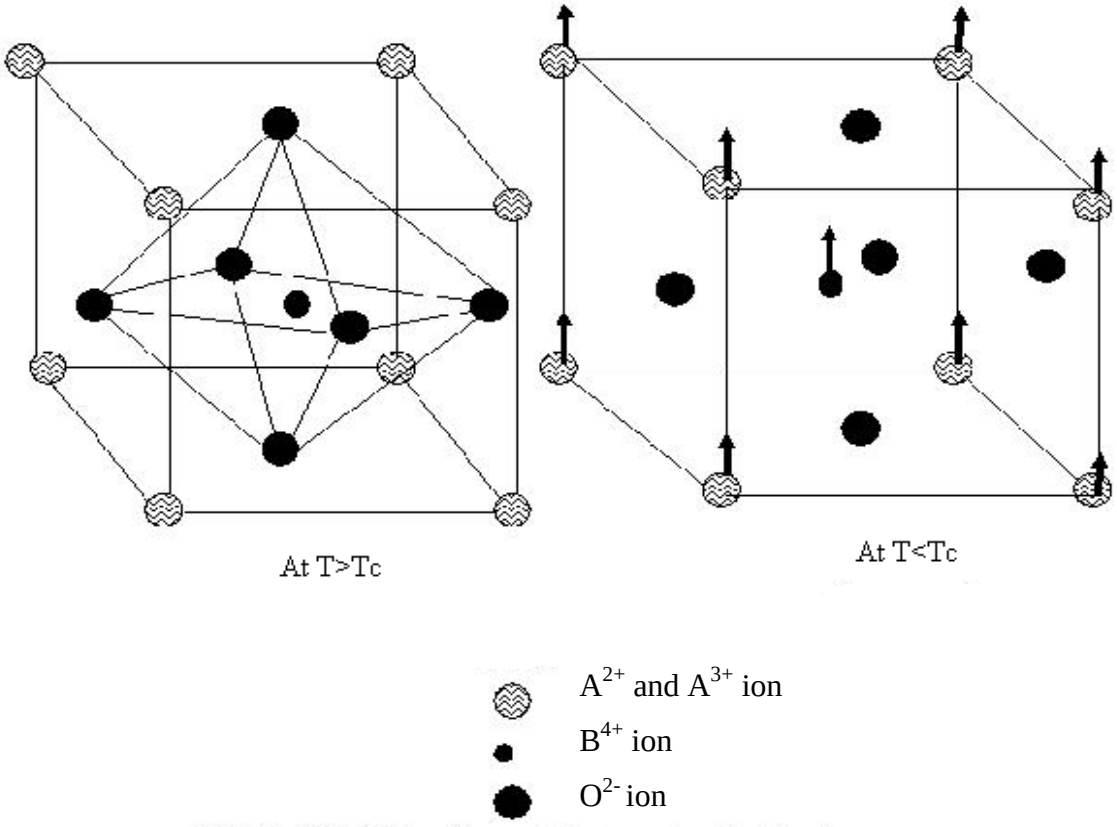

Fig. 1.4 (ABO_3) type perovskite ferroelectric structures

Here, t, R_A, R_B, and R_O represent the tolerance factor, ionic radii of large cation, small cation and anion respectively. In case of ideal cubic perovskite t=1.0, but generally those structures whose tolerance factor "t" is about 0.95-1.0 are slightly distorted but non- ferroelectric and those slightly over 1.0 are ferroelectric [10].

1.4 Barium Titanate (BT) System

Barium titanate (BT) is the most extensively investigated environmental friendly ferroelectric material, because it is extremely interesting from the point of view of practical applications [22-31] It is chemically and mechanically very stable and it exhibits ferroelectric properties at and above room temperature (RT) and it can be easily prepared and used in the form of ceramic polycrystalline samples [32]. Therefore, since the discovery of BT system in the early 1940's, great deals of efforts have been devoted to study the dielectric properties of barium titanium based materials [33-38]. $BaTiO_3$ ceramics are widely used in the fabrication of multilayer ceramic capacitors (MLC) and nonvolatile memory devices because of high dielectric constant (ε_r) and low dissipation factor ($\tan\delta$) at RT. Many efforts have been made to further modify the

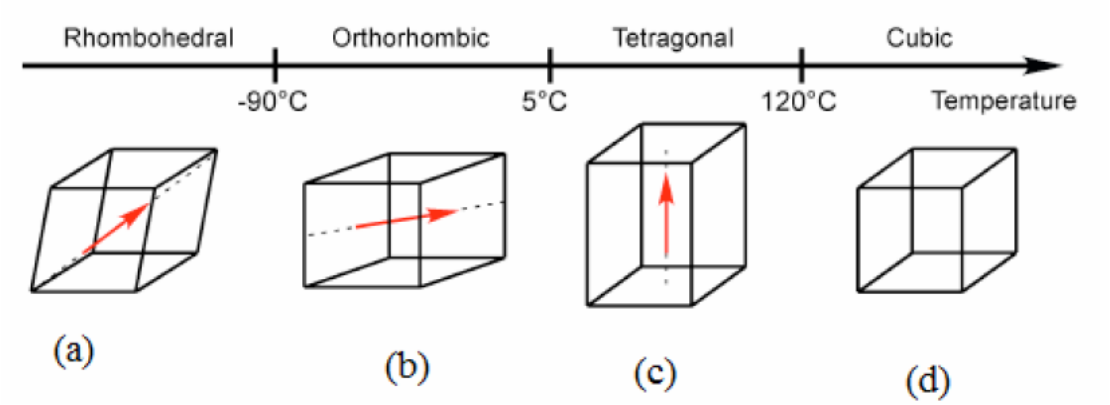

Fig. 1.5 Phase transitions in BT system

dielectric properties of these ceramics. Fig. 1.5 shows the phase transitions in BT system [10]. Additives which change the microstructure can also modify the dielectric properties of $BaTiO_3$ ceramics. Substitution of isovalent/off-valent ions for the host lattice cations in BT perovskite lattice plays a significant role in these modifications. These materials form solid solutions with $BaTiO_3$ and alter its structural features, resulting in a shift in phase transition temperature along with modified dielectric

properties [10, 39-44]. Tetragonal $BaTiO_3$ is a ferroelectric perovskite (ABO_3) at room temperature that finds applications as a dielectric material in multilayer capacitors (MLCs) and as an over load protection device in electrical appliances. For MLC applications, dielectric materials need to be electrically insulating (>10^{10} Ω) and exhibit high permittivity values (>1000) at room temperature. As overload protection devices, they are required to be semiconducting (<100 Ω) at room temperature and undergo a sharp rise in resistivity (~4–6) orders of magnitude) when heated above the ferro to para-electric (tetragonal to cubic) phase transition temperature, T_c. Such devices are called positive temperature coefficient of resistance (PTCR) thermistors. For many years, A- and B-site dopants have been used to modify the electrical properties of $BaTiO_3$; however, in many cases the doping mechanism(s) and defect chemistry remain poorly understood and/or controversial. This is because ceramics, processed at high temperatures, accompany oxygen vacancies [45]. Also, the substation at A and B site can lead to charge imbalance and creation of vacancies. Following are some of the mechanisms of creation of defects in BT ceramics:

$$O^{2-} \Rightarrow 1/2O_2 + 2e^- \qquad \text{----------1.2}$$

For the origin of defects by off-valent ion substitution, it was reported that by addition of divalent and trivalent ions with ionic radii similar to that of Ti, and demonstrated that the acceptors were compensated by oxygen vacancies, shown in equation 1.3 [46]. Additionally, it was also found that the electrons will be generated when off valent like Sm^{3+} ions substitute for Ba sites as donor by the equation 1.4

$$2BaO + Sm_2O_3 \rightarrow 2Ba_{Ba} + 2Sm'_{Ti} + 5O_O + V^{**}_O \qquad \text{----------1.3}$$

$$Sm_2O_3 + 2TiO_2 \rightarrow 2Sm^*_{Ba} + 2Ti_{Ti} + 6O_O + 1/2O_2 + 2e' \qquad \text{--------1.4}$$

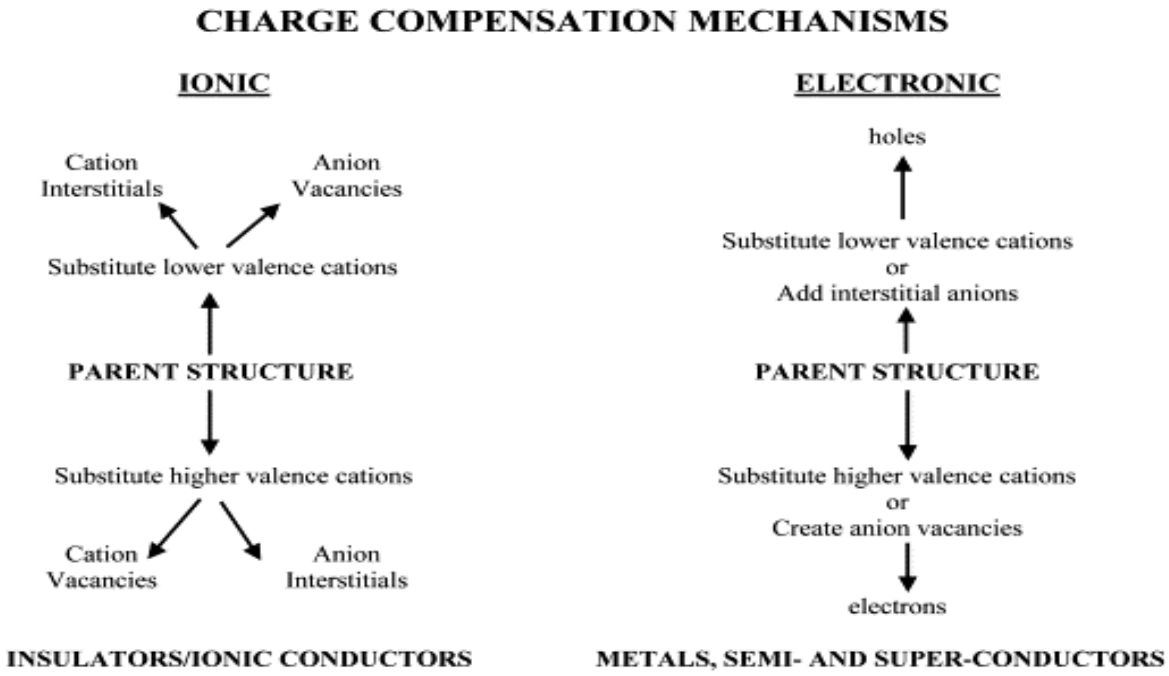

1.4.1 Modifications in BT System

A lot of study has been done on the isovalent/off-valent substitution in BT system [10]. The desired temperature-stability in dielectric properties of BT system are achieved by substitution of isovalent/off-valent ions. Isovalent dopants are commonly used to alter T_c and lower the orthorhombic/tetragonal [$T_{O/T}$] and rhombohedral /orthorhombic [$T_{R/O}$] phase transition temperatures. A-site doping with cations of the same valence as Ba causes the Curie temperature Tc (~120^0C in $BaTiO_3$) to either decrease (Sr substitution) or increase (Pb substitution), without any significant broadening of phase transition [10]. Fig.1.6 shows the effect of several elemental substitutions on the Curie temperature of BT [10-11].

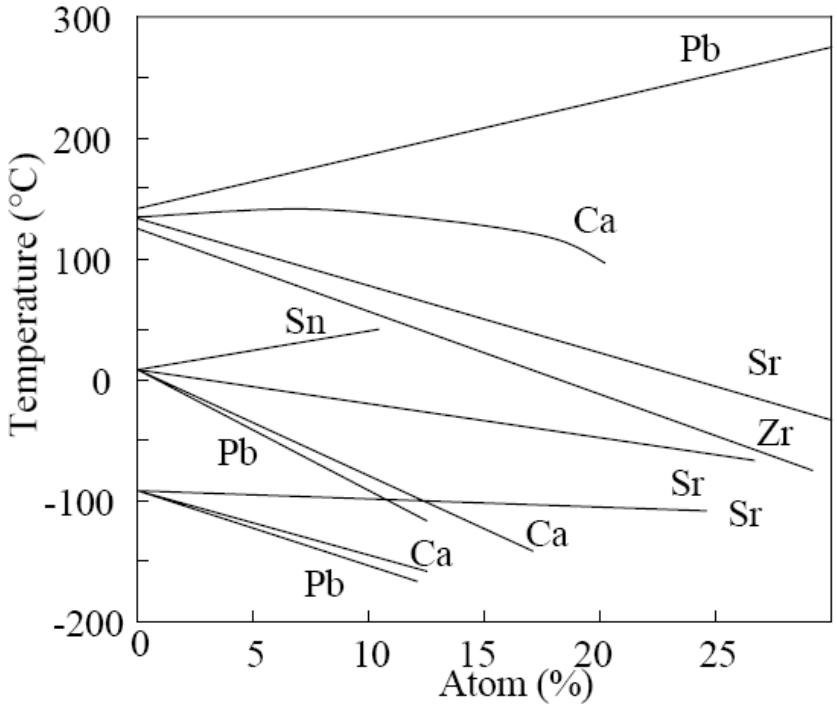

Fig. 1.6 Effect of elemental substitution on the T_c of the BT system.

There are reports of anomalous behaviour of off-valent substitution in BT system [47, 48]. A small amount of off-valent substitution in BT system greatly reduces the transition temperature (T_c) and hence ε_r at RT increases. For example when Nd^{3+} replaces Ba^{2+} this is called Donor doping. It is found that adding Nd_2O_3 into barium titanate can broaden and shift the Curie temperature to lower temperature, and thus enhance the diffuse phase transformation. The grain-growth inhibition effect is also found in $BaTiO_3$ ceramic with high Nd_2O_3 concentration [42]. Therefore, there is a need for studying the iso-valent and off-valent ion substitution effects on BT system in detail. In order to increase volume efficiency, the dielectric layers of BT system and inner electrodes are stacked layer by layer to form a multilayered structure. This is known as a multilayer ceramic capacitor (MLCC). In order to use low-cost metal electrodes, such as Ni and Cu for replacing the more expensive Ag-Pd system inner electrode in multilayer ceramic capacitors (MLCC) the $BaTiO_3$ based compounds must be sintered at a temperature low enough to suppress electrode oxidation [49, 50].

1.5 Various Synthesis Routes

Unfortunately, lowering the sintering temperature may result in a significant decrease in the dielectric constant. The processing temperature and microstructure of a ferroelectric ceramic depends on the synthesis route. The purity of the starting precursors affects the processing temperatures and hence the material properties. The solid state route (SSR) requires high calcination temperature to get perovskite phase and often results in the formation of multiphase and inhomogeneous powders [51-54]. Mostly the iso-valent and off-valent substituted BT ceramics are prepared by solid state reaction route [48, 54-56]. The complex double metal salts methods involve the use of solid precursors for the manufacture of pure $BaTiO_3$. The process suffers from the use of costly materials, multi steps, uncontrolled particle size and inter particle agglomeration. Pechini's autocombustion method is also reported to produce 10 nm particle size where costly materials are used but the approach suffers from small batch volume. Hydrothermal process [57] also involves the incorporation of costly materials. High energy ball milling [54] is also reported to produce 10nm particle size but the approach suffers from small batch size, high processing time and energy consumption. Whereas, chemical solution methods are used to produce more homogeneous, finer particle size and low impurity level powders than that produced by the SSR route [58-60]. But, chemical solution methods require expensive high purity chemicals and the method is complex [61]. Both chemical and solid state reaction routes have relative advantages and disadvantages over each other. It becomes imperative to devise some modifications in these routes to combine the advantages of both these routes. Therefore, in the present study, iso valent and off valent modified BT systems have been synthesized by modified solid state reaction route (MSSR), which combines the advantages of solid state and chemical routes like:

low cost of starting precursors and low processing temperatures with better dielectric properties. Therefore, the MSSR processing of iso valent and off valent modified BT ceramics is new of its type.

1.5.1 Microwave (MW) Synthesis Route

Synthesis of ferroelectric titanate based on conventional ceramic methods involves long reaction times due to slow diffusion rates in the solid state and often necessitate intermittent grinding [62]. The sintering of ceramics in conventional furnaces requires generally rather long times owing to the inertia of the furnaces and much energy is lost by radiation It is well documented in the literature that the various properties such as $\varepsilon_{r,}$ $\tan\delta$ and electromechanical properties of ferroelectric ceramics are influenced by microstructure and grain size. We can achieve higher density and uniform microstructure in ceramics by the addition of solid solution forming additives, which inhibit grain growth; and by the application of suitable process control, such as hot pressing or fast firing. Very recently, there is a growing interest on microwave sintering (MS) in order to get fine grains and uniform microstructure [63-66]. It is also worth pointing out that the use of microwaves allows heating to be started at the core of the sample contrary to classical heating which starts at the surface; this could change the microstructure of the ceramics and consequently their physical properties. Moreover the quenching of the ceramics in order to stabilize a high-temperature property should be easier with microwave devices. It is also reported that microwave sintering (MWS) is superior to conventional sintering (CS) due to its unique characteristics, such as rapid heating, enhanced densification rate and improved microstructure [67-76]. Microwave heating is fundamentally different from conventional heating. In the microwave process, the heat is generated internally within the material instead of originating from external sources, and hence there is an

inverse heating profile. The heating is very rapid as the material is heated by energy conversion rather than by energy transfer, which occurs in conventional techniques. Therefore, microwave processing of the samples is energy efficient and promising good microstructure and density [67-76]. But, MW processing of iso valent and off valent modified BT ceramics is rarely reported in literature. In the present work, both iso-valent and off-valent substituted BT systems, with better dielectric properties have also been synthesized by microwave processing technique and compared with conventionally processed samples.

1.6 Aim of the Present Work

As mentioned earlier, BT system is the best system for MLC applications. But, in multilayer ceramic capacitors (MLCC), the $BaTiO_3$-based compounds must be sintered at a temperature low enough to suppress electrode oxidation for its practical applications in devices. There is also a need to modify BT systems for getting higher density, uniform microstructure, higher dielectric constant at room temperature, diffuse phase transition nature, stable capacitors with satisfactory operational capacity with increased temperature stability. In the present work, the processing temperatures of $BaTiO_3$-based compounds are lowered by using MSSR and MWS routes. The effect of MSSR and MWS processing routes on the perovskite phase evolution, structural, density, microstructural, dielectric, ferroelectric and strain vs. electric field (S-E) properties of iso-valent and off-valent substituted $BaTiO_3$-based compounds are studied in detail.

Briefly, following are the aims of the present research work:

- To lower the processing temperatures of $BaTiO_3$-based compounds than the conventional processing routes.

- To optimize the processing steps of modified solid state reaction route (MSSR) for obtaining single perovskite phase formation in modified BT compounds.
- To study how the substituent variation and the MSSR route influences the perovskite phase evolution, structural, density, microstructural, dielectric, ferroelectric and strain vs. electric field (S-E) properties of modified BT systems.
- To suggest best modified BT systems synthesized by MSSR route for dielectric applications.
- To reduce the sintering temperature of modified BT systems using MW sintering technique.
- To study how the substituent variation and MW sintering process influence the perovskite phase evolution, structural, density, microstructural, dielectric, ferroelectric and strain vs. electric field (S-E) properties of modified BT systems.

Following series are synthesized by MSSR route:

(i) $Ba_{1-x}Ca_xTiO_3$/BCT

(ii) $Ba_{1-x}Mg_xTiO_3$ /BMT

(iii) $Ba_{1-x}Sr_xTiO_3$/BST

(iv) $Ba_{1-x}Sm_xTi_{(1-x/4)}O_3$ /BSmT{y}; where y=x/0.02

(v) $Ba_{1-x}La_xTi_{(1-x/4)}O_3$/BLT {y} samples, where x=0.02, 0.04. 0.06 & 0.08

In the present work for x=0.02, 0.04. 0.06 & 0.08, we have used BCT1, BCT2, BCT3, BCT4, BMT1, BMT2, BMT3, BMT4, BST1, BST2, BST3, BST4, BSmT1, BSmT2, BSmT3, BSmT4 & BLT1, BLT2, BLT3, BLT4 notations.

$Ba_{1-x}Ca_xTiO_3$ & $Ba_{1-x}La_xTi_{(1-x/4)}O_3$ samples, where x=0.02, 0.04. 0.06 & 0.08, respectively synthesized by MSSR route are showing better dielectric properties. Therefore, these two series were sintered using MW process.

References

1. W.D. Kingery, H.K. Bowen and D.R. Uhalmann, Introduction to ceramics, 2nd Edition, John Wiley and sons, New York (1976).
2. N. Setter, J. Euro. Ceram. Soc., **21** (2001) 1279.
3. D.W. Richerson, Modern Ceramic Engineering, Marcel Dekker, New York (1992).
4. J.S. Reed, Principles of Ceramic Processing, John Wiley and Sons, Inc., New York (1995).
5. I.D. Marinescu, H.K. Tonshoff , I. Inasaki, Handbook of Ceramic Grinding and Polishing, Noyes Publications, USA (2002).
6. J. Valasek, Phys. Rev., **17** (1921) 475.
7. C. Kittel, Introduction to Solid State Physics, 7th Edition, John Wiley & sons, New York (1995).
8. G. Sirane, S. Hoshino, K. Suzuki, J. Phys. Soc., Japan, **5** (1950) 453.
9. G. Goodman, Am. Cearm. Soc. Bull., **31** (1952) 113.
10. B. Jaffe, W. Cook, H. Jaffe, Piezoelectric Ceramics, Academic Press, London (1971).
11. A. Safari, R. K. Panda, V. F. Janas, Ferroelectric Ceramics : Processing, Properties & Applications (Review Paper).
12. G. Haertling, J. Am. Ceram. Soc., **82** (1999) 797.
13. J.W. Waanders, Piezoelectric Ceramics-Properties and Applications, Philips Components, Eindhoven (1991).
14. Y. Saito, H. Takao, T. Tani, T. Nonoyama, K. Takatori, T. Homma, T.Nagaya, M. Nakamura, Nature **432** (2004) 84.
15. G. Z. Zang, J. F. Wang, H. C. Chen, W. B. Su, C. M. Wang, P. Q. Ming, J. Du, L. M. Zheng, S. Zhang, T.R. Shrout, Appl. Phys. Lett., **88** (2006) 212908.

16. M. Matsubara, K. Kikuta, S. Hirano, Jpn. J. Appl. Phys., **44** (2005) 6618.

17 Y Guo, K Kakimoto, H Ohsato, Appl. Phys. Lett., **85** (2004) 4121.

18. J Wu, Y. Wang, D. Xiao, J. Zhu, P. Yu, L. Wu, W. Wu, Jpn. J. Appl. Phys., **46** (2007) 7375.

19. H. Takao, Y. Saito, Y. Aoki, K. Horibuchi, J. Am.Ceram. Soc., **89** (2006) 1951.

20. E. Hollenstein, M. Davis, D. Damjanovic, N. Setter, Appl. Phys. Lett., **87** (2005) 182905.

21. L E Cross, Nature, **432** (2004) 24.

22. S. Komarneni & H. Katsuki,Ceramics International, **36** [3] (2010) 1165.

23. P. Kumar, S. Singh, M. Spah, J.K. Juneja, C. Prakash, K.K. Raina J. Alloys & Compounds, **489** [1, 7] (2010) 59.

24. N. Horchidan, A. C. Ianculescu, L. P. Curecheriu, F. Tudorache, V. Musteata, S. Stoleriu, N. Dragan, D. Crisan, S. Tascu, L. Mitoseriu, J. Alloys & Compounds, 509 [14] (2011) 4731-4737.

25. X. Deng, X. Guan, P. Chen, C. Lu, Z. Tan, D. Li, J. Li, X. Wang, L. Li, Thin Solid Films, **518** [24] (2010) e75.

26. S. Marković, Č. Jovalekić, L. Veselinović, S. Mentus, D. Uskoković, Journal of the European Ceramic Society, **30** [6] (2010) 1427.

27. B. Schumacher, H. Geßwein, J. Haußelt, T. Hanemann Microelectronic Engineering, **87** [10] (2010) 1978.

28. S. Tsukada, Y. Akishig, Scripta Materialia, **64** [3] (2011) 268.

29. Fang, D. X. Zhou, S. Gong, Physica B: Condensed Matter, 406 [6-7] (2011) 1317-1322.

30. H. N. Zadeh, C. Glitzky, W. Oesterle, T. Rabe, Journal of the European Ceramic Society, **31** [4] (2011) 589.

31. K. Niesz, T. Ould-Ely, H. Tsukamoto, D.E. Morse Ceram. International, **37** [1] (2011) 303.

32. B. D. Stojanovic, V. R. Mastelaro, C. O. Paiva Santos, J. A. Varela, Sci. Sintering, **36** (2004) 179.

33. Q. Jia, B. Shen, X. Hao, S. Song, J. Zhai, Materials Letters, **63** (2009) 464.

34. C. Zhou, X. Liu, W. Li, C. Yuan, Mater. Chem. Phys., **114** (2009) 832.

35. Y. Saito, H. Takao, T. Tani, T. Nonoyama, K. Takatori, T. Homma, T. Nagaya, M. Nakamura, Nature, **432** (2004) 84.

36. M. Suzuki, H. Nagata, J. Ohara, Jpn. J. Appl. Phys., **42** (2003) 6090.

37. T. Sawada, A. Ando, Y. Sakabe, D. Damjanovic, Jpn. J. Appl. Phys., **42** (2003) 6094.

38. C.R. Zhou, X.Y. Liu, Mater. Chem. Phys., **108** (2008) 413.

39. P. Victor, R Ranjith, S. B. Krupanidhi , J. Appl. Phys., **12** (1994) 7702.

40. V. S. Tiwari, N. Singh, D. Pandey, J. Phys. Condens. Matter, **7** (1995) 1441.

41. Yu Zhi, C. Ang, R. Guo, A. S. Bhalla, J. Appl. Phys., **92** (2002) 2655.

42. Z. Yao, H. Liu, Y. Liu, W. Wu, Z. Shen, Y. Liu, M. Cao, Mat. Chem. & Phys., 109 (2008) 475.

43. C. Masingboon, P. Thongbai, S. Maensiri, T. Yamwong, S. Seraphin, Mater. Chem. Phy., **109** (2008) 262.

44. W.P. Chen, W. Xiang, M.S. Guo, W.C. You, X.Z. Zhao, H.L.W. Chan, J.Alloys Compd., **422** (2006) L9.

45. F.D. Morrison, D.C. Sinclair, A.R. West, Int. J. Inorg. Mat., **3** (2001) 1205.

46. Y. Li, Y. Qu, Materials Research Bulletin, **44** (2009) 82.

47. F.D. Morrison, D.C. Sinclair, J.M.Skakle, A.R.West, J. Am. Ceram. Soc., **81** (1998) 1957.

48. F.D. Morrison, D.C. Sinclair, A.R.West, J. Appl. Phys., **86** (1999) 6355.

49. H. Kishi, Y. Mizuno, H. Chazono , Jpn. J. Appl. Phys., **42** (2003) 1.

50. Y. Sakabe, Current Opinion in Solid State and Materials Science, **2**[5] (1997) 584.

51. A. Beauger, J.C. Mutin, J.C. Niepce, J. Mater. Sci., **18** (1983) 30416.

52. A. Beauger, J.C. Mutin, J.C. Niepce, J. Mater. Sci., **183** (1982) 3543.

53. Y. H. Hu, M. P. Harmer, D.M. Smyth, J. Am. Ceram. Soc., **68** (1985) 372.

54. N.J. Welham, J. Mater. Res., **13** (1998) 1607.

55. M. Aparna, T. Bhimasankaram, S.V. Suryanarayana, G. Prasad, G.S. Kumar, Bull. Mater, Sci., **24** (5) (2001) 497.

56. P. Yongding, L. Yunhe, Y. Wenhu, J. Rare Earths, **25** (2007) 167.

57. S. Ghosh, S. Dasgupta, A. Sen, H. Sekhar Maiti, Mater. Lett., **61** (2007) 538.

58. A. Beauge, J.C. Mutin, J.C. Niepce , J. Mat. Sci., **18** (1983) 3041.

59. J. Bera, S.K. Rout, Mater. Lett., **59** (2005) 135.

60. D.F.K. Hennings, B. Schreinemacher, H. Schreinemacher, J. Eur. Ceram. Soc., **13** (1994) 81.

61. H. K. Guo, X. G. Tang, J. X. Zhang, S. W. Shan, M. M. Wu, Y. J. Luo, Journal of Materials Science Letters, **17** [18] (1998) 1567.

62. A.J. Moulson and J.M. Herbert, Electroceramics: Materials, properties and Applications , 2nd Edition, Wiley, New York (2003).

63. P. Yadoji, R. Peelamedu, D. Agrawal, R. Roy, Materials Science and Engineering B **98** (2003) 269.

64. D. Agrawal, Journal of Materials Education, **19** (1999) 49.

65. D.E. Clark, D.C. Folz, J.K. West, Materials Science and Engineering A**287** (2000) 153.

66. C. Leonelli, P. Veronesi, L. Denti, A. Gatto, L. Iuliano, Journal of Materials Processing Technology, **205** (2008) 489.

67. M. Oghbaei, O. Mirzaee, Journal of Alloys and Compounds, **494** (2010) 175.

68. C. T. Hu, *et.al*., Jpn. J. Appl. Phys., **37** (1) (1998) 186.

69. E. T. Thostenson, T. W. Chen, Compos. Part A, **30** (1999) 1055.

70. O.P. Thakur, C. Prakash, D. Agrawal, Int. J. Ceram. Process. Research, **3**(2) (2002) 75.

71. O.P. Thakur, C. Prakash, D. Agrawal, J. Mater. Sci. Engg B, **96** (2002) 221.

72. O.P. Thakur, C. Prakash, D. Agrawal, Mater. Letters, **56** (2002) 970.

73. M. Fu, D. Agrawal, Y. Fang, J. of Microwave Power & Electromagnetic Energy, **40** [3] (2007) 133.

74. C. Y. Fang, C. Wang, A. V. Polotai, D. K. Agrawal, M. T. Lanagan, Materials Letters **62** (2008) 2551.

75. N. Yoshikawa & T. Kato, J. Phys. D: Appl. Phys., **43** (2010) 425403

76. N. Yoshikawa, Fundamentals and Application of Microwave heating of Metals, Materia, Japan (Bulletin of Japan Inst.Metals), **48** [1] (2009) 3.

CHAPTER II

INVESTIGATED PARAMETERS

2.1 Introduction

This chapter presents a brief background of the parameters investigated in the present work. The properties of ferroelectric materials are strongly influenced by preparation methodology. There may be excellent compositional control of the material with improper processing, but the properties of the resulting ceramics are not necessarily good. Generally, in BT based systems synthesized by solid state reaction (SSR) route, processing temperatures are high. In the present work, modified solid state reaction (MSSR) and microwave (MW) processing techniques are used to reduce the processing temperatures, time and promising better dielectric properties of modified BT based systems. MSSR and MW processing routes are new of its type therefore it is important to understand the various processes intricacies taking place during material synthesis. A study of calcination and sintering parameters is also essential. Phase and microstructure, dielectric constant and loss, piezoelectric and ferroelectric properties characterize a ferroelectric material for various applications. Discussion on each one of these parameters is presented in following sections.

2.2 Material Synthesis Routes

Modified BT samples were prepared by MSSR and microwave processing routes. In MSSR route both oxide/carbonates and acetates of the starting precursors are used to combine the advantage of both SSR and chemical routes. Modified BT samples with best dielectric and ferroelectric properties are also prepared with microwave processing technique. In the following sections, first SSR, Chemical and then MSSR routes are discussed followed by microwave (MW) processing technique.

2.2.1 Solid State Reaction (SSR) Route

A solid solution is prepared by mixing two or more compounds and if the characteristics of starting components are retained, the mixture is formed. But, if the solid solutions of these compounds form one single compound then it does not retain the characteristics of its components. Usually, polycrystalline materials are prepared by the solid state reaction (SSR) route [1]. Solids usually do not react at room temperature and in order to facilitate the reaction, they are heated to higher temperature [2].

In SSR method, first of all raw materials are weight out according to the stoichiometry of the compound with due consideration for impurity and moisture contents. The selection of reactant chemicals depends on the reaction conditions and expected nature of the product. The reactants are dried thoroughly prior to weighing. As increase in surface area enhances the reaction rate, fine grained materials should be used if possible. Raw materials are mechanically mixed and then grinding operations are performed to control the particle size and to make mixture homogeneous. For this purpose milling operation is performed which can reduce the particle size to 1-10 μm range [3]. An attempt to reduce the size of the particles further may affect the homogeneity and purity of the material. Distilled water is usually used as wetting medium as it is available with adequate purity at low cost and is non-inflammable. Next step is the solid state reaction between the constituents of starting materials at suitable temperature [3, 4]. This process is called firing or calcination. During calcination, control over stoichiometry is essential, and for it, volatile constituents have to be compensated. Calcination causes the constituents to interact by inter diffusion of their ions and resulting in a homogeneous body. Hence, it is considered that calcination is the part of the

mixing process [1]. Calcination also controls the shrinkage during sintering. After calcination powder is given desired shape, known as green body, and this green body is densified through sintering process. One major drawback of SSR route is that it requires high calcination temperature to get single phase and often results in the formation of multiphase and inhomogeneous powders [2,3].

2.2.2 Metal Organic Decomposition (MOD)/Chemical Route

This technique often referred to as sol-gel processing, in which metal-containing organic chemicals (alkoxides) react with water in a non-aqueous solvent to produce a metal hydroxide or hydrous oxide, or in special cases, an anhydrous metal oxide. These gels are dried at low temperature to yield mixed oxide powder for ceramic processing. High surface area of dried gels enables higher reactivity, which in turn allows low processing temperature [5]. A major advantage of the MOD method is the control over purity and stoichiometry, which can be achieved with powder crystalline size of the order of 5-50nm [6]. Materials produced with this technique have lower sintering temperatures and grains of submicron size, which allows thinner layers and enhanced dielectric breakdown strength [7]. But, chemical solution methods require expensive high purity chemicals and the method is complex. Sometimes the processing may take place several days [8].

2.2.3 Modified Solid State Reaction (MSSR) Route:

Generally, the solid state reaction (SSR) route requires high calcination temperature to get single phase. Whereas, chemical solution methods are used to produce more homogeneous, finer particle size and low impurity level powders than that produced by the SSR route [9-11]. But, as discussed above both these SSR and chemical routes have relative advantages and disadvantages. Therefore, for better processing of ceramics with good properties at low processing temperature, it

becomes imperative to devise some modifications in these two routes so as to combine the advantages and avoid the disadvantages. In the present study, a modified solid state reaction route is used to synthesize iso valent and off valent modified BT systems. In the MSSR route barium acetate trihydate, calcium acetate/strontium acetate/magnesium acetate/lanthanum acetate/samarium acetate (all from Aldrich, USA with 99.8% purity) and fumed TiO_2 (Degussa) were used as starting precursors. Barium acetate and off-valent and iso-valent acetates are chosen since it is easy to dissolve these chemicals in acetic acid whereas, fumed TiO_2 (Degussa) was chosen to avoid the separate ball milling of this compound. With this set up of chemical reagents we are combining the advantages of chemical routes (easy decomposition of barium acetate and off-valent and iso-valent acetates) and fine powder of fumed TiO_2 (Degussa).

2.2.4 Microwave Processing Technique

Microwave energy is a form of electromagnetic energy with the frequency range of 300MHz to 300 GHz and the corresponding wavelengths are between 1mm and 1m [12]. The frequency and wavelength range of microwaves are shown in Fig. 2.1 [12]. Microwave heating is a process in which the materials couple with microwaves, absorb the electromagnetic energy volumetrically, and transform into heat. This is different from conventional methods where heat is transferred between objects by the mechanisms of conduction, radiation and convection. In conventional heating, the material's surface is first heated followed by the heat moving inward. This means that there is a temperature gradient from the surface to the inside as shown in Fig. 2.2. However, microwave heating generates heat within the material first and then heats the entire volume [24].

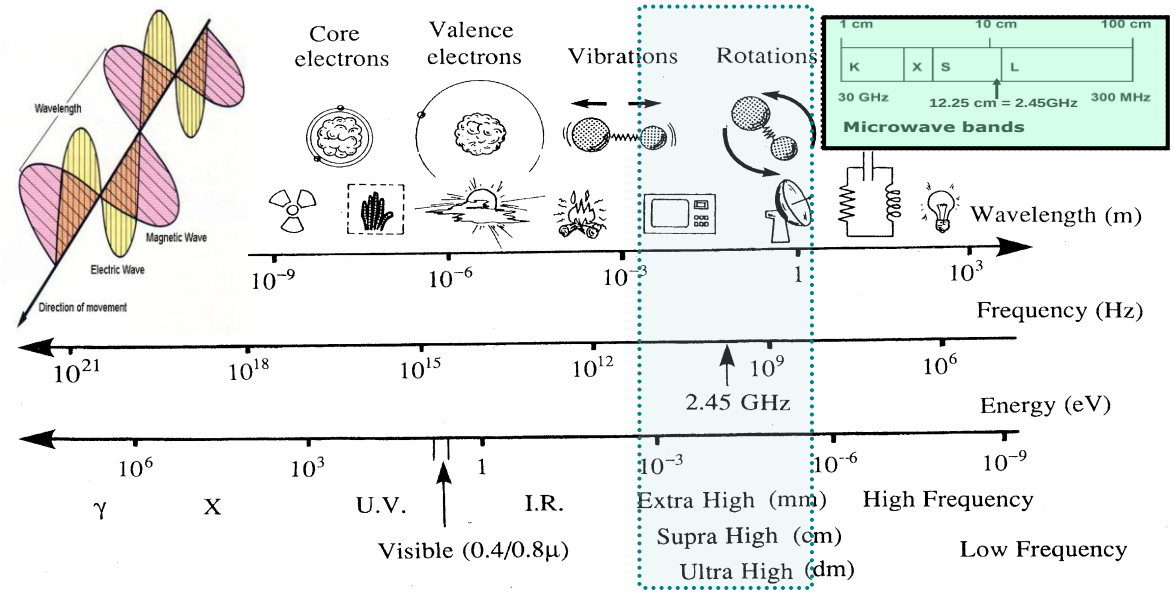

Fig. 2.1 The frequency and wavelength range of electromagnetic waves

This heating mechanism is advantageous due to the following facts: enhanced diffusion processes, reduced energy consumption, very rapid heating rates and considerably reduced processing times, decreased sintering temperatures, improved physical and mechanical properties, simplicity, unique properties, and lower environmental hazards.

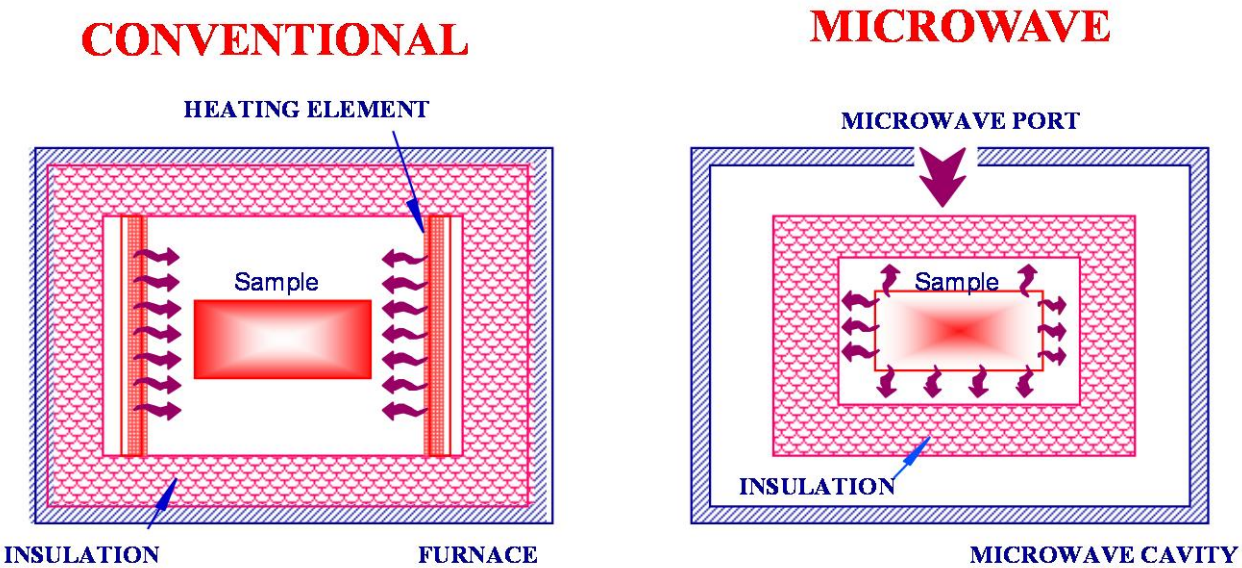

Fig. 2.2 Temperature gradient in conventional & microwave furnaces.

The dielectric interaction of materials with microwaves can be described by two important parameters: absorbed power (P) and depth of microwave penetration (D). They will determine the uniformity of heating throughout the material. The average absorbed power, P, which is volumetric absorption of microwave energy (W/m3) in material, is expressed as Eq. 2.1 [14, 15]:

$$P = \sigma|E|^2 = 2\pi f\varepsilon_0\varepsilon''_{\text{eff}}|E|^2 = 2\pi f\varepsilon_0\varepsilon'_r \tan\delta|E|^2 \qquad \text{.....2.1}$$

tanδ is the loss tangent, which indicate the ability of the material to be polarized and heated. It can be expressed as Eq. 2.2:

$$\tan\delta = \frac{\varepsilon''}{\varepsilon'} \qquad \text{.....2.2}$$

The loss factor measures the ability of the material to transfer microwave energy into heat and the dielectric constant measures the ability of the material to be polarized [15]. The absorbed microwave power in material is converted to heat and lead to increase in its temperature. Temperature increase is shown as Eq.2.3 [14]:

$$\frac{\Delta T}{\Delta t} = \frac{2\pi f\varepsilon_0\varepsilon''_{\text{eff}}|E|^2}{\rho C_p} \qquad \text{.....2.3}$$

The penetration depth D (m) is another important parameter that determines the depth of penetration at which the incident power is reduced by one half exhibiting the uniformity of heating throughout the material. The penetration depth can be expressed as in Eq. 2.4 [14,-16]:

$$D = \frac{3\pi_0}{8.686\pi\ \tan\delta(\varepsilon'_r/\varepsilon_0)^{1/2}} = \frac{C}{2\pi f\sqrt{2\varepsilon'}(\sqrt{1+\tan^2\delta}-1)^{1/2}} \qquad \text{.....2.4}$$

As seen in Eq. (4), the higher the values of tanδ and ε_r, the smaller the depth of penetration for a specific wavelength. High frequencies and large values of the

dielectric properties will result in surface heating, while low frequencies and small values of dielectric properties will result in more volumetric heating [14]. For a conductive metallic material, an incident wave is mainly reflected, and the rest cannot pass through the superficial layer of the metal itself. The penetration depth of the microwaves at a given frequency "f" depends on the electrical and magnetic properties of the material and is a very important parameter, because it constitutes an upper limit to the thickness of the material which can be heated directly by microwaves. The skin depth "d" (m) is defined as the depth into the conductor from the surface at which the current density is 1/e of its value at the surface [17, 18], given by Eq. 2.5

$$d = \sqrt{\frac{1}{\pi f \sigma \mu_a}} \qquad \text{.....2.5}$$

Materials with high conductivity and permeability present a lower penetration depth, for a given frequency, but there is also implicit temperature dependence due to the changes of σ and μa. Most metals generally have a penetration depth of the micrometer order, so the direct heating tends to remain superficial, but using powders with particle size of the penetration depth order, it is possible to heat them directly and use microwave in the sintering process [17]. As seen from the above equations, the dielectric properties (ε_r', ε_{eff}" and tanδ) act as an important role in the extent of power absorbed by a material. There are no structural parameters (atomic, microstructural or otherwise) in the equations. Structural features

are assumed to be accounted for by changes in the dielectric properties (ε_r', ε_{eff}" and tanδ) [14]. The particular requirements of sintering material powders make this process one of the most challenging applications for microwave processing. These requirements often include some or all of the following: high temperature, high

heating rates, uniform temperature, and equivalent thermal history throughout the specimen.

Therefore, microwave processing of the samples is energy efficient and promising good microstructure and density of the microwave processed samples. In the present work, both iso-valent and off-valent substituted BT systems, with better dielectric properties have also been synthesized by microwave processing technique and compared with conventionally processed samples.

2.3 Synthesis of Ceramic Samples

In this work, polycrystalline modified BT ceramics have been synthesized using MSSR and microwave processing technique. Both these synthesis techniques involve calcination and sintering. Therefore, a general discussion on calcination and sintering is given. A general discussion on the shaping of the material used in the present work is also presented.

2.3.1 Calcination

Calcination process involves chemical reactions between the starting precursors used and during it either the partial or complete phase of the compound is formed. It also helps in removing the unwanted gases and unwanted products during the decomposition of the starting precursors. Calcination process also helps in homogenizing the materials and reducing the shrinkage during the subsequent sintering process of the finally shaped samples.

In general, following four physical processes are involved in the calcination of the raw materials:

(i) Linear expansion of the particles (< 400^0C) (ii) Solid phase reaction (400-750^0C) (iii) Contraction of product (750-850^0C) and (iv) Grain growth (>850^0C).

Synthesis of the phase of a compound takes place by solid-phase reaction, which involves the chemical reaction through atomic diffusion among grains at temperature below the melting points of the raw materials [19]. Usually, the calcination temperature is chosen high enough to cause complete reaction, but low enough to cause subsequent grinding. In the materials, having volatile constituents, the calcination temperature must be kept low enough to avoid loss of the volatile parts. To lower the calcination temperature and avoid the loss of volatile constituents, other processing techniques such as MOD (sol-gel processing), Co-precipitation etc. are used [20]. Several non-conventional routes are also employed to reduce the calcination temperature, which results in better quality ferroelectrics at relatively lower sintering temperature. But, these methods are complex, use expensive precursors and sometimes processing of ceramics may take several days [2].

2.3.2 Shaping

Calcined powders are ball-milled again to give suitable shaping to the powder. Generally, an organic binder is incorporated into the powder, for giving sufficient strength to dry shapes, so that handling between shaping and sintering may not be difficult. One of the most important requirements of the binder is that it should be possible to remove the binder from the pressed shapes without any disruptive effect. Out of various shaping methods, dry pressing has been used in the present work

2.3.3 Dry Pressing

Dry pressing is used for giving simple tablet/pellet like shapes to the calcined powder. It is carried out in a die having movable top. A cavity is formed at the bottom in lower portion. This cavity is filled with free flowing granulated powder

and then it is struck with the top of the die. With the help of the top-punch, pressure in the range of 70-275MPa is applied.

2.3.4 Sintering in MSSR

In the sintering process the shaped materials are consolidated into strong and dense polycrystalline aggregates. During sintering at an appreciable temperature, the atomic motion is more violent and the area between grains in contact increases due to the thermal expansion of the grains and finally only one interface between two grains remains. This corresponds to a state with much lower surface energy. In this state, the atoms on the grain surfaces are affected by neighboring atoms in all directions, which results in densified ceramic [19].

At the beginning of the sintering process, but rather at high temperature, the lattice distortion and internal strain are reduced by atomic diffusion and this is frequently called as 'the recovery process'. With the further increase in temperature, a recrystallization process occurs through atomic diffusion. During recrystallization, new crystal nuclei form and grow at grain boundaries and in other regions inside the grain with higher free energies. Meanwhile, some grains grow by swallowing up other grains. In the recrystallization stage, grain growth is usually realized through the motion of grain boundaries. In general, higher the sintering temperature, larger the grains would grow, as the grain growth is caused by atomic diffusion, which increases with the increase in sintering temperature. However, the density of a ceramic is affected by the sintering temperature and time in a more complex fashion. If the sintering temperature is too high or the sintering time is too long, the density of the volatile based ceramics will be reduced owing to evaporation of the volatile element of the compound. Since, the grain growth is caused by atomic

diffusion, it follows that a higher sintering temperature and a larger hold time would result in larger grains.

The oxide ceramics should be sintered in an oxidizing atmosphere or in air and a reducing atmosphere must be avoided. Therefore, no organic substances should be mixed with the semifinished products, as they can produce a reducing atmosphere (i.e CO) during sintering.

2.3.5 Sintering in Microwave Processing Technique

The process of sintering materials in the conventional methods is incorporated with mixing of material powder with additive, milling, and pressing into green parts followed by sintering with indirect heating of green pellets at about 0.6–0.8Tm in a refractorytype electrical resistance furnace, induction furnace or fossil fuel furnace. These furnaces use a large number of expensive heating elements, fuel and refractory materials to achieve and maintain the high temperature for a long time. Moreover, it consumes much electrical energy,muchfuel, and longer time. These kind of furnaces with indirect heating are called conventional sintering furnace and the heating mechanism is called conventional heating. The fundamental difference between microwave sintering and conventional sintering is in the heating mechanism. The temperature profile for both methods is shown in Fig. 2.3. For conventional sintering, heat is generated by heating elements and transferred to samples via radiation, conduction, and convection. In microwave sintering, however, the materials themselves absorb microwave energy, and then transform it into heat within their bodies [21, 22]. The microwave heating presents a potential economical sintering process with shortened processing time for the materials. This method is expected to overcome many of the shortcomings of the conventional sintering process [23]. Thus, there has been considerable interest in microwave heating for the synthesis and

processing of materials. Microwave processing has gained worldwide acceptance as a novel method for heating and sintering a variety of materials, as it offers many advantages in terms of enhanced diffusion processes, reduced energy consumption and processing cost, very rapid heating rates and significantly reduced processing times, decreased sintering temperatures, improved physical and mechanical properties, simplicity, unique properties, new materials and products and lower environmental hazards, which are not observed in conventional processes [13,14, 17 24, 25].

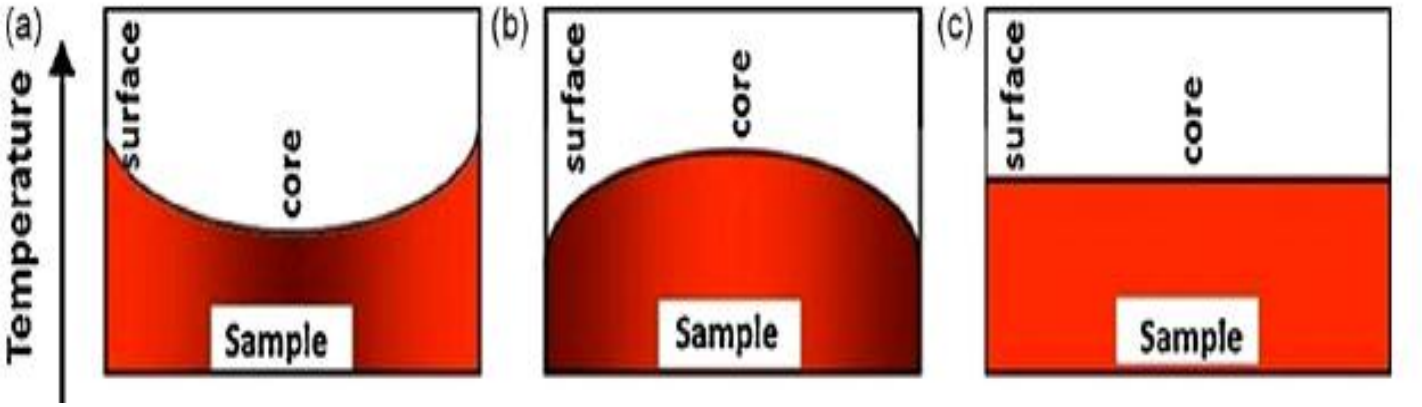

Fig. 2.3 Temperature profile within the sample in: (a) conventional heating, (b) microwave heating and (c) microwave hybrid heating.

2.4 Dielectric Polarization

Polarization of a dielectric material is defined as dipole moment per unit volume and is given as

$$P = \alpha E. \qquad \ldots 2.6$$

here P is the polarization of the material under an applied external electric field E and α is the polarizability of the dielectric material. Generally, the overall polarizability, α, of a material is made up of four contributions:

$$\alpha = \alpha^d + \alpha^i + \alpha^e + \alpha^f \qquad \ldots 2.7$$

here α^d = Dipolar polarizability

α^i = Ionic polarizability

α^e = Electronic polarizability

α^f = Interfacial polarizability

shown in Fig. 2.4 [26] and the discussion on these different polarizations is as follows

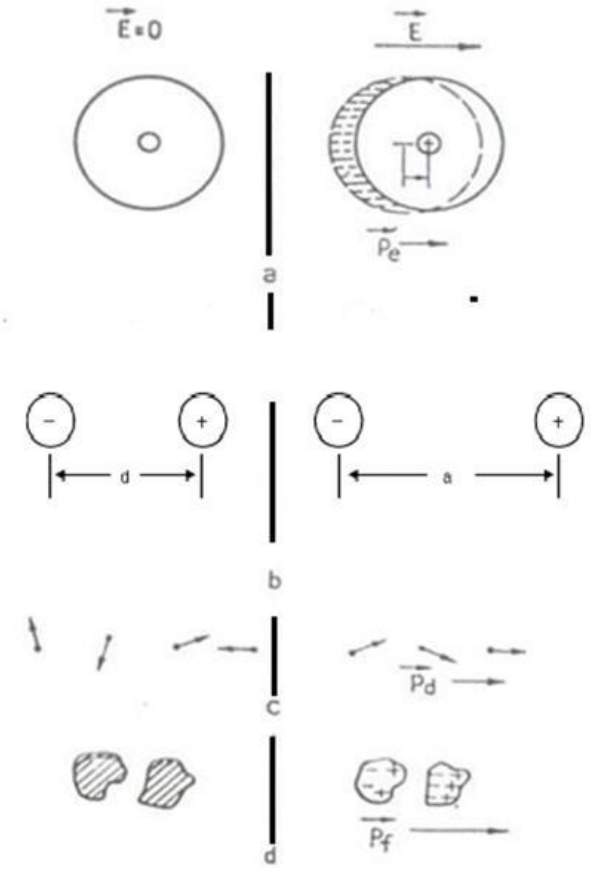

Fig. 2.4 Different polarization mechanisms; (a) Electronic polarization, (b) Ionic polarization, (c) Dipolar polarization & (d) Interfacial polarization.

2.4.1 Dipolar Polarization (Orientational Polarization)

In a system composed of heteronuclear molecules the disposition of the individual atoms within a molecule can be such that the molecule itself has a permanent dipole

moment and its magnitude does not change with the local field magnitude and this polarization is known as dipolar polarization. In zero field, the permanent dipoles will be randomly oriented and the system has no net polarization, but an applied electric field will tend to align the dipoles and the material will acquire a net polarization, also known as orientational polarization. Due to the randomizing effect of the thermal vibrations this type of polarization is more effective at low temperatures or in other words decreases with the increase in temperature. Dipolar polarization is frequency dependent, and active in low and microwave frequency range [26].

2.4.2 Ionic Polarization

It originates with the displacement of ions from the equilibrium positions under an applied electric field. As the name suggests, ionic polarization occurs in ionic materials. It occurs when an electric field is applied to an ionic material then cations and anions get displaced in opposite directions giving rise to a net dipole moment. Ionic polarization is active in infrared frequency range and temperature independent.

2.4.3 Electronic Polarization

Due to the relative displacement of the centers of the +ve charges with respect to the centre of the –ve charges of an atom when subjected to an external electric field, E electronic polarization arises. It is operative in all dielectrics and is temperature independent. Electronic polarization is active in the optical (visible-ultravoilet) frequency range.

2.4.4 Interfacial Polarization

In polycrystalline materials, the inter-grain boundaries are zones, where free charges (interstitial ions, vacancies, injected electrons etc.) can accumulate and cause polarization of crystallites, which is known as interfacial polarization. The notion of interface polarization is related to separated surfaces between crystallites, which act

as barriers to the motion of free charges from one crystallite to the other and is a characteristics of polycrystalline materials [27]. Interfacial polarization is prominent in microwave frequency range and temperature dependent. Frequency ranges of different polarizations is given in given in Fig. 2.5.

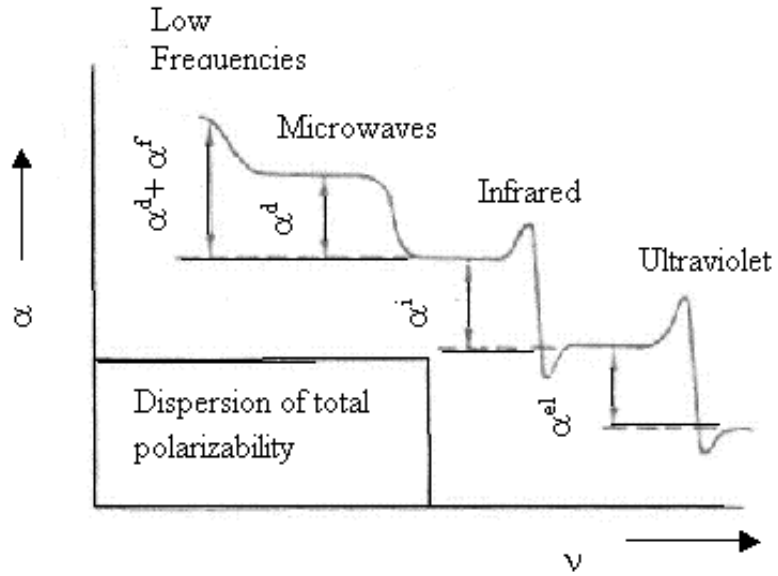

Fig. 2.5 Frequency range of different polarizations

2.5 Dielectric Properties

Very often **f**erroelectric materials are dielectrics. For most applications of ferroelectric materials, the dielectric constant (ε_r) and dielectric loss ($\tan\delta$) are important practical parameters, and studies of the dielectric properties provide a great deal of information about the suitability of the material for various applications.

2.5.1 Dielectric Constant (ε_r)

The ratio between the charge stored on an electroded slab of material brought to a given voltage and the charge stored on a set of identical electrodes, separated by vacuum defines the relative dielectric constant (ε_r) of a material. It is defined as

$$\varepsilon_r = 1+P/(\varepsilon_o E) \qquad \ldots 2.8$$

where ε_r = Dielectric constant

P = (Induced dipole moment/volume), under an applied electric field E

ε_o= Permittivity of the free space

And, for an alternating electric field, the dielectric constant can be written as

$$\varepsilon_r = \varepsilon' - i\varepsilon'' \quad \ldots 2.9$$

where ε'is the real component of the dielectric constant, in phase with the applied field. ε" is the imaginary component, 90^o out of phase with the applied field, caused by either resistive leakage or dielectric absorption. For normal substances, the value of ε_r is low, usually under 5 for organic materials and under 20 for most inorganic materials. Generally, ferroelectric ceramics have much higher ε_r, typically several hundreds to several thousands [28].

2.5.2 Dielectric Loss (tanδ)

The charging current in an ideal dielectric/capacitor leads the applied voltage by π/2 radians (90^o). However, in real dielectrics in addition to the charging current associated with the storage of electric charge by the dipoles, a loss current must also be considered. This loss current arises from the long-range migration of charges, e.g., dc ohmic conduction and the dissipation of energy associated with the rotation or oscillation of dipoles [28]. As the dielectric is not loss free, it is generally represented by a complex dielectric constant, defined in equation 2.9**.** The total current in the real dielectric is a complex quantity which leads the voltage by an angle (90-δ), where δ is called the loss angle. Dielectric loss (tanδ) also known as dissipation factor is defined as $\tan\delta = \varepsilon''/\varepsilon'$. The inverse of the loss tangent, Q = (1/tanδ), is used as a figure of merit in high frequency applications.

2.5.3 Curie Temperature (T_c)

The temperature above which the spontaneous polarization (P_s) of the ferroelectric materials vanishes and the material goes into paraelectric state is known as Curie

point, denoted by T_c. When the temperature increases through the Curie point, a ferroelectric crystal undergoes a structural phase transition from a ferroelectric (non-centrosymmetric) to paraelectric phase (symmetric) and above T_c the material does not exhibit ferroelectricity. Thermodynamic properties including dielectric, elastic, optical and thermal constants show an anomalous behavior near the vicinity of T_c, [19]. If there are two or more ferroelectric phases in a material, the Curie point only specifies the temperature at which a ferroelectric - paraelectric phase transition occurs.

2.5.4 Phase Transition

Generally, the spontaneous polarization, P_s, in a ferroelectric material decreases with the increase in temperature. It becomes zero at T_c, where transition takes place from ferroelectric phase to paraelectric phase. If this transition is a discontinuous change in P_s at T_c then phase transition is known as first order phase transition. However, if P_s becomes zero gradually with temperature, then the transition is called second order phase transitions [28]. The first & second order phase transitions are shown in Fig. 2.6 [29]

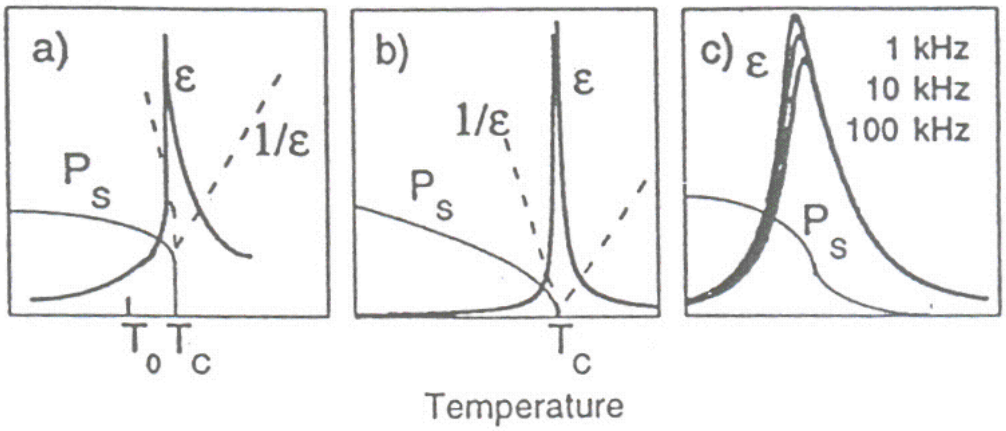

Fig. 2.6 Ferroelectric phase transition behaviors (a) first order (b) second order and (c) relaxor type.

2.5.5 Diffuse Phase Transition

A diffuse phase transition (DFT) is generally characterized by broadening in dielectric constant versus temperature curve. i.e the transition temperature is not sharply defined. This DFT is not only observed in relaxors but may be realized in normal dielectrics under certain special circumstances. It is known that the dielectric permittivity of a normal ferroelectric above the Curie temperature follows the Curie-Weiss law described by

$$\varepsilon' = C/(T - T_0), \ (T > T_C) \qquad \text{.....2.10}$$

A modified Curie-Weiss law has been proposed to describe the diffuseness of a phase transition,

$$\frac{1}{\varepsilon'} - \frac{1}{\varepsilon_m} = (T - T_m)^{\gamma} / C' \qquad \text{.....2.11}$$

where : and C' are assumed to be constant. The parameter γ gives information on the character of the phase transition; for γ:=1, a normal Curie Weiss law is obtained, for γ:=2, it reduces to the quadratic dependency which describes a complete diffuse phase transition. The slope of the plot of log ($1/\varepsilon_r - 1/\varepsilon_{rmax.}$) vs log (T-Tm) gives us γ factor.

Broadening of phase transition in ceramics depends on the composition fluctuations and structural disorderness. In systems, where structural order is distributed due to the disturbance in the composition phase transition is generally gradual and bandwidth depends on the degree of the disorder. Ferroelectric behavior of these materials within the Curie range can be described by considering the material as a collection of small regions, each having normal ferroelectric features with different Curie temperatures [29]. Other features like Lorentz parameter etc. may vary from region to region and the macroscopic properties of the crystal depend on the

average behavior over the entire volume. Following factors may affect the ferroelectric behavior of the material undergoing diffused phase transition (DPT):

(1) Macroscopic inhomogeneties due to errors in fabrication techniques.

(2) Microscopic inhomogeneties due to compositional fluctuations.

(3) Thermal polarization.

(4) Relaxation polarization

(5) Lattice defects

2.6 Ferroelectric Domains

The regions of uniformly oriented spontaneous polarization within the material defines the ferroelectric domains. Onset of the spontaneous polarization at T_c, leads to the formation of a surface charge. These surface charges produce an electric field, called depolarizing field, E_d. The depolarizing field may be very strong of the order of several kV/cm, rendering the single–domain state of the ferroelectric energetically unfavorable [30, 31]. The electrostatic energy associated with the depolarizing field may be minimized if

(i) The ferroelectric splits into domains with oppositely oriented polarization.

(ii) The depolarizing charge is compensated for by electrical conduction through the material or by charges from the material surrounding.

Splitting of a ferroelectric crystal into domains may also occur due to the influence of mechanical stresses [32].

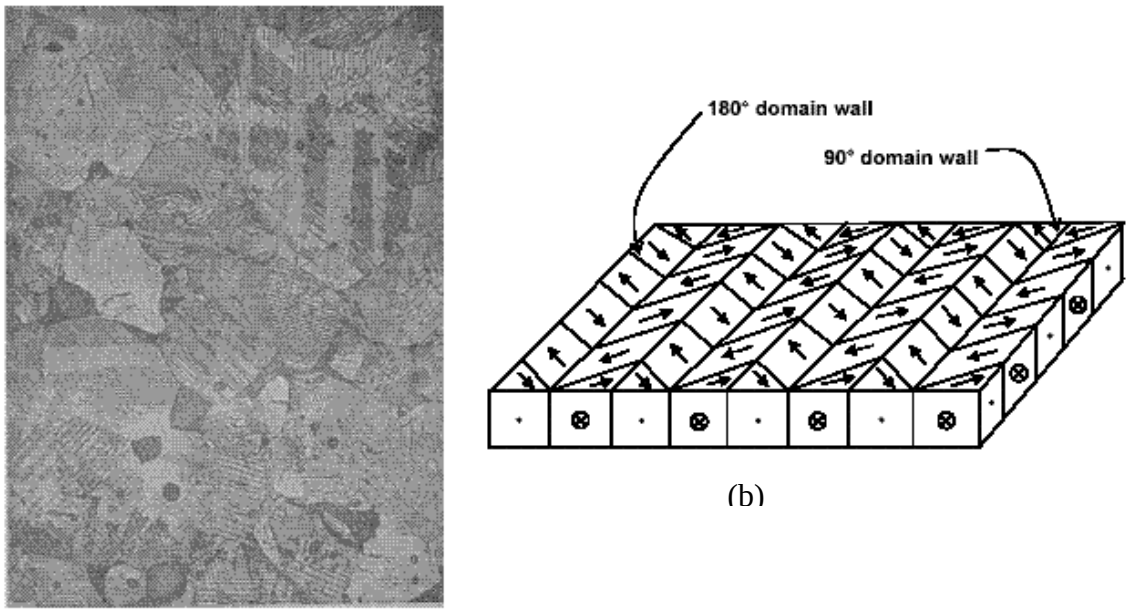

(a) (b)

Fig. 2.7 Ferroelectric (a) domains and (b) domain walls

The walls, which separate domains with oppositely oriented polarization, are called 180^o walls and those, which separate regions with mutually perpendicular polarization, are called 90^o walls [33]. 180^o and 90^o domain walls are shown in Fig. 2.7 [3]. Both 90^o and 180^o walls may reduce the effects of depolarizing fields but only the formation of 90^o walls may minimize the elastic energy [34]. 90^o domain wall motion results in large deformation and their movements require higher fields. The types of domain walls that can occur in a ferroelectric material depend on the symmetry of both the non-ferroelectric and ferroelectric phases of the material. Ferroelectric domain walls are much narrower than domain walls in ferromagnetic materials.

2.7 Poling

Poling is a process during which a high electric field is applied on the ferroelectric ceramic samples to force the domains to reorient in the direction of the applied

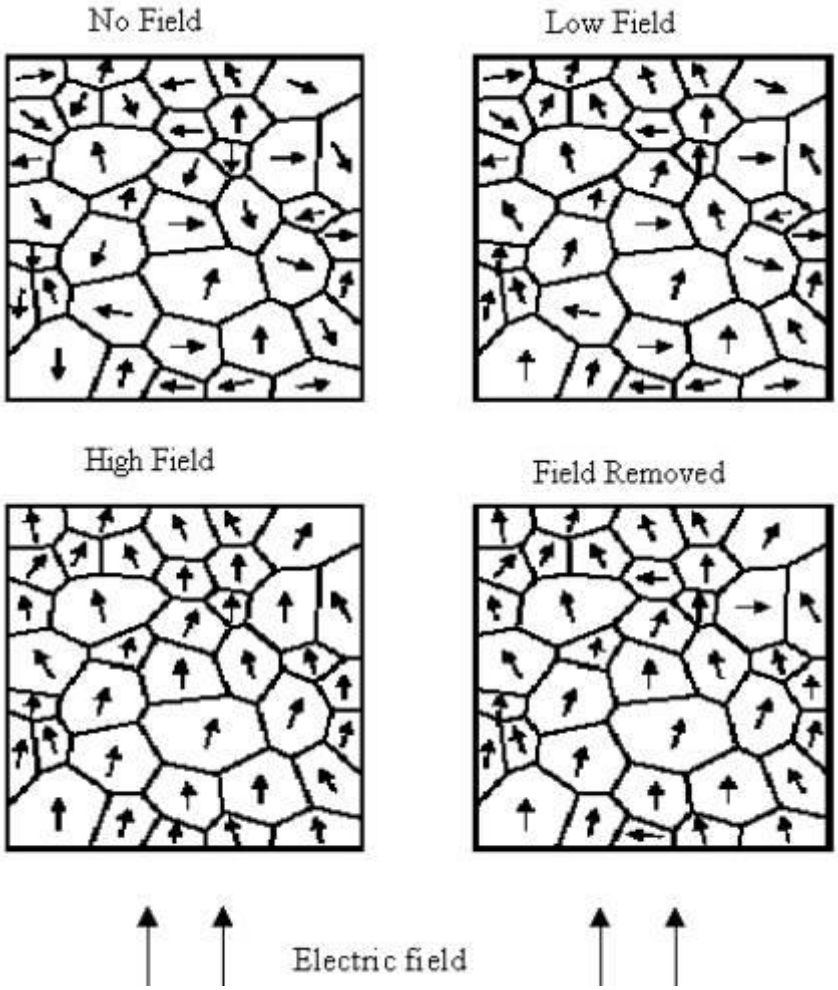

Fig. 2.8 Poling steps of a ferroelectric material

electric field. The poling is possible only in ferroelectric materials and poling steps are shown in Fig 2.8[3]. Pyroelectric or piezoelectric polycrystalline materials, with randomly oriented grains can not be poled as they lack more than one equilibrium state of the polarization vector. Before poling, the ferroelectric ceramic does not possess any piezoelectric and pyroelectric properties owing to the random orientation of the ferroelectric domains in the ceramics. For domain reorientation, a poling field must be applied on the sample and maintained for a certain length of time. For a given

field and poling time, better domain rearrangement results at higher temperature [28], but less than T_c. This happens because with the increase in poling temperature, crystalline anisotropy and coercive field, E_c, of the ferroelectric materials decreases [28]. Also, with increasing temperature, space charges, which act against domain motion, decreases in the ceramic. However, when the poling temperature is too high, problems arise as the electrical conductivity increases and the consequent increase in leakage current would result in sample breakdown during the period of poling. After poling, the electric field is removed and a remnant polarization and remnant strain are maintained within the material, and it starts exhibiting piezoelectric and pyroelectric effects [28].

2.8 Piezoelectric Coefficients

2.8.1 Piezoelectric Charge Coefficient (d)

'd' is piezoelectric charge coefficient and is measured in Coulomb/Newton (C/N). d_{33} is the piezoelectric coefficient, related to the direction of the applied electric field to the direction of the faces on which charges induced. d_{33} is the piezoelectric constant when the direction of the applied stress is along the direction of the faces of the ceramic on which charges are developed as shown in Fig. 2.9 [30]. In converse piezoelectric effect, an applied field E may produce a proportional strain S in the material, which is given by

$$S = d \bullet E \qquad \ldots 2.12$$

where d is expressed in pico-meter/volt.

High ‘d’ constant is desirable for materials intended to develop motion or vibration, such as sonar or ultrasonic cleaner transducers [28]. Piezoelectric constants and strain induced by electric field behavior is desired for actuator applications [35].

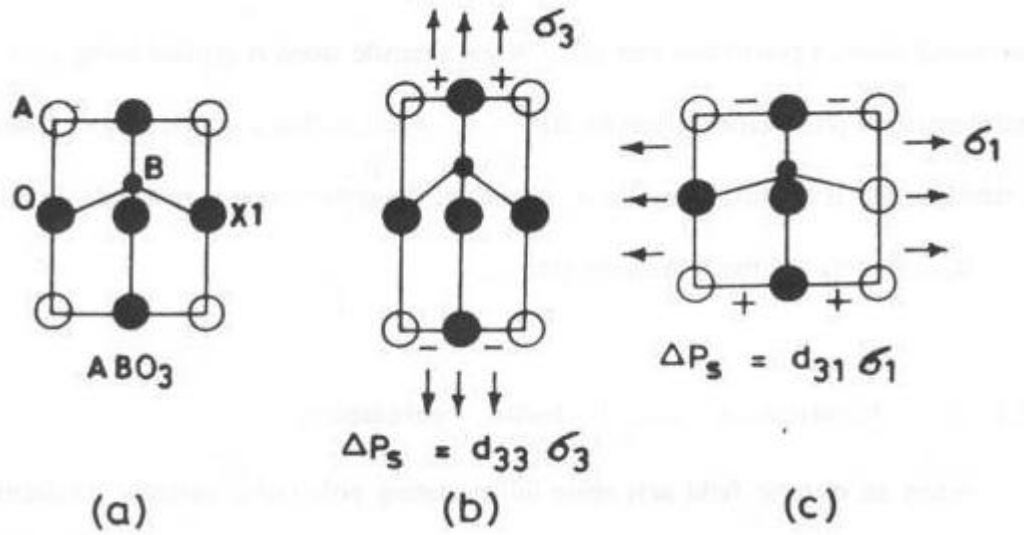

Fi. 2.9 (a) A two dimensional view of the perovskite structure (ABO_3) showing the displacement of B-ions in the x_3 direction, (b) The ame structure with a tensile stress σ_3 applied along x_3, and (c) A tensile stress σ_1 applied along x_1.

2.9 Hysteresis Loop Behavior

It is the most important property of ferroelectric materials and measured by the behavior of polarization reversal or switching by an applied external electric field in the material. The domain-wall switching in a ferroelectric material, results a ferroelectric hysteresis loop, shown in Fig. 2.10 [5]. This hysteresis loop can be observed experimentally by using a Sawyer –Tower circuit [36]. As shown in Fig. 2.13, at small values of the ac electric field, the polarization increases linearly with the field amplitude and in this region, the field is not strong enough to switch the domains with the unfavourable direction of the polarization. As, the field is increased, the polarization of domains with an unfavourable direction of polarization starts to

switch in the direction of field and rapidly increasing the measured charge density. The polarization reversal takes place by the growth of existing antiparallel domains,

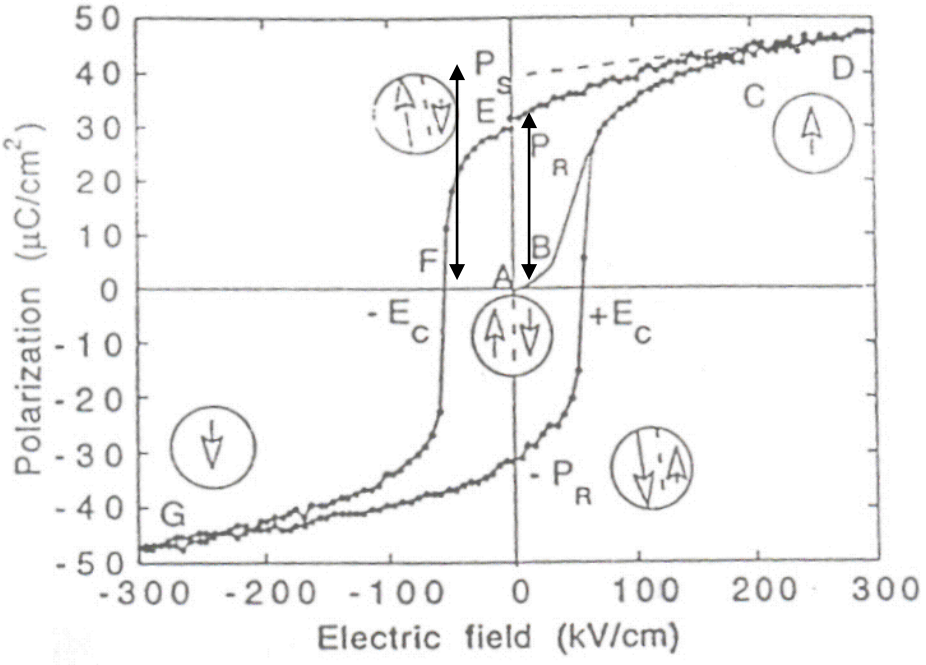

Fig. 2.10 Polarization vs. electric field loop behavior of a ferroelectric material.

by domain-wall motion and by nucleation and growth of new antiparallel domains [30, 37]. The polarization response in this region is strongly nonlinear and once all the domains are aligned, the ferroelectricity again behaves linearly. With the decrease in field strength, some domains back–switch, but at zero field the polarization is non zero and to reach a zero polarization state, the field must be reversed. Further increase of the field in the negative direction causes a new alignment of dipoles and saturation. The field strength is then reduced to zero and reversed to complete the cycle. The value of polarization at zero field is called the remnant polarization, P_r, and the field necessary to bring polarization to zero is called the coercive field, E_c. The spontaneous polarization, P_s, is usually taken as the intercept of the polarization axis, tangent to the saturated polarization. In polycrystalline materials, true spontaneous polarization equal to that of a single

crystal can never be reached and here it is more correct to speak of saturated rather than of spontaneous polarization [38].

Generally, an ideal hysteresis loop is symmetrical. In some materials the coercive field, spontaneous and remnant polarizations and the shape of the loop may be affected by a number of factors including the thickness, the presence of charged defects, mechanical stresses, preparation conditions and pinning centers [39].

Polarization electric field (P-E) hysteresis loop is also a function of temperature and usually the area of the loop shrinks with the increase in temperature until a phase transition takes place [28]. At this point no P-E loop is observed and this temperature is called Curie temperature T_c.

2.10 Strain Electric (S-E) Field Curve

Polarization switching by an electric field in ferroelectric materials leads to strain – electric field effect. Generally the strain - electric field curves are attributed to:

(i) Electrostrictive phenomenon

(ii) Piezoelectric phenomenon

(iii) Switching and movement of domain walls.

Here, the word “electrostriction” is used in a general sense to describe electric-field induced strain and frequently also implies the “converse piezoelectric effect”. However, in solid state theory, the converse piezoelectric effect is defined as a primary electromechanical coupling effect, that is, the strain is linearly proportional to the electric field, while electrostriction is a secondary coupling in which the strain is proportional to the square of the electric field and is independent of the direction of the applied electric field. Thus, strictly speaking, they should be distinguished.

Some Ferroelectric material, show the electrostrictive effect, shown in Fig. 2.11 [5], which is expressed as

$$x = ME^2 \qquad \ldots 2.13$$

where x=strain induced with the application of applied electric field E, and M=electrostrictive constant.

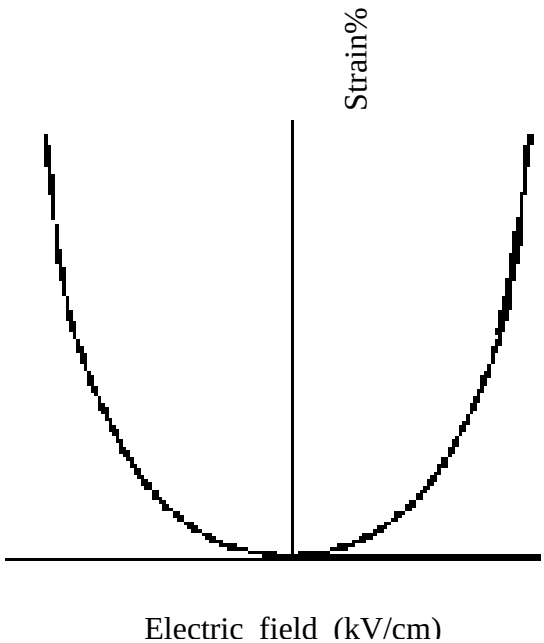

Fig. 2.11 Strain induced by electric field in a electrostrictive material

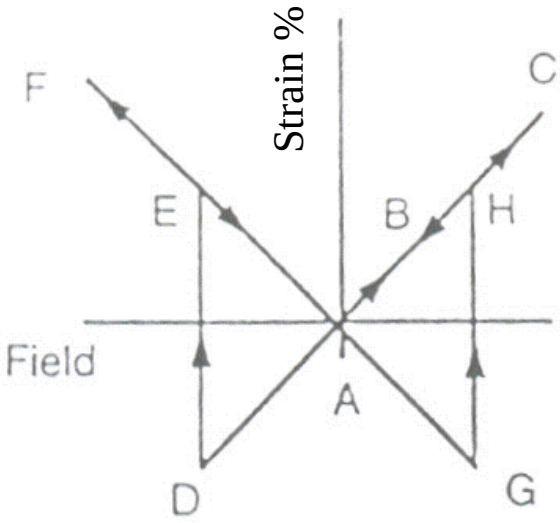

Fig. 2.12 Strain induced by electric field behavior in a piezoelectric material.

When strain induced in a material is proportional to the applied electric field and depends on the direction of electric field, the phenomenon is known as converse piezoelectric effect, which is expressed as

$$x = d \bullet E \qquad \ldots 2.14$$

where x is induced strain with the application of electric field E and d is the piezoelectric constant. Pure piezoelectric effect is shown in Fig. 2.12 [38, 41]. As, shown in Fig. 2.12, initially the strain of the material is taken to be zero and the electric field is applied in the direction of spontaneous polarization (P_s). As, the field is increased, the crystal expands through the piezoelectric effect and the strain traces the line A-B-C and the expansion continues until the maximum field is reached. At point C, the field starts to decrease, but is still parallel to P_s. The strain of the sample traces the same line but in the opposite direction (from C to A) and becomes again zero at point A. The field then changes its direction, becoming antiparallel to P_s. As, the field strength increases in the negative direction, the material starts contracting with respect to point A. At point D the field is large enough to switch the direction of polarization. After switching, the polarization again becomes parallel to the field, and again strain becomes positive (point E). During further increase of the field in the negative direction, strain increases to point F, and decreases back to point A as the field is decreased. The reversal of the polarization and sudden change of the strain happens at point G. The strain – field curve is linear for purely piezoelectric effect as shown in the Fig 2.12.

In reality, the strain electric field curves for a piezoelectric material have a hysteresis loop, which resembles the shape of a butterfly as shown in Fig. 2.13 [38,

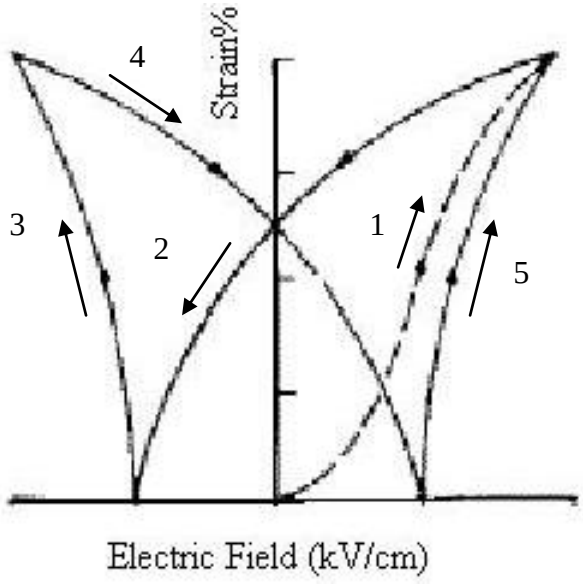

41]. This

Fig. 2.13 Strain versus electric field behavior of a general ferroelectric material

results because of the combined effect of electrostrictive and piezoelectric phenomenon and switching and movement of domain walls in the material. Also, ceramic samples usually contain a number of non-180^o domains. The movement and switching of non-180^o walls may involve a significant change in the dimensions. During the field cycling, a residual (or remnant) strain may be observed at zero field if domains in general do not switch to their original positions at zero field [40, 41]. As, the contribution to the strain from movement of domain walls is strongly nonlinear and hysteretic, and it is this part of the strain–electric field relationship that is most often observed. Hysteresis free strain-electric field behavior is desired for actuator applications [42].

References:

1. Himanshu Narayan *et al*, Nanotechnology, **20** (2009) 255601
2. M. N. Rahaman, Ceramic Processing and Sintering, 2nd Edition, Marcel Dekker Inc., (2003).
3. A.J. Moulson and J.M. Herbert, Electroceramics: Materials, properties and Applications, 2nd edition, Wiley, New York (2003).
4. G. C. C. da Costa, A. Z. Simões, A. Ries, C. R. Foschini, M. A. Zaghete, J. A. Varela, Mater. Letters, **58** (2004) 1709.
5. G.H. Haertling, J. Am. Ceram. Soc., **50** (1967) 329.
6. M. Veith, S. Mathur, N. Lecerf, V. Huch, T. Decker, H. Pech, W. Eiser, R. Haberkorn, J. Sol–Gel Sci. Tech., **15** (2000) 145.
7. M. H. Frey, D. A. Payne, Appl. Phys. Lett., **63**(1993) 2753.
8. H. K. Guo, X. G. Tang, J. X. Zhang, S. W. Shan, M. M. Wu, Y. J. Luo, Journal of Materials Science Letters, **17** [18] (1998) 1567.
9. X.G. Tang, Q.F. Zhou, J.X. Zhang, J. Appl. Phys., **86** (1999) 5194.
10. M. Veith, S. Mathur, N. Lecerf, V. Huch, T. Decker, H.P. Beck, W. Eiser, R. Haberkorn, J. Sol–Gel Sci. Technol., **17** (2000) 145.
11. X.G. Tang, J. Wang, X.X. Wang, H.L.W. Chan, Solid State Commun., **131** (2004) 163.
12. M. Oghbaei, O. Mirzaee, Journal of Alloys and Compounds, **494** (2010) 175.
13. P. Yadoji, R. Peelamedu, D. Agrawal, R. Roy, Materials Science and Engineering B **98** (2003) 269.
14. D.E. Clark, D.C. Folz, J.K. West, Materials Science and Engineering A **287** (2000) 153.
15. W.H. Sutton, American Ceramic Society Bulletin **68** (2) (1989) 376.

16 Y. Zhao, Y. Chen, Progress in Nuclear Energy, **50** (2008) 1.

17 C. Leonelli, P. Veronesi, L. Denti, A. Gatto, L. Iuliano, Journal of Materials Processing Technology, **205** (2008) 489.

18 R.J. Meredith, Engineers' Handbook of Industrial Microwave Heating. IEE Power The Institution of Electrical Engineers, London, UK (1998).

19 Yuhuan Xu, Ferroelectric Materials and Their Applications, Elsevier Science Pub. Co. New York, USA, 1991.

20 T. R. Shrout, S. L. Swartz, IEEE Ultrasonic Symposium (1997).

21 A. Goldstein, N. Travitzky, A. Singurindi, M. Kravchik, Journal of the European Ceramic Society **19** (12) (1999) 2067.

22 V. Tsakaloudi, E. Papazoglou, V.T. Zaspalis, Materials Science and Engineering, B **106** (2004) 289.

23. J.H. Yang, K.W. Song, Y.W. Lee, J.H. Kim, K.W. Kang, K.S. Kim, Y.H. Jung, Journal of Nuclear Materials, **325** (2004) 210.

24. D. Agrawal, Journal of Materials Education, **19** (1999) 49.

25 R.R. Menezes, P.M. Souto, R.H.G.A. Kiminami, Journal of Materials Processing Technology, **190** (2007) 223.

26. I. Bunget, M. Popescu, Physics of Solid Dielectrics, Elsevier, New York (1984).

27. L. L. Hench, J. K. West, Principles of Electronic Ceramics, John Wiley & Sons, New York (1989).

28. B. Jaffe, W. Cook and H. Jaffe, Piezoelectric Ceramics, Academic Press, London (1971).

29. L. E. Cross, Ferroelectrics, **76** (1987) 241.

30. M. E. Lines and A. M. Glass, Principles and Applications of Ferroelectrics and Related Materials, Oxford, Clarendon (1979).

31. J. C. Burfoot and G. W. Taylor, Polar Dielectrics and Their Applications, London: Macmillan (1979).

32. G. Arlt, J. Mater. Sci., **25** (1990) 2655.

33. S. Stemmer, S. K. Streiffer, F. Ernst, M. Ruhle, Phil. Mag. A, **71** (1995) 713.

34. R. E. Newnham, Structure–property relations, Berlin: Springer (1975).

35. S. E. Park, T.R. Shrout, J. Appl. Phys., **82** (1997) 1804.

36. C. B. Sawyer, C. H. Tower, Phys. Rev., **35** (1930) 269.

37. V. Shur, E. Rumyantsev, J. Korean Phys. Soc., **32** (1988) S727.

38. D. Damjanovic, Rep. Prog. Phys., **61** (1998) 1267.

39. R. Ramesh, S. Aggarwal, O. Auciello, Mater. Sci. Engg., **32** (2001) 191.

40. M. J. Zipparo, K. K. Shung, T. R. Shrout, IEEE Tranns. UFFC, **44** (1997) 1038.

41. K. Uchino, Am. Ceram. Soc. Bull., **65** (1986) 647.

42. K. Furuta, K. Uchino, Advanced Ceramic Materials, **1** (1986) 61.

CHAPTER III

EXPERIMENTAL DETAILS

3.1 Introduction

Methodology of the iso-valent and off-valent substituted BT systems synthesized by MSSR and microwave processing techniques and detailed description of various characterization techniques are given in this chapter. It includes the experimental methods and the details of instruments, used for the study of various properties.

3.2 Sample Preparation

This section comprises the details of the methods used for the preparation of iso-valent and off-valent substituted BT systems by MSSR and microwave processing techniques.

3.2.1 Modified BT Systems by Modified Solid State Reaction Route (MSSR)

The following polycrystalline iso-valent and off-valent substituted BT systems were prepared using MSSR route.

- $Ba_{1-x}Ca_xTiO_3$
- $Ba_{1-x}Mg_xTiO_3$
- $Ba_{1-x}Sr_xTiO_3$
- $Ba_{1-x}Sm_xTi_{(1-x/4)}O_3$/BSmT
- $Ba_{1-x}La_xTi_{(1-x/4)}O_3$/BLT samples, where x=0.02, 0.04. 0.06 & 0.08

In the modified solid state reaction route (MSSR) barium acetate trihydate, calcium acetate/magnesium acetate/lanthanum acetate/samarium acetate (all from Aldrich, USA with 99.8% purity) and fumed titanium oxide (Degussa) were used as starting precursors. Stoichiometric proportion of barium acetate and calcium acetate/magnesium acetate/strontium acetate/lanthanum acetate/samarium acetate were dissolved and transparent solution was prepared using 2-methoxy ethanol as the solvent and acetic acid as the catalyst using earlier reports and the flowchart as given in Fig. 3.1. Finally, the

stoichiometric proportion of titanium oxide was mixed in the transparent solutions and stirred for 4 h to make the solution homogeneous. After drying the slurry in the oven decomposition behavior of the dried modified BT powder was investigated using a NETZSCH thermal analyzer based on the principle of TGA/DTA where single heating chamber is used. Based on TGA study, isovalent and off valent substituted BT samples were calcined at 800 & 900^{o}C for 4h, respectively. Single perovskite phase formation was confirmed by X-ray diffraction (XRD) technique. at 900^{o}C calcination temperature. The powder calcined at 900^{o}C was mixed thoroughly with 2wt% polyvinyl alcohol (PVA) binder & pressed into disks of diameter ~10mm and a thickness of ~1.5mm under a pressure ~60MPa. Sintering was optimized at 1300^{o} for 4 h with a heating rate of 5^{o}C/minute. In order to examine the phases present in the system XRD analysis of the sintered modified BT systems was performed on a PW 3020 Philips diffractometer using Cu Kα (λ=0.15405 nm) radiation. The sintered microstructures were observed using a JEOL T-330 scanning electron microscope (SEM). The experimental densities (d_{ex}) of the samples were measured by the Archimedes method. Silver paste was applied on both sides of the samples for the electrical measurements. Dielectric constant (ε_r) and dielectric loss ($\tan\delta$) were measured as a function of temperature using a computer interfaced HIOKI 3532-50 LCR-HITESTER. A conventional Sawyer–Tower circuit was used to measure the electric field Vs polarization hysteresis (P–E) loop at 20 Hz frequency. The samples for the piezoelectric property measurements were poled by a corona poling unit at a temperature 25^{o}C below than transition temperature (Tc) by applying a dc electric field of 3 kV/mm for 30min.

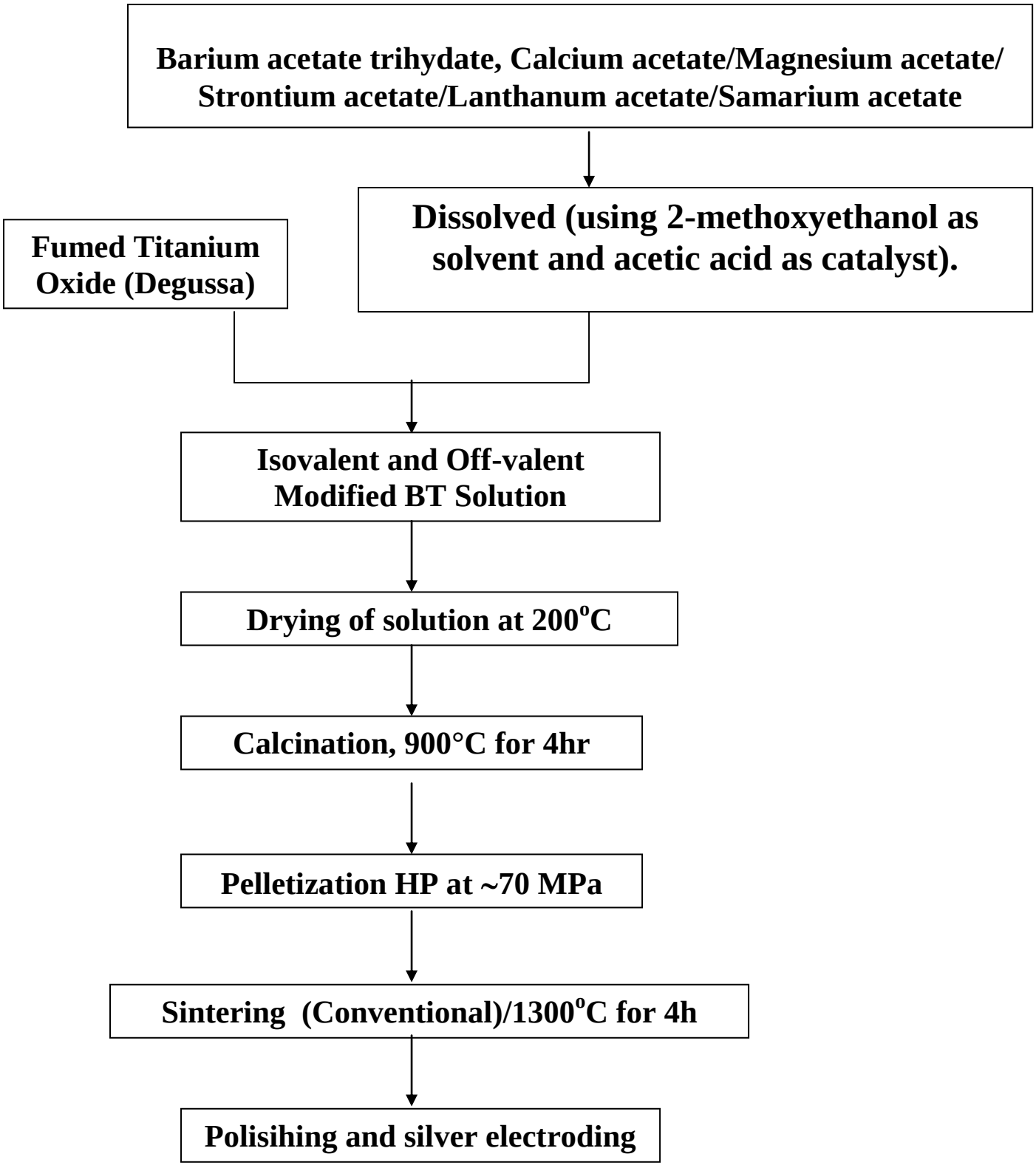

Fig. 3.1Flow chart of synthesis of iso-valent & off-valent modified BT ceramics by MSSR route

3.3 Structural Characterizations

This section describes the procedures used for the structural characterizations of iso-valent and off-valent substituted BT systems using different instruments.

3.3.1 TGA/DTA

Unlike structural or microscopic method of material characterizations, differential scanning calorimetry (DSC) is a thermo analytical technique in which the difference in the amount of heat required to increase the temperature of a sample and reference is measured as function of temperature. It can give information on how a substance "got from here to there" during thermal processing. Thermo gravimetric analysis (TGA) is the study of weight changes of a material with respect to temperature. The technique is useful strictly for transformations involving absorption or evolution of gases from a specimen consisting of condensed phase. Decomposition behavior of the selected raw material was investigated using a NETZSCH thermal analyzer based on the principle of DTA where single heating chamber is used. These devices have a disk (constantan alloy) on which the sample and reference pans rest symmetrically placed platform. Thermocouple (chromel alloy) is welded to the underside of each platform. The chromel constantan junctions make up the differential thermocouple junctions with the constantan disk acting as one leg of the thermocouple pair. A calibration constant within the computer software converts the amplified differential thermocouple voltage to energy per unit time which is plotted on y-axis of the DSC output.

In typical TGA experiment, specimen powder is placed on refractory pan (porcelain or platinum). The pan in the hot zone of the furnace is suspended from a high precision balance. A thermocouple is in the close proximity to the specimen but not in contact, so as not to interfere with the free float of the balance. The balances are

electronically compensated so that the specimen pan does not move when the specimen gains or loses weight. The effect of particle packing affects both DSC and TGA analysis therefore this is taken into account while doing the experiments.

3.3.2 X-ray Diffraction

The diffraction of X-ray by crystals was discovered by von Laue in 1912. Following the experimental observation of X-ray diffraction, von Laue showed that the phenomenon could be described in terms of diffraction from a three dimensional grating. In the same year, while engaged in experimental studies, W. L. Bragg noticed the similarity of diffraction to ordinary reflection and deduced a simpl equation treating diffraction as reflection from planes in the crystal lattice i. e the Bragg law:

$$2d\sin\Theta=n\lambda$$

Where d is the interplanar spacing between two parallel planes, Θ is the angle between incident rays and the parallel planes, n is an integer number and order of diffraction and λ is wavelength of X-rays.

The process of reflection is described in terms of incident and reflected rays each making an angle Θ with a fixed crystal plane. It can also be viewed as invoving a fixed incident beam, in which case reflection occurs from planes set at an angle Θ with respect to the beam and generates a reflected ray deviating through 2Θ as shown in Fig. 3.2. X-ray diffraction has been extensively used in this work for monitoring the purity of phases after chemical reactions and for determining the crystal symmetry of the phase. There are seven three- dimensional co-ordinate systems that describe all the crystal structures and form the basis for their classification. The observed X-ray diffraction is realted to the crystal symmetry. When a crystal structure undergoes a symmetry transition, the lattice parameters change and accordingly the X-ray diffraction pattern also change.

Powdered X-ray diffraction was done using Philips Analytical XRD machine. The X-ray radiation used was emitted by copper whose characteristic wavelength for the K_α radiation was 1.5418 Å.

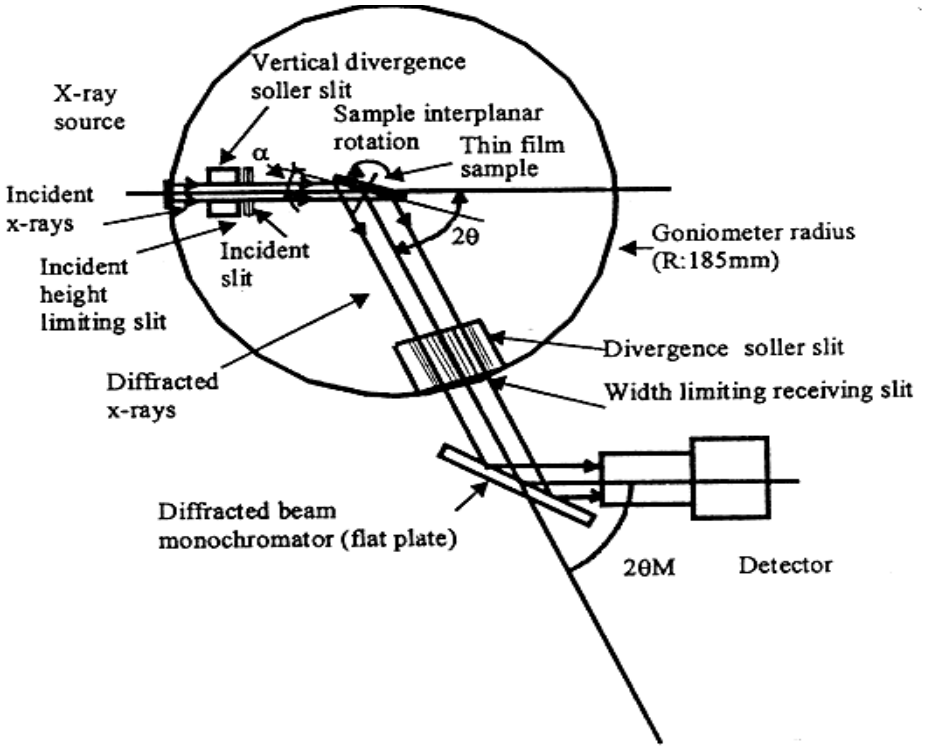

Fig. 3.2 The diffraction of X-rays by a family of crystal planes.

The counter was set to scan over a range of 2θ values at a constant angular velocity from 20^0 to 70^0 at a scanning rate of 2^0 per minute. The 2θ values, corresponding to the peaks were noted from the diffraction patterns. Taking the intensity of the highest peak to be 100%, the relative intensity of other peaks was measured. These diffraction lines were indexed in different crystal systems and unit cell configurations, using a computer program package 'Powdmult'.The voltage and current were set at a value of 40KV and 30mA, respectively.

3.4 Density

As per Archimedes principle of buoyancy when a object is immersed in a fluid we have the relation

$$\frac{\text{density}}{\text{density of fluid}} = \frac{\text{weight}}{\text{weight of displaced fluid}},$$

Where, density and weight are of the object, which is immersed in the fluid.

Therefore, the experimental or observed density, d_o, was determined using Archimedes method:

$$d_o = (W_a / W_a\text{-}W_w) \times (\text{density of the fluid})\text{g/cc.} \qquad \ldots 3.1$$

Here d_o is the density of the sample and W_a and W_w are the weights of the material in air and in water, respectively. Since, the fluid taken in this work is water, which is having a density of 1g/cc, therefore we can write eq. 3.1

$$d_o = (W_a / W_a\text{-}W_w)\ \text{g/cc.}$$

The accuracy of the balance is ± 0.1 mg = 0.0001 g. And the accuracy of the fluid density is 1.00; therefore in the density calculation three significant figures are used. The error bar is ±0.01.

3.5 Scanning Electron Microscope (SEM)

The scanning electron microscopy was used to determine the surface morphology and average crystallite size of the modified BT samples. SEM gives information about the grain size and grain evolution in the modified BT samples. It also gives the information about the inter-granular and the intra-granular pores and the distribution of grains in the samples. SEM photographs of the modified BT samples were obtained using the JEOL T-330 scanning electron microscope. SEM measurements are based on the principle of irradiating the specimen with a finely focused electron beam. The secondary electrons, backscattered electrons, auger electrons, characteristic x-rays and several other radiations are released from the specimen. Generally, the secondary electrons are collected to form the image in the SEM mode. A thin layer of gold ~100nm was deposited on the fractured surfaces of the modified BT samples to avoid electric charging problems.

3.6 Energy-dispersive X-ray (EDX/EDS) spectroscopy

EDX systems are most commonly found with SEM units. Since, SEM are equipped with a cathode and magnetic lenses to create and focus a beam of electrons, and since the 1960s they have been equipped with elemental analysis capabilities. A detector is used to convert X-ray energy into voltage signals; this information is sent to a pulse processor, which measures the signals and passes them onto an analyzer for data display and analysis. EDX/EDS is an analytical technique used for the elemental analysis or chemical characterization of a sample. It is based on the principle of analyzing X-rays emitted by the matter in response to being hit with charged particles. Its characterization capabilities are due in large part to the fundamental principle that each element has a unique atomic structure allowing X-rays that are characteristic of an element's atomic structure to be identified uniquely from one another. To stimulate the emission of characteristic X-rays from a specimen, a high-energy beam of charged particles such as electrons or protons (see PIXE), or a beam of X-rays, is focused into the sample being studied. At rest, an atom within the sample contains ground state (or unexcited) electrons in discrete energy levels or electron shells bound to the nucleus. The incident beam may excite an electron in an inner shell, ejecting it from the shell while creating an electron hole where the electron was. An electron from an outer, higher-energy shell then fills the hole, and the difference in energy between the higher-energy shell and the lower energy shell may be released in the form of an X-ray. The number and energy of the X-rays emitted from a specimen can be measured by an energy-dispersive spectrometer. As the energy of the X-rays are characteristic of the difference in energy between the two shells, and of the atomic structure of the element from which they were emitted, this allows the elemental composition of the specimen to be measured.

3.7 Electrode Deposition

The silver electrical contacts were made on both sides of the modified BT samples for carrying out the electrical properties study. The sintered pellets were polished to a smooth finish and cleaned with alcohol. Care was taken to ensure that the pellets faces were parallel. Silver paste was then applied on both sides of the modified BT samples and heated up 350^{o}C for 1 hr. Silver electroding on the the modified BT samples gives the metal-insulator-metal structure to the pellets. The pellets act as dielectric medium between the two parallel metallic plates. Now, the samples are ready for electrical measurements. For piezoelectric measurements, the pellets were properly poled.

3.8 Dielectric Measurements

Dielectric measurements of the modified BT samples were carried out by using computer interfaced HIOKI 3532-50 LCR-HITESTER. This instruments can measure a capacitance from 1pF to 100mF, with a maximum resolution of 0.1pF and tanδ with a resolution of 0.0001. This system includes a LCR meter model HIOKI 3532-50 LCR-HITESTER interfaced to a PC via IEEE 488, programmable temperature chamber connected to PC via RS 485, measurement jig and software,

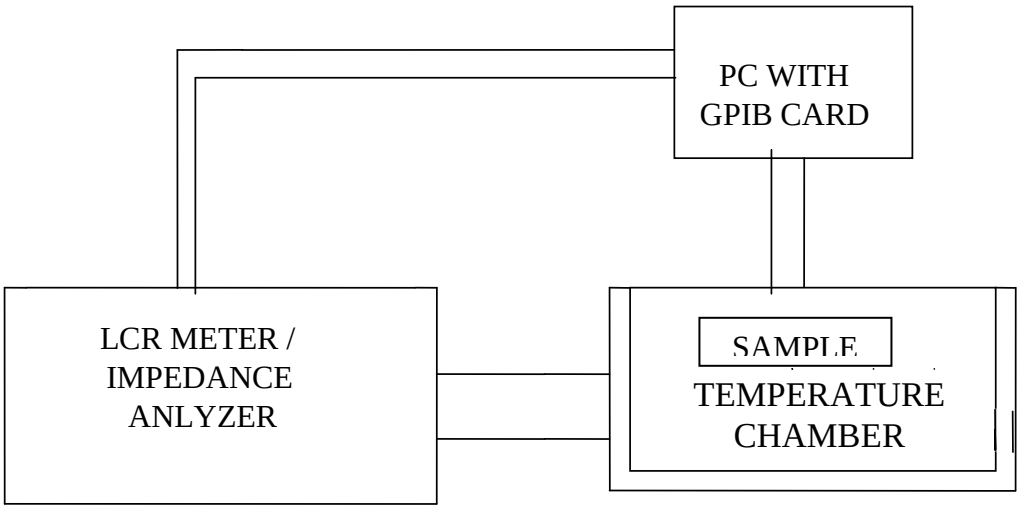

Fig 3.3 Dielectric measurement setup for bulk samples

shown in Fig. 3.4. A signal of 1V was applied to the sample. Measurements of the samples were done as a function of frequency and temperature. Data were recorded at the interval of 5 degrees. Software calculates dielectric constant, ε_r, using the relation

$$\varepsilon_r = C \times t / (\varepsilon_0 \times A) \qquad \text{----------3.2}$$

where C is the measured capacitance, t is thickness, A is the area and ε_o is the permittivity of the free space, ($\approx 8.854 \times 10^{-12}$ F/m). The frequencies were varied from 100Hz to 1MHz and temperature was varied from 35^{o}C to 135^{o}C. Peak in the dielectric constant versus temperature behavior gives the Curie temperature, T_c.

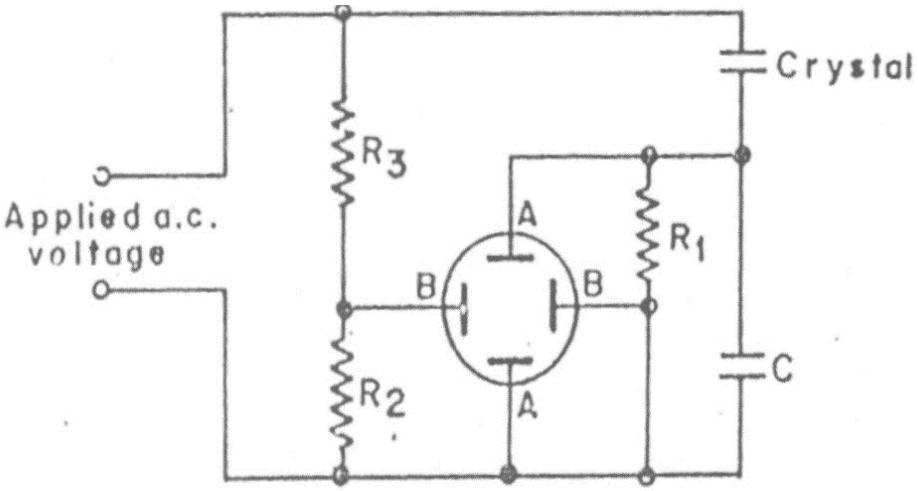

Fig. 3.4 Sawyer-Tower circuit for P-E loop measurements of bulk samples

3.9 Hysteresis Measurements

Ferroelectric hysteresis (P-E) loops at room temperature for all the modified BT samples were recorded using an Automatic PE Loop Tracer of M/S AR Imagetronics. The system consists of a PC, Software, programmable voltage source (up to 5kV) and Silicon oil bath. The measurement is based on modified Sawyer Tower circuit, shown in Fig. 3.5, operating at 50 Hz. For measurement, specimen is kept in a spring loaded jig and immersed in silicon oil. The loop is recorded by the system and the software computes all the parameters e.g. P_s, P_r and E_c. Software has the facility of cycling and averaging of the data points.

3.10 Strain vs. Electric Field Measurements

The strain vs. electric field is measured by an MTI-2000fotonic sensor (Mech. Tech. Inc), shown in Fig. 3.6. The MTI-2000 photonic probe modules contain two sets of optical fibers. Light-transmitting fibers and light receiving fibers are bundeled together. The displacement is based on the interaction between the field of illumination of the transmitting fibers and the field of view of the receiving fibers. The platelet sample with electrode on both sides is connected into an external voltage source. The distance between the sample and the photonic probe is contralooed by a screw device.

At contact, or zero gap, most of the light existing the transmitting fibers is reflected directly back into those fibers. No light is provided to the receiving fibers and the output electrical signal (in the voltage scale) is "zero". As the probe to the target distance increases by tuning the screw in one direction [Figure 2.8(b)], increasing amounts of the light are captured by the receiving fibers. This relationship will continue until the entire face of the receiving fibers is illuminated with reflected light. This point is called the "optical peak " and corresponds to maximum voltage output of the electrical signal. Any further tuning of the screw in the same direction will cause the diverging field of the reflected light to exceed the field of view of the receiving fibers, thus causing a reversal in the output-versus-distance signal relationship. Therefore the point at "optical peak" is set as a maximum point. Before the measurement starts, the distance between the sample and the Fotonic probe is first reduced by screwing backwards to get away from the optical peak to the point that gives rise to minimum intensity of received light, then the electrical signal is applied. Any displacement of the sample in response to the electric field will then be compared with the optical peak and gives the relationship of displacement versus electric field.

The d_{33} piezoelctric coefficient is calculated from the slope of strain vs. electric field plots.

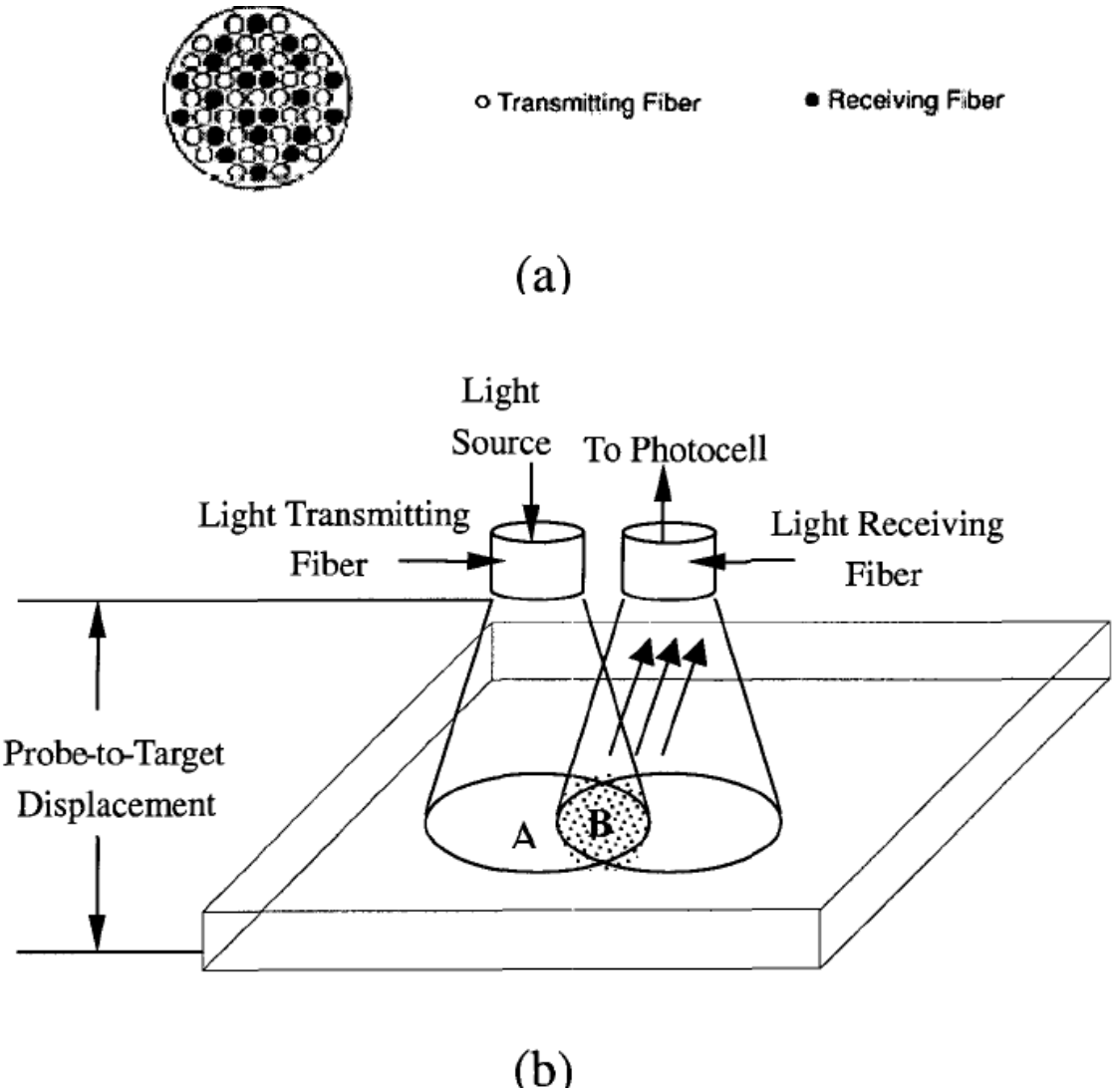

Fig. 3.5 A setup for measurements of the strain vs. electric filed loop. (a) Fiber – optical probe tip configurations; (b) Displacement sensing mechanism of adjacanet fiber-optical elements.

CHAPTER IV

THE PEROVSKITE PHASE EVOLUTION, STRUCTURAL AND MICROSTRUCTURAL PROPERTIES

4.1 Introduction

With the modification of solid state reaction route, perovskite phase evolution study in iso-valent and off-valent substituted BT systems is essential as in these materials the perovskite phase can be accompanied by unwanted phases [1-6] which significantly affects the material properties [7]. Therefore, optimization of processing conditions for the single perovskite phase evolution in iso-valent and an off-valent substituted BT system is essential. Modifications in a ferroelectric material affects its properties; most likey the perovskite phase evolution, microstructure and density [7, 9-10]. Therefore, in this chapter, the effect of modifications on perovskite phase evolution, structural and microstructural properties of iso-valent and off-valent substituted BT systems are discussed using TGA/DTA, X-ray diffraction (XRD) and scanning electron microscopy (SEM) techniques. Density measurements have also been discussed.

4.2 Thermo Gravimetric Analysis (TGA) Study

4.2.1 TGA of BT Powder Synthesized by SSR Route

Fig. 4.1 shows the TGA/DTA curves of dried $BaTiO_3$ powder synthesized by SSR. Two processes of weight loss in the temperature ranges of RT-700^oC and 700-1000^oC are observed. The first weight loss ~2% in the temp. range of RT-700^oC is due to loss of water. The second weight loss ~14% in the temperature range of ~700°C to 1000°C is due to loss of carbon dioxide:

$$BaCO_3+TiO_2=BaTiO_3+CO_2 \qquad \text{……..4.1}$$

molecule according to the reaction . Above 1000°C, no substantial weight loss is observed. The first endothermic peak ~680^{o} corresponds to physical transformation of precursors. Second endothermic peak at ~790^{o}C corresponds to the polymorphic transformation of witherite to α-$BaCO_3$ [11]. The third endothermic peak ~990^{O}C huge endothermic peak corresponds to the major decomposition of $BaCO_3$ in the precursor. Therefore, TGA/DTA study of BT powder synthesized by SSR route is hinting that the calcination temperature should be above 1000°C.

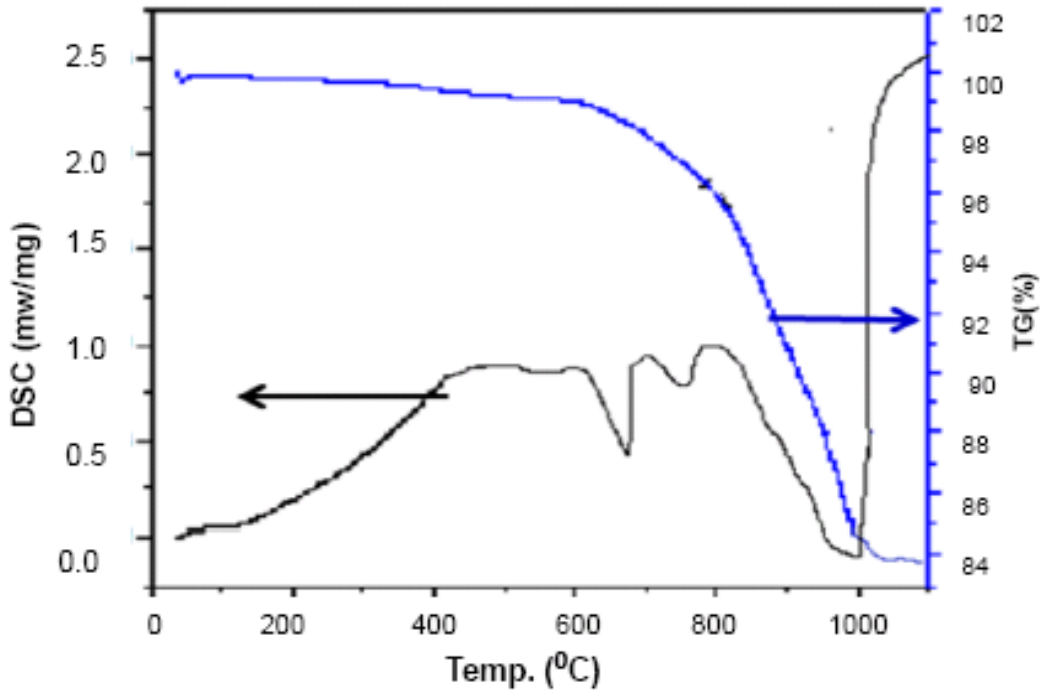

Fig.4.1 TGA/DSC graph of dried BT powder synthesized by SSR route

4.2.2 TGA of BT Powder Synthesized by MSSR Route

Fig. 4.2 shows the TGA/DTA graph of $BaTiO_3$ powder synthesized by modified solid state reaction (MSSR) route. A weight loss of ~10.23% was observed up to 200^{o}C, which is attributed to the evaporation of absorbed water and solvent. Further a large wt. loss of ~16% around 300^{o}C is due to the decomposition of acetyl and bonded alkyl groups and their combustion [12]. The weight loss at around 800 °C (5.65%) is

due to the decomposition of residual $BaCO_3$. From DSC curve, the first endothermic peak near 100^{o}C is attributed to the loss of water molecules and the exothermic peak

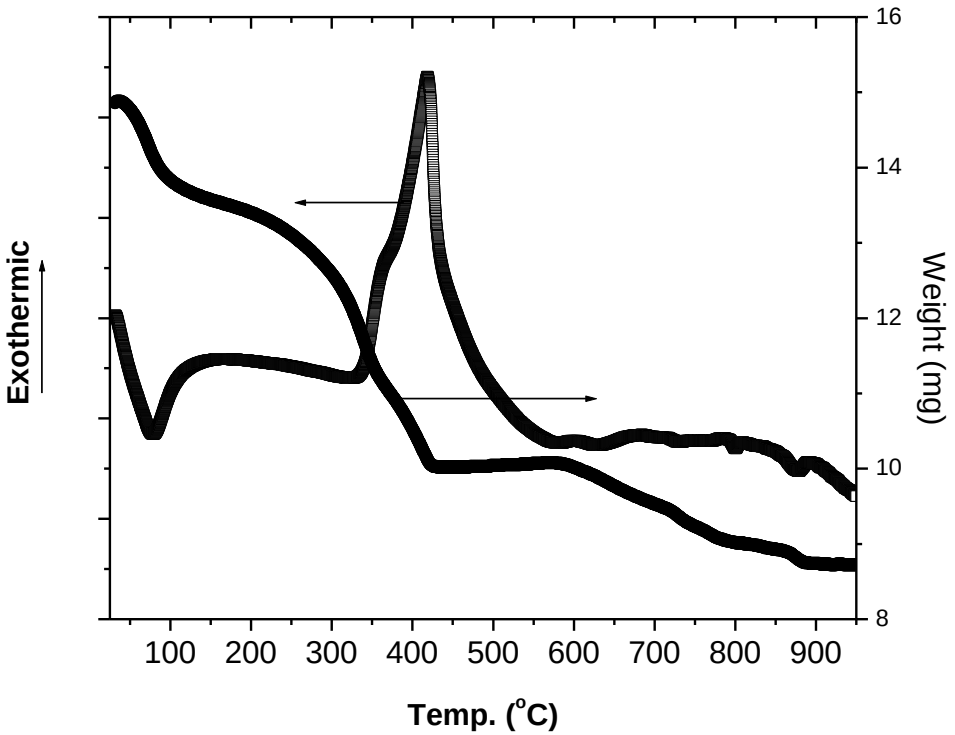

Fig.4.2 TGA/DSC graph of dried BT powder synthesized by MSSR route

near 400^{o}C is due to the formation of CO_2 molecules [13]. When the temperature is higher than 900^{o}C, the weight of the $BaTiO_3$ dry gels no longer decreased, which hints about the calcination temperature to be ~900^{o}C.

4.3 X-ray Diffractions (XRD)

4.3.1 BT Samples Synthesized by SSR & MSSR Route

The starting calcination temperatures for single perovskite phase formation are decided based on TGA/DSC studies (section 4.2.1 & 4.2.2) of BT systems synthesized using SSR and MSSR routes. TGA/DSC studies hints that the calcinations temperature for single perovskite phase formation of BT powder synthesized using SSR and MSSR route are ~ 1000 & 800^{o}C, respectively. Therefore, we have chosen 1000 & 800^{o}C as the starting calcinations temperatures for SSR and MSSR route, respectively. Figs. 4.3 and 4.4 show XRD pattern at RT of BT samples

calcined at different temperatures by using SSR and MSSR routes. The diffraction pattern shows the development of intense lines of single perovskite phase of BT system calcined at 1100 and 900^{o}C by SSR and MSSR routes, respectively. In SSR route at 1000^{o}C calcinations temperature, we are getting secondary phase peaks of $BaCO_3$ and intermediate phase along with small intense peaks of pervoskite phase. As, the calcinations temperature is raised to 1100^{o}C single perovskite phase peaks are observed with no trace of secondary phase peaks, which is also confirmed by TGA/DTA study. But, in MSSR route single perovskite phase peaks with no trace of any secondary phase is observed at 900^{o}C, which is also confirmed by TGA/DTA study. From the above study, we are seeing the significant reduction of calcinations temperature in MSSR route than SSR route. Low calcinations temperature in BT samples synthesized by MSSR route can be attributed to the fine particle size of the precursors [14]. In MSSR route the particle size of the precursors used is lower than the size of the precursors used in SSR route. Lower the particle size, higher is the ratio of surface area to volume ratio. Since surfaces are higher energy regions, they will always act to minimize their area, and thus lower their energy whenever possible [15], which lead to lower calcinations temperature. It is well known that larger the surface area to volume ration of the solid, the faster the reaction will be. Smaller particles have a bigger surface area to volume ratio than larger particle for the same mass of solid. Therefore, we can summarize following reasons for the increase in rate of reaction with the decrease in particle size:

- Increasing the surface area to volume ratio of the reactants results in a higher number of reaction sites.
- Increasing the number of reaction sites increases the number of total collisions.

- The greater the frequency of total collisions, the greater the frequency of effective collisions.
- If the frequency of effective collisions increases, so does the reaction rate.

In addition, the difference in particle size between the precursors used may also accelerate the calcination reaction and lower the processing temperature. Since in MSSR route, the particle size for barium acetate trihydrate is of nano meter size order and fumed titanium oxide is of sub-micro meter size order [16]. Diffraction peaks are found to be sharp, distinct indicating good homogeneity and crystallization of the BT system [17]. The XRD lines of BT samples synthesized by SSR and MSSR routes are indexed in different crystal structures using a computer program package 'Powdmult'[18]. Standard deviation (SD), $\Sigma\Delta d(=d_{obs}-d_{cal})$, where 'd' is inter-plane spacing, was found to be minimum for tetragonal structure of BT samples synthesized by SSR and MSSR routes, respectively.

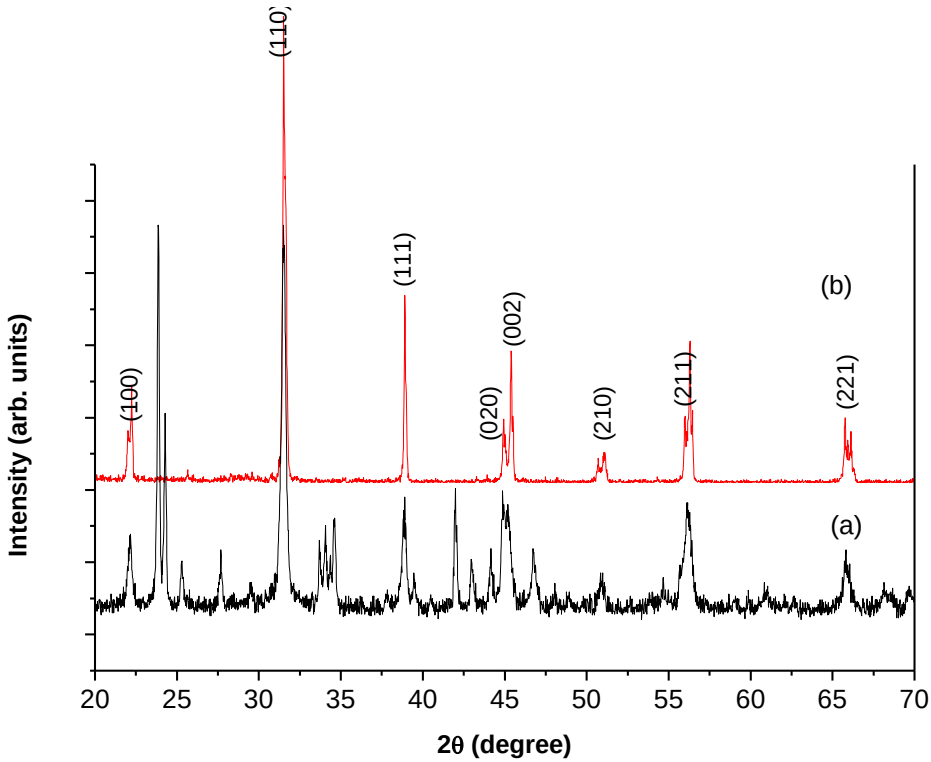

Fig. 4.3 XRD patterns of BT samples synthesized by SSR route and calcined at (a) 1000 and (b) 1100^{o}C.

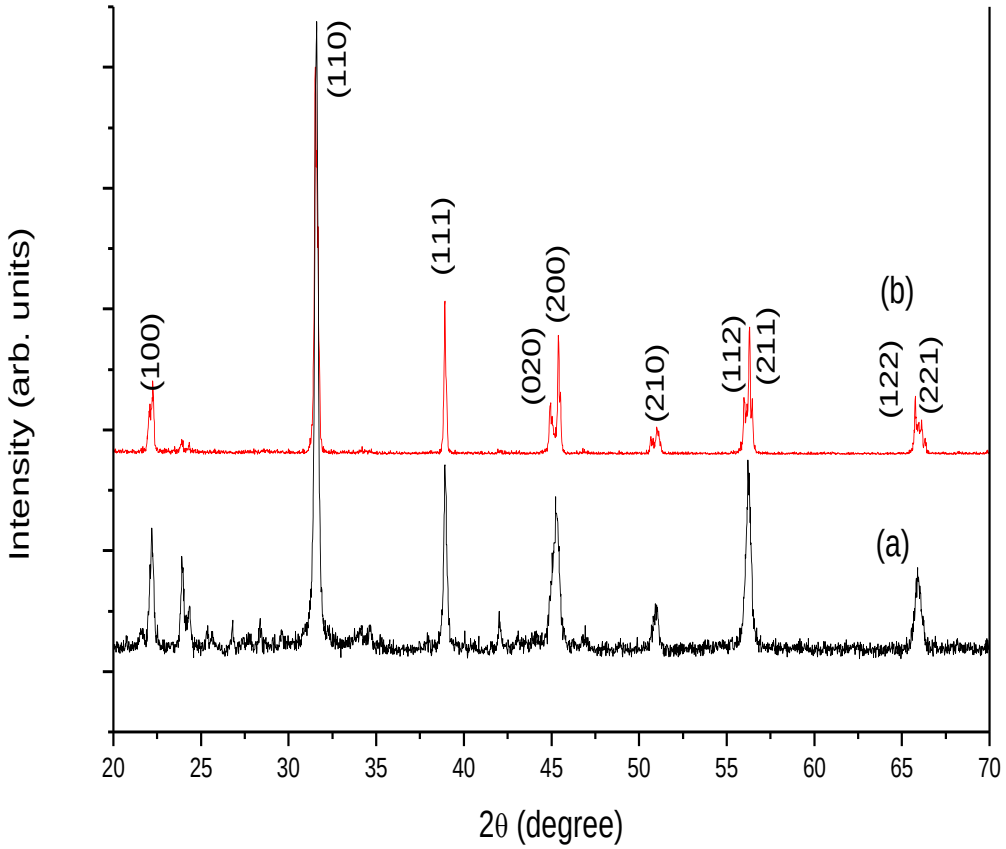

Fig. 4.4 XRD patterns of BT samples synthesized by MSSR route and calcined at (a) 800 and (b) 900°C.

Therefore, from above study, in our present work, off-valent and iso-valent modified BT systems are synthesized by MSSR route and calcination temperature was optimized at ~900°C.

4.3.2 Sintering of BT system by SSR & MSSR routes

Sintering temperature of the BT samples synthesized by SSR route is well established in literature and it is 1450°C for 4h when the heating rate is 5°C/minute while raising the temperature from RT to 1450°C. Therefore, we have sintered BT samples synthesized by SSR route at 1450°C for 4h and from RT to 1450°C the heating rate was 5°C/minute. Since the calcination temperature for single perovskite phase formation has been lowered using MSSR route than the SSR route, which gives hint of lowering of sintering temperature also. Sintering of BT samples synthesized by

MSSR routes was carried out at 1100, 1200 and 1300^{o}C for 4h, respectively. Densities of BT samples synthesized by MSSR route and sintered at 1100, 1200 and 1300^{o}C for 4h are 5.51, 5.62 & 5.72(g/cc), respectively. Here, density of the BT samples synthesized by MSSR routes and sintered at 1300^{o}C for 4h is better than the density of the BT samples synthesized by SSR route and sintered at 1450^{o}C for 4h (5.64g/cc). Therefore, **s**intering temperatures of the BT systems synthesized by SSR and MSSR routes were 1450 and 1300^{o}C for 4h, respectively. At 1300^{0}C sintering temperature BT ceramic samples synthesized by MSSR route are showing better density (Given in Table 1) than the BT samples sintered at 1450^{o}C by SSR route. Sintering temperature of BT systems synthesized by MSSR route is significantly lower than the same systems processed through SSR route in the present study and earlier study [19-22]. Lowering of sintering temperature can be attributed to the fine particle size of the precursors. This fine particle size gives higher surface area to volume ratio of the modified BT particle and hence increase in diffusion process and lowering of sintering temperature [14, 23].

Table.4.1 Structures BT systems synthesized by SSR & MSSR routes:

Systems	**Structure**	**Density (g/cc)**
$BaTiO_3$ (SSR route) (Sintered at 1450^{o}C)	Tetragonal, c/a=1.0147	5.64
$BaTiO_3$ (MSSR route) (Sintered at 1300^{o}C)	Tetragonal, c/a=1.0149	5.72

4.3.3 Phase Evolution study of Iso-valent and off-valent Modified BT Samples Synthesized by MSSR Route

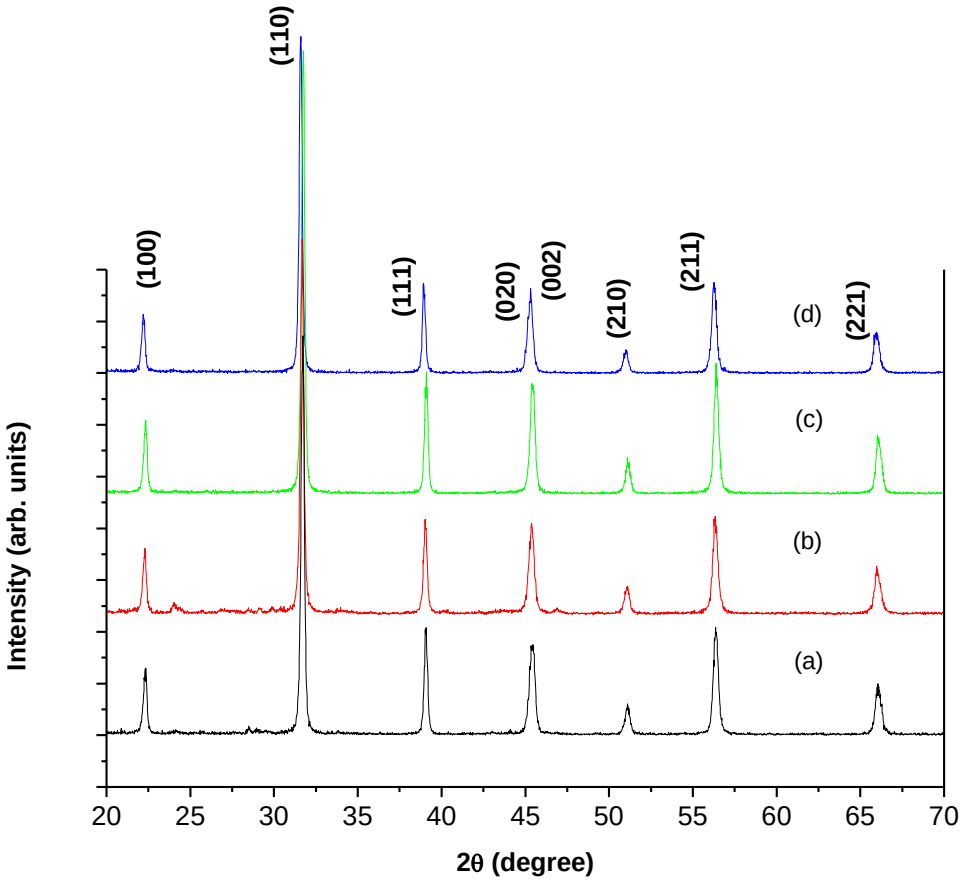

Fig. 4.5 XRD patterns of (a) BMT1 (b) BMT2 (c) BMT3 & (d) BMT4 samples.

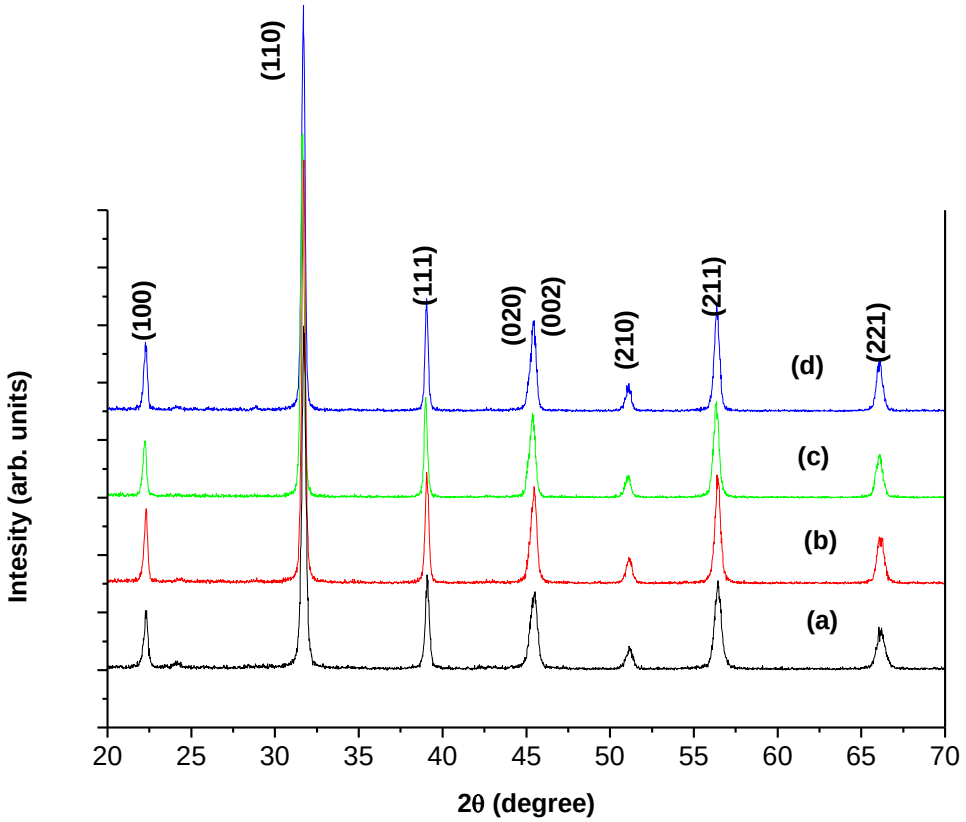

Fig. 4.6 XRD patterns of (a) BCT1 (b) BCT2 (c) BCT3 & (d) BCT4 samples

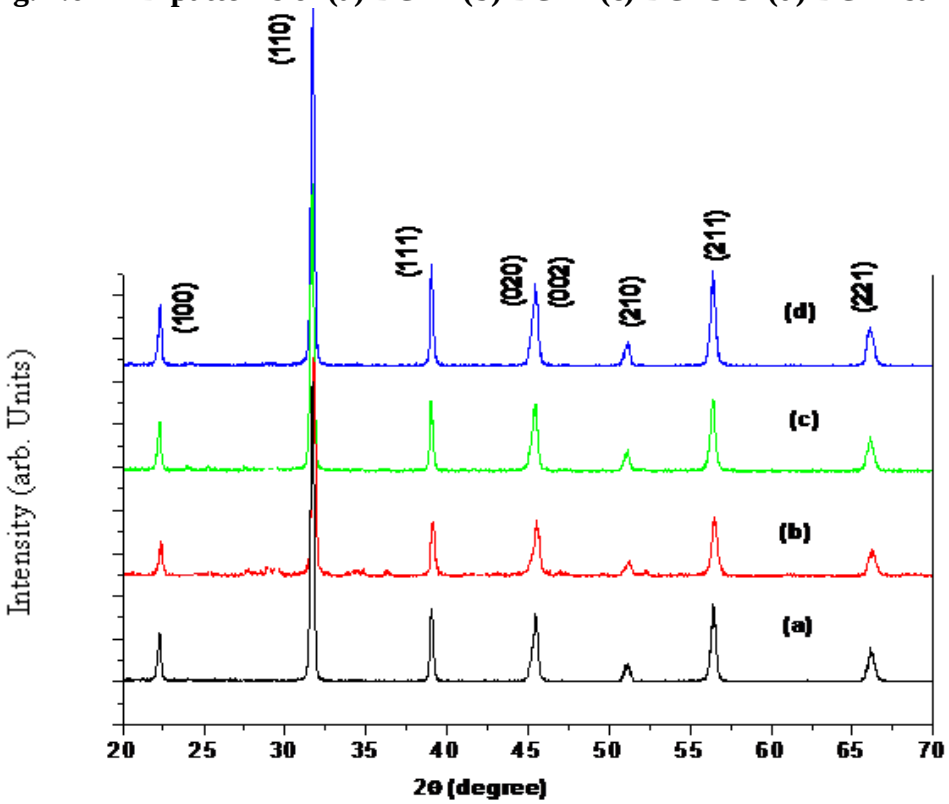

Fig. 4.7 XRD patterns of (a) BST1 (b) BST2 (c) BST3 & (d) BST4 samples.

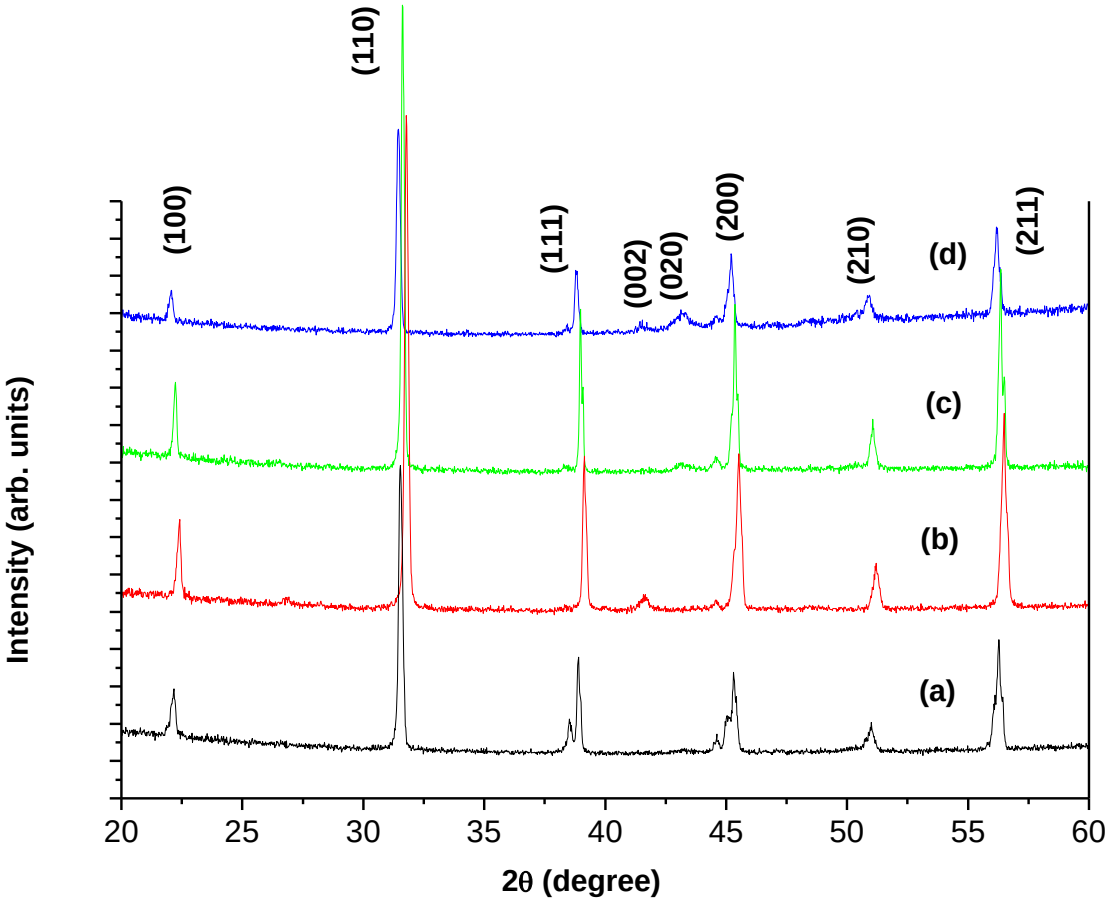

Fig. 4.8 XRD patterns of (a) BSmT1 (b) BSmT2 (c) BSmT3 & (d) BSmT4 samples.

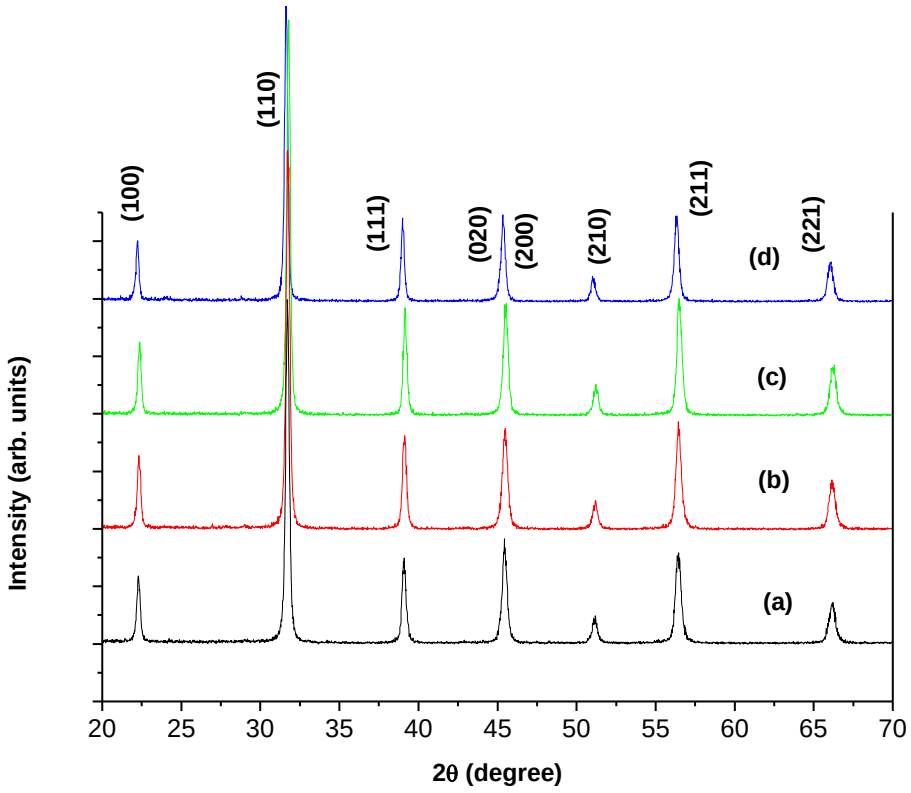

Fig. 4.9 XRD patterns of (a) BLT1 (b) BLT2 (c) BLT3 & (d) BLT4 samples.

Figs. 4.5-4.9 shows the XRD patterns of calcined iso-valent and off-valent substituted BT systems. Single perovskite phase without any trace of secondary phase developed in Ca^{2+}, Sr^{2+} and Mg^{2+} modified BT systems at 900^{o}C calcinations temperature. Whereas with the increase of La^{3+} and Sm^{3+} ions substitution% in modified BT samples, calcination temperature for single perovskite phase without any trace of secondary phase is increasing from 900^{o}C to 950^{o}C respectively. This can be explained on the basis of effect of melting temperatures of substituent elements on reaction kinetics in modified BT systems. Since, modifiers in a system can also decrease the process reaction temperature during calcination. Generally, modifiers with low melting temperature improve the contact between reacting components during the calcination process. Modifiers with a lower melting point than the host components temperature should enable the formation of a liquid phase in the system, and improve contacts between mixture components [14, 23] and hence lower the calcination temperature. As, melting temperature of La (1193^{o}K) and Sm(1345^{o}K) is higher than Ba (1002^{o}K), therefore the calcination temp. of La and Sm modifid BT systems is higher than iso valent modified BT systems.

In Figs. 4.5-4.7 intensities of XRD peaks is increasing with the increase in Ca^{2+}, Mg^{2+} and Sr^{2+} ions substitution% in BT system. This suggests Ca^{2+}, Mg^{2+} and Sr^{2+} ions in BT system are mixing well. Since the ionic size of Ca^{2+} (0.99Å), Mg^{2+} (0.66Å) and Sr^{2+} (1.12Å) ions is smaller than the replacing Ba^{2+} (1.34Å) ions in modified BT system and we know reactivity of a particle increases with the decrease of particle size [14, 15]. Therefore, with the increase of incorporation of smaller ionic size Ca^{2+}, Mg^{2+} and Sr^{2+} ions in place of larger size Ba^{2+} ions in modified BT systems, the reactivity between the modified BT precursors increases giving rise the increase in crystallinity. In Fig. 4.8, single perovskite phase peak appear for all the modifications

of Sm% in BT system but the calcination temperature increases with the increase of Sm substitution% in modified BT system. Single perovskite phase without any trace of secondary phase is formed at 900 and 950^{o}C in XRD patterns of BSmT1, BSmT2 & BSmT3, BSmT4 samples, respectively. Similarly, single perovskite phase without any trace of secondary phase is formed at 900 and 950^{o}C in XRD patterns of BLT1, BLT2 & BLT3, and BLT4 samples, respectively. This has already been explained on the basis of higher melting temperature of Sm and La atoms than the Ba atoms. As, can be seen from Fig. 4.8, with the increase in Sm substitution% the XRD peak intensity decreases, suggesting the decrease in homogeneity and crystallization with the increase in Sm fraction in BT system [17]. In Fig. 4.9, all peaks are sharp and distinct in La modified BT system suggesting the better solubility of La in BT system. In all the iso valent and off-valent modified BT systems there is a peak shift towards higher 2θ side (as can be seen from the XRD plots In Figs. 4.5-4.9). This is because of the smaller size of substituted ions than the Ba^{2+} ions in modified BT system, which is well established in earlier study of modified ferroelectric systems [14, 15, 23].

Sintering temperature of the iso-valent and off-valent substituted BT systems synthesized by MSSR route was optimized at 1300^{o}C. Sintering temperature of the iso-valent and off-valent substituted BT systems synthesized by MSSR route with better density (given in Table 4.3) than the same systems synthesized by SSR (sintering temperature at 1450^{o}C) route is optimized at 1300^{o}C, which is again significantly lower than the same systems processed through SSR route [19-22, 24]. Lowering of sintering temperature can be attributed to the fine particle size of the precursors. This fine particle size gives higher surface area to volume ratio of the modified BT particle and hence increase in diffusion process and lowering of sintering temperature [15].

4.3.4 Structures

The XRD lines of calcined iso-valent and off-valent substituted BT systems synthesized by MSSR route were indexed in different crystal systems and unit cell configurations using a computer program package 'Powdmult'[18]. Standard deviations, S.D, $\Sigma \Delta d$ (= d_{obs} - d_{cal}), where 'd' is inter-plane spacing, were found to be minimum for different structures for iso-valent and off-valent substituted BT systems. Structures of iso-valent and off-valent substituted BT ceramics synthesized by MSSR route are given in Table 4.2. In $Ba_{1-x}Y_xTiO_3$ (Y=Ca, Mg and Sr) ceramics, where x = 0.02, 0.04, 0.06 and 0.08, respectively a tetragonal structure is found. The tetragonality (c/a ratio) decreases with the increase in Mg & Sr substitution % in BT systems, which is as per earlier reports on Mg and Sr substitution effects in BT ceramics [25-28], however the tetragonality (c/a ratio) increases, with the increase of Ca substitution% in BT system, which is again as per earlier reports on the Ca substitution effects in BT ceramics [29]. In $Ba_{1-x}La_xTi_{(1-x/4)}O_3$ ceramics, the tetragonality (c/a ratio) decreases with the increase of x fraction and the structure transforms from tetragonal to cubic above x>0.02. Whereas, again in $Ba_{1-x}Sm_xTiO_3$ ceramics the tetragonality (c/a ratio) decreases with the increase of x fraction and the structure transforms from tetragonal to cubic for x=0.08. The similar structural effect in off-valent modified ferroelectrics is well reported and supports our findings [30-34]. The change of crystal structure with iso-valent and off-valent substitution in BT system can be explained as follows. Crystal structures obtained from unit cell refinement showed that the tetragonality of BT system is changing by introducing the iso-valent and off-valent dopants. It can be attributed to the creation of defects and oxygen vacancies by the iso valent and off-valent ions substitution in BT system [19, 35]. As, established earlier, Ca beyond a limit can go to Ti site and create charge

imbalance [29]. Similarly, the ionic size of Sr and Mg is smaller than Ba ions therefore the unit cell volume is decreasing and tetragonality is decreasing [35]. Whereas, the more pronounced effect of off valent substitution in BT system can be explained by the creation of a higher concentration of various defects in the crystal structure of barium titanate influencing the change of crystal lattice parameters [31, 35].

Table.4.2 Structures of Iso-valent and off-valent modified BT systems synthesized by MSSR:

System	$Ba_{0.98}Ca_{0.02}TiO_3$	$Ba_{0.96}Ca_{0.04}TiO_3$	$Ba_{0.94}Ca_{0.06}TiO_3$	$Ba_{0.92}Ca_{0.08}TiO_3$
Structure	Tetragonal, c/a=1.0150	Tetragonal c/a=1.0158	Tetragonal c/a=1.0162	Tetragonal c/a=1.0167
System	$Ba_{0.98}Mg_{0.02}TiO_3$	$Ba_{0.96}Mg_{0.04}TiO_3$	$Ba_{0.94}Mg_{0.06}TiO_3$	$Ba_{0.92}Mg_{0.08}TiO_3$
Structure	Tetragonal, c/a=1.0134	Tetragonal c/a=1.0131	Tetragonal c/a=1.0128	Tetragonal c/a=1.0126
System	$Ba_{0.98}Sr_{0.02}TiO_3$	$Ba_{0.96}Sr_{0.04}TiO_3$	$Ba_{0.94}Sr_{0.06}TiO_3$	$Ba_{0.92}Sr_{0.08}TiO_3$
Structure	Tetragonal, c/a=1.0142	Tetragonal c/a=1.0138	Tetragonal c/a=1.0131	Tetragonal c/a=1.0120
System	BSmT1	BSmT2	BSmT3	BSmT4
Structure	Tetragonal, c/a=1.0136	Tetragonal c/a=1.01250	Tetragonal c/a=1.0115	Cubic c/a=1
System	BLT1	BLT2	BLT3	BLT4
Structure	Tetragonal c/a=1.01129	Cubic c/a=1.00	Cubic c/a=1	Cubic c/a=1

4.4 Density Measurements:

Densities of the MSSR route processed iso-valent and off-valent modified BT samples were measured using Archimedes' principle. The values are given Table 4.3.

Densities of iso-valent and off-valent modified samples synthesized by MSSR route is better than the same samples synthesized by SSR route [19-22] at significantly lower sintering temperature. This shows the advantage of MSSR route over SSR route. These advantages are:

I) Lowering of calcination and sintering temperature

II) Better density.

Table 4.3 Densities of modified BT systems synthesized by MSSR route

System	$Ba_{0.98}Ca_{0.02}TiO_3$	$Ba_{0.96}Ca_{0.04}TiO_3$	$Ba_{0.94}Ca_{0.06}TiO_3$	$Ba_{0.92}Ca_{0.08}TiO_3$
Density (g/cc)	5.79	5.69	5.61	5.58
System	$Ba_{0.98}Mg_{0.02}TiO_3$	$Ba_{0.96}Mg_{0.04}TiO_3$	$Ba_{0.94}Mg_{0.06}TiO_3$	$Ba_{0.92}Mg_{0.08}TiO_3$
Density (g/cc)	5.70	5.69	5.65	5.59
System	$Ba_{0.98}Sr_{0.02}TiO_3$	$Ba_{0.96}Sr_{0.04}TiO_3$	$Ba_{0.94}Sr_{0.06}TiO_3$	$Ba_{0.92}Sr_{0.08}TiO_3$
Density (g/cc)	5.77	5.76	5.63	5.59
System	BSmT1	BSmT2	BSmT3	BSmT4
Density (g/cc)	5.85	5.80	5.61	5.71
System	BLT1	BLT2	BLT3	BLT4
Density (g/cc)	5.75	5.86	5.79	5.81

4.5 Scanning Electron Micrographs

Fig. 4.10 depicts the surface micrographs of sintered BT samples synthesized by SSR and MSSR routes, respectively. Pore free uniform grains can be seen from the surface micrographs of BT samples synthesized by MSSR route. Grains of ~1.7 and 12μm sizes, estimated by the linear intercept method are observed for sintered BT samples synthesized SSR and MSSR routes, respectively. Pore free uniform distribution of grains in BT samples synthesized by MSSR route shows its superiority over SSR route.

Figs. 4.11-15 depict the scanning electron micrographs (SEM) of iso-valent and off-valent substituted BT systems synthesized by MSSR. The average grain size was calculated using the linear intercept method and is given in Table 4.4.

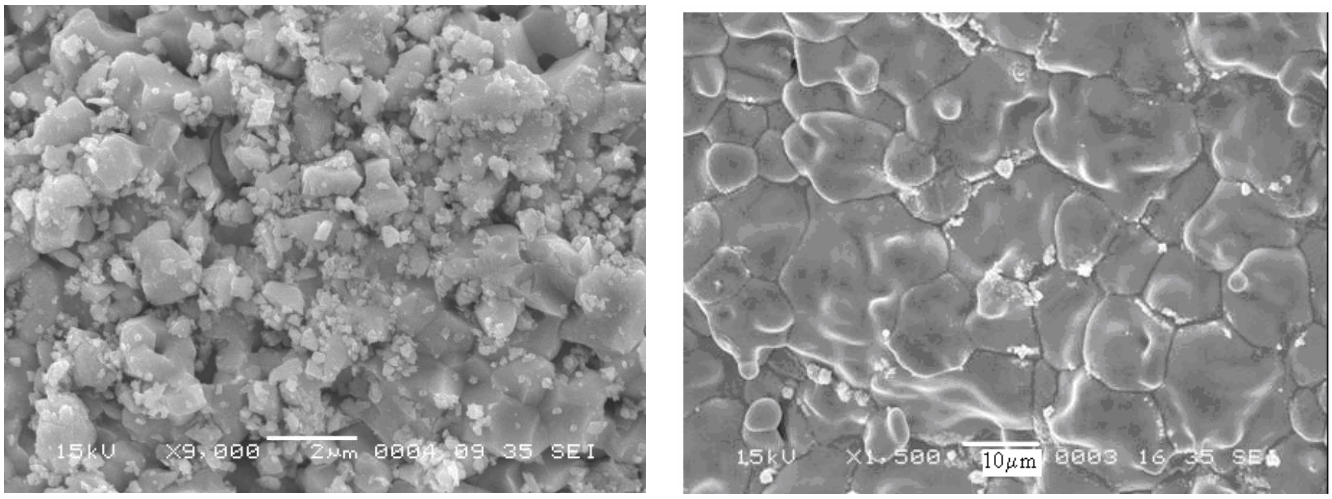

(a) (b)

Fig. 4.10 SEM micrographs of BT samples synthesized by (a) SSR & (b) MSSR routes.

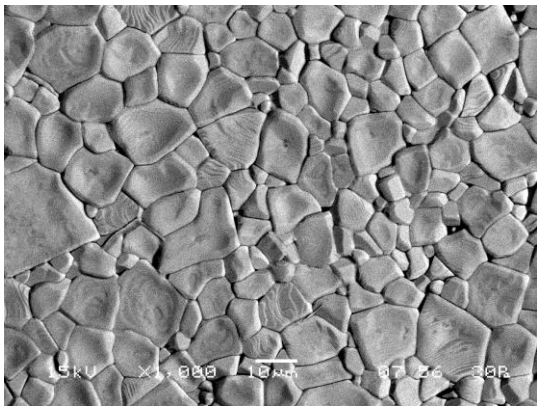

(a)

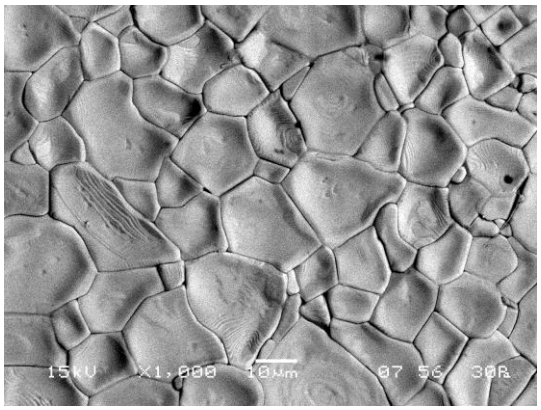

(b)

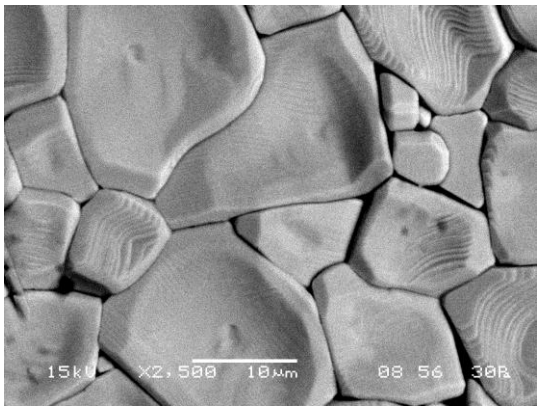

(c)

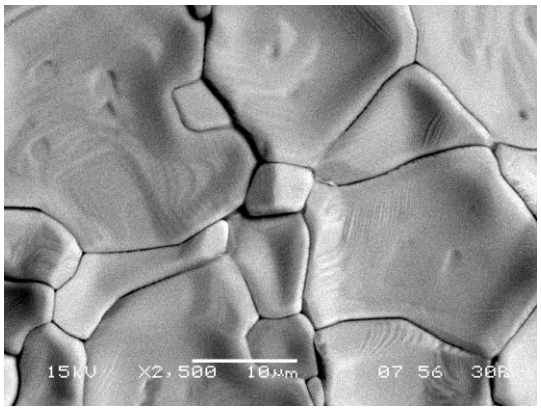

(d)

Fig. 4.11 SEM micrographs of sintered SEM micrographs of sintered (a) BCT1 (b) BCT2 (c) BCT3 & (d) BCT4 samples.

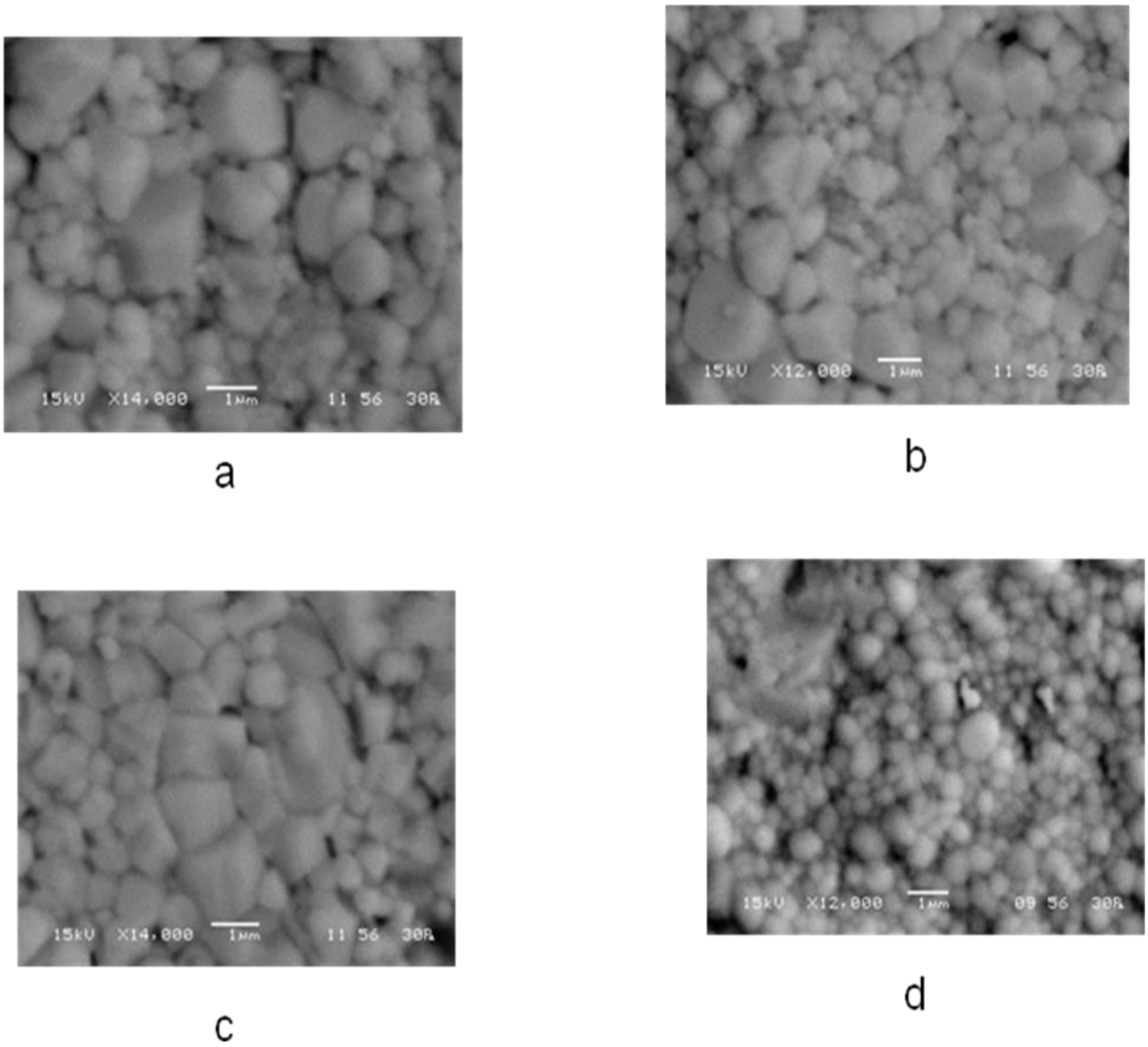

Fig. 4.12 SEM micrographs of sintered SEM micrographs of sintered (a) BMT1 (b) BMT2 (c) BMT3 & (d) BMT4 samples.

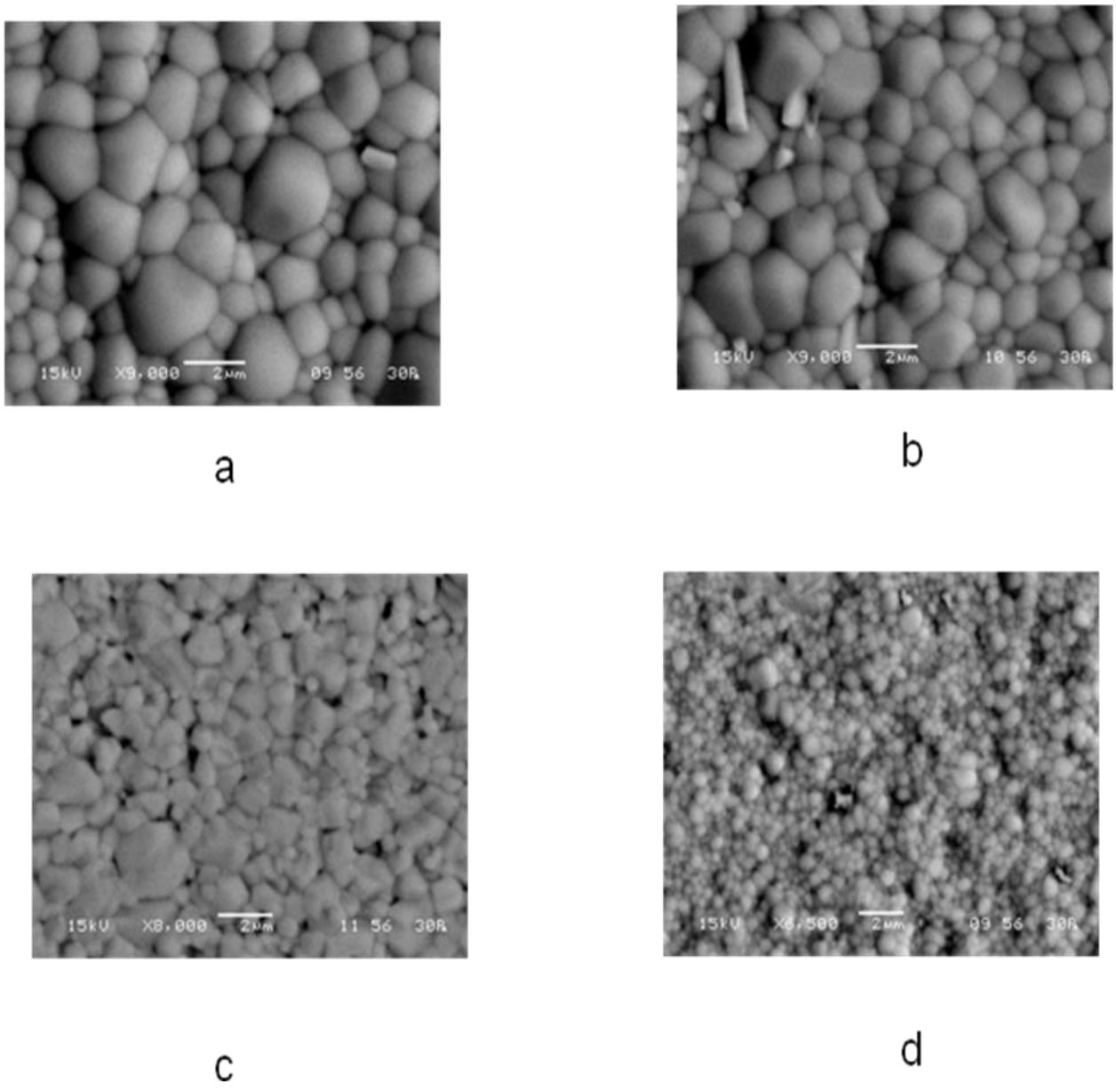

Fig. 4.13 SEM micrographs of sintered (a) BST1 (b) BST2 (c) BST3 & (d) BST4 samples.

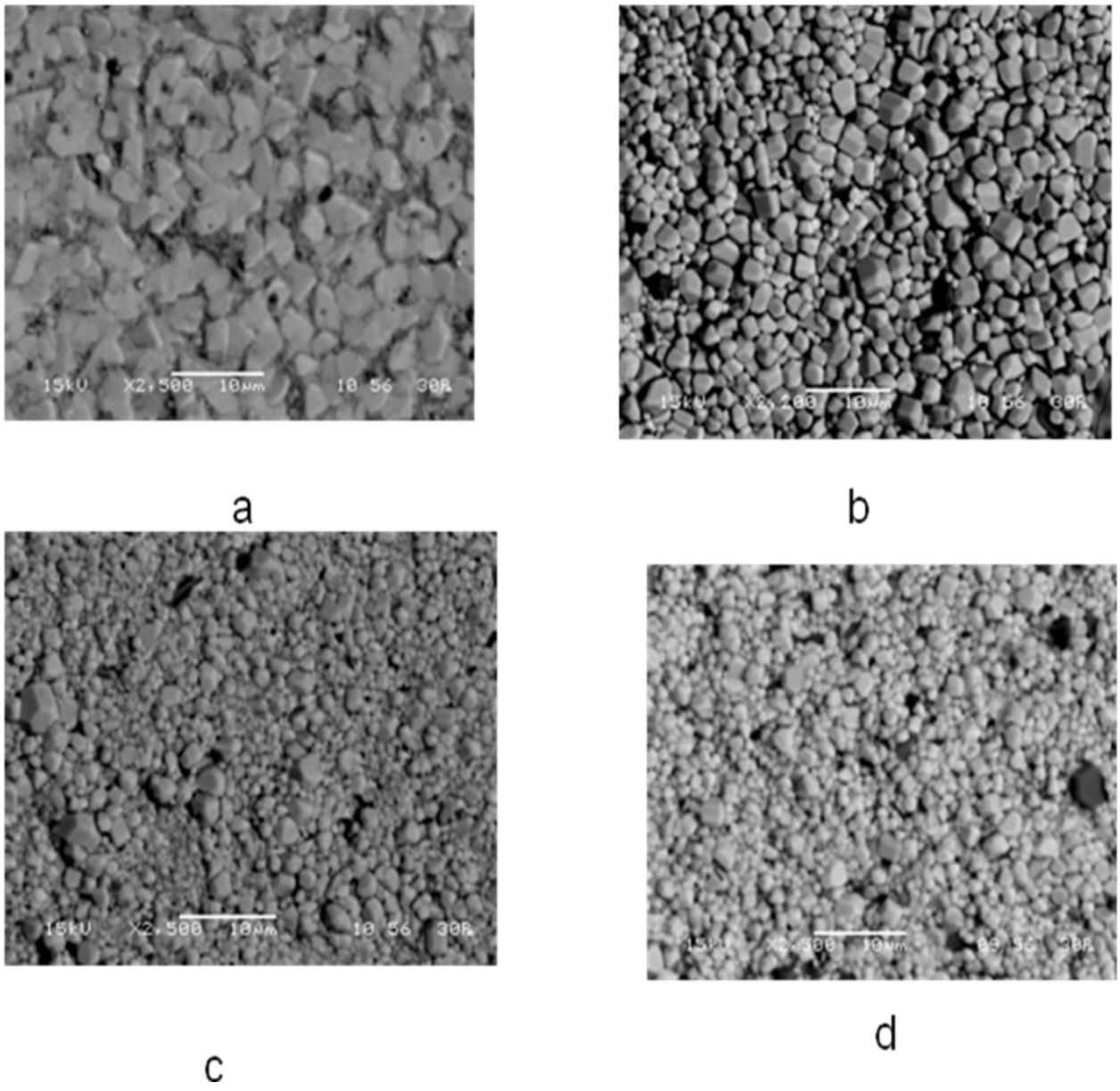

Fig. 4.14 SEM micrographs of sintered (a) BSmT1 (b) BSmT2 (c) BSmT3 & (d) BSmT4 samples.

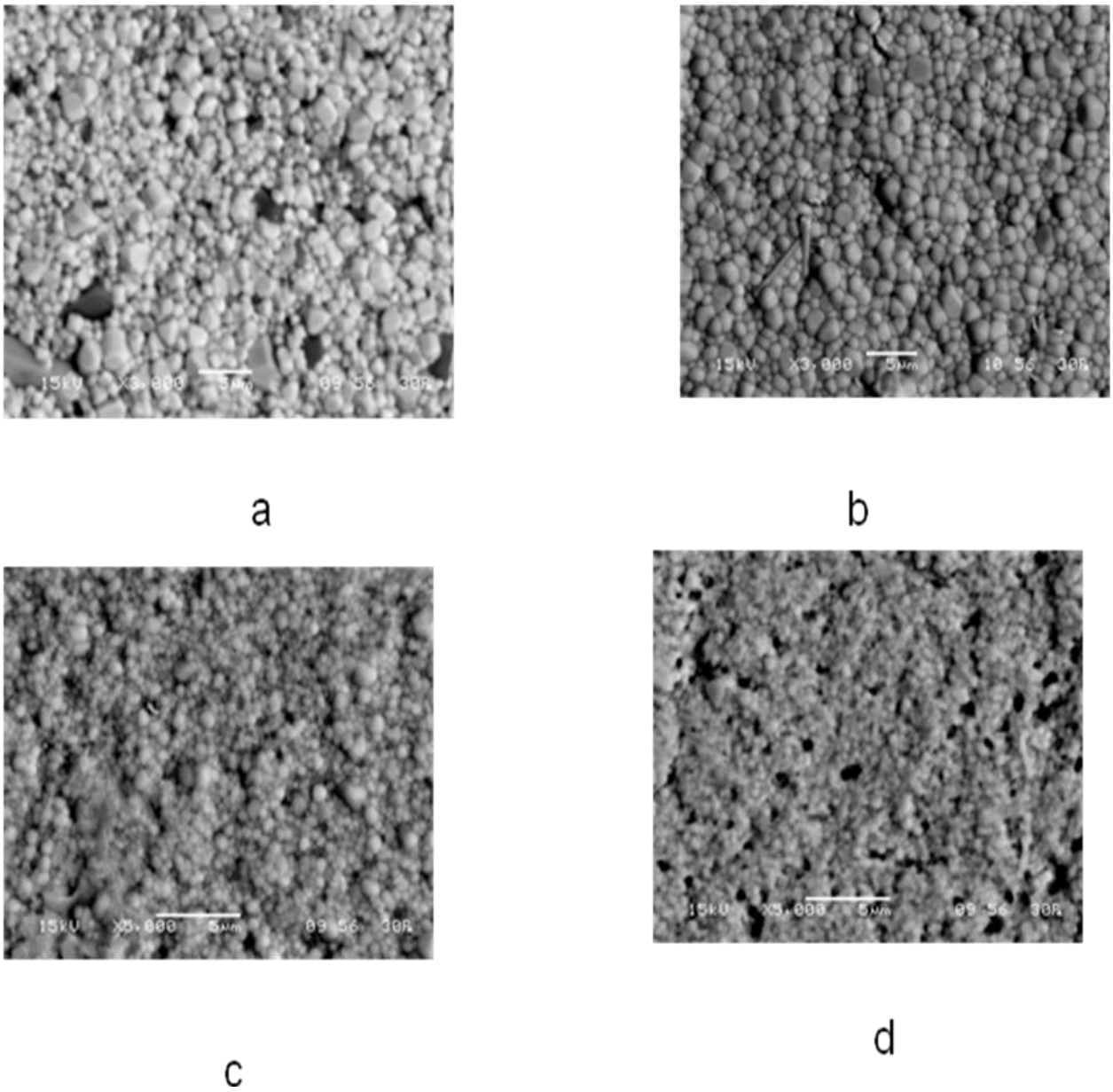

Fig. 4.15 SEM micrographs of sintered (a) BLT1 (b) BLT2 (c) BLT3 & (d) BLT4 samples.

In $Ba_{1-x}Y_xTiO_3$ (Y=Ca) systems, where x = 0.02, 0.04, 0.06 and 0.08, respectively the grain size and uniformity of the grains increases with the increase of Ca substitution% in BT system indicating the good solubility of Ca in BT system. With the increase in Sr, Mg substitution% in BT system, grain size decreases. In $Ba_{1-x}Y_xTi_{(1-x/4)}O_3$ (Y=La and Sm) systems the grain size decreases with the increase of substitution concentration. Therefore, the effect of the Sr, Mg, La and Sm substitutions results in a reduction of grain growth. The melting temperature of the iso-valent and off-valent

substituted BT systems particle may increase with the decrease of the particle size [36, 37], which can lead to decrease in the rate of grain growth and hence smaller grain size in Sr, Mg, Sm and La modified BT ceramics synthesized by MSSR route.

Table 4.4. Grain size of iso-valent and off-valent substituted BT systems synthesized by MSSR route:

System	**$Ba_{0.98}Ca_{0.02}TiO_3$**	**$Ba_{0.96}Ca_{0.04}TiO_3$**	**$Ba_{0.94}Ca_{0.06}TiO_3$**	**$Ba_{0.92}Ca_{0.08}TiO_3$**
Grain Size(μm)	**10**	**18**	**22**	**27**
System	**$Ba_{0.98}Mg_{0.02}TiO_3$**	**$Ba_{0.96}Mg_{0.04}TiO_3$**	**$Ba_{0.94}Mg_{0.06}TiO_3$**	**$Ba_{0.92}Mg_{0.08}TiO_3$**
Grain Size (μm)	**1.33**	**1.23**	**1.14**	**0.7**
System	**$Ba_{0.98}Sr_{0.02}TiO_3$**	**$Ba_{0.96}Sr_{0.04}TiO_3$**	**$Ba_{0.94}Sr_{0.06}TiO_3$**	**$Ba_{0.92}Sr_{0.08}TiO_3$**
Grain Size (μm)	**2.05**	**1.29**	**1.17**	**0.94**
System	**BSmT1**	**BSmT2**	**BSmT3**	**BSmT4**
Grain Size (μm)	**2.96**	**2.30**	**1.661**	**1.28**
System	**BLT1**	**BLT2**	**BLT3**	**BLT4**
Grain Size (μm)	**1.56**	**1.47**	**0.86**	**0.62**

Table 4.5 Compositions analysis by EDX of (i) BLT4 & (ii) BMT3 samples

Element	App Conc.	Intensity Corrn.	Weight%
O K	19.91	1.1611	21.35
Ti K	13.26	1.0336	15.97
Ba L	40.69	0.9305	54.43
La L	5.35	0.979	6.81
Totals			100

Element	App Conc.	Intensity Corrn.	Weight%
O K	17.95	1.1002	21.1
Mg K	0.33	0.6642	0.63
Ti K	13.09	1.0188	16.62
Ba L	40.82	0.917	57.56
Totals			100

(i)

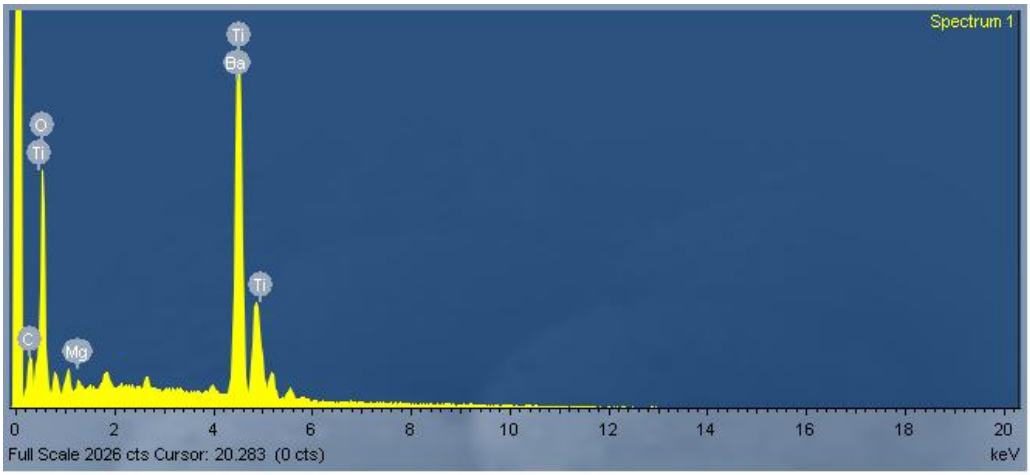

Fig. 4.16 EDX of BMT3 samples

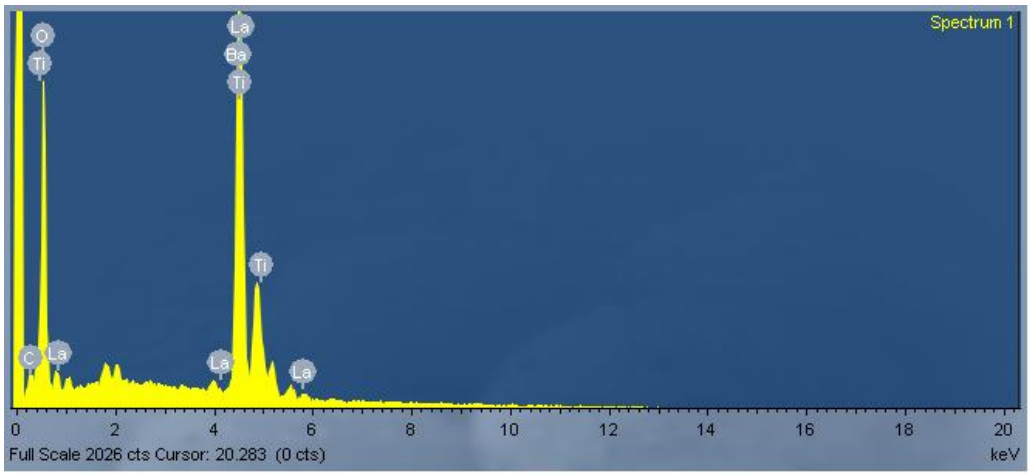

Fig. 4.17 EDX of BLT4 sintered samples

The chemical composition analysis of the iso-valent & off-valent modified BT samples synthesized by MSSR route was achieved by energy dispersive x-ray spectrometry (EDX), using an EDX spectrometer attached to the same SEM unit. Figs. 4. 16 & 4.17 shows the EDX results of BLT4 & BMT3 samples. Table 4.5, corresponding to Figs. 4. 16 & 4.17 confirms the stoichiometry of BLT4 & BMT3 samples. Element% & Atomic% are calculated from the data of the Table 4.5 by using the relations

Element% = Apparent conc./Intensity Correction.

Atomic% =weight% / atomic weight;

the sum of atomic weights for all elements in the sample was then normalized to 100%.

References

1. W.D. Kingery, H.K. Bowen, D.R. Uhalmann, Introduction to ceramics, 2nd Edition, John Wiley and sons, New York (1976).
2. N. Setter, J. Euro. Ceram. Soc., **21** (2001) 1279.
3. D.W. Richerson, Modern Ceramic Engineering, Marcel Dekker, New York (1992).
4. J.S. Reed, Principles of Ceramic Processing, John Wiley & Sons, Inc., New York (1995).
5. I.D. Marinescu, H.K. Tonshoff , I. Inasaki, Handbook of Ceramic Grinding and Polishing, Noyes Publications, USA (2002).
6. J. Valasek, Phys. Rev., **17** (1921) 475.
7. C. Kittel, Introduction to Solid State Physics, 7th edition, Wiley Publications (1995).
8. T. R. Shrout, A. Halliyal, Am. Ceram. Soc. Bull., **66** (1987) 704.
9. Yuhuan Xu, Ferroelectric Materials and Their Applications, Elsevier Science Pub. Co. New York, USA (1991).
10. K. Katayama, M. Abe , T. A. Yanagida, J. of Euro. Ceram. Soc., **5** (1989) 183.
11. Perry's Chemical Engineers' Handbook, 6th Edition, edited by Robert H. Perry, Don W. Green, and James O. Maloney, McGraw-Hill Book Company, New York (1984).
12 S. Tangwiwat, S. J. Milne, J. Non-Crystalline Solids, **351** (2005) 976.
13. J. Bera, D. Sarkar, J. Electroceramics, **11**[3] (2003) 131.
14. A.J. Moulson and J.M. Herbert, Electroceramics: Materials, properties and Applications, 2nd edition, Wiley, New York (2003).
15. J. Ravez , A. Simon, J. Solid State Chemistry **162** (2001)260.
16. P. Kumar, S.N. Kumar, Sonia, R. K. Patel & C. Prakash, Appl. Sur. Sci., **255** (2009) 5686.
17. H. R. Rukmini, R. N. P. Choudhary and D. L. Prabhakara, Mater. Chem. Phys., **64** (2000) 171.
18. E Wu, POWD, an interactive powder diffraction data interpretation and indexing program, Ver. 2.1, School of Physical Science, Finder's University of South Australia, Bedford Park.

19. F.D. Morrison, D.C. Sinclair, A.R.West, J. Appl. Phys., **86** (1999) 6355.
20. F.D. Morrison, D.C. Sinclair, A.R. West., Int. J. Inorg. Mater., **3** (2001) 1205.
21. M. Aparna, T. Bhimasankaram, S.V. Suryanarayana, G. Prasad, G.S. Kumar Bull. Mater. Sci., **24** (5) (2001) 497.
22. P. Yongding, L. Yunhe, Y. Wenhu, J. Rare Earths, **25** (2007) 167.
23. M. N. Rahaman, Ceramic Processing and Sintering, 2nd Edition. Marcel Dekker Inc., (2003).
24. Naratip Vittayakorn, Journal of Applied Sciences Research, **2**(12) (2000) 1319.
25. Noor Jawad Ridha, W. Mahmood Mat Yunus, S.A. Halim, Z.A. Talib, Firas K. Mohamad Al-Asfoor, Walter C. Primus, American J. of Engineering and Applied Sciences **2**(4) (2009) 661.
26. A. G. Belous, O. I. V'yunov, L. L. Kovalenko, V. Buscaglia, M. Viviani, P. Nanni, Inorganic Materials, **39**(2) (2003) 133.
27. Toru Nagai, Kenji Iijima, Hae Jin Hwang, Mutsuo Sando, Tohru Sekino, Koichi Niihara, Journal of the American Ceramic Society, **83** (2000) 107.
28. R. C. Pullar, Y. Zhang, L. Chen, S. Yang, J. R. G. Evans, A. N. Salak, D. A. Kiselev, A.L. Kholkin, V. M. Ferreira, N. M. Alford, J. Electroceram., **22** (2009) 245.
29. K. Aliouane, A. Guehria-Laidoudi, A. Simon, J. Ravez, Solid State Sciences, **7** (2005) 1324.
30. Finlay D. Morrison, Derek C. Sinclair*, Anthony R. West, International Journal of Inorganic Materials **3** (2001) 1205.
31. R. Zhang,† J. F. Li, D. Viehland*, J. Am. Ceram. Soc., **87** [5] (2004) 864.
32. N. Kohzu , Y. Iguchi , T. Okuda, Solid State Ionics, **108** (1998) 129.
33. Y. Li *, Y. Qu, Materials Research Bulletin, **44** (2009) 82.
34. B.D.Stojanović, V.R.Mastelaro, C.O. Paiva Santos, J.A.Varela, Science of Sintering, **36** (2004) 179.
35. H. Saka, Y. Nishikawa, T. Imura, Philo. Mag. A **57** (1988) 895.
37. W.H. Qi, M.P. Wang, Mater. Chem. Phys., **88** [2-3] (2004) 280.

CHAPTER V

DIELECTRIC PROPERTIES OF MODIFIED BT SYSTEMS

5.1 Introduction

For multilayer capacitors (MLCs) [1-4], dynamic random access memory (DRAM) [5], bolometer [6] and high power applications [7], the ferroelectric materials should have high dielectric constant (ε_r) with low dielectric loss (tanδ). BT ceramics are widely used in the fabrication of multilayer ceramic capacitors (MLC) and dynamic random access memory (DRAM) devices because of their high dielectric constant (ε_r) and low dissipation factor (tanδ) at RT. Many efforts have been made to further modify the dielectric properties of these ceramics [8-13]. Substitution of iso-valent/off-valent ions for the host lattice cations in BT perovskite lattice plays a significant role in these modifications [14–22]. These materials form solid solutions with $BaTiO_3$ and alter its structural features, resulting in a shift in phase transition temperature along with modified dielectric properties. In this chapter effect of synthesis route and iso-valent/off-valent ions substitution on dielectric properties of BT system have been carried out and discussed in detail. In order to examine the effect of substitution on transition temperature (T_c) and dielectric properties, variation of dielectric parameters at different frequencies with temperature have been reported and discussed in detail. Variation of dielectric properties of modified BT system as a function of frequency at room temperature (RT) has also been reported and discussed in detail.

5.2 Dielectric Properties

In this section variation of dielectric properties of BT & modified BT system as a function of frequency at RT has been reported followed by discussion on variation of dielectric properties at different frequencies with temperature.

5.2.1 Dielectric Properties of BT & Modified BT Samples

In this section, first dielectric properties of BT samples synthesized by SSR and MSSR route are presented. This follows the dielectric properties of modified BT samples synthesized by MSSR route.

5.2.1.1 Variation of Dielectric Properties with Frequency at Room Temperature of BT Samples Synthesized by SSR and MSSR Route

(i)

(ii)

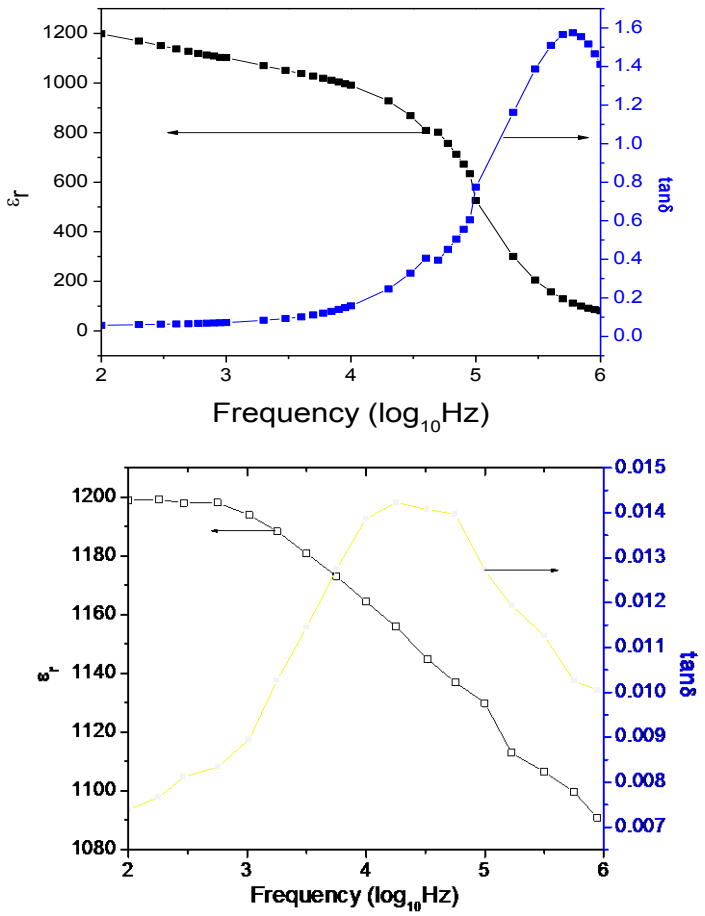

Fig. 5. 1 Variation of ε_r and tanδ with frequency of BT samples synthesized by (i) SSR and (ii) MSSR routes.

Fig. 5.1 shows the frequency dependence of dielectric constant (ε_r) and tanδ at RT of BT samples synthesized by SSR and MSSR routes, respectively. Value of ε_r & tanδ at 1kHz are found to be ~1100 & 1200 and 0.07 & 0.008 of BT samples synthesized by SSR and MSSR routes, respectively. High value of dielectric constant (ε_r) and low value of tanδ

of BT samples synthesized by MSSR route is due to the better purity of the starting precursors used in this route [23, 24]. This signifies the importance of modified solid state reaction (MSSR) route over SSR route. Here, we are getting better dielectric properties of BT samples synthesized by MSSR route than SSR route at significantly lower processing temperatures [25-28]. This is one of the main achievements of the present work. ε_r decreases with the increase in frequency in BT samples synthesized by both the routes, which is a characteristic feature of the ferroelectric materials [29]. The appearance of peak in tanδ near 5.7kHz and 4kHz frequencies suggest the existence of resonance frequencies near about these frequencies for BT samples synthesized by SSR and MSSR routes, respectively. It, is well known that the dielectric loss becomes max. near at resonance frequencies compare to its near frequencies [30]. Further, the decrease of tanδ with the increase in frequency after max. tanδ value can be explained by Debye formula [31]. According to this formula tanδ is inversely proportional to frequency which explains the decrease in tanδ with the increase in frequencies beyond max. tanδ.

5.2.1.2 Temperature variation of Dielectric Properties at Different Frequencies of BT Samples Synthesized MSSR Route:

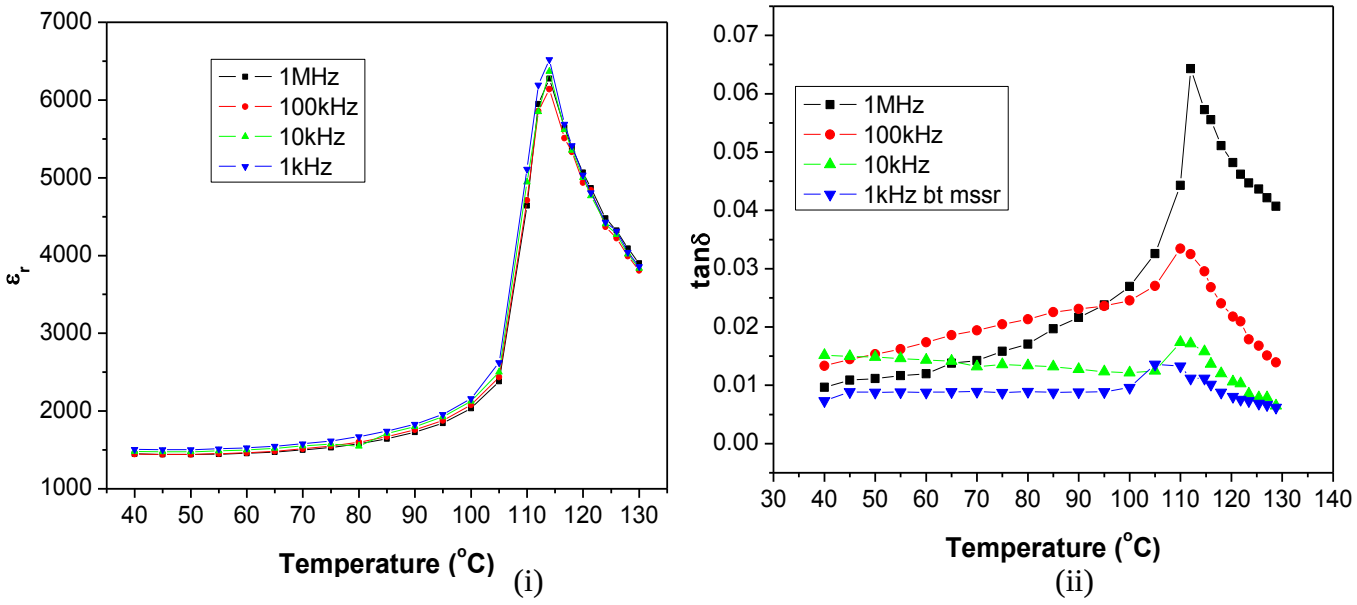

Fig. 5.2 Temperature variation of (i) ε_r and (ii) tanδ at different frequencies of BT samples synthesized by MSSR route.

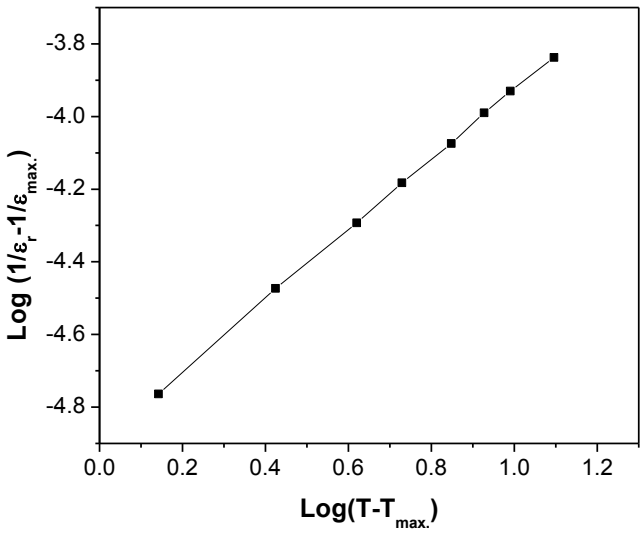

Fig. 5.3 Variation of $\log(1/\varepsilon_r - /\varepsilon_{r\ max.})$ vs. $\log(T - T_{max})$ of BT samples synthesized by MSSR route.

Fig. 5.2 shows the temperature variation of ε_r and tanδ at different frequencies (1 kHz–1 MHz) of BT samples synthesized by MSSR route. Values of ε_r and tanδ at different frequencies increases with the increase in temperature and transition temperature (T_c) was found to be around ~115^{o}C. The value of T_c is nearly same of the same system synthesized by solid state reaction route.

Fig.5.3 shows the variation of $\log(1/\varepsilon_r - 1/\varepsilon_{r\ max.})$ vs. $\log(T - T_{max})$ for BT samples synthesized by MSSR route. From the slope of the graph, value of 'γ' is calculated. Value of γ is found to be ~1, which suggests that the phase transition is of normal type, which is as per the earlier reports on BT system synthesized by SSR route [31].

5.2.2 Variation of Dielectric Properties with Frequency at Room Temperature of Modified BT Samples Synthesized MSSR Route:

In the following section the variation of dielectric properties with frequency at room temperature of iso-valent and off-valent modified BT samples synthesized by MSSR route is presented and discussed in detail.

(a)

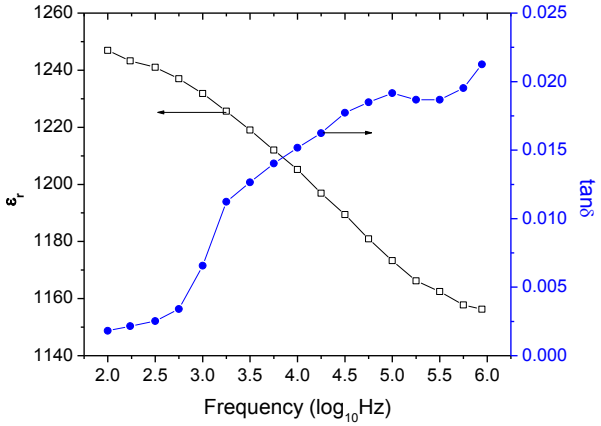

(b)

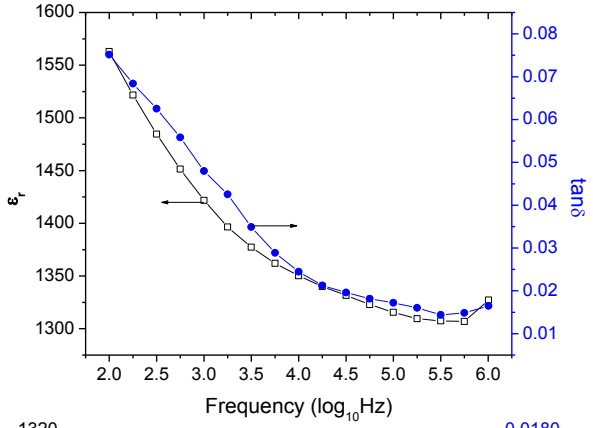

(c)

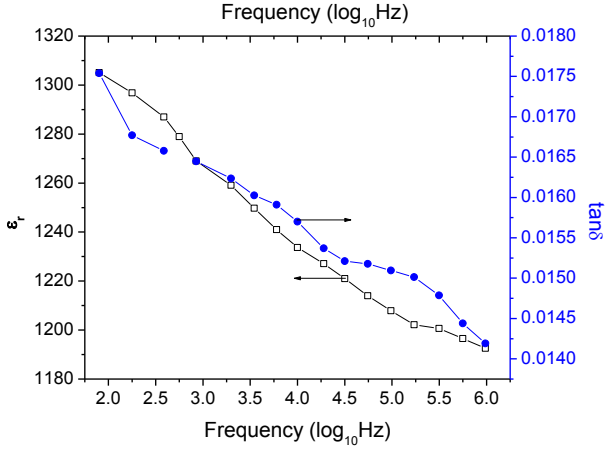

(d)

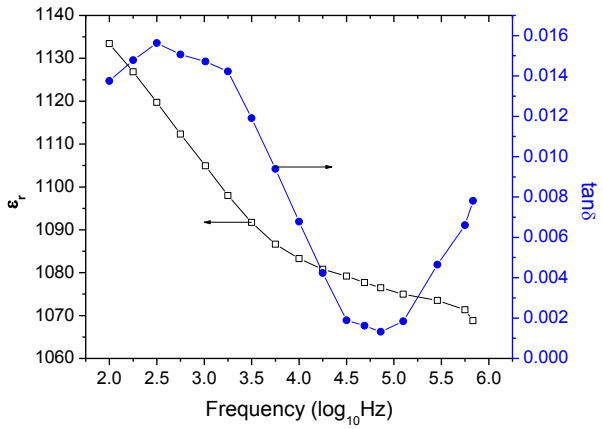

Fig. 5.4 Variation of ε_r and tanδ with frequency of (a) $Ba_{0.98}Ca_{0.02}TiO_3$ (b) $Ba_{0.96}Ca_{.0.04}TiO_3$ (c) $Ba_{0.94}Ca_{0.06}TiO_3$ & (d) $Ba_{0.92}Ca_{0.08}TiO_3$ samples

(a)

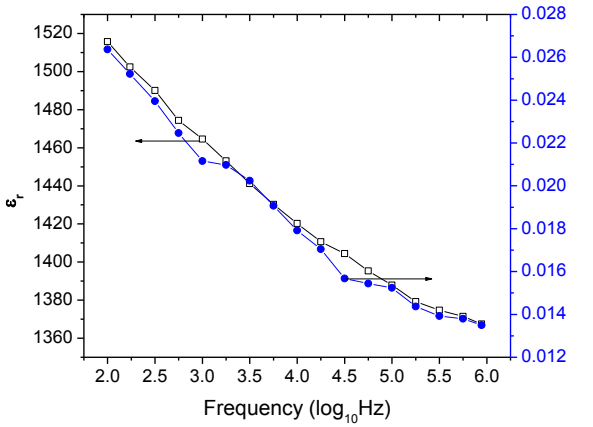

(b)

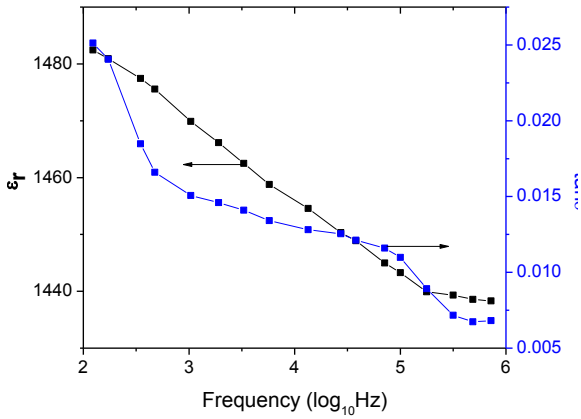

(c)

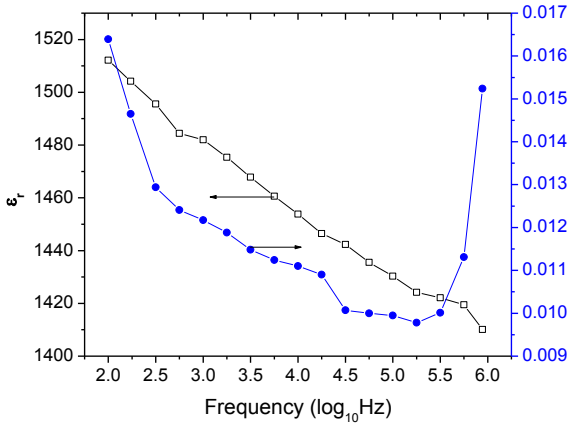

(d)

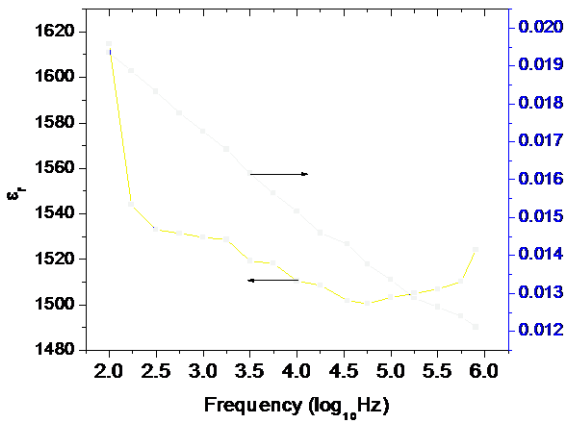

Fig. 5.5 Variation of ε_r and tanδ with frequency of (a) $Ba_{0.98}Mg_{0.02}TiO_3$ (b) $Ba_{0.96}Mg_{0.04}TiO_3$ (c) $Ba_{0.94}Mg_{0.06}TiO_3$ & (d) $Ba_{0.92}Mg_{0.08}TiO_3$ samples.

(a)

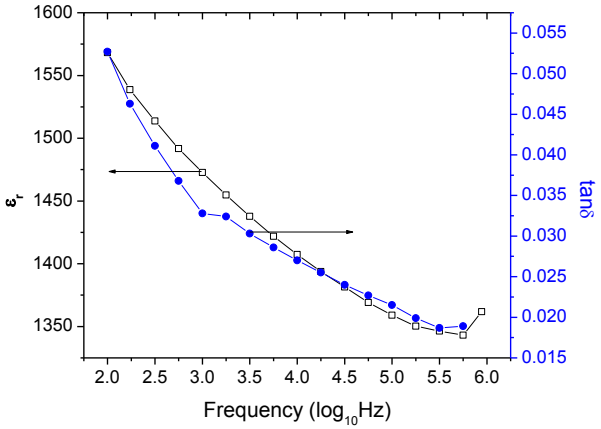

(b)

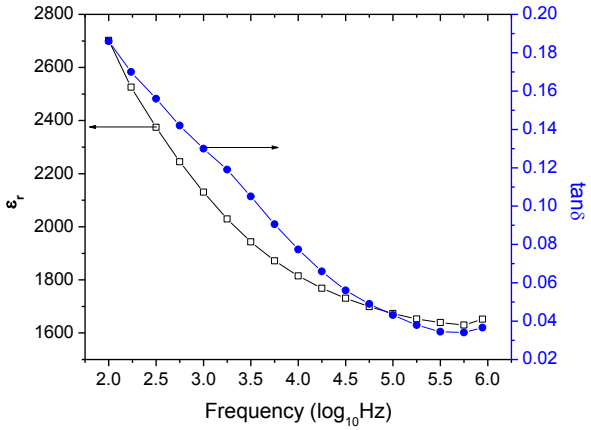

(c)

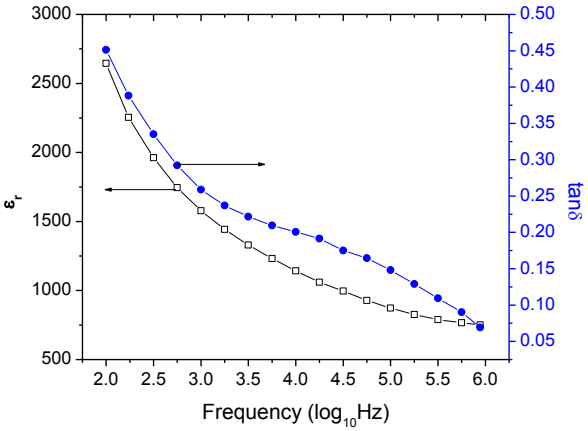

(d)

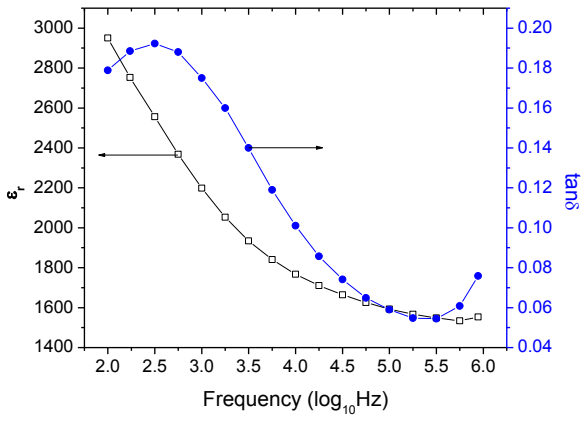

Fig. 5.6 Variation of ε_r and tanδ with frequency of (a) $Ba_{0.98}Sr_{0.02}TiO_3$ (b) $Ba_{0.96}Sr_{.0.04}TiO_3$ (c) $Ba_{0.94}Sr_{0.06}TiO_3$ & (d) $Ba_{0.92}Sr_{0.08}TiO_3$ samples.

(a)

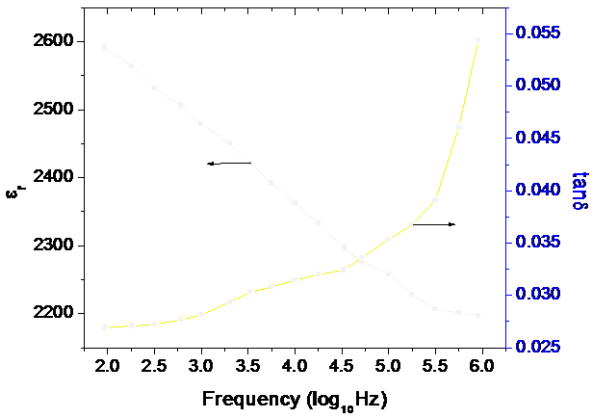

(b)

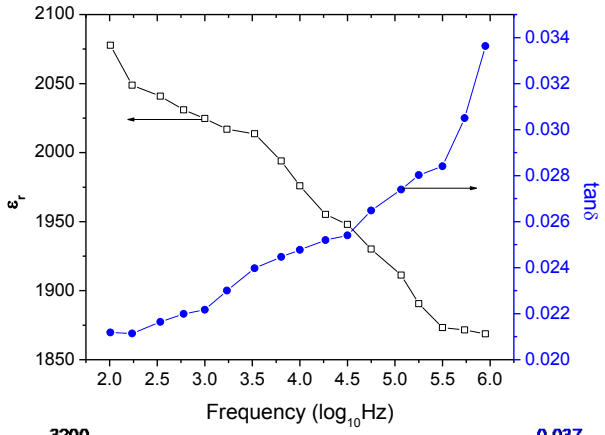

(c)

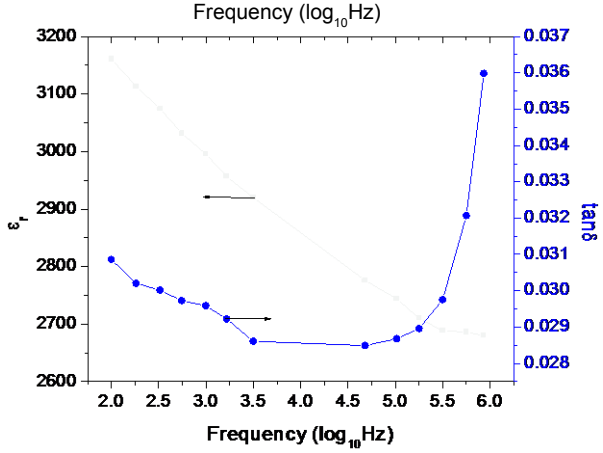

(d)

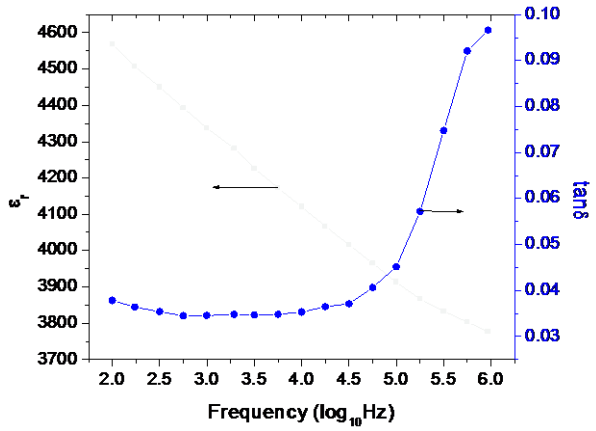

Fig. 5.7 Variation of ε_r and tanδ with frequency of (a) BSmT1 (b) BSmT2(c) BSmT3& (d) BSmT4 samples.

(a)

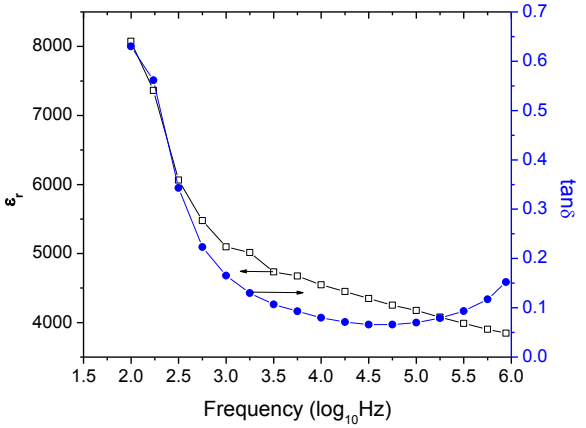

(b)

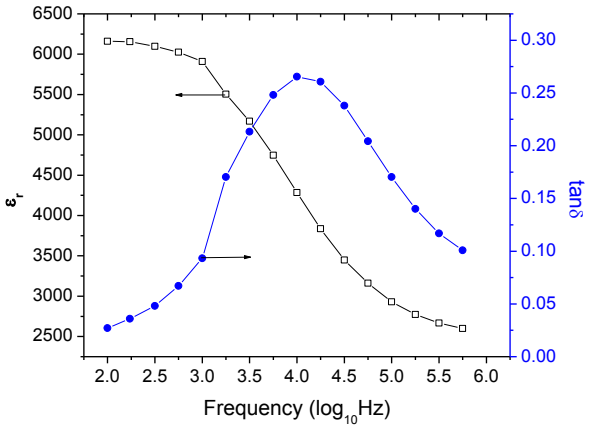

(c)

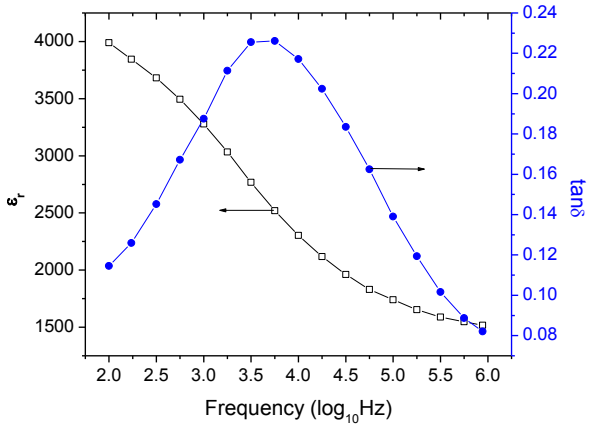

(d)

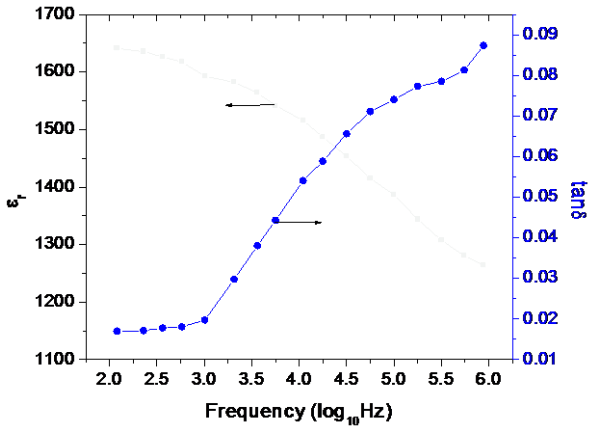

Fig. 5.8 Variation of ε_r and tanδ with frequency of (a) BLT1 (b) BLT2 (c) BLT3 & (d) BLT4 samples.

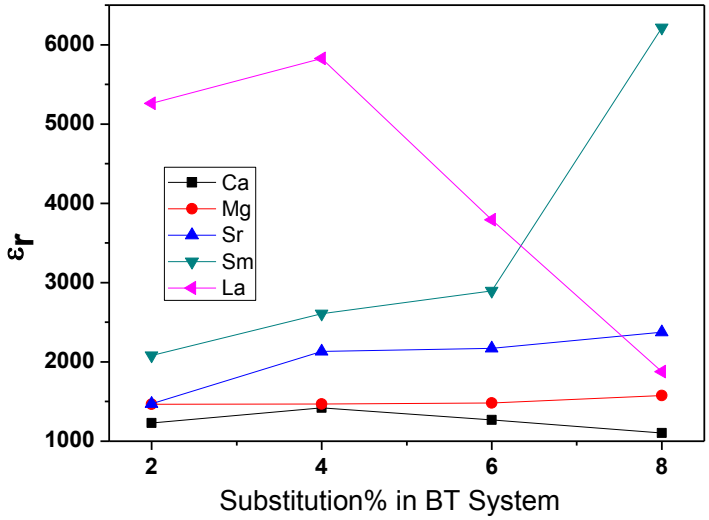

Fig. 5.9 Variation of ε_r (at 1kHz & at room temperature) with iso-valent and off-valent substitution% in BT system.

Figs. 5.4-5.8 shows the frequency dependence of ε_r and tanδ at room temperature (RT) of iso-valent and off-valent modified BT sintered samples synthesized by MSSR route. In all the modified BT samples, ε_r decreases with the increase in frequency. The fall in ε_r arises from the fact that polarization does not occur instantaneously with the application of the electric field, which is further due to the inertia of the dipoles and the delay in response towards the impressed alternating electric field leads to dielectric loss and decline in ε_r [31]. As shown in Fig. 5.10, at low frequencies, all types of polarizations contributes and as the frequency is increased, polarizations with large relaxation times cease to respond and hence the decrease in ε_r [33]. At lower frequencies ε_r is maximum because the contributions from the space charge polarization is large [33]. The space charge polarization arises by the accumulation of charges mainly due to vacancies of oxygen at the grain boundaries and at the electrode interface [34]. At higher frequencies, contributions from the polarizations having high relaxation time ceases resulting in the decrease in ε_r [35]. The same type of frequency-dependent dielectric behaviour is found in all other ferroelectric ceramic systems [14, 29]. As shown in Fig.5.9, it, is well known that the dielectric loss (tanδ) becomes max. near resonance frequencies compare to its neighboring frequencies [30]. Ferroelectric materials can have more than one resonance frequencies. Therefore, the decrease of tanδ with the

increase of frequency from 100Hz suggest we are going away from one resonance frequency and the resonance frequency lies below 100Hz.

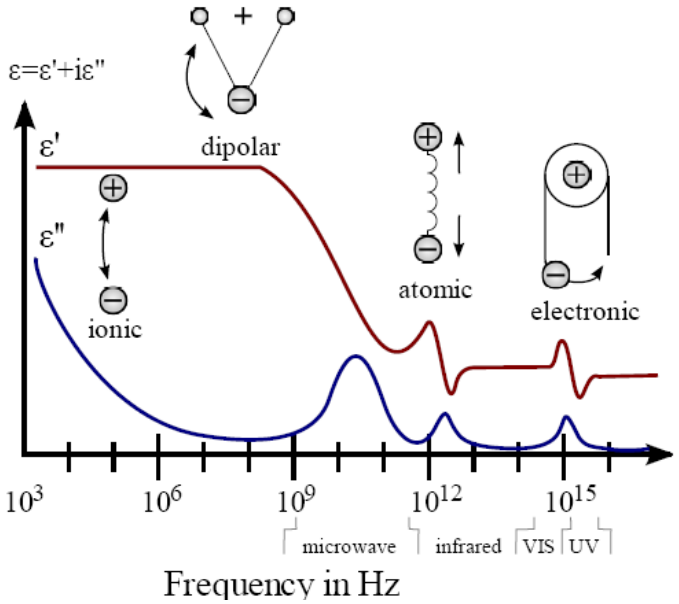

Fig. 5.10 Variation of real and imaginary parts with frequency of a dielectric material

Values of dielectric constant at 1kHz and at RT are given in Table 5.1 and shown in Fig. 5.9.

With the increase of Ca substitution concentration in BT system, the value of ε_r at RT first increases and then decreases beyond 0.04 substitution concentration. As, reported earlier, as we increase the Ca substitution concentration beyond 0.04, Ca can go to Ti sites, which would lead to creation of oxygen vacancies [39]. These oxygen vacancies would pins the movement of the ferroelectric domains walls and hence result in the decrease in dielectric constant [40]. With the increase of Mg and Sr ions substitution concentration in BT system, the value of ε_r at 1kHz & at RT increases (as given in Table 5.1). This is due to decrease in T_c [discussed in section 5.2.3]. Lowering of T_c shifts the position of temperature corresponding to ε_{rmax}. towards the RT side and hence increase in ε_r at RT with the increase in Sr ions substitution concentration in BT system [14, 29].

The value of ε_r at 1kHz at RT (given in Table 5.1 & shown in Fig. 5.9) increases with the increase of Sm ion substitution from 2080 to 6214. Whereas in the case of La ions

substitution in BT system, the value of ε_r at 1kHz at RT (given in Table 5.1 & shown in Fig. 5.9) increases upto 0.04 substitution concentration and then decreases with the increase of La substitution concentration in BT system**.** This is again due to decrease in T_c [discussed in section 5.2.3]. Lowering of T_c shifts the position of temperature corresponding to ε_{rmax}. towards the RT and hence increase in ε_r at RT with the increase in Sm and La ions substitution concentration in BT system. Since in the case of 0.06 & 0.08 La ions substitution concentration in BT system, the T_c is far below RT, therefore the position of ε_{rmax}. lies far below RT and as we know above the transition temperature the ε_r decreases, giving rise to low value of ε_r at RT.

Table 5.1 Values of dielectric constant at 1kHz and at RT of Iso-valnet and off-valnet modified BT Samples Synthesized by MSSR Route

System	**$Ba_{0.98}Ca_{0.02}TiO_3$**	**$Ba_{0.96}Ca_{0.04}TiO_3$**	**$Ba_{0.94}Ca_{0.06}TiO_3$**	**$Ba_{0.92}Ca_{0.08}TiO_3$**
ε_r at 1kHz	**1231**	**1422**	**1270**	**1104**
T_C	**120**	**121.5**	**123.**	**124.5**
System	**$Ba_{0.98}Mg_{0.02}TiO_3$**	**$Ba_{0.96}Mg_{0.04}TiO_3$**	**$Ba_{0.94}Mg_{0.06}TiO_3$**	**$Ba_{0.92}Mg_{0.08}TiO_3$**
ε_r at 1kHz	**1465**	**1470**	**1482**	**1576**
T_C	**75**	**75**	**75**	**80**
System	**$Ba_{0.98}Sr_{0.02}TiO_3$**	**$Ba_{0.96}Sr_{0.04}TiO_3$**	**$Ba_{0.94}Sr_{0.06}TiO_3$**	**$Ba_{0.92}Sr_{0.08}TiO_3$**
ε_r at 1kHz	**1473**	**2131**	**2170**	**2374**
T_C	**111**	**105**	**94.7**	**90**
System	**BSmT1**	**BSmT2**	**BSmT3**	**BSmT4**
ε_r at 1kHz	**2080**	**2609**	**2896**	**6214**
T_C	**100**	**65**	**50**	**Less than RT**
System	**BLT1**	**BLT2**	**BLT3**	**BLT4**
ε_r at 1kHz	**5260**	**5826**	**3791**	**1878**
T_C	**53**	**Just Below RT**	**< RT**	**<< RT**

5.2.3 Temperature Variation of Dielectric Properties at Different Frequencies of Modified BT Samples Synthesized by MSSR Route:

In the following section the temperature variation of dielectric properties at different frequencies of iso-valent and off-valent modified BT samples synthesized by MSSR route is presented an discussed in detail.

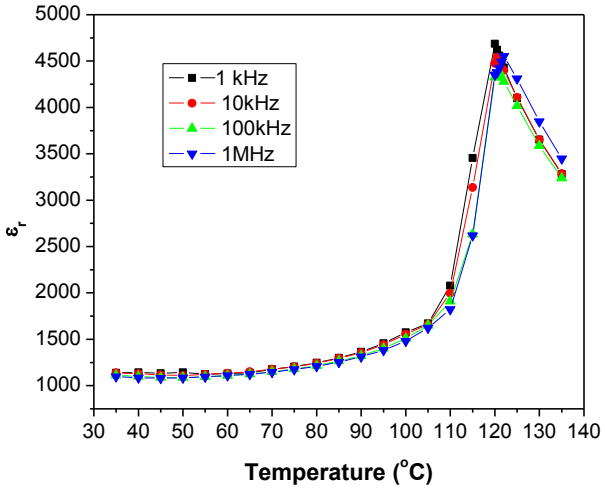

(a)

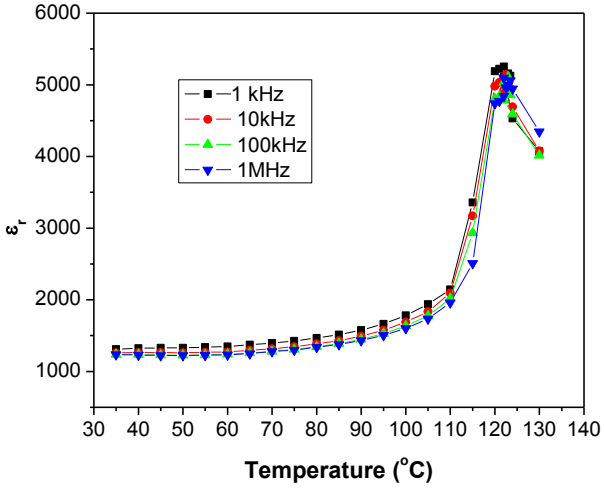

(b)

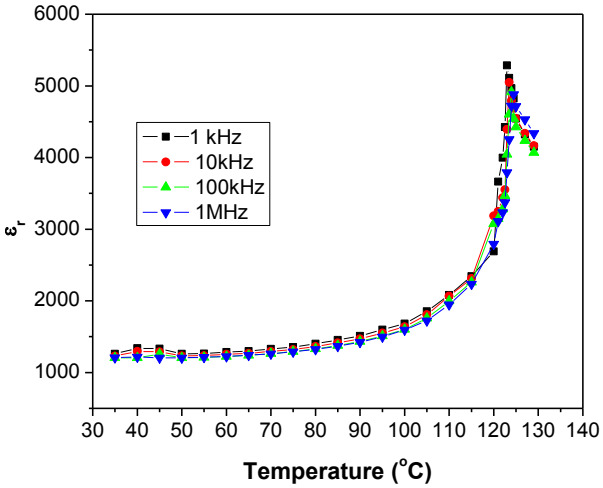

(c)

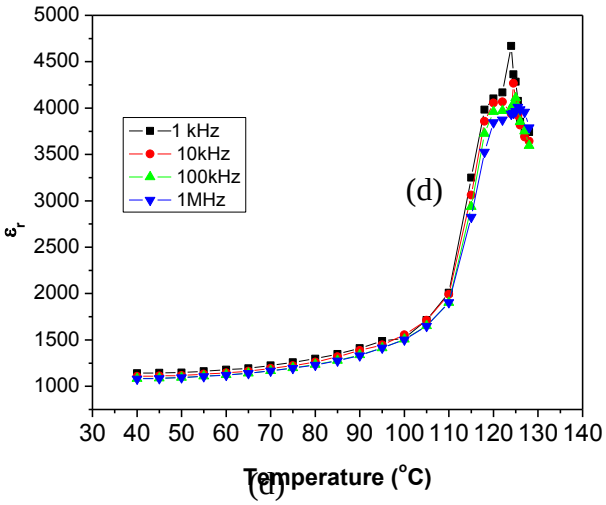

(d)

Fig. 5.11 Temperature variation of ε_r at different frequencies of sintered (a) BCT1 (b) BCT2 (c) BCT3 & (d) BCT4 samples.

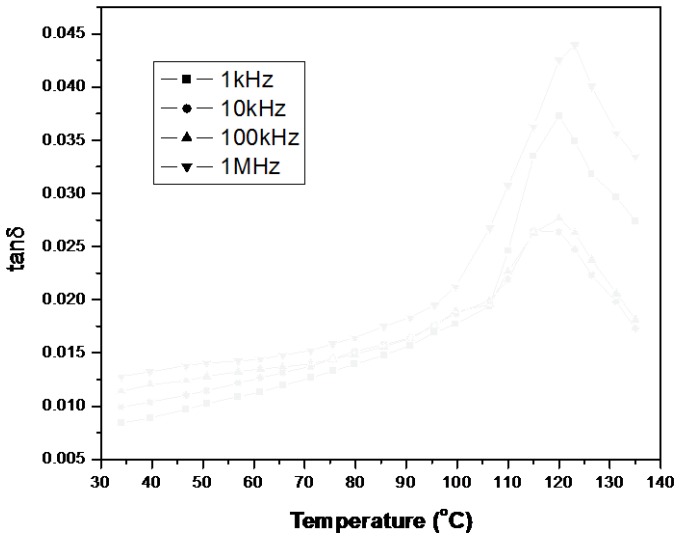

(a)

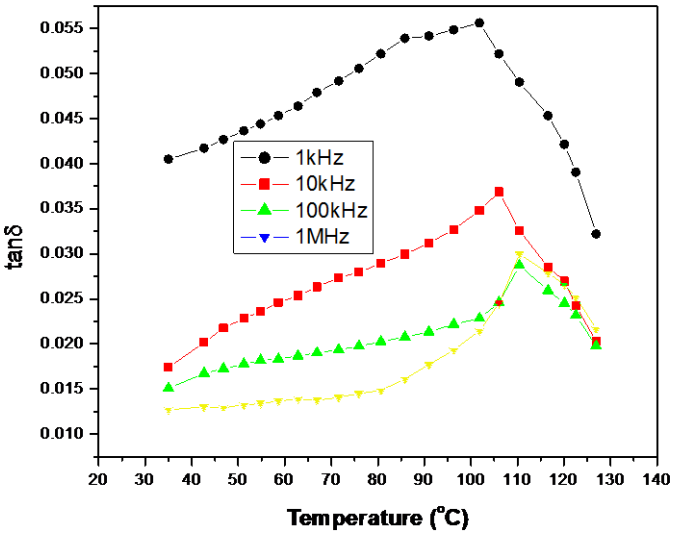

(b)

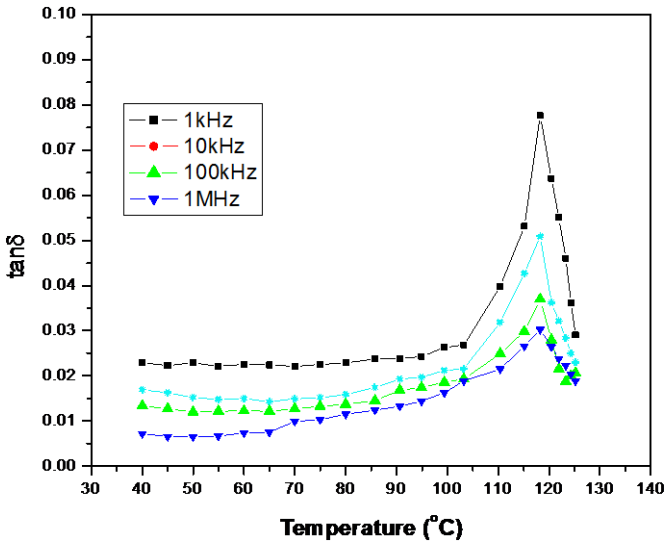

(c)

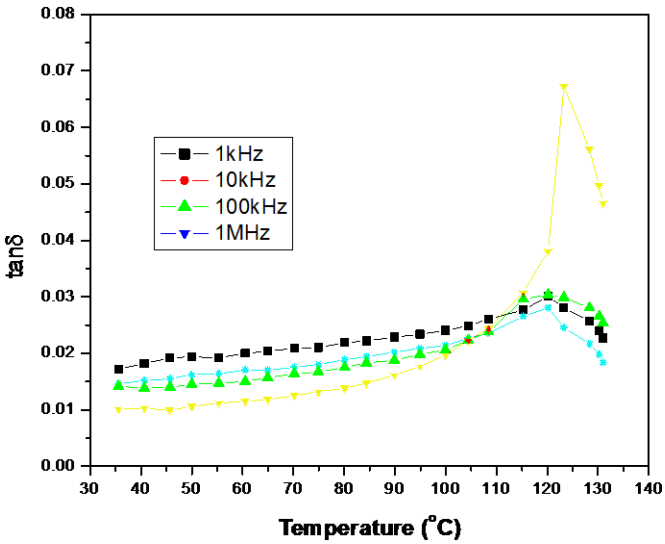

(d)

Fig. 5.12 Temperature variation of tanδ at different frequencies of sintered (a) BCT1 (b) BCT2 (c) BCT3 & (d) BCT4 samples.

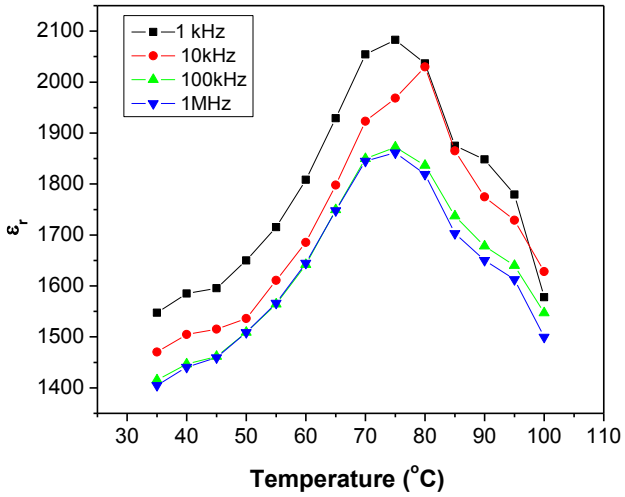

(a)

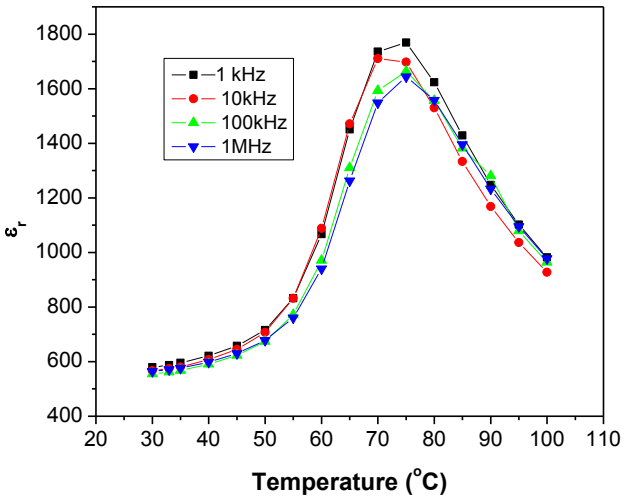

(b)

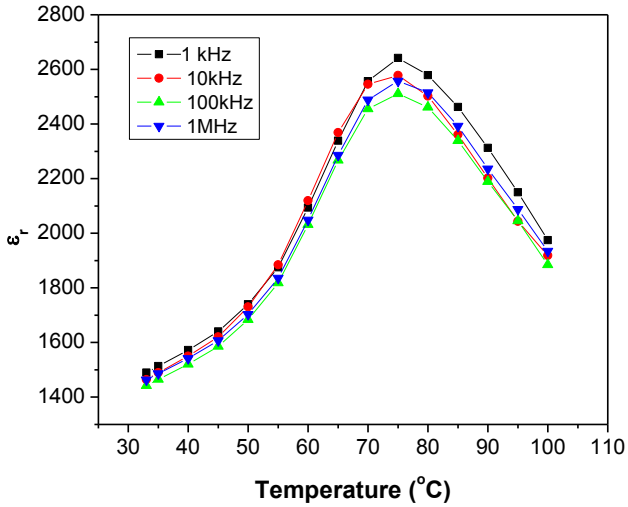

(c)

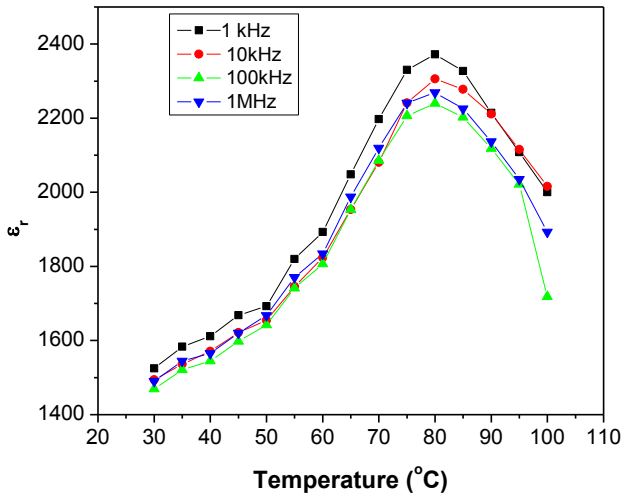

(d)

Fig. 5.13 Temperature variation of ε_r at different frequencies of sintered (a) BMT1 (b) BMT2 (c) BMT3 & (d) BMT4 samples.

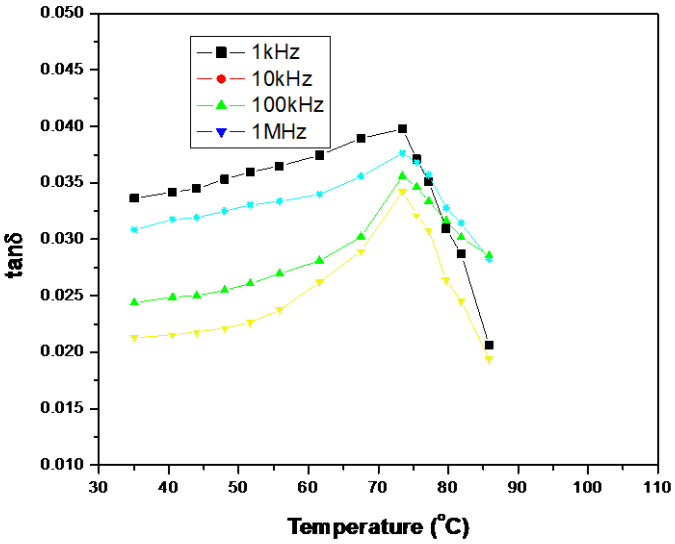

(a)

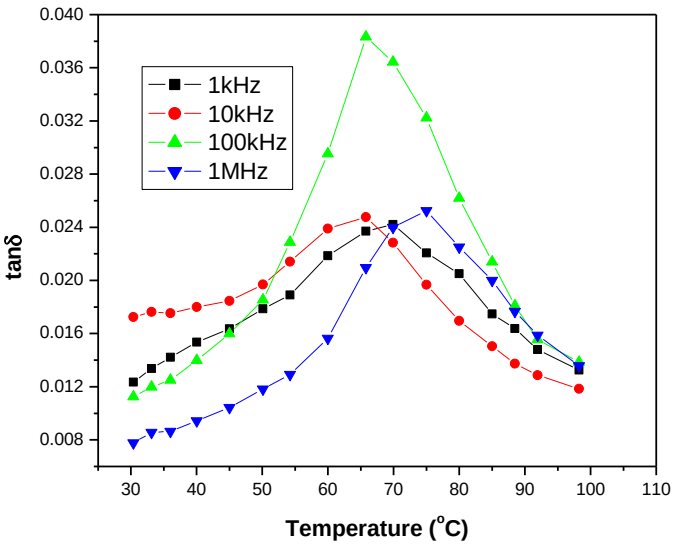

(b)

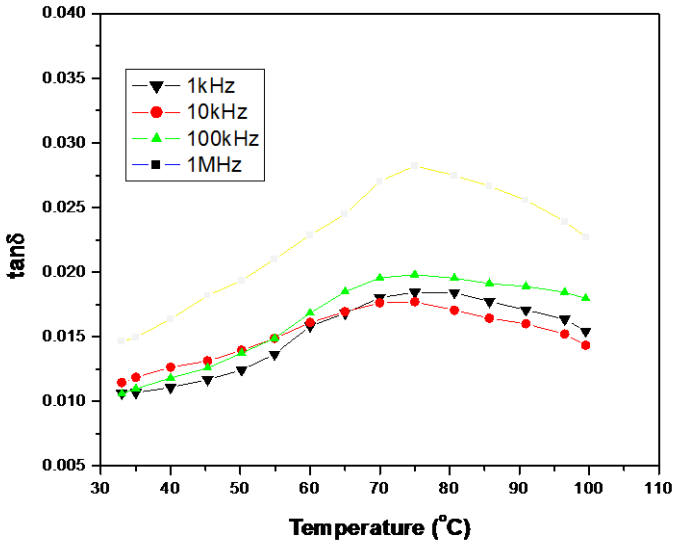

(c)

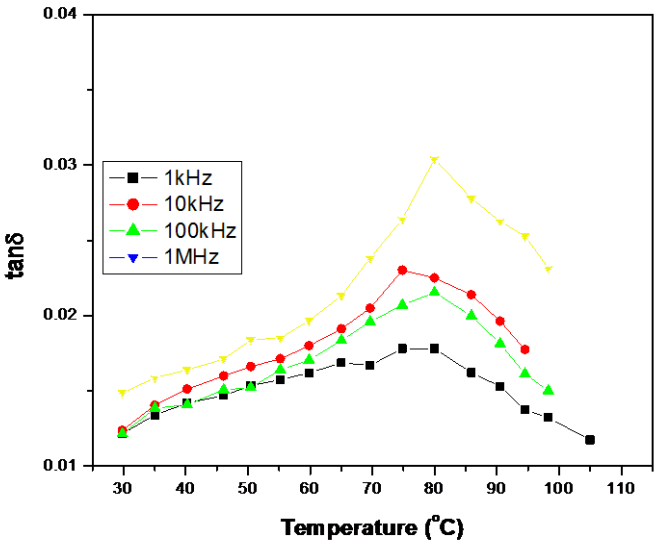

(d)

Fig. 5.14 Temperature variation of tanδ at different frequencies of sintered (a) BMT1 (b) BMT2 (c) BMT3 & (d) BMT4 samples.

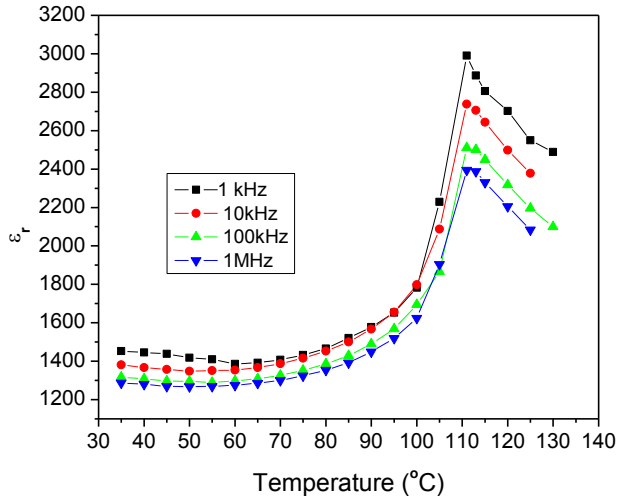

(a)

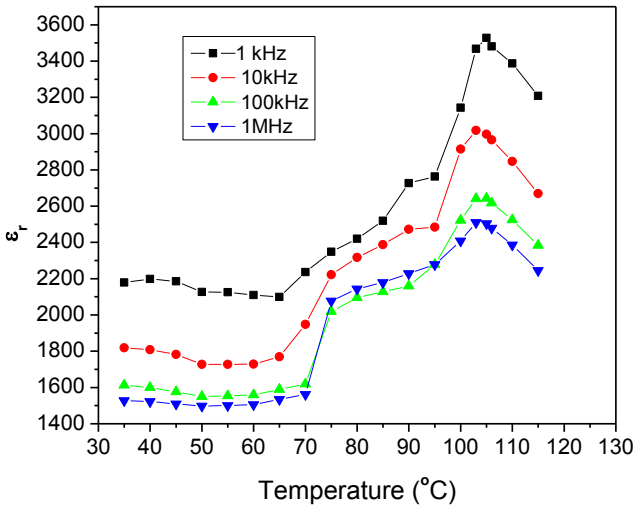

(b)

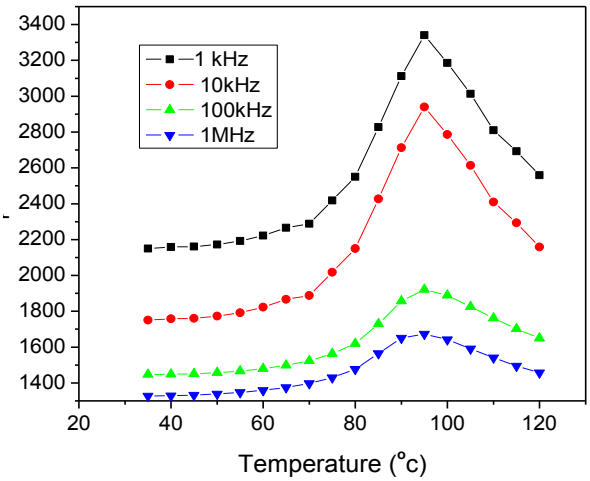

(c)

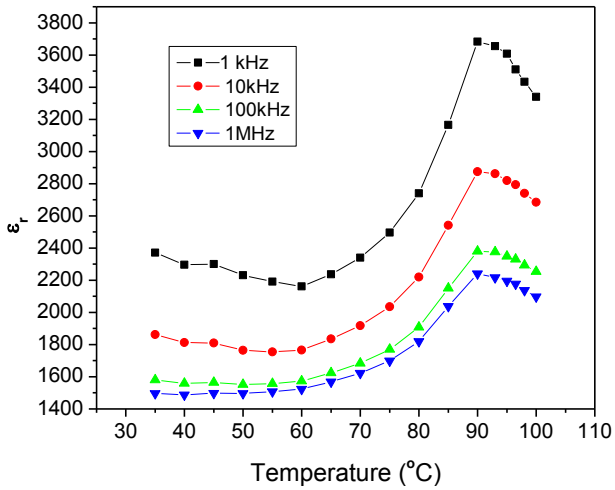

(d)

Fig. 5.15 Temperature variation of ε_r at different frequencies of sintered (a) BST1 (b) BST2 (c) BST3 & (d) BST4 samples.

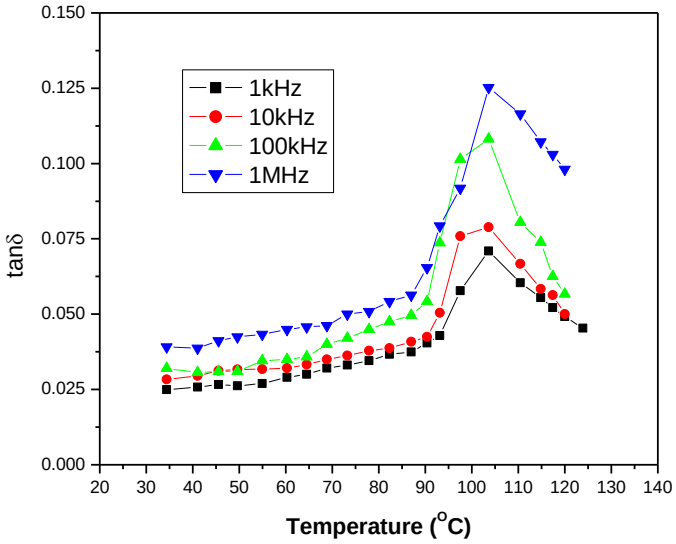

(a)

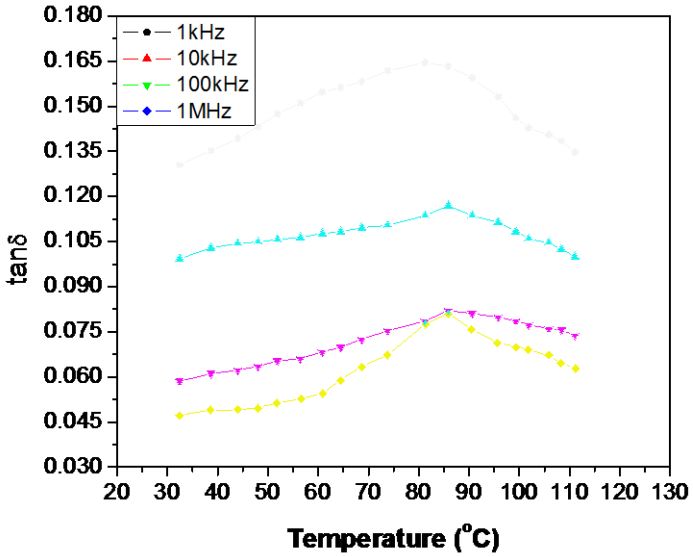

(b)

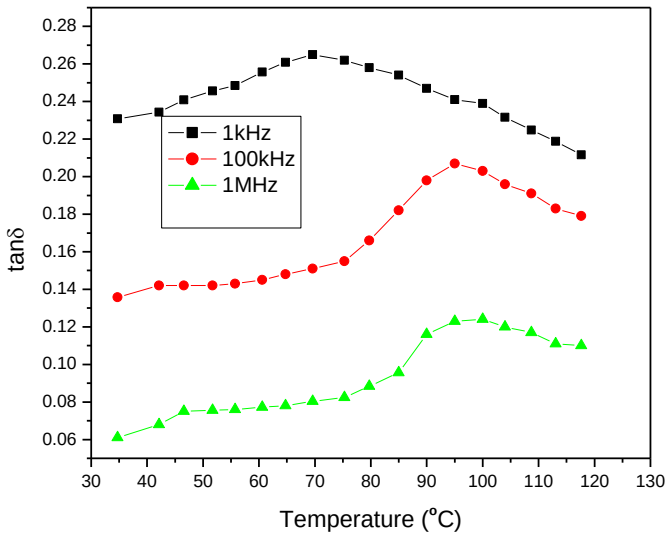

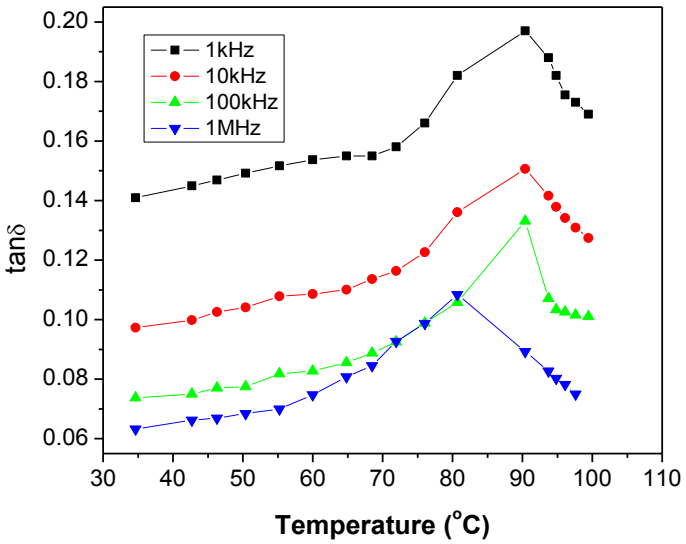

(d)

Fig. 5.16 Temperature variation of tanδ at different frequencies of sintered (a) BST1 (b) BST2 (c) BST3 & (d) BST4 samples.

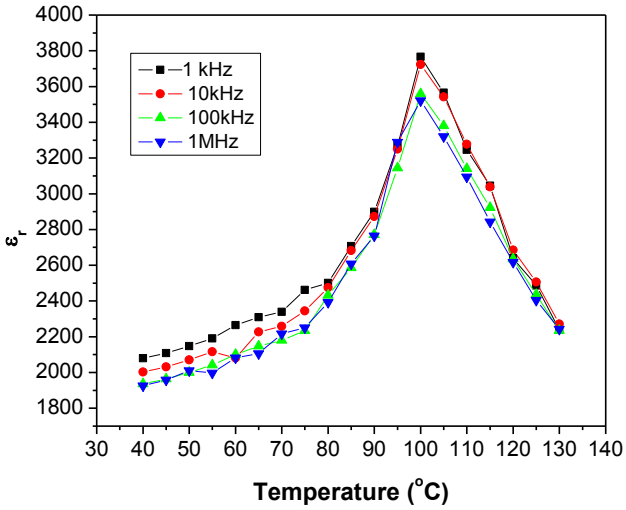

(a)

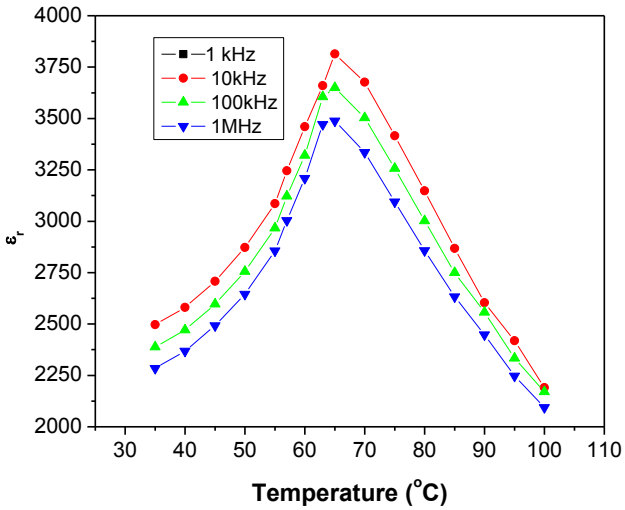

(b)

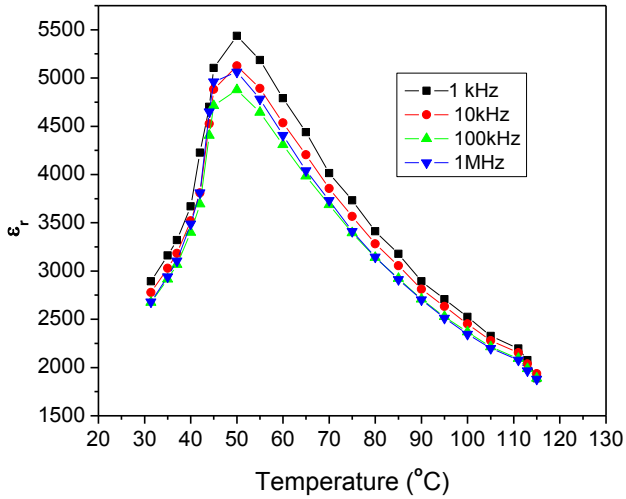

(c)

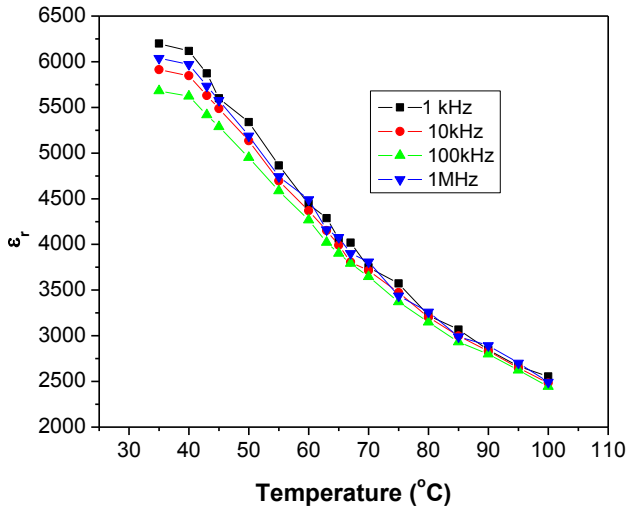

(d)

Fig. 5.17 Temperature variation of ε_r at different frequencies of sintered (a) BSmT1 (b) BSmT2 (c) BSmT3 & (d) BSmT4 samples.

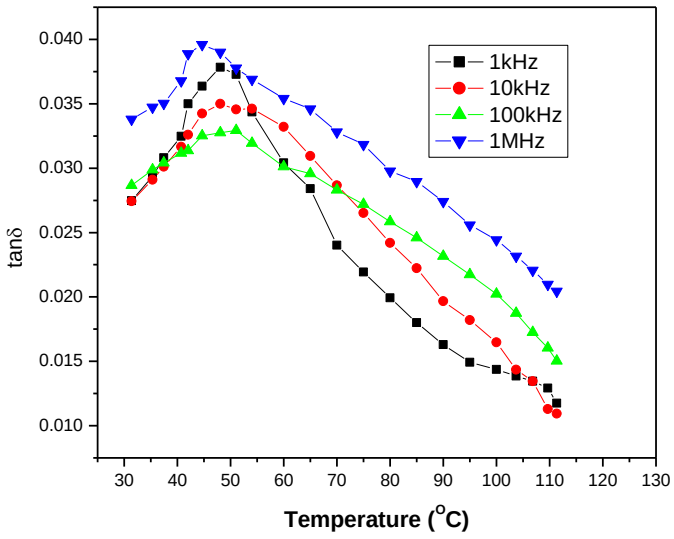

(a)

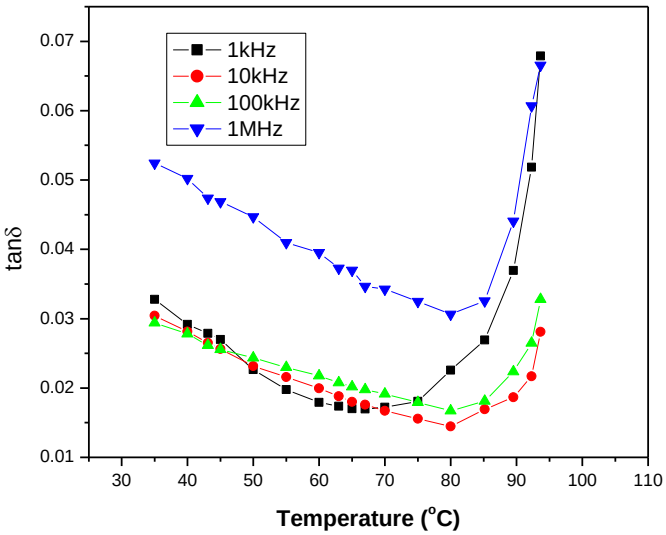

(b)

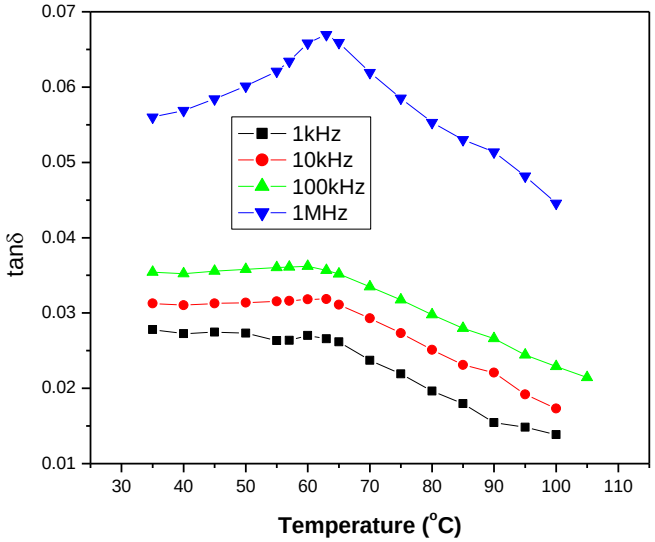

(c)

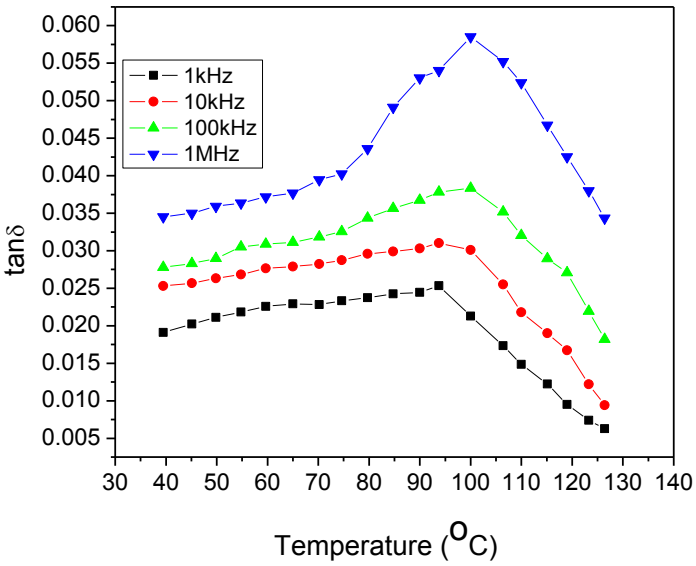

(d)

Fig. 5.18 Temperature variation of tanδ at different frequencies of sintered (a) BSmT1 (b) BSmT2 (c) BSmT3 & (d) BSmT4 samples.

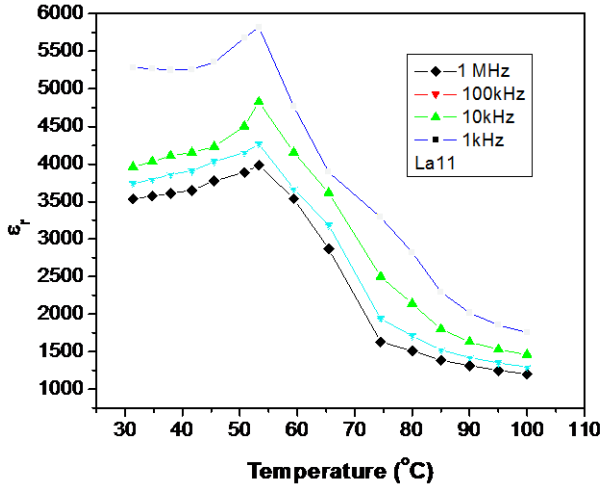

(a)

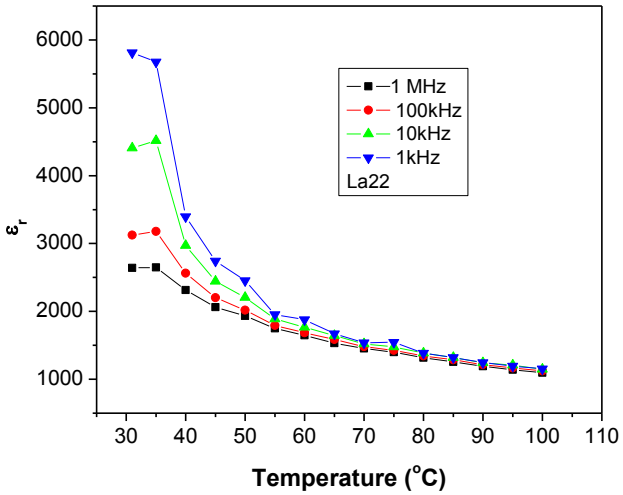

(b)

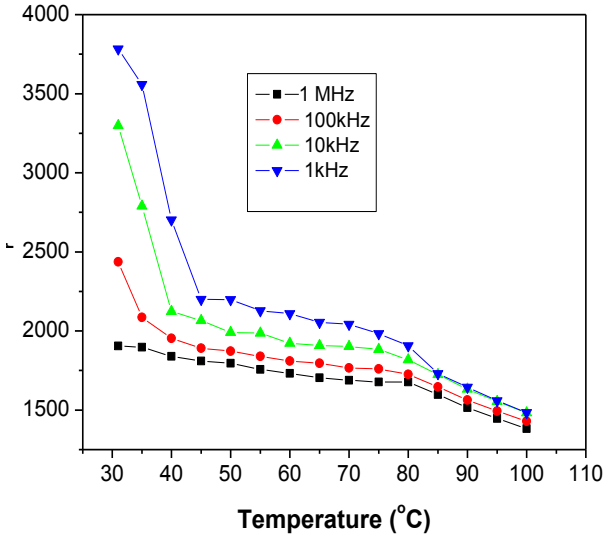

(c)

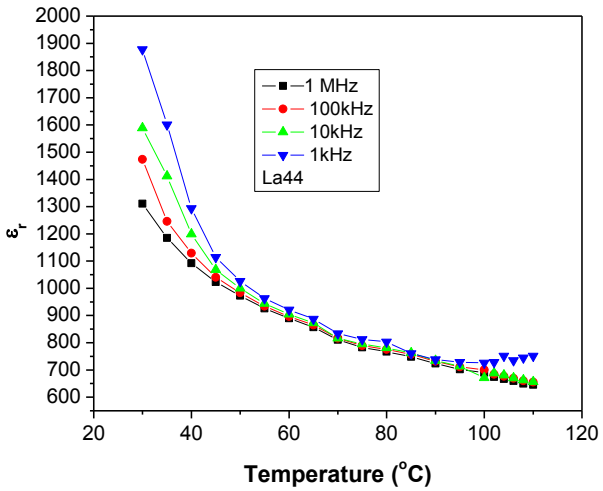

(d)

Fig. 5.19 Temperature variation of ε_r at different frequencies of sintered (a) BLT1 (b) BLT2 (c) BLT3 & (d) BLT4 samples.

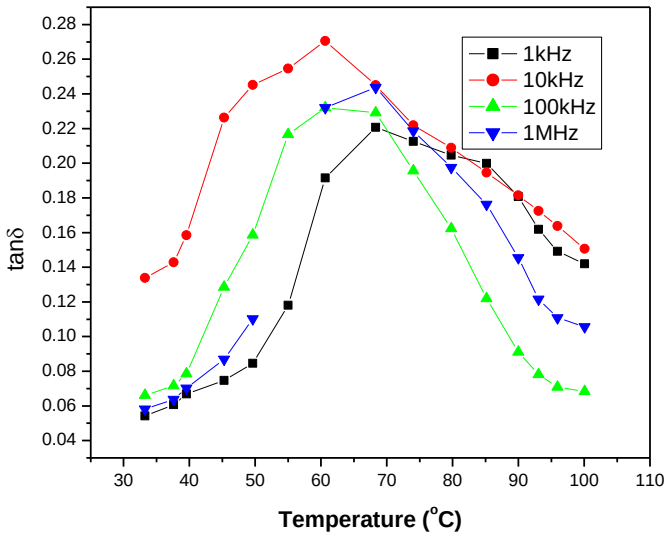

(a)

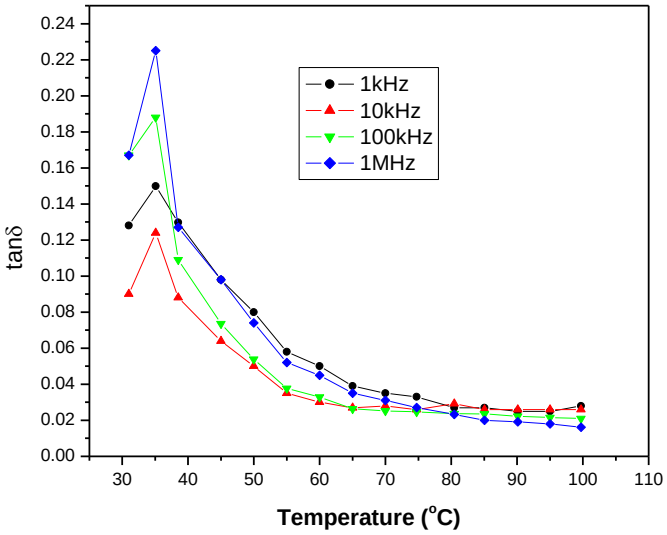

(b)

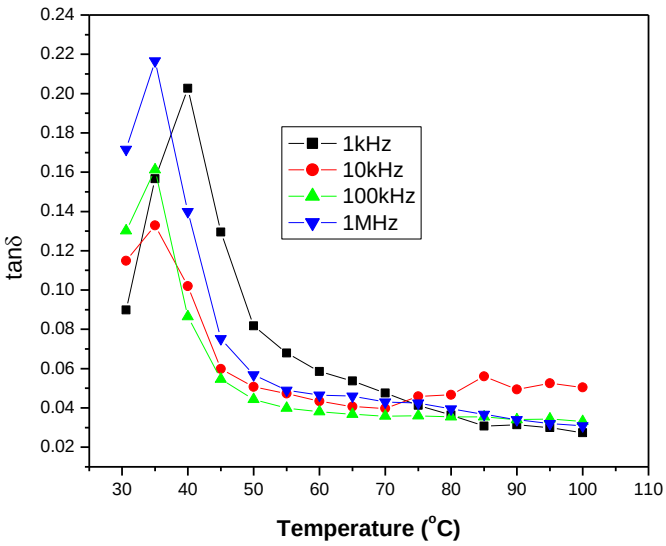

(c)

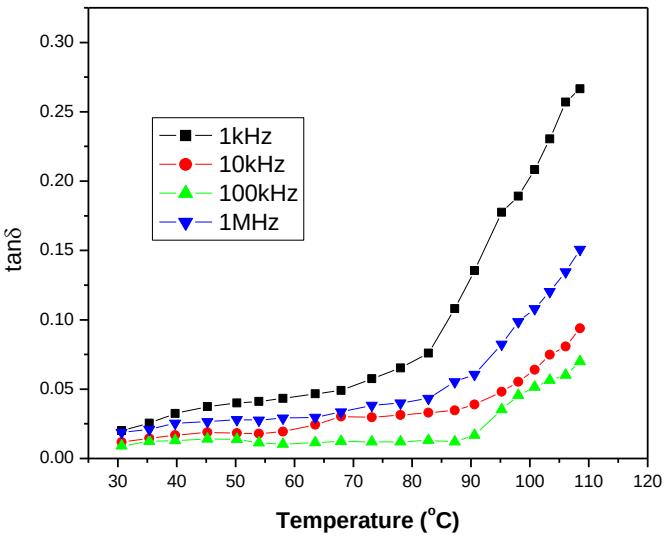

(d)

Fig. 5.20 Temperature variation of tanδ at different frequencies of sintered (a) BLT1 (b) BLT2 (c) BLT3 & (d) BLT4 samples

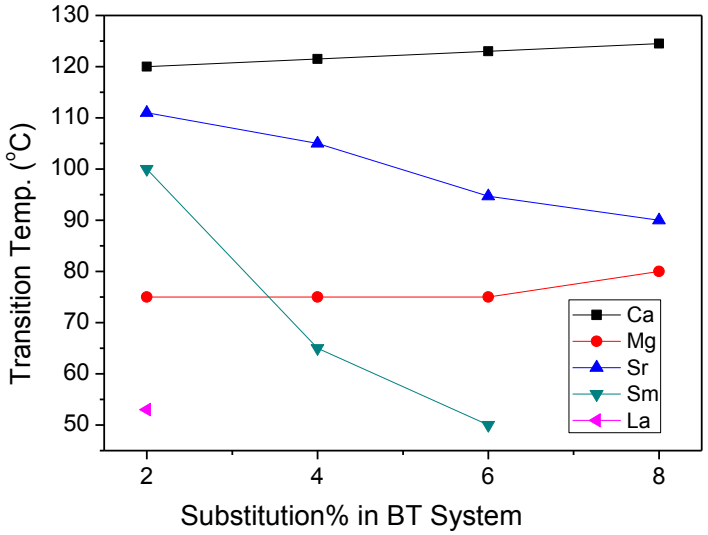

Fig. 5.21 Variation of T_c with iso-valent and off-valent substitution% in BT system.

5.2.3.1 Results & Discussion on Iso-valent Modified BT Samples:

Figs. 5.10-5.15 represent the temperature variation of ε_r and tanδ at different frequencies of iso-valent modified BT samples synthesized by modified solid state reaction route (MSSR). ε_r at different frequencies increases with the increase in temperature. ε_r of any material, in general, is influenced by dipolar, electronic, ionic and interfacial polarizations [34]. Interfacial polarization increases due to the creation of crystal defects and dipolar polarization decreases due to the increase in randomness of the dipoles with temperature. However, the temperature effect on ionic and electronic polarizations is very small [33]. The increase in ε_r with temperature suggests the increase in interfacial polarization in these materials.

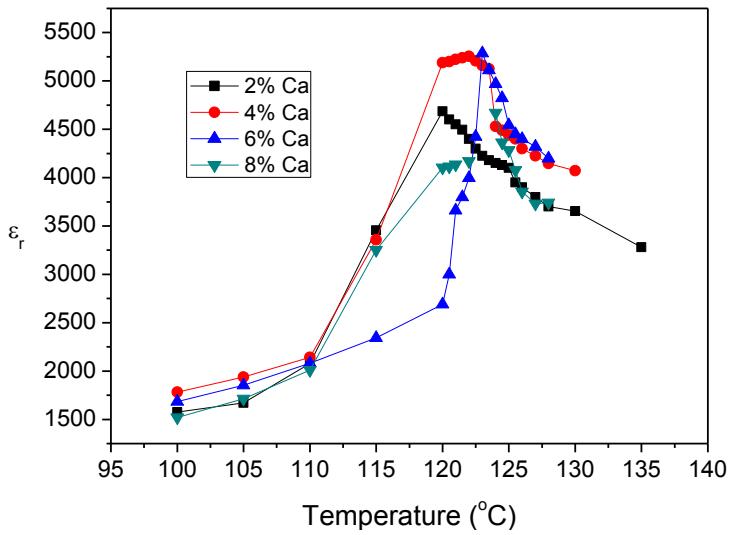

Fig. 5.22 Temperature variation of ε_r at 1kHz with different substitution% of Ca in BT system.

Fig. 5.11 & 5.12 represents the effect of variation of Ca ions substitution concentration and temperature on the dielectric properties of BT samples. The temperatures corresponding to maximum ε_r and where the structure of the material transform from non-cubic to cubic structure is known as Curie temperature (T_c) [14, 29, 36] . It can be seen from the Fig. 5.11 & Fig. 5.22 that with the increase of Ca substitution concentration in BT system the transition temperature increases. This can be explained on the basis of decrease of internal compressive stress with the increase in Ca substitution concentration in BCT system. Since, it is well established that internal compressive stress decreases with the increase of grain size [37], and here the grain size increases with the increase in Ca substitution concentration in BCT system [reported in Chapter 4]. As, transition temperature (T_c) is inversely proportional to internal compressive stress [38] therefore larger the grain size, less the internal compressive stress and higher the T_c. This is also supported by XRD study. With the increase of Ca substitution concentration in BT system, the tetragonality, determined by X-ray diffraction study, given in Table 4.2, increases. It is also well established that the increase in tetragonality leads to increase in T_c [14]. This explains the increase of T_c with the increase of Ca substitution concentration in BT system. The values of ε_r at 1kHz and at RT are given in Table 5.1. With the increase of Ca substitution concentration in BT system, the value of ε_r at RT first increases and then decreases beyond 0.04 substitution concentration. As, reported earlier, with the increase of Ca substitution concentration beyond 0.04, Ca can go to Ti sites, which would lead to creation of oxygen vacancies [39]. These oxygen vacancies would pins the movement of the ferroelectric domains walls and hence result in the decrease in dielectric constant [40]. Dielectric loss ($\tan\delta$) increases with the increase in temperature and there exists a max. peak around the T_c. It is observed that a higher value of $\tan\delta$ is obtained with increasing temperature which may be due to the increase in the mobility of ions and imperfections in the material [41].

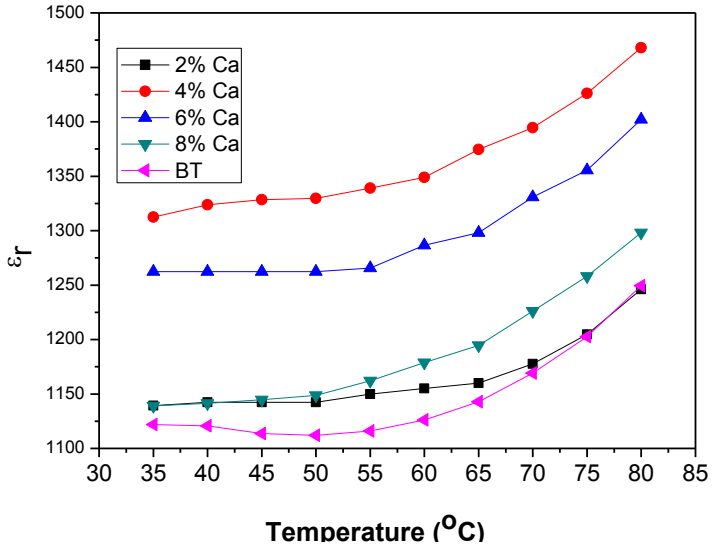

Fig. 5.23 Temperature variation of ε_r at 1kHz with different substitution% of Ca in BT system from room temp. to 80°C.

As can be seen in Fig. 5.23 that the temperature coefficient of capacitance from RT to 70°C in BCT1, BCT2 & BCT3 samples is almost negligible compare to unmodified BT samples, which signifies the importance of Ca modification in BT system for its use in multilayer capacitors [42].Figs. 5.13 - 5.16 represent the effect of variation of Mg and Sr ions substitution concentration on the dielectric properties of BT samples. With the increase of Mg ions substitution concentration the transition temperature (T_c) decreases to 75°C and does not decrease with the further increase in Mg ions substitution concentration. Whereas, with the increase of Sr ions substitution concentration in BT system, the position of T_c decreases gradually from 111 to 90°C. The same type of dielectric phenomena is observed in earlier repots on Mg and Sr ion substitution in BT system [15-17]. The decrease in T_c with the substitution of Mg ions in BT system is supported by the XRD study, where with the substitution of Mg ions in BT there is decrease of tetagonality and hence lowering of T_c. The decrease in T_c with the increase in substitution concentration of Sr ions in BT system is also supported by the XRD study, where with the increase in substitution concentration of Sr ions in BT there is decrease of tetagonality and hence lowering of T_c. The SEM study of Mg & Sr

ions substitution in BT system also supports the decrease in T_c. As reported in chapter 4, the average grain size decreases with the increase of Mg and Sr ions substitution concentration in BT system. As stated earlier, the internal compressive stress increases with the decreases of grain size [37]. Since, T_c is inversely proportional to internal compressive stress, therefore there is decrease of T_c in Mg and Sr substituted BT samples. With the increase of Mg and Sr ions substitution concentration in BT system, the value of ε_r at 1kHz & at RT increases (as given in Table 5.1). This is due to decrease in T_c. Lowering of T_c shifts the position of temperature corresponding to ε_{rmax}. towards the RT side and hence increase in ε_r at RT with the increase in Sr ions substitution concentration in BT system [14, 29].

5.2.3.2 Results & Discussion on Off-valent Modified BT Samples:

Figs. 5.17-5.20 represent the temperature variation of ε_r and tanδ at different frequencies of Sm and La ions substitution in BT samples synthesized by modified solid state reaction route (MSSR). As can be seen in Fig. 5.21, even the small amount of off-valent substitution (2%) in BT system is modifying the T_c to the larger extent. This agrees with the earlier report on off-valent substitution in BT system [19-22]. The ionic radii of Ba^{2+}, La^{3+}, and Sm^{3+} ions are 135, 117 and 110pm, respectively. Here, the La and Sm substitution reduces the lattice distortion, i.e., the *c*/*a* ratio as given in Table 4.2 [19, 20], and hence the T_C decreases with increase in La and Sm substitution concentration in BT system. This is expected since the ionic radius of La and Sm is smaller than that of Ba and confirmed by XRD study. With the 0.08 substitution concentration of Sm and 0.04, 0.06 and 0.08 substitution concentration of La, the T_c shifts below RT. This is as per earlier study on La and Sm ions substitution in BT system [19-22]. The value of ε_r at 1kHz at RT (given in Table 5.1) increases with the increase of Sm ion substitution from 2080 to 6214. Whereas in the case of La ions substitution in BT system, the value of ε_r at 1kHz at RT (given in Table 5.1) increases upto 0.04 substitution concentration and then decreases with the increase of La substitution

concentration in BT system**.** This is again due to decrease in T_c. Lowering of T_c shifts the position of temperature corresponding to ε_{rmax}. towards the RT and hence increase in ε_r at RT with the increase in Sm and La ions substitution concentration in BT system. Since in the case of 0.06 & 0.08 La ions substitution concentration in BT system, the T_c is far below RT, therefore the position of ε_{rmax}. lies far below RT and as we know above the transition temperature the ε_r decreases, giving rise to low value of ε_r at RT.

Dielectric loss (tanδ) increases with the increase in temperature in all the iso-valent and off-valent modified BT samples and there exists a max. peak of tanδ around the T_c. This increase in tanδ with temperature can be explained on the increase of mobility of ions leading to increase in a.c conductivity and hence increase in dielectric loss [41]. Creation of oxygen vacancies at higher temperature may also increase the dielectric loss at higher temperature [43, 44]. Temperature of max. tanδ of all the iso valent & off-valent ion substituted BT ceramics is different from temperature of max. ε_r, which is a characteristic of ferroelectric [29] materials. Kramers-Kronig relation indicates that this may be due to temperature dependent relaxation near Curie temperature [29].

5.2.4 Diffusivity Study

Broadening of phase transition in ceramics depends on the composition fluctuations and structural disorder [29]. In systems, where structural order is distributed due to the disturbance in the composition phase, transition is generally gradual and bandwidth depends on the degree of the disorder. ε_r of these type of materials in the paraelectric region obey the following quadratic equation [45]:

$$1/\varepsilon_r = 1/\varepsilon_{r\,max} + (T-T_{max.})^{\gamma} / C \qquad \ldots 5.1$$

rather than the Curie Weiss law [29, 45]. As per eqn. 5.1, $\gamma = 1$ corresponds to Ist order phase transition or sharp transitions and for diffuse phase transitions the value of γ is more than 1. In other words, for Ist order phase transition the value of $\varepsilon_{rmax.}$ is strongly temperature

dependent, whereas for diffuse phase transitions the $\varepsilon_{rmax.}$ dependence on temperature decreases. Generally, in multilayer capacitor (MLC) applications, the value of ε_r should be high with less temperature dependence. Therefore, more the transition of a dielectric material diffuse, more the material is suitable for MLC applications. Figs. 5.20 & 5.21 show the plots between log $(1/\varepsilon_r - 1/\varepsilon_{rmax.})$ versus log $(T-T_{max.})$ at 1kHz of iso-valent and off-valent modified BT samples. The nature of phase transition is ascertained by calculating the degree of diffusion (γ). Fitting ε_r at 1kHz in the region of $T > T_{max}$ in equation 5.1 and a graph between $\log(1/\varepsilon_r - 1/\varepsilon_{r\ max})$ versus $\log(T-T_{max})$ is plotted, as shown in Figs 5.24 & 5.25**.** Diffusivity factor (γ), calculated from the slopes of these plots in the higher temperature region are given in Table 5.2.

Diffusivity factor (γ) is increasing slightly with the increase of Ca substitution concentration in BT system., but remains near to 1, which represents normal phase transition [29, 45]. This establishes the good solubility of Ca in BT system [39] and as a result less compositional fluctuations. Whereas with the increase of Mg and Sr ions substitution concentration in BT system the value of γ factor increases, indicating the increase in diffusive nature of phase transition [29, 46]. Similarly, in case of Sm and La ions substitution, value of γ factor is more than 1 and indicates the diffuse phase transition nature of these modified BT systems [29, 46]. This diffuse phase transition nature in these compounds suggests the introduction of structural disorder and compositional fluctuations by modifications of Sr, Mg, Sm & La ions substitution in BT system [47]. The diffuse transition behaviour might be due to the larger probability of the Sr, Mg, Sm & La ions ions occupying the Ti ions site in modified BT system, eventually introducing larger compositional and structural disorder, which gives rise to diffuse phase transition [47, 48].

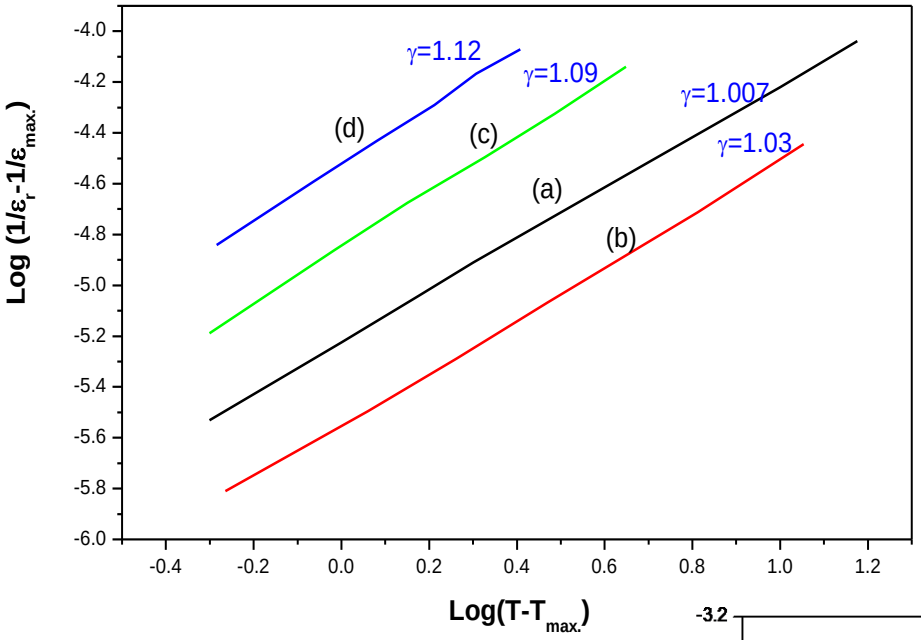

(i)

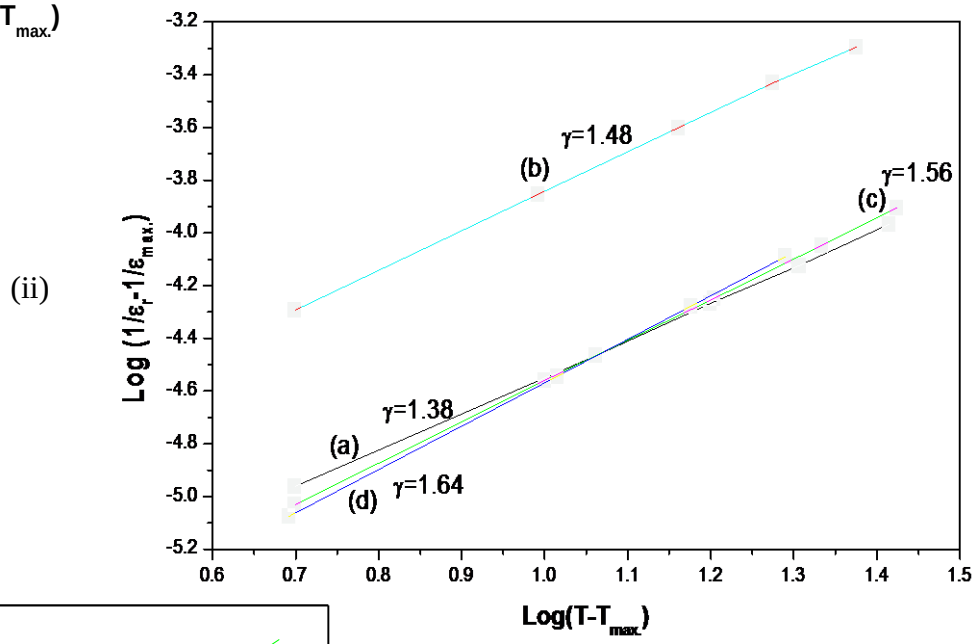

(ii)

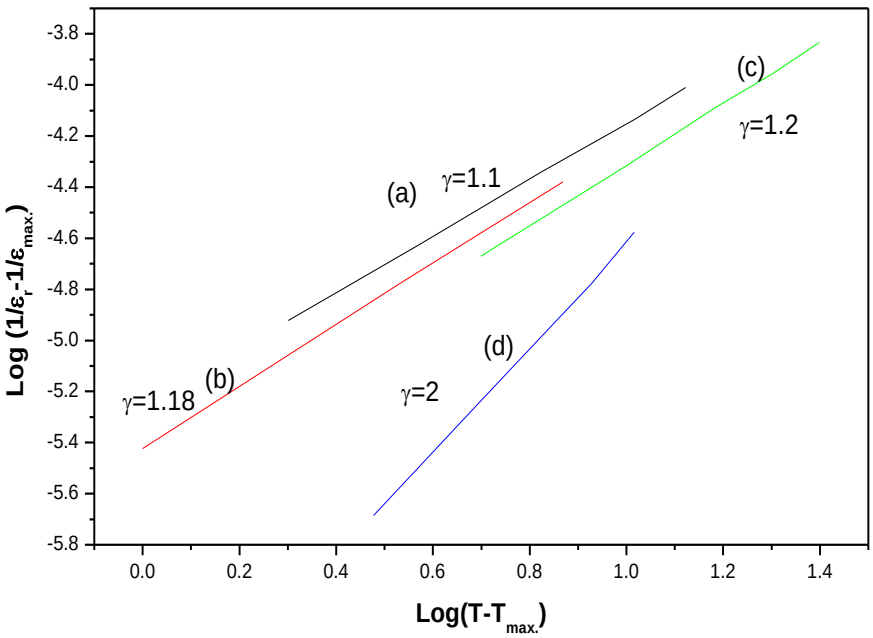

(iii)

Fig. 5.24 Variation of log($1/\varepsilon_r - /\varepsilon_{r\ max.}$) vs. log($T - T_{max}$) of (i) $Ba_{1-x}Ca_xTiO_3$(ii) $Ba_{1-x}Mg_xTiO_3$ (iii) $Ba_{1-x}Sr_xTiO_3$ samples., where x= (a) 0.02, (b) 0.04, (c) 0.06 & (d) 0.08.

(i)

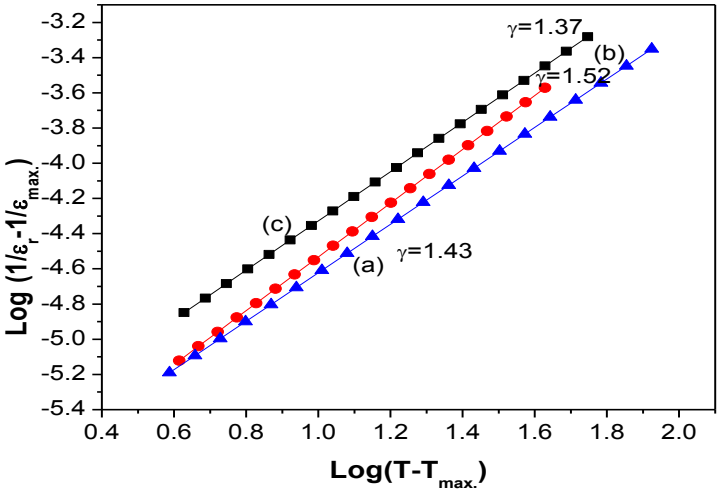

(ii)

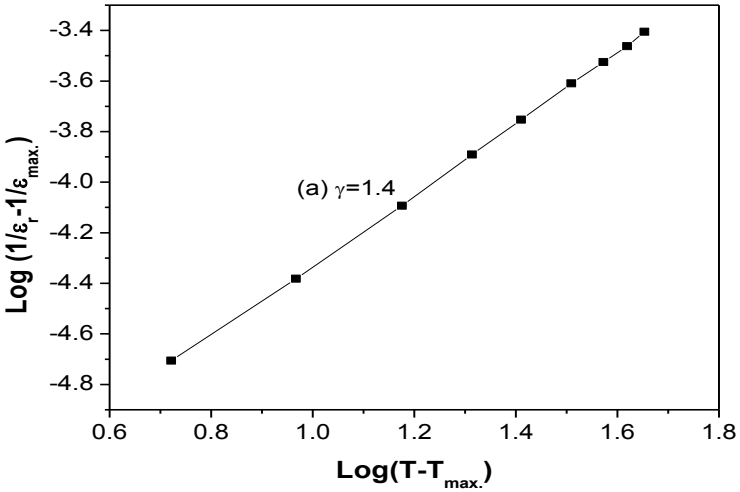

Fig. 5.25 Variation of $\log(1/\varepsilon_r - /\varepsilon_{r\ max.})$ vs. $\log(T - T_{max})$ of (i) $Ba_{1-x}Sm_xTi_{(1-x)/4}O_3$ & (ii) $Ba_{1-x}La_xTi_{(1-x)/4}O_3$ samples, where x= (a) 0.02, (b) 0.04, (c) 0.06 & (d) 0.08).

Table 5.2 Diffusivity factor (γ) of iso-valent and off-valent modified BT samples

System	**$B_{0.98}Ca_{0.02}TiO_3$**	**$Ba_{0.96}Ca_{0.04}TiO_3$**	**$Ba_{0.94}Ca_{0.06}TiO_3$**	**$Ba_{0.92}Ca_{0.08}TiO_3$**
γ	**1.003**	**1.07**	**1.09**	**1.12**
System	**$Ba_{0.98}Mg_{0.02}TiO_3$**	**$Ba_{0.96}Mg_{0.04}TiO_3$**	**$Ba_{0.94}Mg_{0.06}TiO_3$**	**$Ba_{0.92}Mg_{0.08}TiO_3$**
γ	**1.38**	**1.48**	**1.56**	**1.64**
System	**$Ba_{0.98}Sr_{0.02}TiO_3$**	**$Ba_{0.96}Sr_{0.04}TiO_3$**	**$Ba_{0.94}Sr_{0.06}TiO_3$**	**$Ba_{0.92}Sr_{0.08}TiO_3$**
γ	**1.1**	**1.18**	**1.2**	**2**
System	**BSmT1**	**BaSmT2**	**BSmT3**	**BSmT4**
γ	**1.43**	**1.52**	**1.37**	**-**
System	**BLT1**	**BLT2**	**BLT3**	**BLT4**
γ	**1.4**	**-**	**-**	**-**

References

1. F. Chaput, J. P. Boilot, M. Lejeune, R. Papiernik, L. G. H. Pfalzgraf, J. Am. Ceram. Soc., **72** (1989) 1355.
2. K. R. Han, S. Kim, H. J. Joo, J. Am. Ceram. Soc., **81** (1989) 2998.
3. K. Kusumoto, T. Sekiya, Mater. Res. Bulletin, **33** (1998) 1367.
4. T. Yamamoto, K. Okazaki, J. Am. Ceram. Soc., **69** (1986) 188.
5. K. Uchino, Ferroelectric Devices, Marcel Dekker, New York (2000).
6. S.E. Park ,T.R. Shrout, J. Appl. Phys., **82** (1997) 1804.
7. Y. H. Chen, S. Hirose, D. Viehland, S. Takahashi and K. Uchino, Jpn. J. Appl. Phys., **39** (2000) 4843.
8. Q. Jia, B. Shen, X. Hao, S. Song, J. Zhai, Materials Letters, **63** (2009) 464.
9. C. Zhou, X. Liu, W. Li, C. Yuan, Mater. Chem. Phys., **114** (2009) 832.
10. Y. Saito, H. Takao, T. Tani, T. Nonoyama, K. Takatori, T. Homma, T. Nagaya, M. Nakamura, Nature, **432** (2004) 84.
11. M. Suzuki, H. Nagata, J. Ohara, Jpn. J. Appl. Phys., **42** (2003) 6090.
12. T. Sawada, A. Ando, Y. Sakabe, D. Damjanovic, Jpn. J. Appl. Phys., **42** (2003) 6094.
13. C.R. Zhou, X.Y. Liu, Mater. Chem. Phys., **108** (2008) 413.
14. B. Jaffe, W.R. Cook , H. Jaffe, Piezoelectric ceramics, Academic Press, London (1971).
15. N. J. Ridha, W. M. M. Yunus, S.A. Halim, Z.A. Talib, F. K. Mohamad Al-Asfoor, W. C. Primus, American J. of Engineering & Applied Sciences, **2**(4) (2009) 661.

16 A. G. Belous, O. I. V'yunov, L. L. Kovalenko, V. Buscaglia, M. Viviani, P. Nanni, Inorganic Materials, **39**(2) (2003) 133.

17. T. Nagai, K. Iijima, H. J. Hwang, M. Sando, T. Sekino, K. Niihara, J. American Ceramic Society, **83** (2000) 107.
18. R. C. Pullar, Y. Zhang, L. Chen, S. Yang, J. R. G. Evans, A. N. Salak, D. A. Kiselev, A.L. Kholkin, V. M. Ferreira, N. M. Alford, J Electroceram., **22** (2009) 245.
19. F. D. Morrison, D.C. Sinclair, A. R. West, Int. J. of Inorg. Mater., **3**(2001) 1205.
20. R. Zhang,† J. F. Li, D. Viehland, J. Am. Ceram. Soc., **87** [5] (2004) 864.
21. Y. Li, Y. Qu, Materials Research Bulletin, **44** (2009) 82.
22. B.D.Stojanović, V.R.Mastelaro, C.O. Paiva Santos, J.A.Varela, Science of Sintering, **36** (2004) 179.
23. H. Xu, L. Gao**,** Materials Lettes, **58** [10] (2004) 1582.
24. Y. Xie, S. Yin, T. Hashimoto, Y. Tokano, Savakis, T. Sato, Materials Research Bulletin, **45** [10] (2010) 1345.

25. F.D. Morrison, D.C. Sinclair and A.R.West, J. Appl. Phys., **86** (1999) 6355.
26. F.D. Morrison, D.C. Sinclair, A.R. West, Int. J. Inorg. Mater. **3** (2001) 1205.
27. M. Aparna, T. Bhimasankaram, S.V. Suryanarayana, G. Prasad, G.S. Kumar, Bull. Mater. Sci., **24** (5) (2001) 497.
28. P. Yongding, L. Yunhe, Y. Wenhu, J. Rare Earths, **25** (2007) 167.
29. M. E. Lines, A. M. Glass, Principles and Applications of Ferroelectrics and Related Materials, Oxford, Clarendon (1979).
30. D.J. Griffiths, Introduction to Electrodynamics , 3rd edition, Prentice Hall (1998).
31. A. K. Singh, T. C. Goel, R. G. Mendiratta, O. P. Thakur, C.Prakash, J. Appl. Phys., **91** (2002) 6626.
32. Y. Kumar, Md. A. Mohiddon, A. Srivastava, K. L. Yadav, Indian J. Engg. Mat., **16** (2009) 390.
33 C. Kittel, Introduction to Solid State Physics, 7th Edition, John Wiley & sons, New York (1995).
34 I. Bunget, M. Popescu, Physics of Solid Dielectrics, Elsevier, New York (1984).
35 S. Chopra, S. Sharma, T. C. Goel, R. G. Mendiratta, Appl. Sur. Sci., **230** (2004) 207.
36 K. Tkacz-Śmiech, A. Koleżyński, W. S. Ptak, Solid State Comm., **127** (2003) 557.
37 F. J. Chen, Y. N. Pan, C. Y. Lee, C. S. Lin, J. Electrochem. Soc., **157** [3] (2010) D154.
38. T. Sun, X. Wang, H. Wang, X. Zhang, Z. Cheng, J. American Ceramic Society **93** [9] (2010) 2571.
39. R. C. Pullar, Y. Zhang, L. Chen, S. Yang, J. R. G. Evans, A. N. Salak, D. A. Kiselev, A.L. Kholkin, V. M. Ferreira, N. M. Alford, J Electroceram (2009) 22:245
40. Y. Li, Y. Qu, Materials Research Bulletin, **44** [1] (2009) 82.

40. P. Kumar, S. Singh, O.P. Thakur, C Prakash, T.C. Goel, J. J. Appl. Phys., **43** (2004) 1501.
41. N. Baskaran, H. Chang, Mater. Chem. Phys., **77** (3) (2002) 889
42. M. Raghavender, G S. Kumar, G Prasad, Indian J. Pure & applied Physics, **44** (2010)
43. S. Jain, A. K. Jha, J. Electroceram., **24** (2010) 58.
44. M. Kuwabara, S. Takahashi, K. Goda, K. Watande, Jpn. J. Appl. Phys., **31** (1992) 3241
45. G. H. Heartling, J. Amer. Ceram. Soc., **82** (1999) 797.
46. N. Setter, L.E. Cross, J. Mat. Sci., **15** (1980) 1573.
47. L. E. Cross, Ferroelectrics, **76** (1987) 241.

CHAPTER VI

FERROELECTRIC & STRAIN vs. ELECTRIC FIELD PROPERTIES OF MODIFIED BT SYSTEMS

6.1 Introduction

Polarization vs. electric field (P-E) hysteresis loop is an important property of a ferroelectric material. High value of remanant polarization, P_r, with low coercive field, E_c, is required for non-volatile ferroelectric random access memory (NVFRAM) applications [1-3]. In this chapter, effect of synthesis route and iso-valent/off-valent ions substitution in BT system on the development of P-E hysteresis loops have been discussed. Strain induced by electric field behavior of modified BT samples has also been discussed.

6.2 Ferroelectric Properties

In this section, the polarization versus electric field (P-E) hysteresis loop properties of unmodified BT samples synthesized by SSR & MSSR routes have been discussed. This follows the(P-E) hysteresis loop properties of modified BT systems synthesized by MSSR route.

6.2.1 Ferroelectric Properties of BT Systems Synthesized by SSR & MSSR Routes:

Fig. 6 (a) & (b) shows the P–E hysteresis loops of BT samples synthesized by SSR and MSSR route, respectively. Development of P-E hysteresis loops confirms the ferroelectric nature of BT samples. Values of remnant polarization (P_r) and coercive filed (E_c) of BT samples synthesized by SSR route are ~3μC/cm^2 and 3.55kV/cm. Whereas, remnant polarization (P_r) and coercive fields (E_c) of the BT samples synthesized by MSSR route are ~5μC/cm^2 and 2.1kV/cm. High value of P_r in the BT samples synthesized by MSSR route may be related to the better crystalline, larger grain size and larger tetragonality (c/a ratio, mentioned in Chapter 4) nature. Large grain size can results in large size of the domains as

latter can grow easily inside a grain [4]. Higher value of E_c of BT samples synthesized by SSR route may be due to smaller grain size of the samples (reported in Chapter 4) as compared to the same system synthesized by MSSR route [4].

(a)

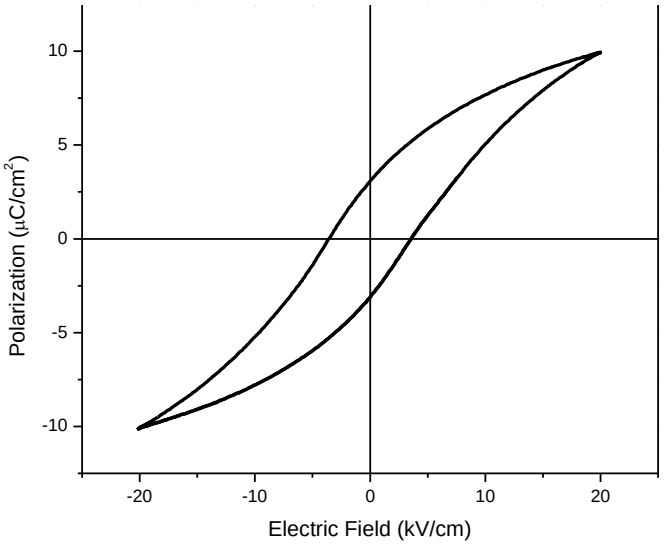

(b)

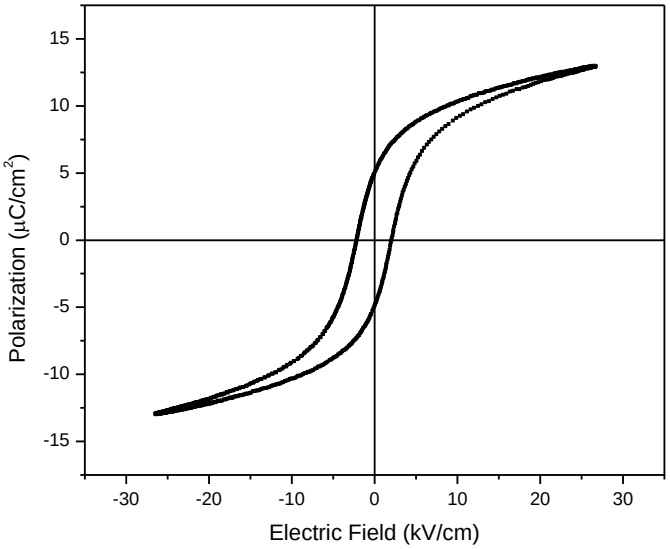

Fig. 6.1. P-E Hysteresis loops of BT samples synthesized by (a) SSR and (b) MSSR routes.

6.2.2 Ferroelectric Properties of Modified BT Systems synthesized by MSSR:

In this section, the polarization versus electric field (P-E) hysteresis loop properties of modified BT systems synthesized by MSSR has been discussed.

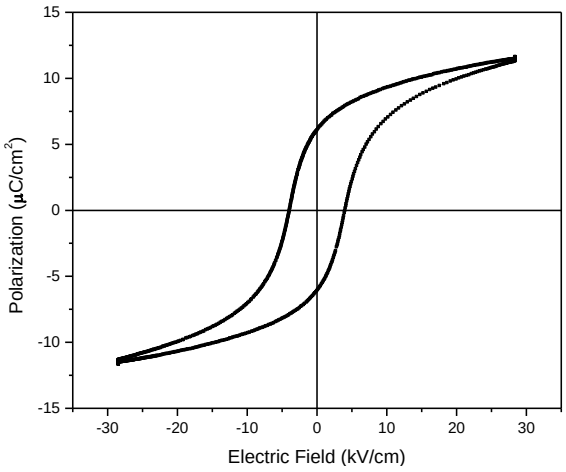

(a)

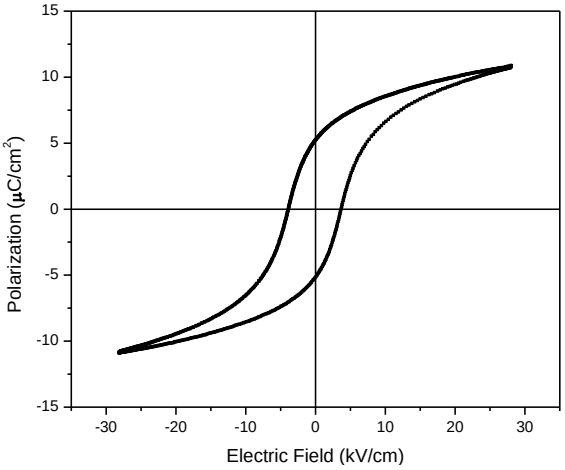

(b)

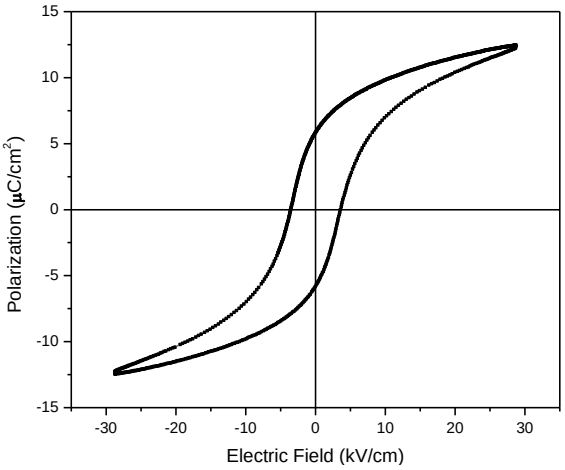

(c)

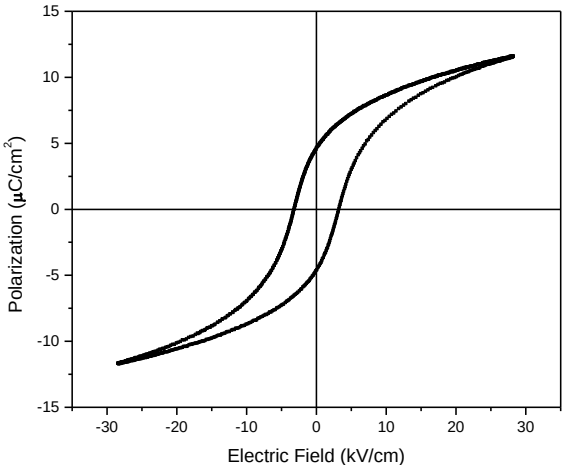

(d)

Fig. 6.2. P-E Hysteresis loops of (a) $Ba_{0.98}Ca_{0.02}TiO_3$ (b) $Ba_{0.96}Ca_{.0.04}TiO_3$ (c) $Ba_{0.94}Ca_{0.06}TiO_3$ & (d) $Ba_{0.92}Ca_{0.08}TiO_3$ samples

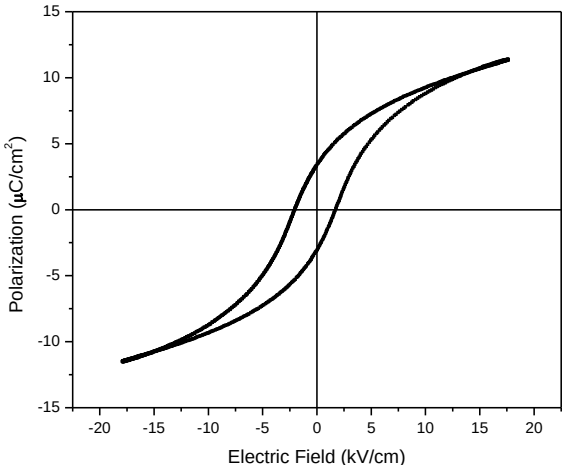

(a)

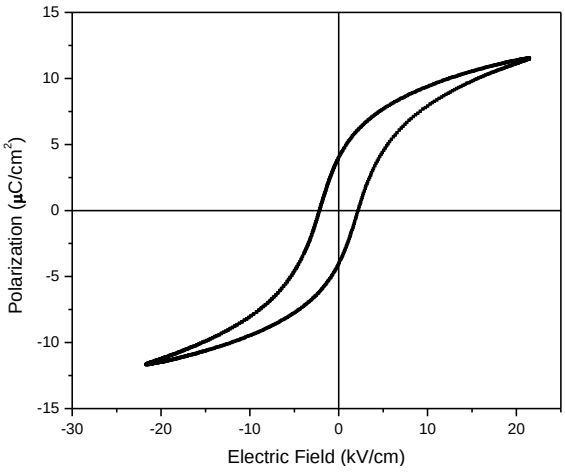

(b)

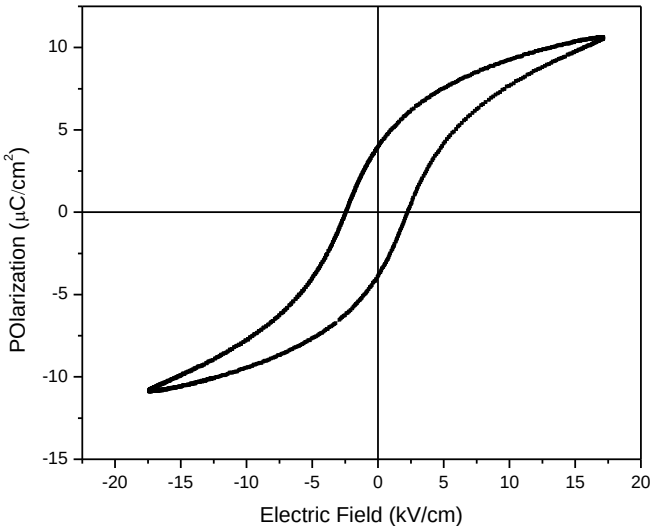

(c)

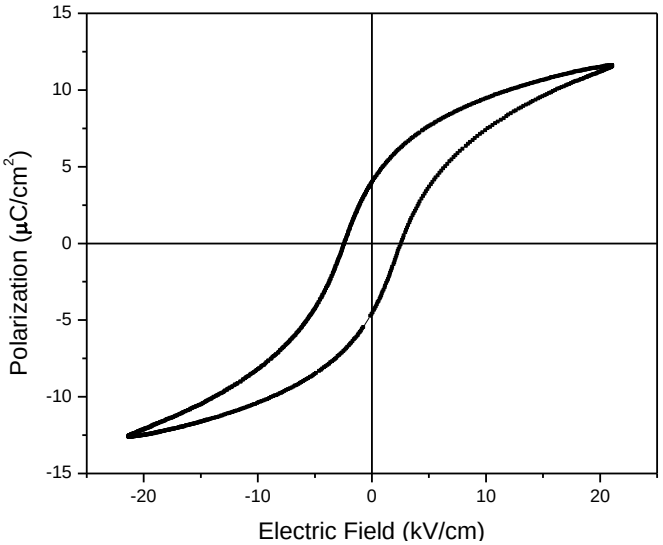

(d)

Fig. 6.3. P-E Hysteresis loops of (a) $Ba_{0.98}Sr_{0.02}TiO_3$ (b) $Ba_{0.96}Sr_{.0.04}TiO_3$ (c) $Ba_{0.94}Sr_{0.06}TiO_3$ & (d) $Ba_{0.92}Sr_{0.08}TiO_3$ samples.

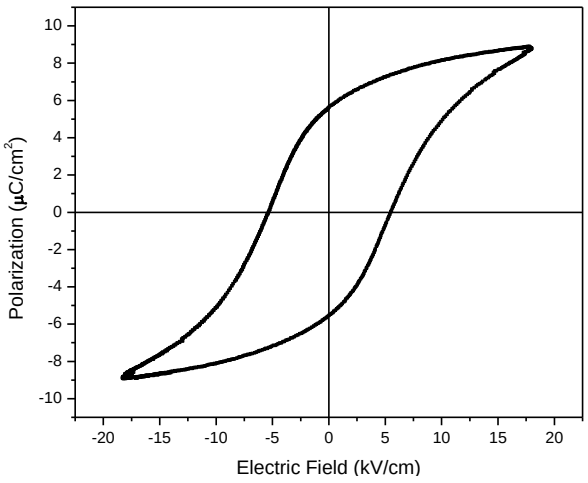

(a)

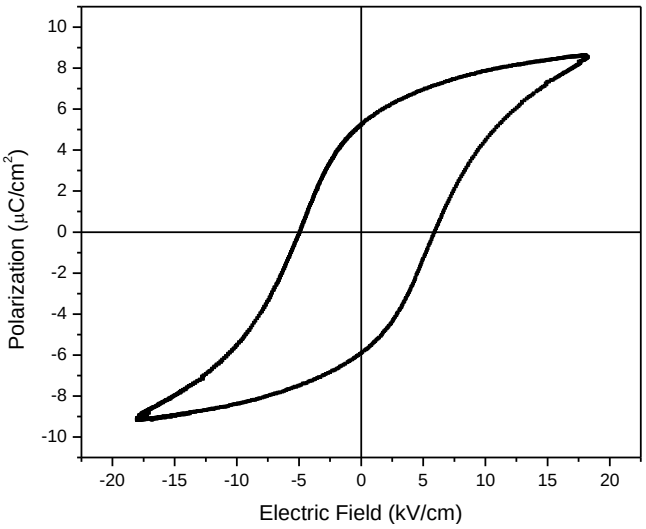

(b)

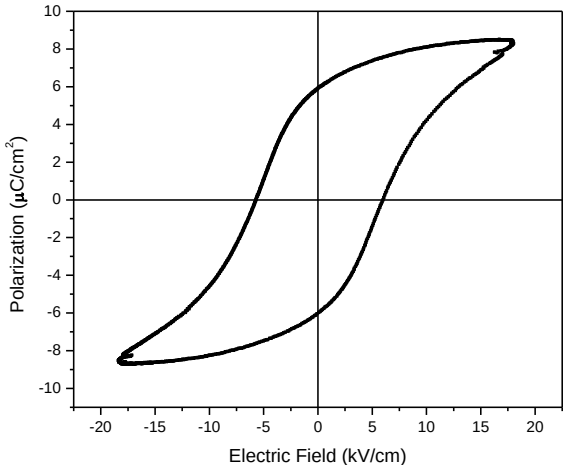

(c)

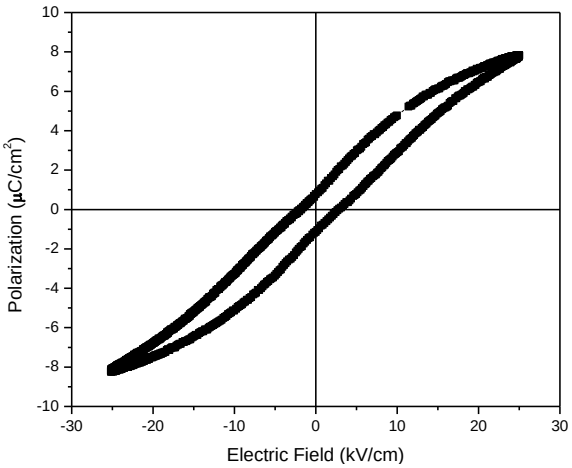

(d)

Fig. 6.4. P-E Hysteresis loops of (a) $Ba_{0.98}Mg_{0.02}TiO_3$ (b) $Ba_{0.96}Mg_{.0.04}TiO_3$ (c) $Ba_{0.94}Mg_{0.06}TiO_3$ & (d) $Ba_{0.92}Mg_{0.08}TiO_3$ samples.

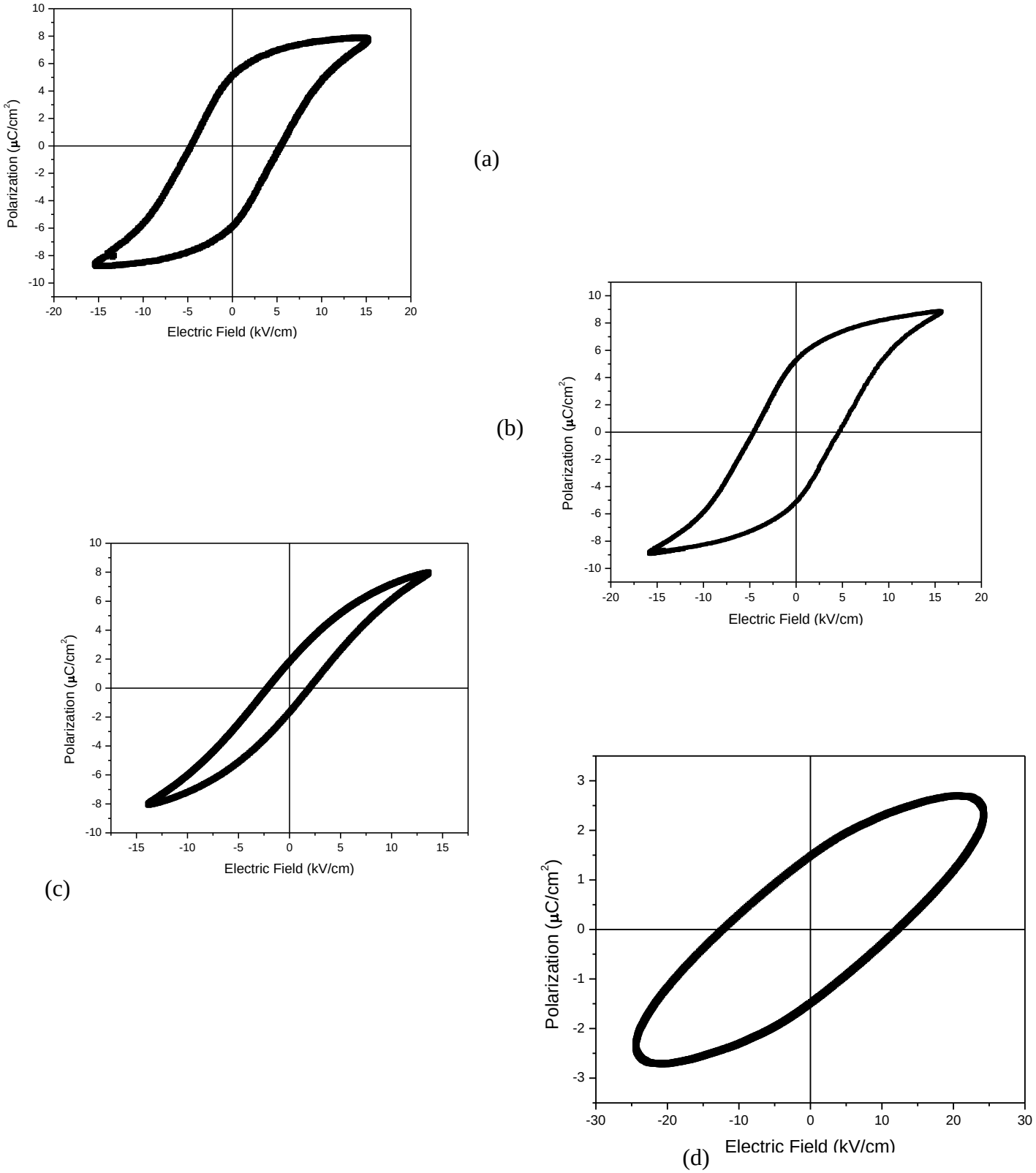

Fig. 6.5. P-E Hysteresis loops of (a) BSmT1 (b) BSmT2 (c) BSmT3 & (d) BSmT4 samples

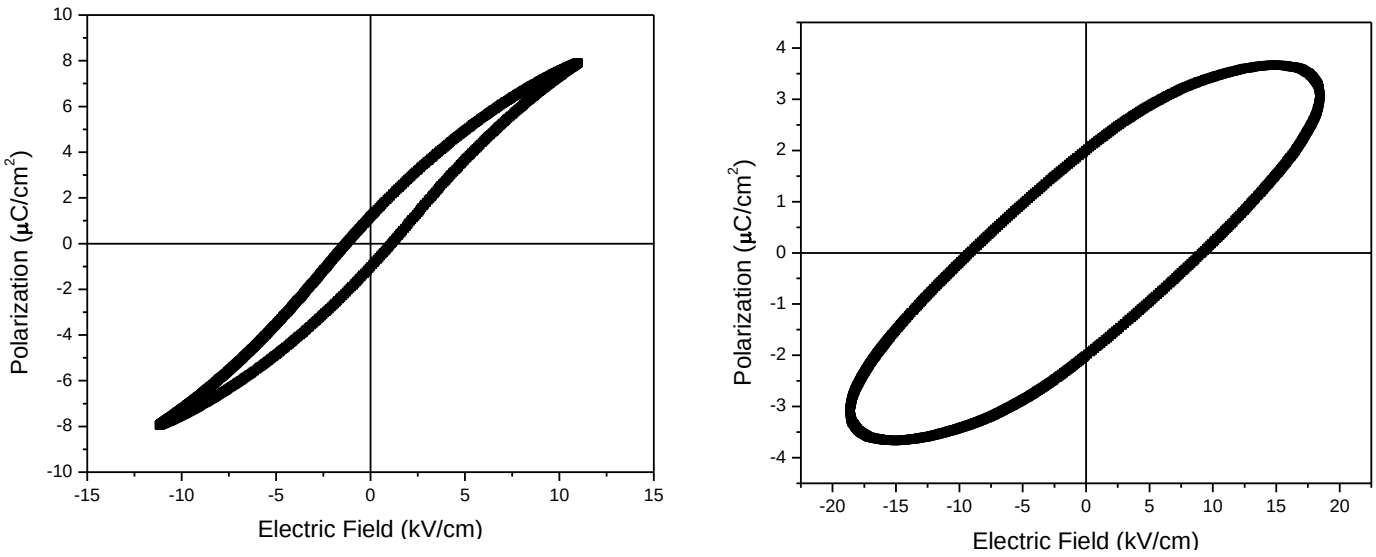

(a) (b)

Fig. 6.6. P-E Hysteresis loops of (a) BLT1 & (b) BLT2 samples.

Polarization vs. electric field (P-E) loops were observed for all the iso-valent and off-valent modified BT systems synthesized by MSSR route except for the La and Sm modified BT samples having centro-symmetric structures. The results are shown in Figs. 6.2-6.6. Well-defined ferroelectric behaviour is observed. The values of coercive field (E_c) and remnant polarization (P_r) were determined from the P-E loops and are given in Table 6.1 for the samples of Ca, Sr, Mg, Sm and La ion substituted BT samples. The results of E_c and P_r are correlated with the average grain size and the amount of substituent, respectively.

Fig. 6.2 represents the effect of variation of Ca ions substitution concentration on the ferroelectric properties of BT samples. Value of P_r of Ca substituted BT samples for $x \leq 0.06$ are above the unmodified BT samples. This decrease of P_r beyond $x>0.06$ can be explained as mentioned earlier. As mentioned in related to dielectric study of Ca modified BT samples, with the increase of Ca substitution concentration beyond 0.06, Ca can go to Ti sites, which would lead to creation of oxygen vacancies [5]. These oxygen vacancies would

pins the movement of the ferroelectric domains walls and hence result in the decrease in P_r [6].

Table 6.1 Variation of coercive field, E_c (kV/cm), remnant polarization, P_r ($\mu C/cm^2$) & saturated polarization Ps ($\mu C/cm^2$) with different x.

	E_c (kV/Cm)				P_r ($\mu C/cm^2$)				P_s ($\mu C/cm^2$)			
$Ba_{1-x}Ca_xTiO_3$	x				x				x			
	1	2	3	4	1	2	3	4	1	2	3	4
	3.95	3.66	3.56	3.30	6.1	5.24	5.87	4.61	11.42	10.8	12.35	11.65
$Ba_{1-x}Sr_xTiO_3$	x				x				x			
	1	2	3	4	1	2	3	4	1	2	3	4
	1.88	2.16	2.45	2.94	3.23	4	3.8	3.7	11.45	11.6	9.25	12.11
$Ba_{1-x}Mg_xTiO_3$	x				x				x			
	1	2	3	4	1	2	3	4	1	2	3	4
	5.52	5.91	5.96	2.28	5.62	5.25	5.92	0.93	8.8	8.55	8.33	8.04
$Ba_{1-x}Sm_xTi_{(1-x/4)}O_3$	x				x				x			
	1	2	3	4	1	2	3	4	1	2	3	4
	5.05	4.60	2.05	2.83	5.51	5.20	1.85	0.73	8.36	8.86	8.03	4.78
$Ba_{1-x}La_xTi_{(1-x/4)}O_3$	x				x				x			
	1	2	3	4	1	2	3	4	1	2	3	4
	1.19	2.32			1.10	2.05			7.93	4.49		

Fig. 6.3 represents the effect of variation of Sr ions substitution concentration on the ferroelectric properties of BT samples. Value of P_r of is nearly same for all the samples but less than unmodified BT samples. Fig. 6.4 represents the effect of variation of Mg ions

substitution concentration on the ferroelectric properties of BT samples. Value of P_r of all the samples except x=0.08 are higher than unmodified BT samples. For x=0.08, the P-E loop has shirked and moving towards antiferroelctric type P-E hysteresis loop [7].

For iso-valent modified BT samples, it can be seen that there is a decrease in the value of coercive field (E_c) with the increase of Ca ion substitution and there is a increase in the value of coercive field (E_c) with the increase of Sr & Mg ion substitution in BT systems. This behaviour can be explained with the average grain size variation (values given in Table 4.4). It is well reported in the literature that with increase in grain size, E_c decreases [8]. This explains the decrease of E_c and increase of E_c with the increase of Ca & Sr, Mg substitution concentration in BT system, respectively, since average grain size increase and decreases with the increase of Ca & Sr, Mg substitution concentration in BT system (reportetd in Chapter 4).

Figure 6.5 shows the (P-E) loops of Sm modified BT samples. Here, development of well saturated ferroelectric hysteresis loops for $x \leq 0.06$ hint towards the ferroelectric nature of the Sm modified BT samples. The (P-E) loop for X=0.08 hints towards the non-ferroelectric nature of the sample, which is supported by XRD and dielectric study. XRD study shows the centro-symmetric structure for x=0.08 (Table 4.2) whereas, dielectric study hints towards that the transition temperature for x=0.08 sample is below RT. We know, if the T_c of a material is below RT then its P-E loop will be representing the non-ferroelectric nature of the sample [9, 10].

Figure 6.6 shows the (P-E) loops of La modified BT samples. Here, development of well saturated ferroelectric hysteresis loops for x=0.02 hint towards the ferroelectric nature of sample. The (P-E) loop for x=0.04 hints towards the non-ferroelectric nature of the sample, which is supported by XRD and dielectric study. XRD study show the centro-symmetric structure for x=0.04, 0.06 & 0.08 (Table 4.2) samples whereas, dielectric study

hints towards that the transition temperature (T_c) for x=0.04, 0.06 & 0.08 sample is below room temperature. Since a material is ferroelectric below T_c [9]. Therefore when the T_c is below RT, there will be no saturated P-E hysteresis loop [9] as confirmed by the above study.

6.3 Strain induced by Electric Field Behavior of Modified BT Samples

In this section, strain induced by bi-polar electric field behavior of modified BT samples synthesized using MSSR route has been discussed.

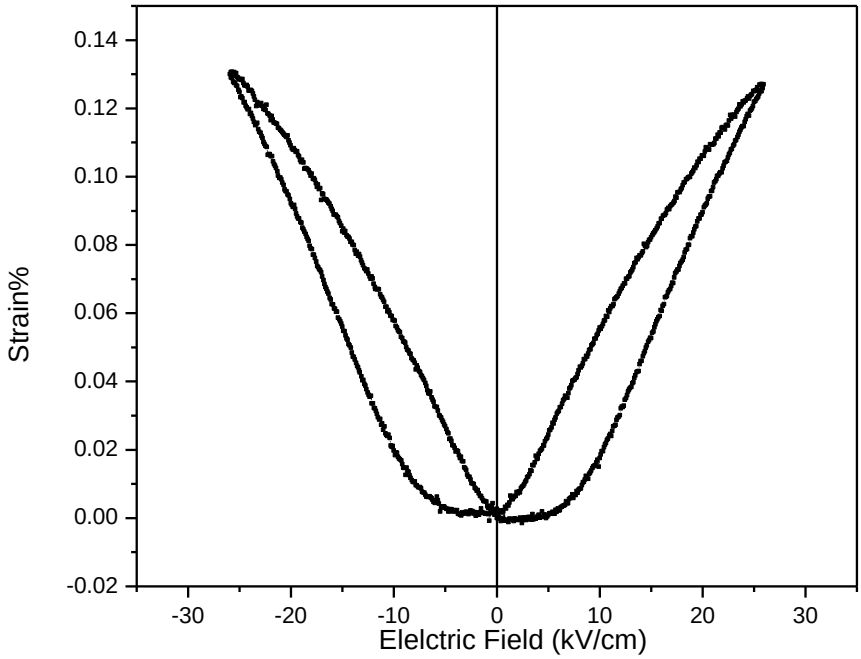

Fig. 6.7 Strain versus bipolar electric field loop of BT samples.

Fig. 6.7 shows the development of S-E butterfly loop with a max. strain `0.13% at 25kV/cm & confirms the piezoelectric nature of the BT samples synthesized by MSSR route [11-27]. Piezoelectric coefficient, d_{33}, has been calculated from converse piezoelectric effect, i.e by using the slope of the strain vs. electric field plot in the higher field region, using the relation [28]

$$d_{33} = (\Delta\text{strain\%} / \Delta\text{Electric field at higher side}) \quad \ldots 8.1$$

The d_{33} piezoelctric coefficient calculated from the slope of strain vs. electric field plot is found to be 335pC/N.

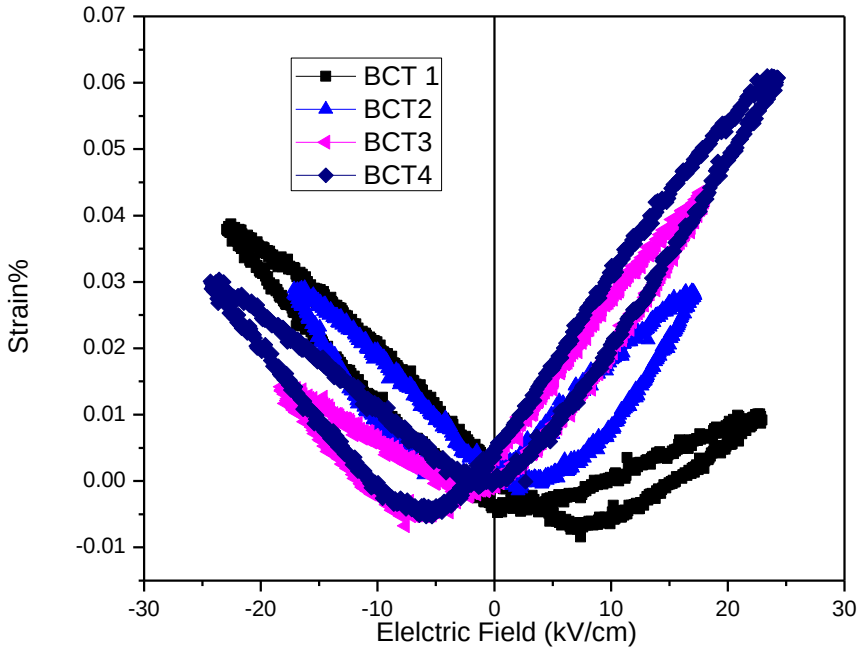

Fig. 6.8 Strain versus bipolar electric field loop of (a) $Ba_{0.98}Ca_{0.02}TiO_3$ (b) $Ba_{0.96}Ca_{.0.04}TiO_3$ (c) $Ba_{0.94}Ca_{0.06}TiO_3$ & (d) $Ba_{0.92}Ca_{0.08}TiO_3$ samples

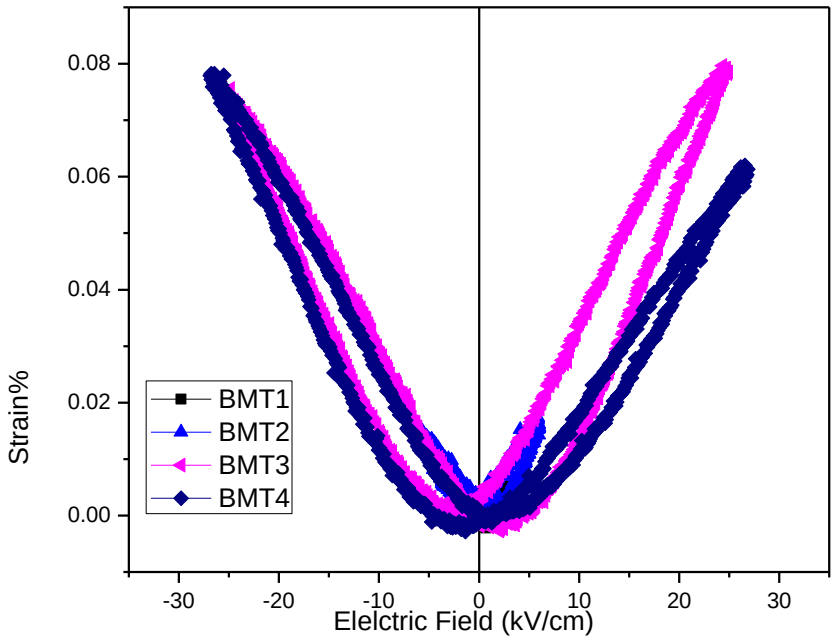

Fig. 6.9 Strain versus bipolar electric field loop of (a) $Ba_{0.98}Mg_{0.02}TiO_3$ (b) $Ba_{0.96}Mg_{.0.04}TiO_3$ (c) $Ba_{0.94}Mg_{0.06}TiO_3$ & (d) $Ba_{0.92}Mg_{0.08}TiO_3$ samples.

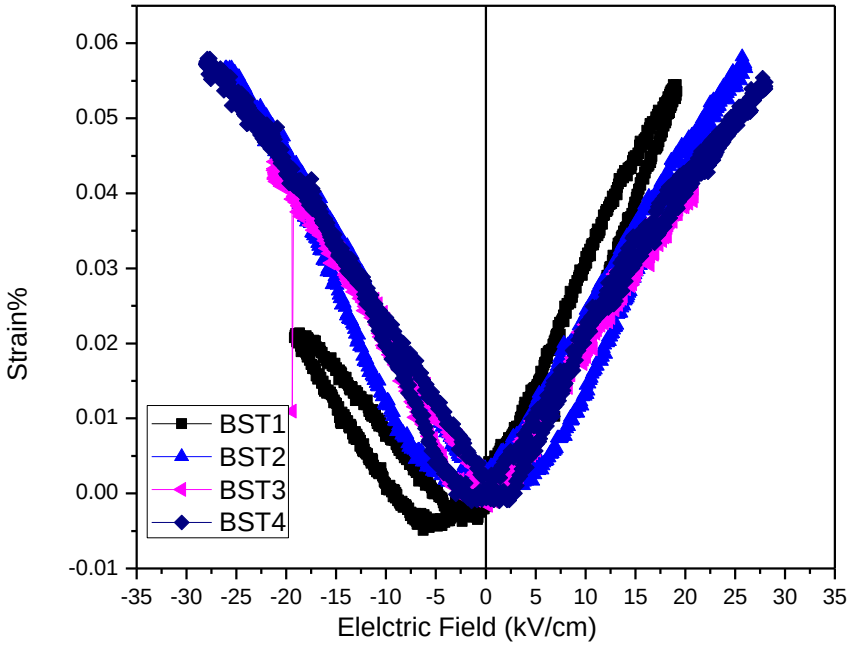

Fig. 6.10 Strain versus bipolar electric field loop of (a) $Ba_{0.98}Sr_{0.02}TiO_3$ (b) $Ba_{0.96}Sr_{.0.04}TiO_3$ (c) $Ba_{0.94}Sr_{0.06}TiO_3$ & (d) $Ba_{0.92}Sr_{0.08}TiO_3$ samples.

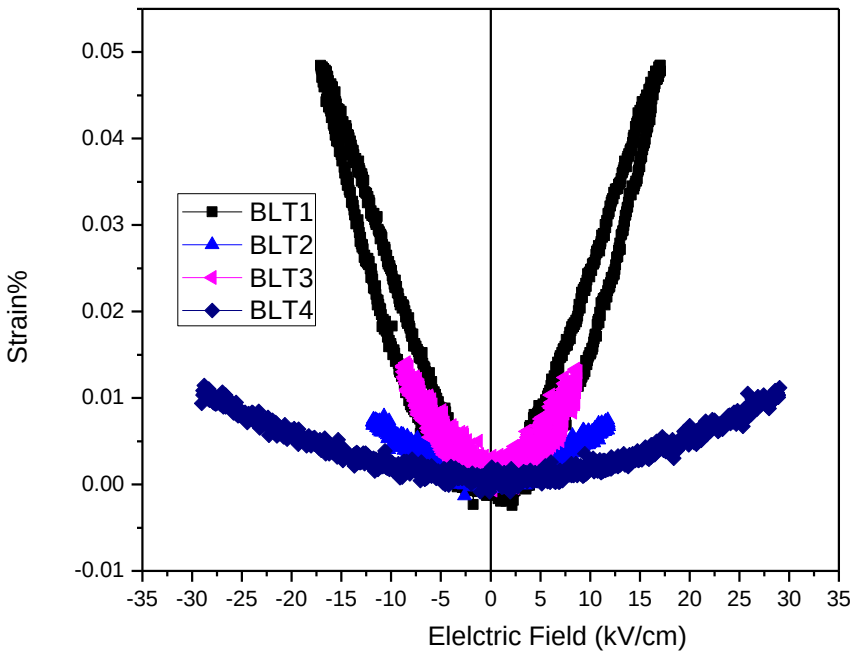

Fig. 6.11 Strain versus bipolar electric field loop of (a) BLT1 (b) BLT2, BLT3 & BLT4 samples.

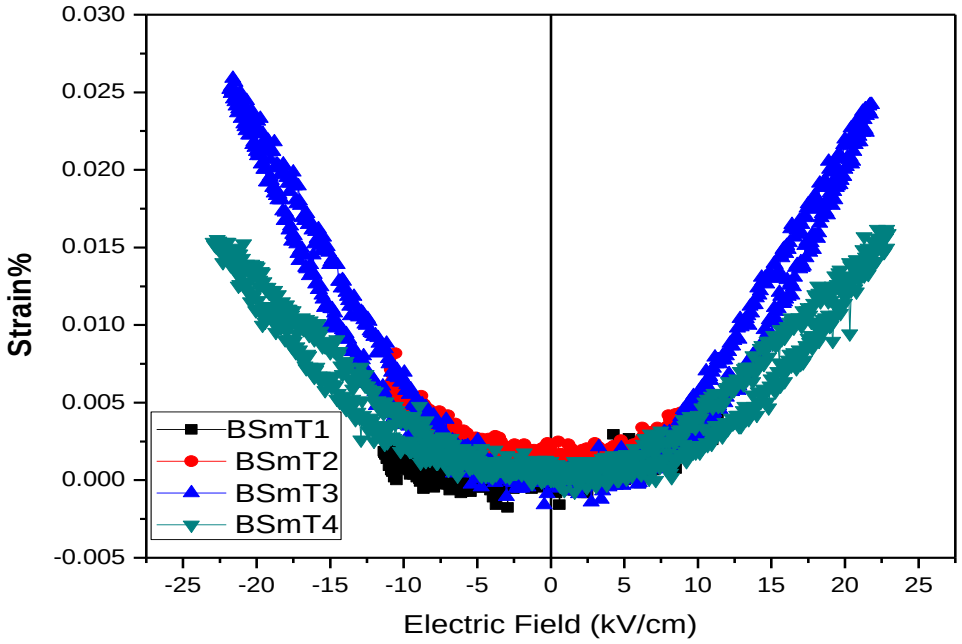

Fig. 6.12 Strain versus bipolar electric field loop (a) BSmT1 (b) BSmT2 (c) BSmT3 & (d) BSmT4 samples

Figs. 6.8-6.13 show the strain vs. electric field loops of the iso-valent and off-valent modified BT systems synthesized by MSSR route. Development of butterfly shape loops in the Ca, Sr and Mg modified BT samples hints towards the piezoelectric nature of these samples [11-27]. Symmetric nature of the S-E loops increases with the increase in Ca substitution% in BCT samples hinting towards the increase in piezoelectric nature [11]. Again symmetric nature of the S-E loops increases with the increase in Sr & Mg substitution% in BST & BMT samples but with the decrease of S-E hysteresis. This decrease of S-E hysteresis hints that with the increase of Sr & Mg substitution% in BST, BMT systems, the BST & BMT systems are transforming from piezoelectric to electrostrictive nature [11]. This is as per XRD and dielectric study (Chapter 4 & 5), where we have reported that with the increase of Sr & Mg substitution% in BST & BMT systems the tetragonality decreases (Chapter 4). Similarly with the increase of La & Sm substitution% in BLT, BSmT systems, max. strain and S-E hysteresis decreases. As, discussed in Chapters 4 & 5 with the increase of La & Sm substitution% in the BLT & BSmT systems the structure is changing from noncentrosymmetric to centrosymmetric

nature. Therefore, the S-E hysteresis loop study of Sr, Mg, La & Sm modified BT samples suggest that these samples are transforming from piezoelectric to electrostrictive nature [11]. Since, in our present study we are relating non-centrosymmetric nature of the crystal structures with the tetragonality of the system [9]. Therefore, decrease in tetragonality hints that we are moving towards centrosymmetric structure (cubic structure in our present study) [9, 24]. It is well established that S-E butterfly loop in dielectric materials comes from piezoelectric nature of the materials [11] and for electrostrictive materials there is no hysteresis in S-E behaviour [11]. The d_{33} piezoelectric coefficient, calculated from the slope of strain vs. electric field plot at lower electric field is given in Table 6.2. Among isovalent modified BT samples, a piezoelectric coefficient as high as 315pC/N is found in BST4 system whereas among off-valent modified BT samples it is found to be ~266pC/N in BLT1samples. High value of d_{33} coefficient of BT, BST4 & BLT1 suggests the suitability of these material for actuator applications [29].

Table 6.2 d_{33} piezoelectric coefficients from S-E study

System	$Ba_{0.98}Ca_{0.02}TiO_3$	$Ba_{0.96}Ca_{0.04}TiO_3$	$Ba_{0.94}Ca_{0.06}TiO_3$	$Ba_{0.92}Ca_{0.08}TiO_3$
d_{33} (pC/N)	**27**	**137**	**228**	**230**
System	$Ba_{0.98}Mg_{0.02}TiO_3$	$Ba_{0.96}Mg_{0.04}TiO_3$	$Ba_{0.94}Mg_{0.06}TiO_3$	$Ba_{0.92}Mg_{0.08}TiO_3$
d_{33} (pC/N)	**91**	**86**	**258**	**172**
System	$Ba_{0.98}Sr_{0.02}TiO_3$	$Ba_{0.96}Sr_{0.04}TiO_3$	$Ba_{0.94}Sr_{0.06}TiO_3$	$Ba_{0.92}Sr_{0.08}TiO_3$
d_{33} (pC/N)	**280**	**210**	**228**	**315**
System	BSmT1	BSmT2	BSmT3	BSmT4
d_{33} (pC/N)	**42**	**197**	**59**	-
System	BLT1	BLT2	BLT3	BLT4
d_{33} (pC/N)	**266**	**81**	-	-

References

1. T. Yamamoto, K. Okazaki, J. Am. Ceram. Soc., **69** (1986) 188.
2. K. Uchino, Ferroelectric Devices, Marcel Dekker, New York (2000).
3. S.E. Park ,T.R. Shrout, J. Appl. Phys., **82** (1997) 1804.
4. G. H. Heartling, J. Amer. Ceram. Soc., **82** (1999) 797.
5. R. C. Pullar, Y. Zhang, L. Chen, S. Yang, J. R. G. Evans, A. N. Salak, D. A. Kiselev, A.L. Kholkin, V. M. Ferreira, N. M. Alford, J. Electroceram. **22** (2009) 245
6. Y. Li, Y. Qu, Materials Research Bulletin, **44** [1](2009) 82.
7. A. Q. Nedelcos, A. Fundora, H. Amorín, J.M. Siqueiros, The Open Condensed Matter Physics Journal, **2** (2009) 1.
8. M. E. Lines, A. M. Glass, Principles and Applications of Ferroelectrics and Related Materials, Oxford, Clarendon (1979).
9. B. Jaffe, W. Cook, H. Jaffe, Piezoelectric Ceramics, Academic Press, London (1971).
10. J. C. Burfoot, G. W. Taylor, Polar Dielectrics and Their Applications, London: Macmillan (1979).
11. K. Uchino, Ferroelectric Devices, Marcel Dekker, New York (2000).
12. S. Bashash, N. Jalili, P. Evans, M. J. Dapino, *J.* of Intelligent Material Systems and Structures December, **20** [18] (2009) 2161.
13. S.T. Zhang, A. B. Kounga, E. Aulbach, W. Jo, T. Granzow, H. Ehrenberg, J. Rödel, J. Appl. Phys., **103** (2008)034108
14. A. Hall, M. Allahverdi, E.K. Akdogan, A. Safari, J. European Ceram. Soc., **25[** 12] (2005) 2991.
15. W. Jiang, R Zhang, B Jiang, W. Cao, Ultrasonics, **41**[2] (2003) 55.

16. Z. Feng, H. Luo, Y. Guo, T. He, H. Xu, Solid State Comm., **126** [6] (2003 347.

17. **J**. B. Lim, S. Zhang, T. R. Shrout, Journal of Electroceramics, Online First™, 1 February 2011.

18. D .Damjanovi, The Science of Hysteresis, **3**[4] (2006) 337.

19. W. Wersing, W. Heywang, H. Beige, H. Thomann, Springer Series in Materials Science 114 (2009) 37.

20. M. Ozgul, S. T. Mckinstry, C. A. Randall, J. Electroceram., **20**[3](2008) 133.

21. A. Pathak, R. Chatterjee, C. Prakash, Ceramics International, **36**[8] (2010) 2263.

22. A. Pathak, C. Prakash, R. Chatterjee, Materials Chem. & Phys.,**123**[1](2010) 132.

23. A. Pathak, C. Prakash, R. Chatterjee, Physica B: Condensed Matter, **404** [20] (2009) 3457

24. M. E. Lines, A. M. Glass, Principles and Applications of Ferroelectrics and Related Materials, Clarendon Press, Oxford (1977).

25. J. X. Zhang, G. Sheng, L. Q. Chen, Appl. Phys. Lett., **96** (2010) 132901

26. S. Zhang, L. Lebrun, C. A. Randall, T. R. Shrout, J. Crystal Growth, **267** [1] (2004) 204.

27. S. Zhang, L. Lebrun, S. Rhee, R.E. Eitel, C. A. Randall, T. R. Shrout, J. Crystal Growth, **236**[1] (2002) 210.

28. M. Kondo, K. Kunhara, Key Engineering Materials, **248** (2003) 15.

29. S. W. Choi, T. R. Shrout, S. J. Jang, A. S. Bhalla, Ferroelectrics, **100** (1989) 29.

CHAPTER 7

SYNTHESIS & CHARACTERIZATION OF UNMODIFIED & MODIFIED BT SYSTEMS BY MICROWAVE (MW) PROCESSING ROUTE

7.1 Introduction

$Ba_{1-x}Ca_xTiO_3$ & $Ba_{1-x}La_xTi_{(1-x/4)}O_3$ samples synthesized by MSSR route, where x=0.02, 0.04. 0.06 & 0.08, respectively are showing better dielectric properties (reported in Chapter 5). Therefore, these two series were also synthesized by MW process. We have studied the MW processing effect on the perovskite phase evolution, structural, density microstructural, dielectric, ferroelectric and piezoelectric properties and compared with the properties of same systems synthesized by conventional sintered route.

7.2 Experimental Procedure

Grade reagents Barium carbonate ($BaCO_3$), calcium carbonate ($CaCO_3$), lanthanum oxide (La_2O_3) and titanium oxide (TiO_2),powders of 99.9% purity were taken as starting materials. The powders were thoroughly mixed in an agate mortar after weighing stochiometrically. The mixture was then subjected to ball milling for 6hr in acetone solution with powder to ball ratio maintained at 1:3. Then the powder were dried and grinding has been done. The dried powder was subjected to TGA/DTA study for deciding about the calcination temperatures. For studying the phase formation behavior and reaction mechanism, mixed powders were calcined at a temperature of 1000 & 1100^0C for 4hr, respectively in an alumina crucible by an indigenous programmable furnace at a heating rate of 5^0C per minute and then cooled in the furnace. Single perovskite phase formation was confirmed by XRD technique for powders calcined at 1100^oC. The calcined powders were grinded in an agate mortar to avoid agglamorization of the particle. The powder calcined at 1100^oC was mixed thoroughly with 2wt% polyvinyl

alcohol (PVA) binder & pressed into disks of diameter ~10mm and a thickness of ~1.5mm under a pressure ~60MPa.2wt% poly vinyl alcohol (PVA) was mixed in the calcined powder sample as binder to impart mechanical strength to the green body. The microwave sintering of the Ca and La substituted BT samples was carried out at 1100^0C for 1 h with a heating rate of 25^0C/min by placing the pellets in the centre of a 4.4 kW, 2.45-GHz multi mode microwave cavity. Schematic diagram of microwave sintering system is shown in Fig.7.1. The microwave furnace temperature was recorded by using a Raytek non-contact sensor (XRTG5). In order to examine the phases present in the modified BT system, XRD analyses of the powder and pellets were performed on a PW 3020 Philips with Cu Kα radiation (λ=1.5405Å).Surface morphology of the samples was studied using Jeol T-330 Scanning Electron Microscope. The sintered pellets were polished and silver paste was applied on the surfaces for doing electrical characterization. The flowchart of MW processing of modified BT samples is given in Fig. 7.2. ε_r and tanδ were measured as the function of frequency and temperature using Hioki 3532-50 LCR HiTESTER. Polarization vs electric field (P-E) hysteresis loops were recorded with computer interfaced loop tracer based on modified Sawyer Tower circuit. The samples for the piezoelectric property measurements were poled by a corona poling unit at a temperature 25^oC below than transition temperature (T_c) by applying a dc electric field of 3 kV/mm for 30min. The piezoelectric and electromechanical parameters are measured in accordance with the 1961 IRE standards on piezoelectric crystals and 1987 IEEE standard of piezoelectricity, ANSI/IEEE std 176-1987.

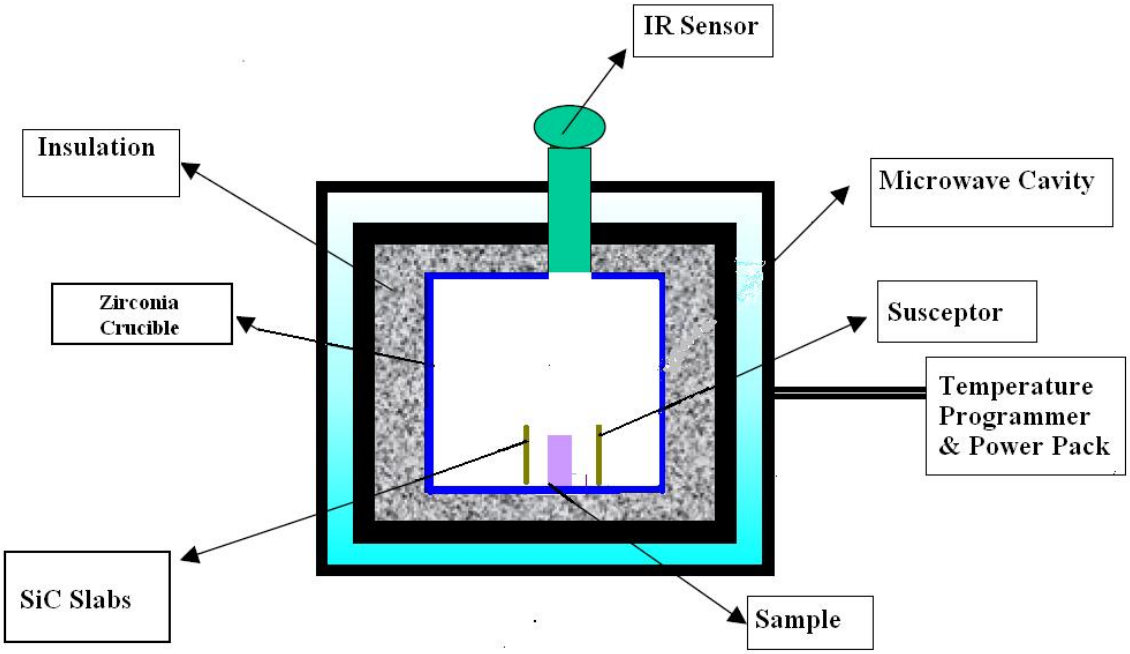

Fig.7.1 Schematic diagram of microwave sintering system.

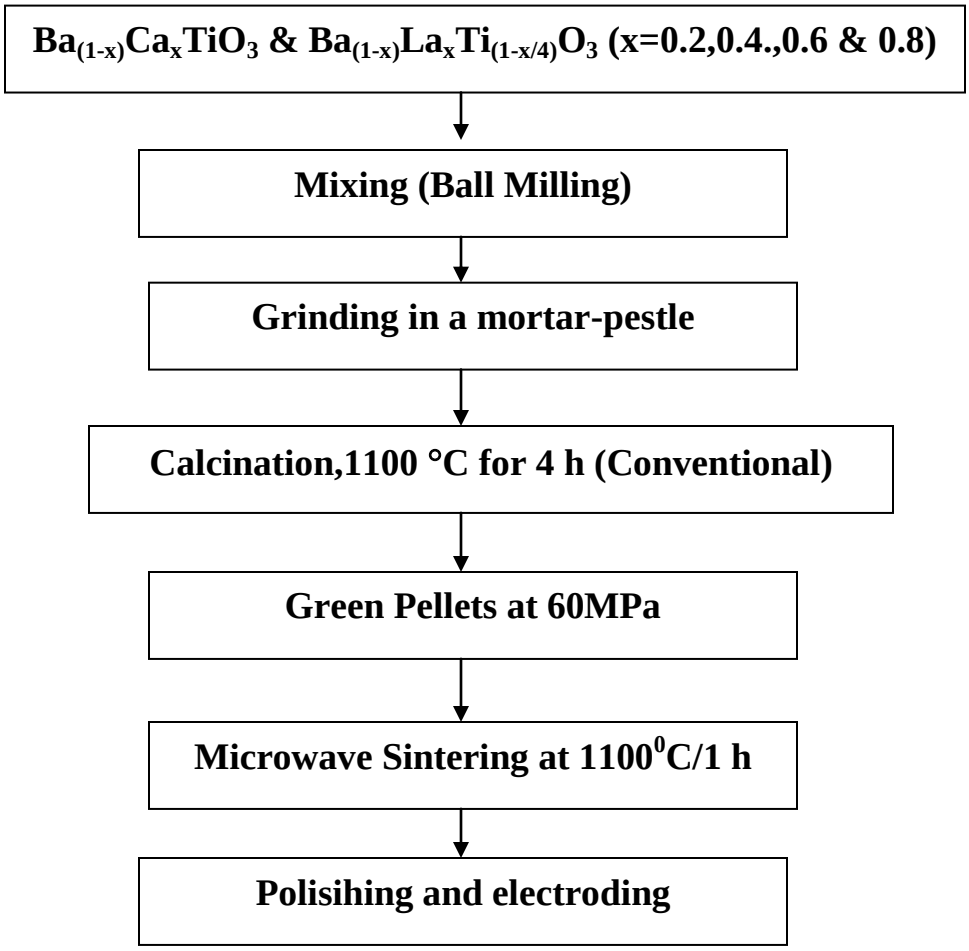

Fig. 7.2 Flow Chart of Microwave Synthesis of Ca & La Modified BT Systems

7.3 Phase Evolution Study

With the modification of solid state reaction route, perovskite phase evolution study in iso-valent and off-valent substituted BT systems is essential as in these materials the perovskite phase can be accompanied by unwanted phases [1-6] which significantly affects the material properties [7]. Therefore, optimization of processing conditions for the single perovskite phase evolution in iso-valent and an off-valent substituted BT system is essential. Modifications in a ferroelectric material affects its properties; most likey the perovskite phase evolution, microstructure and density [7-9]. Therefore, in this chapter, the effect of MW processing on perovskite phase evolution, structural and microstructural properties of iso-valent and off-valent substituted BT systems are discussed using X-ray diffraction (XRD) and scanning electron microscopy (SEM) techniques. Density measurements have also been discussed.

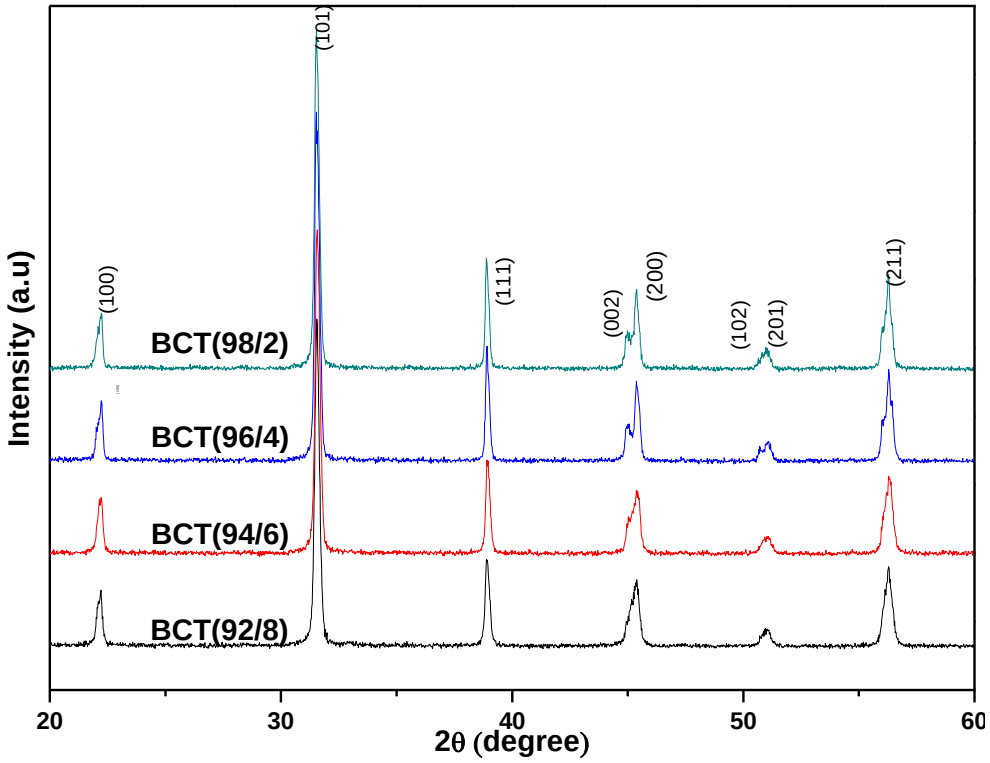

Fig. 7.3 XRD peaks of $Ba_{1-x}Ca_xTiO_3$ (x = 0.02, 0.04, 0.06, 0.08) Microwave Processed at 1100^0C for 4hrs.

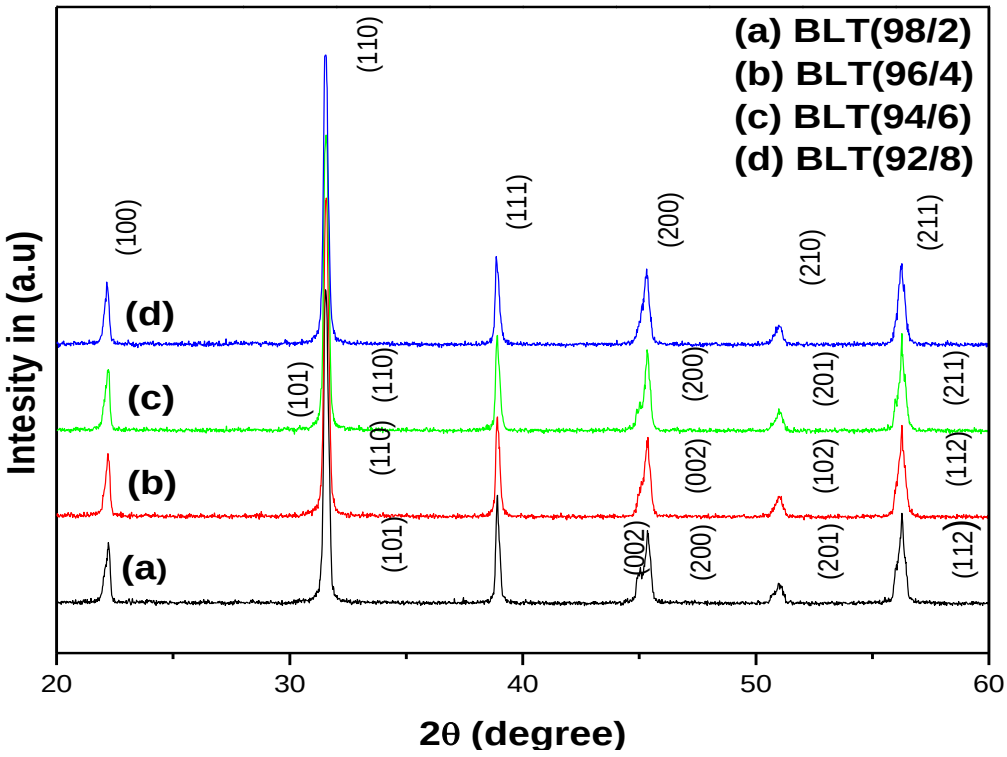

Fig. 7.4 XRD peaks of $Ba_{1-x}La_xTi_{(1-x/4)}O_3$ (x = 0.02, 0.04, 0.06, 0.08) Microwave Processed at 1100^0C for 4hrs.

7.3.1 Structures

Figs.7.3 and 7.4 show the XRD patterns of the $Ba_{1-x}Ca_xTiO_3$ (x = 0.02, 0.04, 0.06, 0.08) and $Ba_{1-x}La_xTi_{(1-x/4)}O_3$ (x = 0.02, 0.04, 0.06, 0.08) samples sintered at 1100^oC for 1hr, respectively by MW route. The XRD patterns confirm the single perovskite phase formation without any trace of secondary phase. Table 1 In the MW processed $Ba_{1-x}Ca_xTiO_3$, samples with the increase in Ca concentration in $BaTiO_3$ system, the splitting at (200) plane decreases indicating the decrease in tetragonality (c/a ratio) [11]. In the MW processed $Ba_{1-x}La_xTi_{(1-x/4)}O_3$, samples with the increase in La concentration in $BaTiO_3$ system, the splitting near $2\theta=45^o$ merges into singlet indicating the structure changes from Tetragonal to cubic [12-14]. The MW processed $Ba_{1-x}La_xTi_{(1-x/4)}O_3$ (x = 0.02, 0.04, 0.06, 0.08) samples for x = 0.02 BLT samples were indexed with tetragonal structure & for x > 0.02 BLT samples were indexed with cubic structure. The more expressed effect of off valent substitution in BT system can be explained by the creation of a higher concentration of various defects in the crystal structure of barium titanate influencing the change of crystal lattice parameters [15, 16]. Table 7.1 represents the type of structures of different compositions of MW sintered BLT and BCT samples.

Table.7.1 Structures of Ca and La Modified BT Systems Synthesized by Microwave Processing Technique:

System Structure	$Ba_{0.98}Ca_{0.02}TiO_3$	$Ba_{0.96}Ca_{0.04}TiO_3$	$Ba_{0.94}Ca_{0.06}TiO_3$	$Ba_{0.92}Ca_{0.08}TiO_3$
	Tetragonal, c/a=1.0162	Tetragonal c/a=1.0159	Tetragonal c/a=1.0157	Tetragonal c/a=1.0153
System Structure	BLT1	BLT2	BLT3	BLT4
	Tetragonal, c/a=1.0139	Cubic c/a=1	Cubic c/a=1	Cubic c/a=1

7.3.2 Densities

Densities of the microwave sintered $Ba_{1-x}Ca_xTiO_3$ and $Ba_{1-x}La_xTi_{(1-x/4)}O_3$(x = 0.02, 0.04, 0.06, 0.08) ceramics were measured using Archimedes' principle. The values are as shown in the given Table 7.2. Table.7.2 shows a better densified microwave processed Ba_{1-x} Ca_xTiO_3(x = 0.02, 0.04, 0.06, 0.08) and $Ba_{1-x}La_xTi_{(1-x/4)}O_3$(x = 0.02, 0.04, 0.06, 0.08) samples then the conventional processed samples. This is due to volumetric and uniform heating in microwave processing of the samples [17-30]. The obtained densities of MW sintered modified BT samples sintered at significantly lower temperatures and time are higher than the earlier reports on modified and unmodified BT ceramic samples processed through other processes including MW technique [24-26, 31]. It is evident that the microwave method takes only a fraction of the time required in the conventional processing to achieve single-phase dense material. Time-Temp. Sintering Profile of Microwave Sintered Ca and La Modified BT Ceramics is shown in Fig. 7.5.This signifies the importance of processing Ca^{2+} & La^{3+} ions modified BT ceramic samples through MW technique.

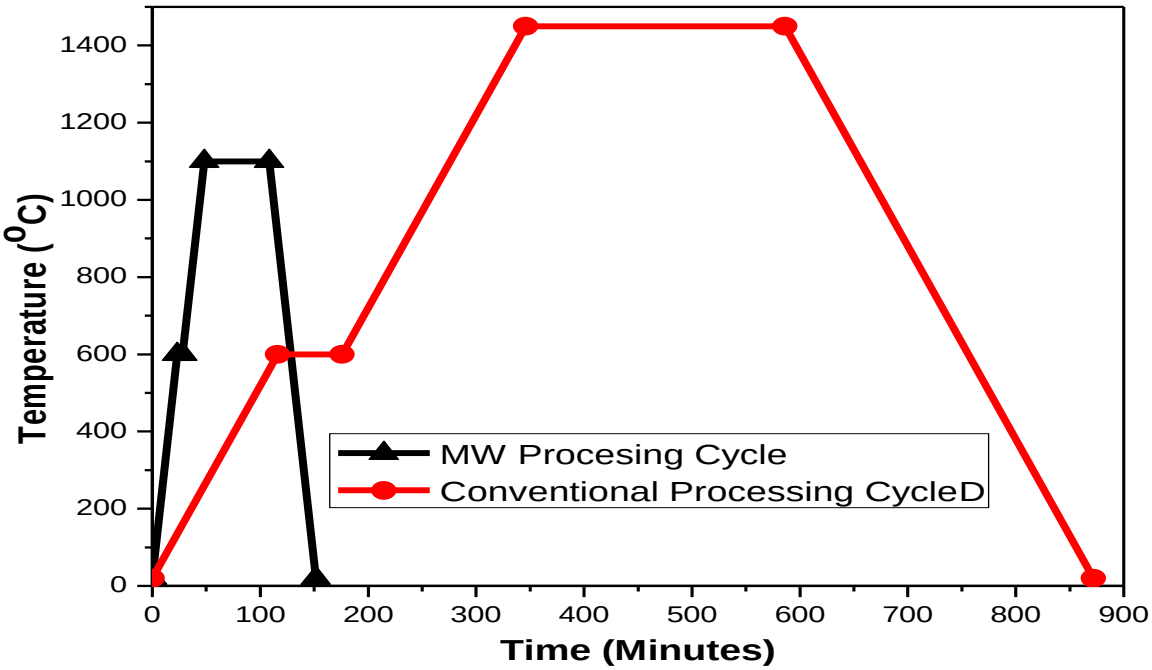

Fig. 7.5 Comparison of time-temp. profile of Ca and La Modified BT ceramics sintered in microwave & conventional furnaces.

COMPARISON OF HEATING MECHANISM IN CONVENTIONAL AND MICROWAVE FURNACE

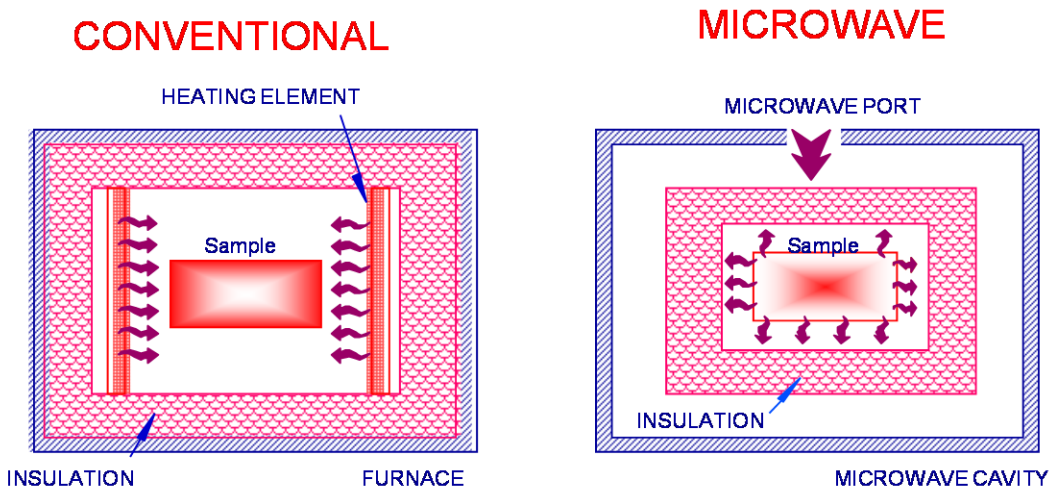

Fig7.6. Heat flow in conventional and microwave furnaces.

Table 7.2. Density & grain size of $Ba_{1-x}Ca_xTiO_3$ and $Ba_{1-x}La_xTi\ O_3$ (x = 0.02, 0.04, 0.06, 0.08) synthesized by MSSR and microwave technique

Sintered Samples	Density in g/cc	Grain Size (μm)
BCT1	5.77	1.3
BCT2	5.68	0.7
BCT3	5.64	0.65
BCT4	5.51	0.5
BLT1	5.75	0.95
BLT2	5.96	0.7
BLT3	6.02	0.52
BLT4	5.95	0.45

7.3.3 Microstructures

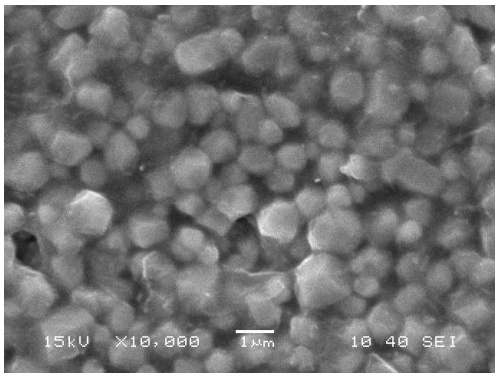

Fig. 7.7 SEM image showing $BaTiO_3$ systems sintered at 1100^0C for 1hr in MW furnace.

Figs. 7.7 shows the SEM of BT system sintered by microwave technique. Here, the grains are with less porosity and with uniformly distributed grains. Grain size of BT system, calculated by linear intercept method, is found to be ~1.4μm. Better densification of the microwave sintered BT samples with the formation of finer and uniform grains than the same system processed through SSR route is due to the rapidity of microwave heating which avoids the undesirable grain growth [21]. This is the characteristic of microwave processing of ceramics as the heating rate is fast and the mechanism of heating rate is

different than conventional sintering process [17-30]. Grain size of microwave sintered Ca^{2+} & La^{3+} ions modified BT ceramic samples is lower than the same systems processed by conventional solid state route [12-17]. Better densification with the formation of finer and uniform grains in the case of microwave sintered samples is due to the rapidity of microwave heating which avoids the undesirable grain growth [21]. This is the characteristic of microwave processing of ceramics as the heating rate is fast and the mechanism of heating rate is different than conventional sintering process [17-30] as shown in Fig. 7.5 & 7.6.

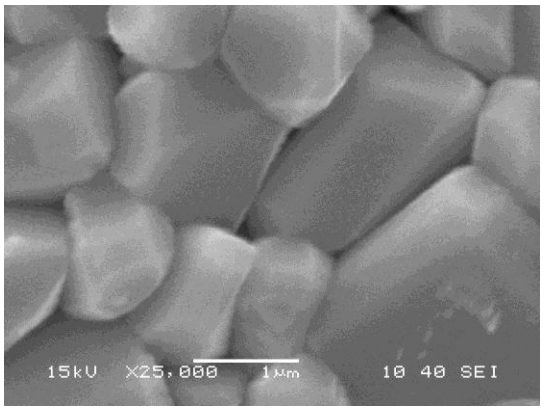

BCT 98-2

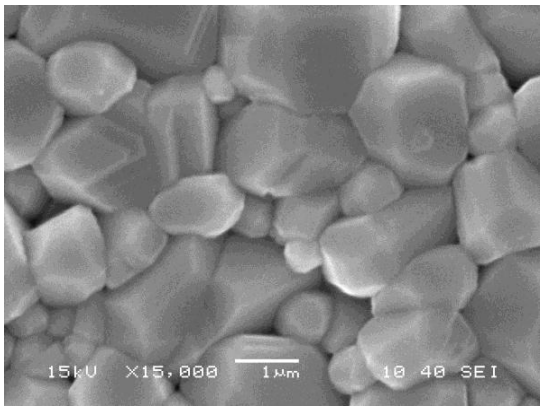

BCT 96-4

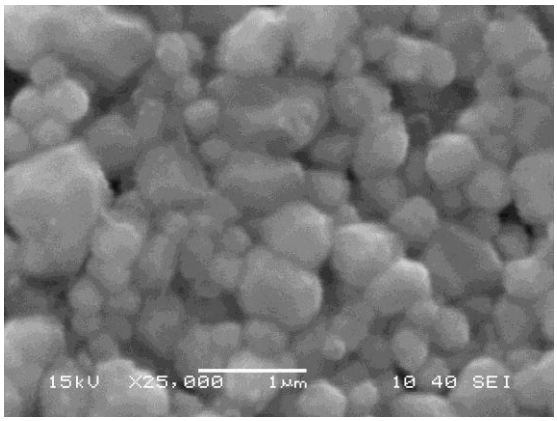

BCT 94-6

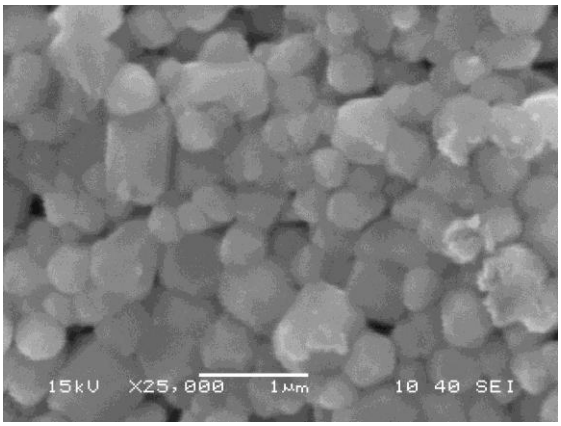

BCT 92-8

Fig. 7.8 SEM image showing $Ba_{1-x}Ca_xTiO_3$ (x = 0.02, 0.04, 0.06, 0.08) systems sintered at 1100^0C for 1hr in MW furnace.

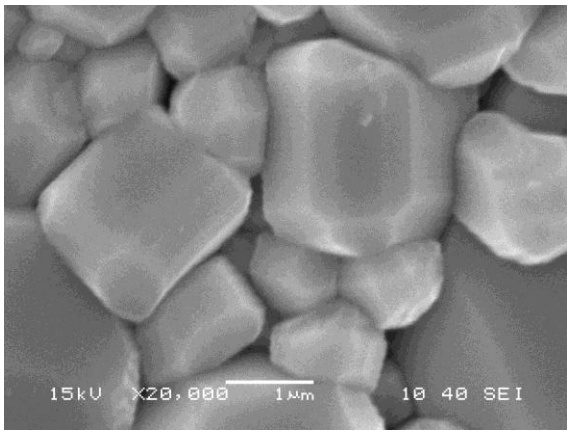

BLT98-2

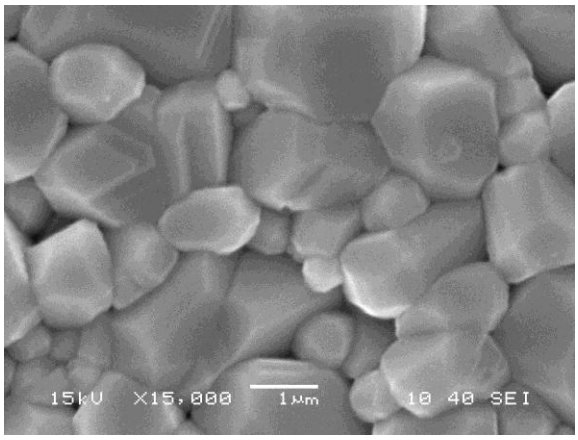

BLT 96-4

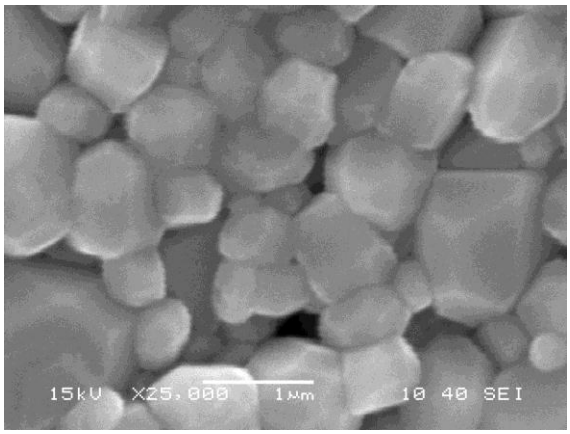

BLT 94-6

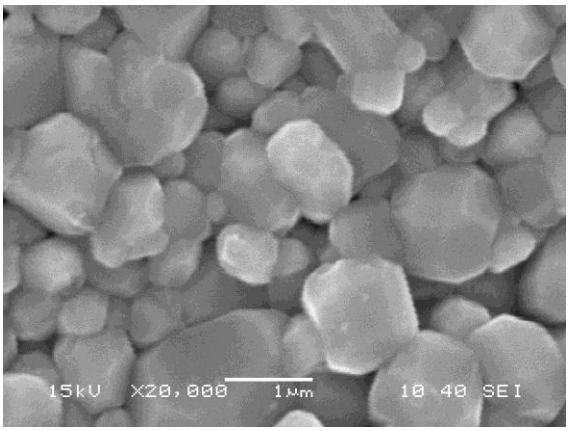

BLT 92-8

Fig. 7.9 SEM images showing $Ba_{1-x}La_xTi_{(1-x/4)}O_3$ (x = 0.02, 0.04, 0.06, 0.08) sintered at 1100^0C for 1hr in MW furnace.

Figs. 7.8 & 7.9 show that the SEM of Ca and La substituted BT system sintered by microwave technique. Here, the grains are with less porosity and with uniformly distributed grains. Grain size of Ca and La substituted BT system are given in Table 7.2. Here, the grain size decreases with the increase in Ca and La substitution % in BT system. This indicates that the increase in Ca and La mol% in BT system inhibits the grain growth.

7.4 Dielectric Properties of MW Sintered samples

(a)

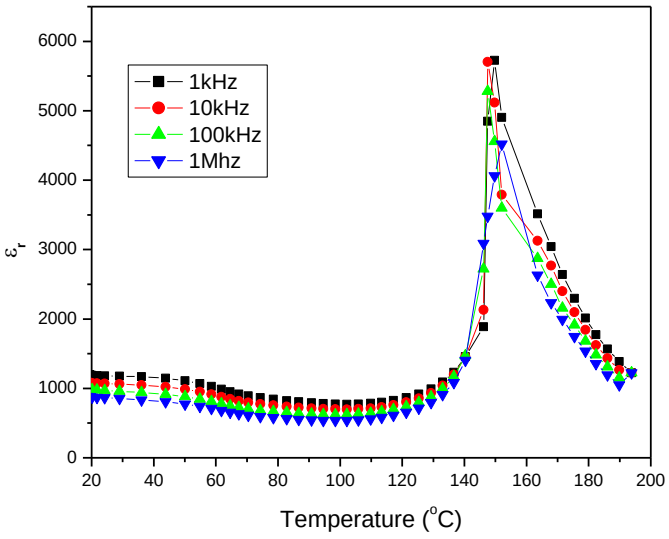

(b)

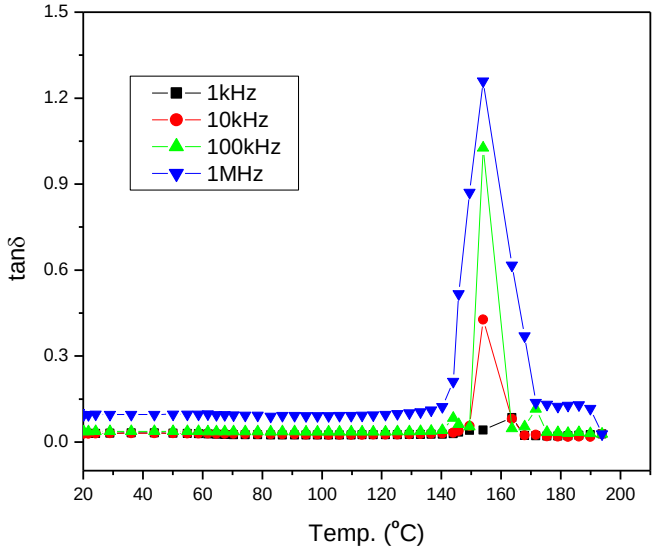

Fig. 7.10 Temperature variation of (a) ε_r and (b) tanδ at different frequencies of MW sintered BT sample.

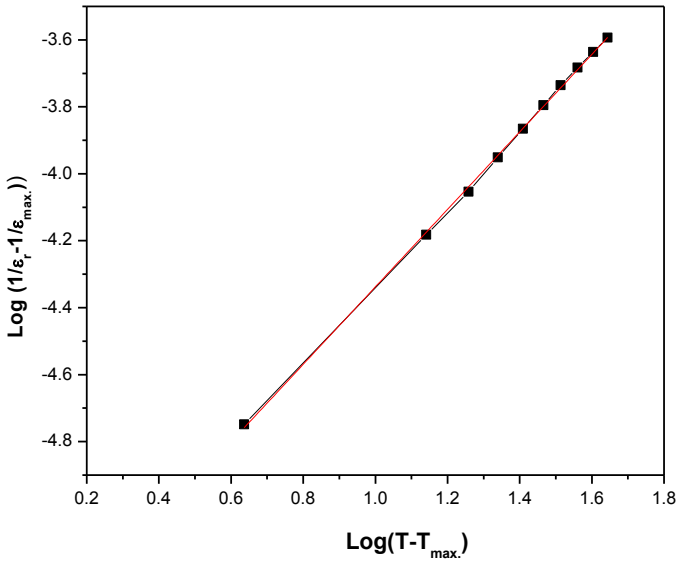

Fig. 7.11 Temperature variation of ε_r at different frequencies of MW sintered BT sample.

Figs. 7.10 show the temperature variation of ε_r and tanδ at different frequencies of BT samples sintered by microwave process. The initial decrease in ε_r with the increase in temperature suggests that the orthorhombic to tetragonal structure transformation temperature, $T_{(o-t)}$, is below room temperature [32]. Since, near $T_{(o-t)}$ temperature, value of ε_r is maximum than nearby temperature values [32]. The temperatures corresponding to maximum ε_r and where the structure of the material transform from non-cubic to cubic structure is known as Curie temperature (T_c) is found to be ~150^{o}C. Fig. 7.10 shows the temperature variation of tan δ at different frequencies (1 kHz–1 MHz). The temperatures of peak dielectric loss and peak dielectric constant do not coincide. Kramers–Kronig relation indicates that this can be the consequence of temperature dependent relaxation near Curie temperature [33]. Temp. variation of tanδ at

different frequencies from RT to 130^{o}C is almost constant. This signifies the importance of using MW processing route over conventional processing route.

Fig. 7.11 shows the plots between log $(1/\varepsilon_r - 1/\varepsilon_{rmax.})$ versus log $(T-T_{max.})$ at 1kHz of MW sintered BT samples. The nature of phase transition is ascertained by calculating the degree of diffusion (γ). Fitting ε_r at 1kHz in the region of $T > T_{max}$ in equation 7.1 and a graph between $\log(1/\varepsilon_r - 1/\varepsilon_{r\ max})$ versus $\log(T-T_{max})$ is plotted. Diffusivity factor (γ), calculated from the slopes of these plots in the higher temperature region is found to be 1.15.

$$1/\varepsilon_r = 1/\varepsilon_{r\,max} + (T-T_{max.})^{\gamma} / C \qquad \ldots 7.1$$

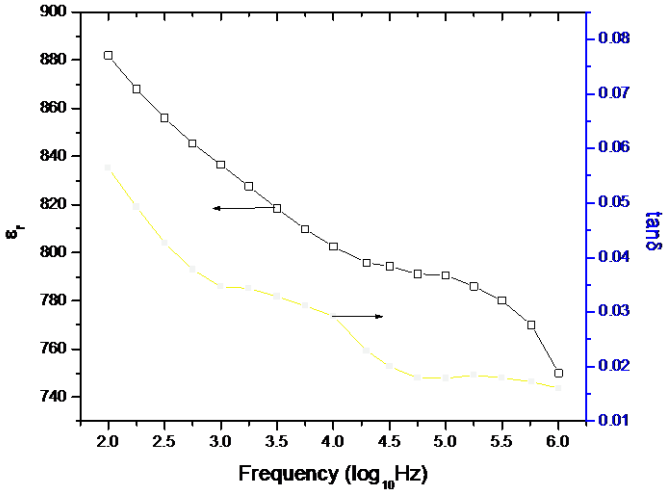

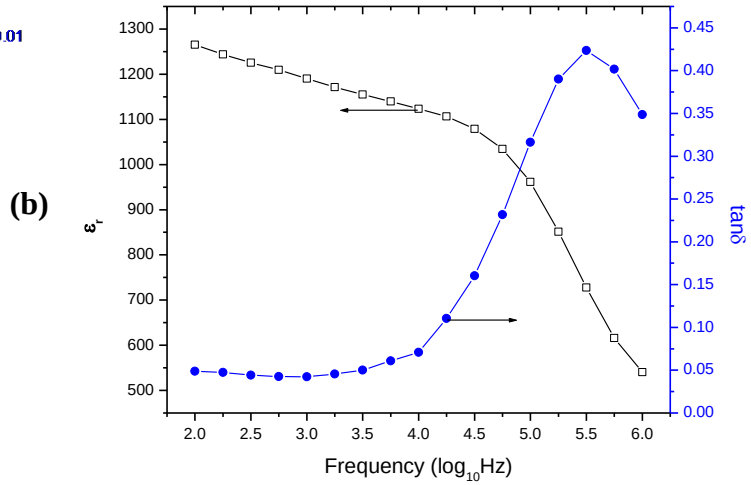

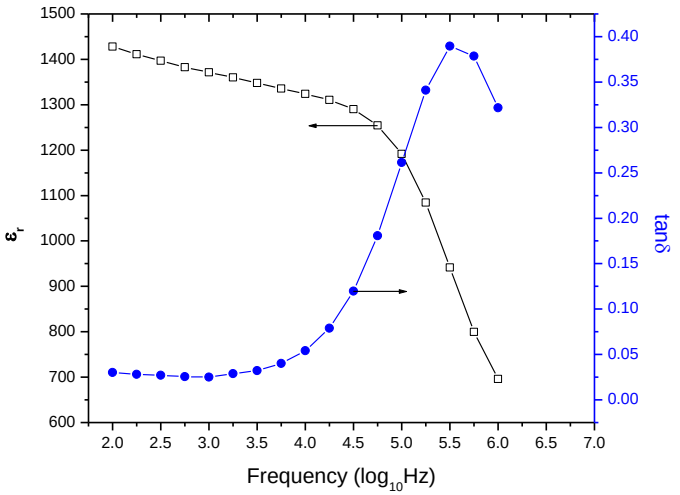

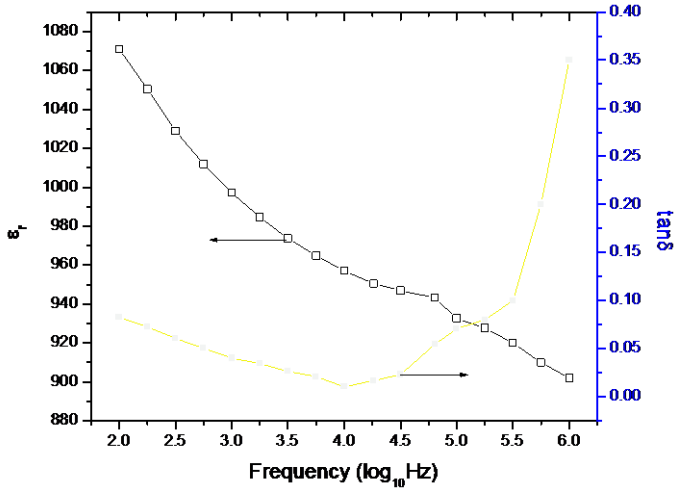

Fig. 7.12 Variation of ε_r and tanδ with frequency of MW sintered (a) $Ba_{0.98}Ca_{0.02}TiO_3$ (b) $Ba_{0.96}Ca_{.0.04}TiO_3$ (c) $Ba_{0.94}Ca_{0.06}TiO_3$ & (d) $Ba_{0.92}Ca_{0.08}TiO_3$ samples.

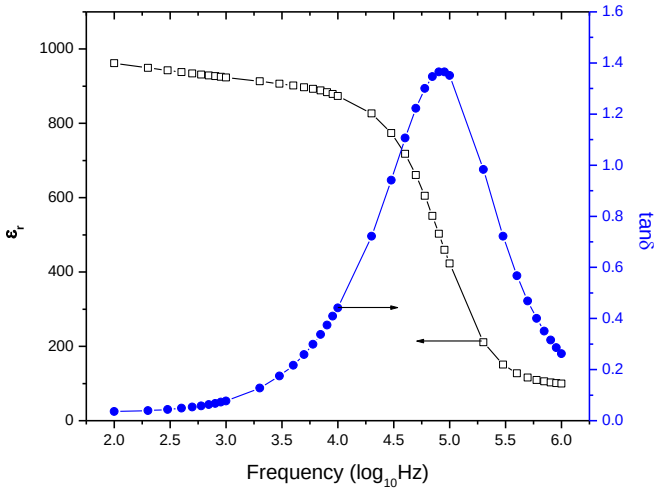

(a)

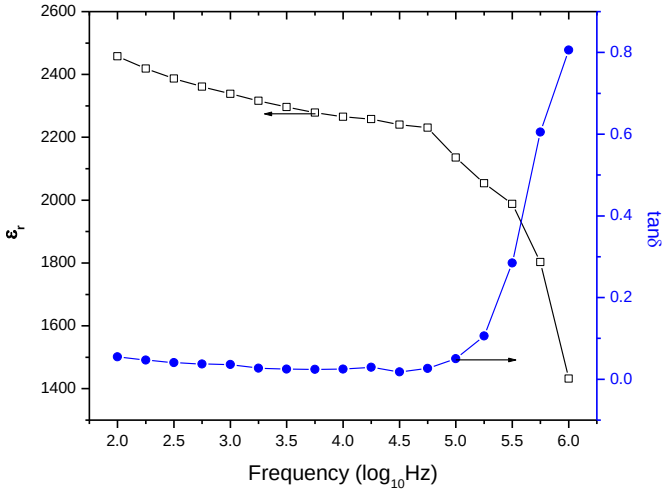

(b)

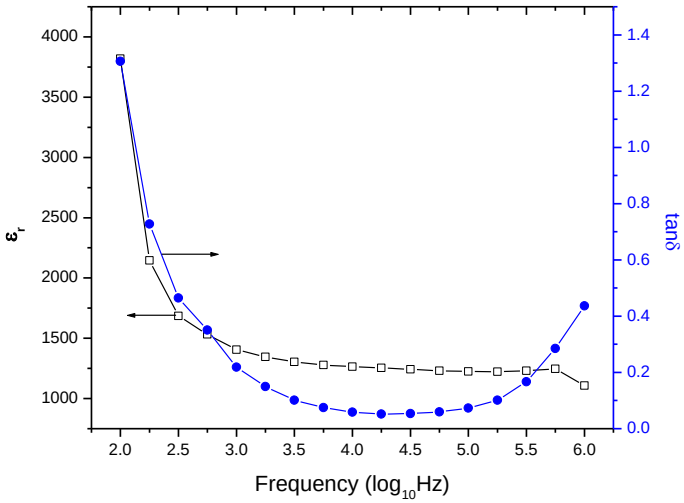

(c)

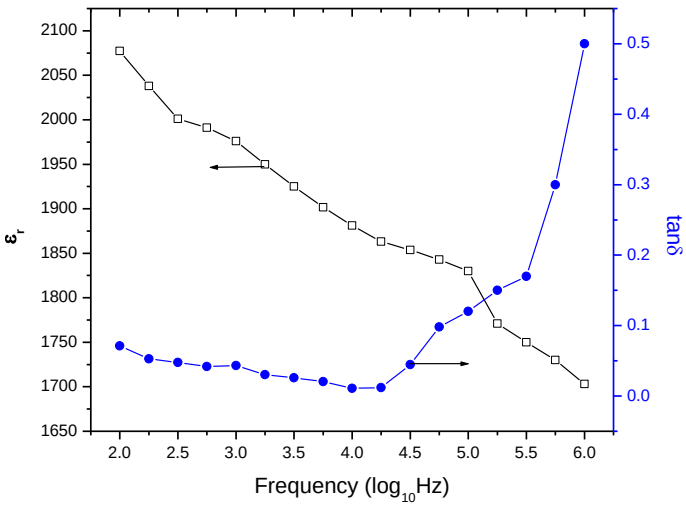

(d)

Fig. 7.13 Variation of ε_r and tanδ with frequency of MW sintered (a) BLT1 (b) BLT2 (c) BLT3 & (d) BLT4 samples.

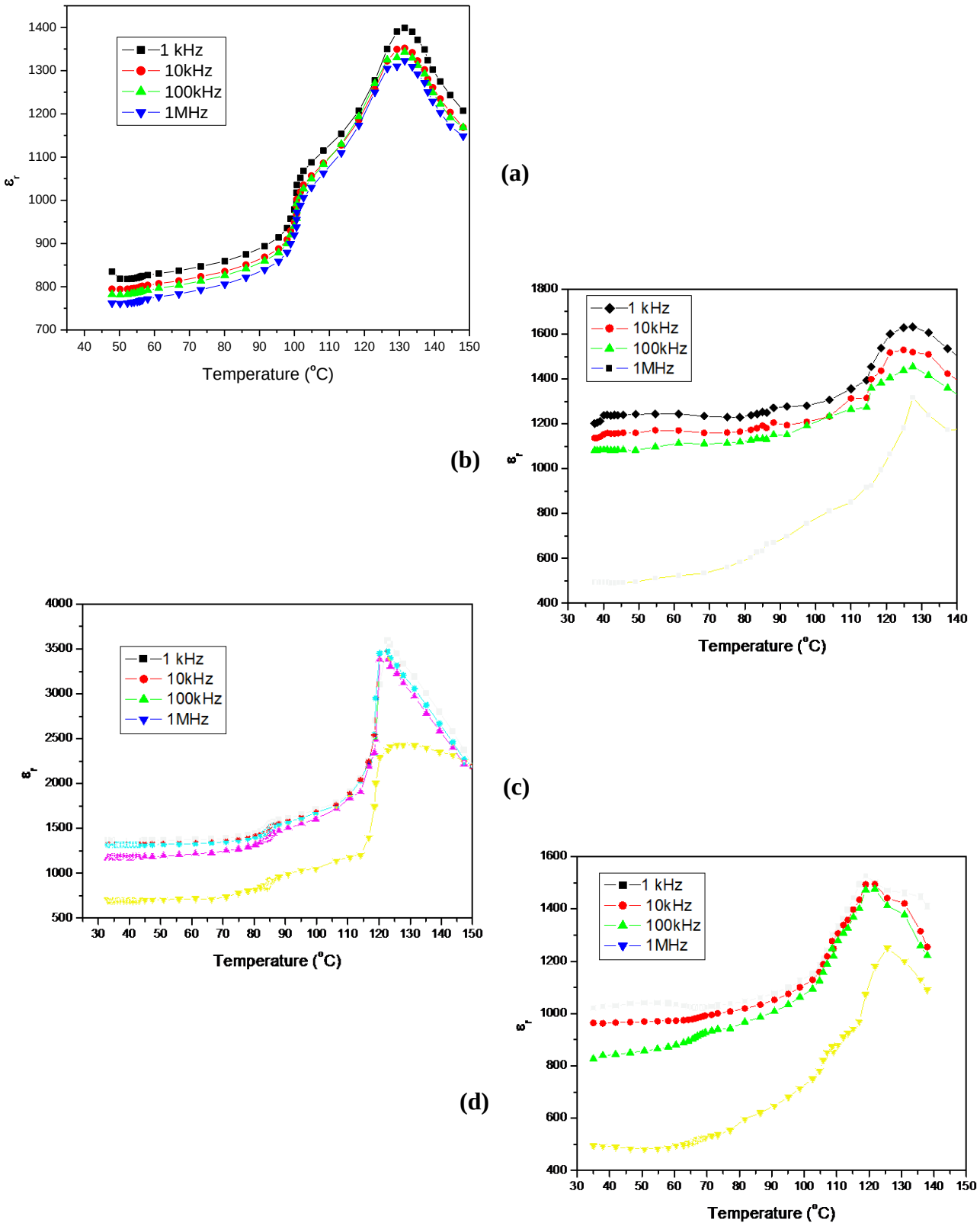

Fig. 7.14 Temperature variation of ε_r at different frequencies of MW sintered (a) $Ba_{0.98}Ca_{0.02}TiO_3$ (b) $Ba_{0.96}Ca_{.0.04}TiO_3$ (c) $Ba_{0.94}Ca_{0.06}TiO_3$ & (d) $Ba_{0.92}Ca_{0.08}TiO_3$ samples.

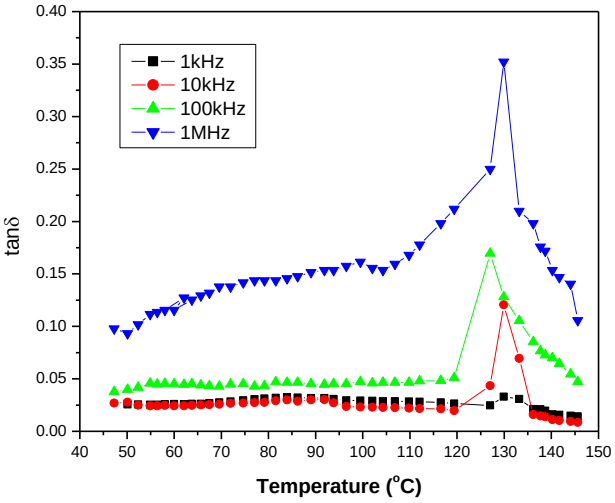

(a)

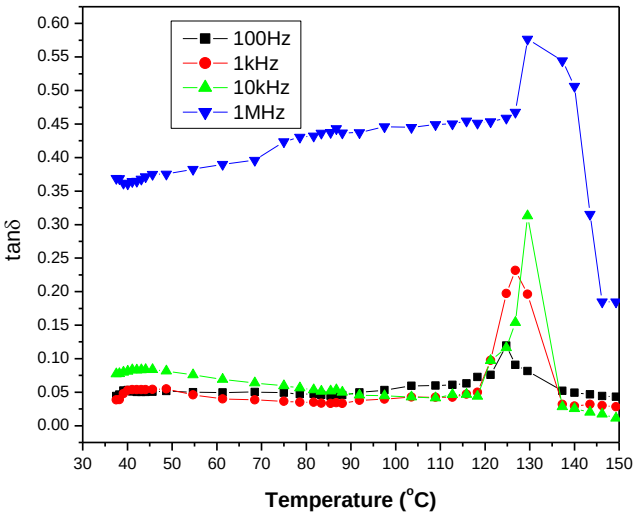

(b)

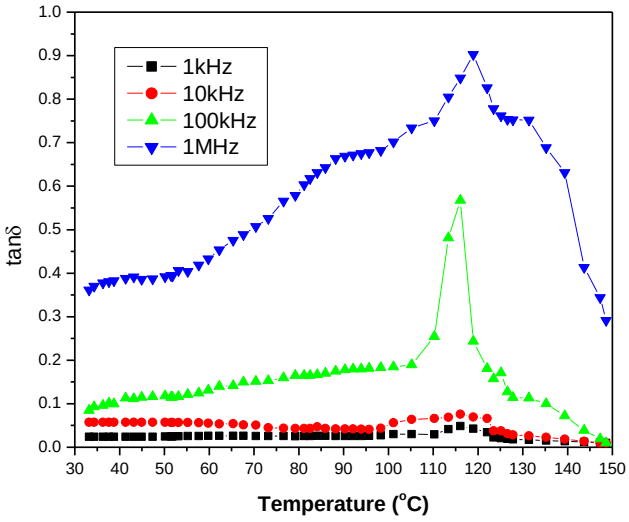

(c)

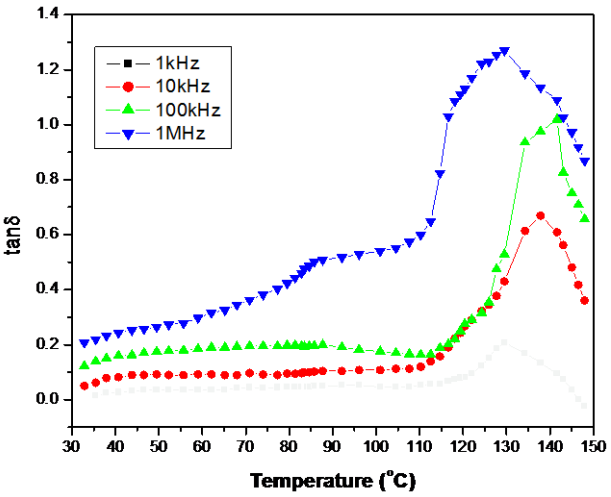

(d)

Fig.7.15 Temperature variation of tanδ at different frequencies of MW sintered (a) $Ba_{0.98}Ca_{0.02}TiO_3$ (b) $Ba_{0.96}Ca_{.0.04}TiO_3$ (c) $Ba_{0.94}Ca_{0.06}TiO_3$ & (d) $Ba_{0.92}Ca_{0.08}TiO_3$ samples.

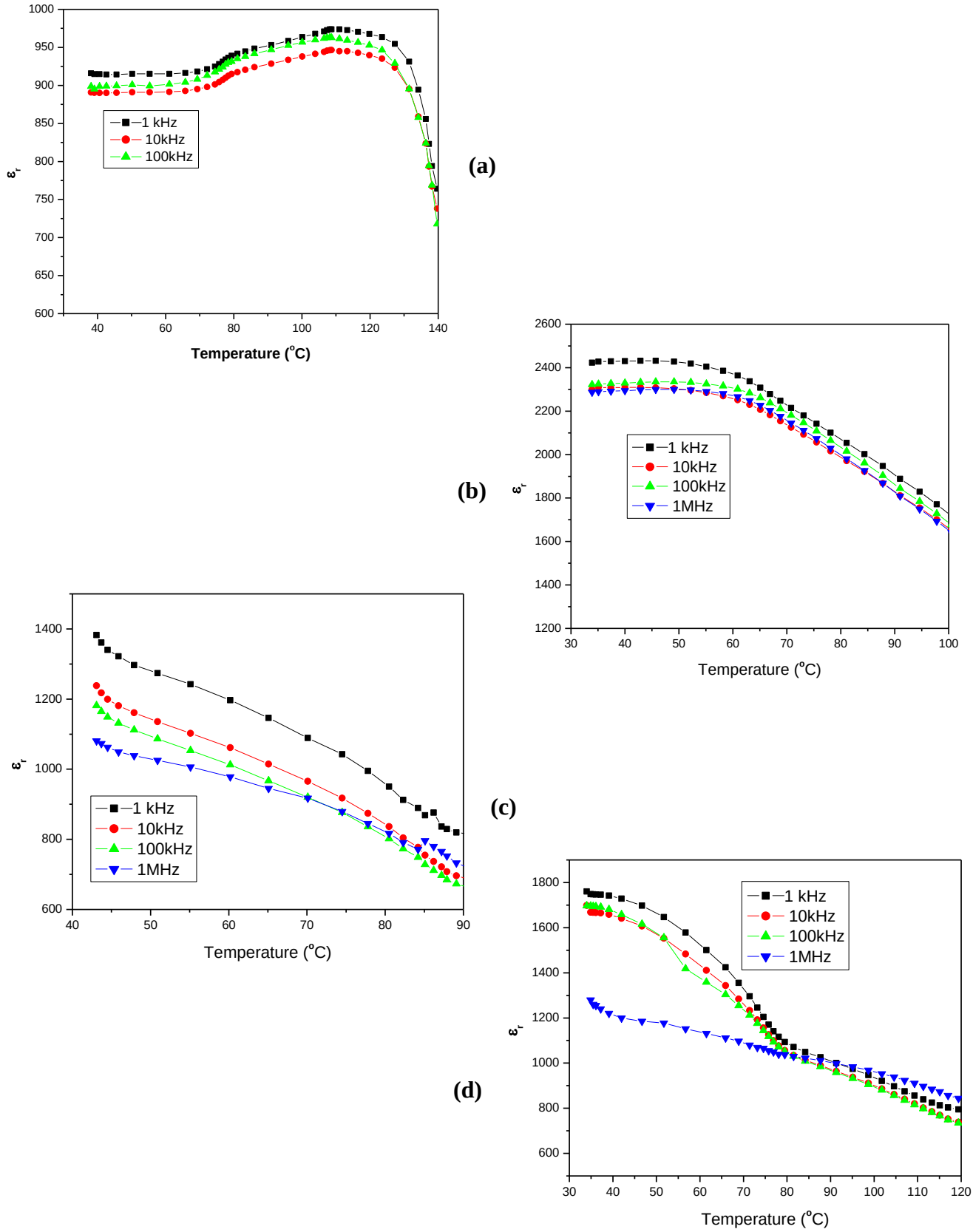

Fig. 7.16 Temperature variation of ε_r at different frequencies of MW sintered (a) BLT1 (b) BLT2 (c) BLT3 & (d) BLT4 samples.

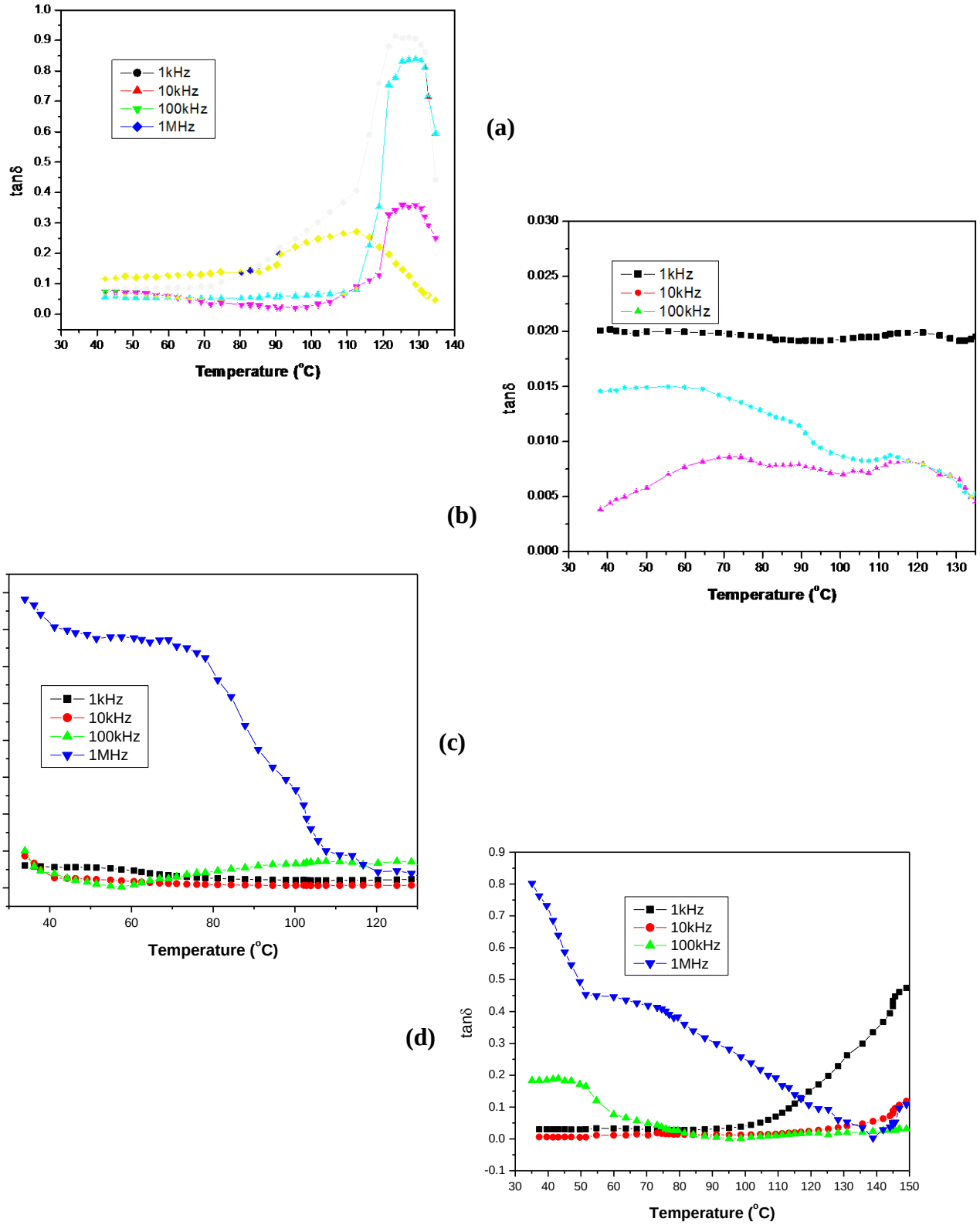

Fig. 7.17 temperature variation of tanδ at different frequencies of MW sintered (a) BLT1 (b) BLT2 (c) BLT3 & (d) BLT4 samples.

Figs. 7.12 & 7.13 show the frequency dependence of ε_r and tanδ at room temperature (RT) of Ca & La modified BT samples sintered by microwave process. In all the modified BT samples, ε_r decreases with the increase in frequency. The fall in ε_r arises from the fact that polarization does not occur instantaneously with the application of the electric field, which is due to the inertia of the dipoles. The delay in response towards the impressed alternating electric field leads to dielectric loss and decline in ε_r. At low frequencies, all types of polarization contributes and as the frequency is increased, polarizations with large relaxation times cease to respond and hence the decrease in ε_r [34]. At lower frequencies, ε_r is maximum because the contributions from the space charge polarization is large, which reduces slowly with the increase in frequency. The space charge polarization arises by the accumulation of charges at the grain boundaries and at the electrode interface. The same type of frequency-dependent dielectric behaviour is found in many ferroelectric materials [33]. In some of the Ca and La modified BT samples, tanδ increases with the increase in frequency and in some the value of tanδ decreases with the increase in frequency. It, is well known that the dielectric loss (tanδ) becomes max. near resonance frequencies compare to its neighboring frequencies, as shown in Fig. 5.9 [35]. Ferroelectric materials can have more than one resonance frequencies. Therefore, the decrease of tanδ with the increase of frequency from 100Hz suggest we are going away from one resonance frequency and the resonance frequency lies below 100Hz. Whereas, increase of tanδ with the increase of frequency suggest we are approaching towards other resonance frequency.

Fig. 7.14 & 7.15 show the temperature variation of ε_r and tanδ at different frequencies of Ca modified BT samples sintered by microwave process. Observed T_c

decreases with the increase in Ca substitution concentration in BCT samples. Here, the Ca substitution reduces the lattice distortion, i.e., the *c*/*a* ratio as given in Table 7.1, and hence the T_C decreases with increase in Ca substitution concentration in BT system (as discussed in chapter V) [36]. This is also supported by SEM study, where with the increase of Ca ions substitution concentration grain size is decreasing. It is well known fact that internal compressive stress increases with the decrease in grain size [37]. Since, transition temperature (T_c) is inversely proportional to compressive stress, therefore with the increase of Ca ions substitution concentration T_c decreases [37]. Values of ε_r and tanδ of different Ca substituted BCT samples at RT are given in Table 7.4. RT value of ε_r of BCT samples at 1kHz increases up to x=0.06 and then decreases at x=0.08. This suggests that with the increase of Ca substitution concentration beyond 0.06, Ca may be going to Ti sites, which would lead to creation of oxygen vacancies. These oxygen vacancies would pins the movement of the ferroelectric domains walls and hence result in the decrease in dielectric constant at x=0.08. Values of ε_r of different Ca modified BT samples are found to be higher than the same systems synthesized by conventional processing [38-40]. This can be explained on the basis of better density and uniform morphology of the Ca substituted BCT samples. Grain size of the Ca substituted BCT samples is lower than the same systems synthesized by conventional processing. It is reported earlier that value of ε_r of fine grained BT samples is higher than coarse grained BT samples [41]. Since, microwave processed Ca modified BT samples have sub micron size grain and therefore increase in ε_r. Temperature coefficient of ε_r from RT to 80^{o}C is almost zero for BCT2 and BCT3 systems. This confirms the dielectric depressor nature of Ca substitution in BCT systems [11]. With the increase in Ca substitution concentration

in BCT samples, the value of ε_r at RT increases up to BCT3 system and then decreases for BCT4 system. This can be explained on the basis of decrease in grain size and porosity of the BCT samples. Increase in ε_r with the decrease in grain size upto 0.65μm (BCT3 system) implies that the internal stress is increasing with the decrease in grain size, which is also confirmed from XRD study. The decrease in ε_r for grain size ~0.5μm (BCT4 system) implies that contribution of 90^o domain walls start increasing below 0.65μm grain size limit. It is known that ε_r increases with the increase in internal stress and it decreases with the increase in 90^o domain wall contribution. Therefore, in the present study, below 0.65μm grain size, 90^o domain wall motion contribution to ε_r becomes prominent and hence there is decrease in ε_r at RT for BCT4 system. The same phenomenon is reported in earlier works on BT system [41, 42]. Dielectric loss (tanδ) increases with the increase in temperature in all the Ca modified BT samples and there exists a max. peak of tanδ around the T_c. It is observed that a higher value of tanδ is obtained with increasing temperature which may be due to the increase in the mobility of ions and imperfections in the material [43, 44]. Temperature of max. tanδ of all the iso valent & off-valent ion substituted BT ceramics is different from temperature of max. ε_r, which is a characteristic of ferroelectric [45] materials. Kramers-Kronig relation indicates that this may be due to temperature dependent relaxation near Curie temperature [33].

Table 7.3 Dielectric properties of MW sintered Ca and La Modified BT at 1kHz & at Room Temperature

System	$Ba_{0.98}Ca_{0.02}TiO_3$	$Ba_{0.96}Ca_{0.04}TiO_3$	$Ba_{0.94}Ca_{0.06}TiO_3$	$Ba_{0.92}Ca_{0.08}TiO_3$
ε_r	830	1202	1363	1021
tanδ	0.065	0.048	0.016	0.015
T_c	132	125	123	119
System	BLT1	BLT2	BLT3	BLT4
ε_r	916	2425	1765	1388
tanδ	0.074	0.036	0.022	0.044
T_c	105	Just Below RT	< RT	<< RT

Figs. 7.16 & 7.17 show the temperature variation of ε_r and tanδ at different frequencies of La ions modified BT samples sintered by microwave process. Observed transition temperature (T_c) decreases drastically with the increase in La^{3+} ions content in BT system. Here, the increase of La substitution concentration in BT system reduces the lattice distortion, i.e., the *c*/*a* ratio as given in Table 7.1 and hence the T_C decreases with increase in La substitution concentration in BT system. This is well supported by XRD study, where the with the increase of La substitution concentration, the structures transforms from tetragonal to cubic. This is also supported by SEM study, where with the increase of La ions substitution concentration, grain size is decreasing. It is well known fact that internal compressive stress increases with the decrease in grain size [37].

Since, transition temperature (T_c) is inversely proportional to compressive stress therefore with the increase of La ions substitution concentration T_c decreases [37]. With the substitution of La^{3+} ions in BT system, the stability of capacitance increases for BLT1 and BLT2 systems. Temperature coefficient of capacitance is negligible from RT to 75^oC and 50^oC for BLT1 and BLT2 systems, respectively. Variation of ε_r with temperature for BLT2, BLT3 and BLT4 systems suggest that the T_c is below RT and BLT2, BLT3 and BLT 4 are in paraelelctric state at RT. This is confirming by the XRD study of BLT3 and BLT 4 systems, which show centro symmetric crystal cubic structure. Temperature variation of dielectric loss (tanδ) at different frequencies follows the same behaviour as that of dielectric constant (ε_r). Low value of tanδ and high value of ε_r at 1kHz frequency and at room temperature hints towards the importance of these materials for multilayer applications.

7.4.1 Diffusivity Study:

In the following section, diffusivity study of Ca and La modified MW sintered BT samples is presented and discussed.

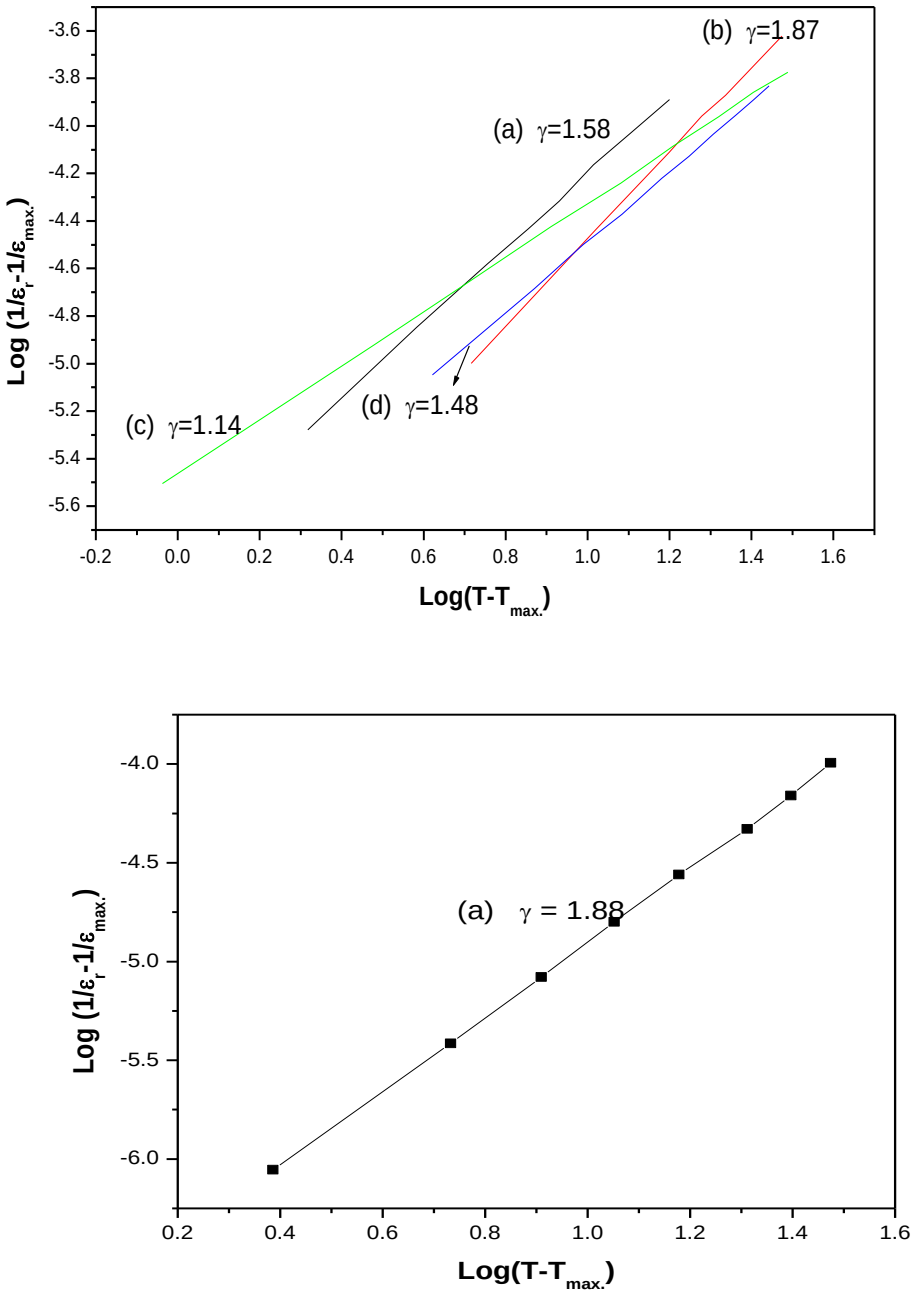

Fig. 7.18 Variation of $\log(1/\varepsilon_r - /\varepsilon_{r\ max.})$ vs. $\log(T - T_{max})$ of (i) $Ba_{1-x}Ca_xTiO_3$(ii) & (ii) $Ba_{1-x}La_xTi_{1-x/4}O_3$ samples., where x= (a) 0.02, (b) 0.04, (c) 0.06 & (d) 0.08

Broadening of phase transition in ceramics depends on the composition fluctuations and structural disorder [33]. In systems, where structural order is distributed due to the disturbance in the composition phase, transition is generally gradual and bandwidth depends on the degree of the disorder. ε_r of these type of materials in the paraelectric region obey the following quadratic equation [47]:

$$1/\varepsilon_r = 1/\varepsilon_{r\,max} + (T-T_{max.})^{\gamma} / C \qquad \ldots\ldots\ldots 7.1$$

rather than the Curie Weiss law [33]. Fig. 7.18 shows the plots between log $(1/\varepsilon_r - 1/\varepsilon_{rmax.})$ versus log $(T-T_{max.})$ at 1kHz of Ca and La modified BT samples. The nature of phase transition is ascertained by calculating the degree of diffusion (γ). Fitting ε_r at 1kHz in the region of $T > T_{max}$ in equation 7.1 and a graph between $\log(1/\varepsilon_r - 1/\varepsilon_{r\,max})$ versus $\log(T-T_{max})$ is plotted, as shown in Fig. 7.18**.** Diffusivity factor (γ), calculated from the slopes of these plots in the higher temperature region are given in Table 7.5.

Table 7.4 Diffusivity factor (γ) of iso-valent and off-valent modified BT samples

System	**$Ba_{0.98}Ca_{0.02}TiO_3$**	**$Ba_{0.96}Ca_{0.04}TiO_3$**	**$Ba_{0.94}Ca_{0.06}TiO_3$**	**$Ba_{0.92}Ca_{0.08}TiO_3$**
γ	**1.58**	**1.87**	**1.14**	**1.48**
System	**BLT1**	**BLT2**	**BLT3**	**BLT4**
γ	**1.88**	**-**	**-**	**-**

High value of dielectric constant with more diffuse phase transition nature than same systems synthesized by SSR route signifies the importance of MW processing of these samples for multilayer capacitor applications.

7.5 Ferroelectric Properties of MW sintered unmodified & Ca and La modified BT Systems:

In this section, the polarization versus electric field (P-E) hysteresis loop properties of MW sintered BT & Ca & La modified BT systems has been discussed

7.5.1 Ferroelectric Properties of MW sintered BT Systems:

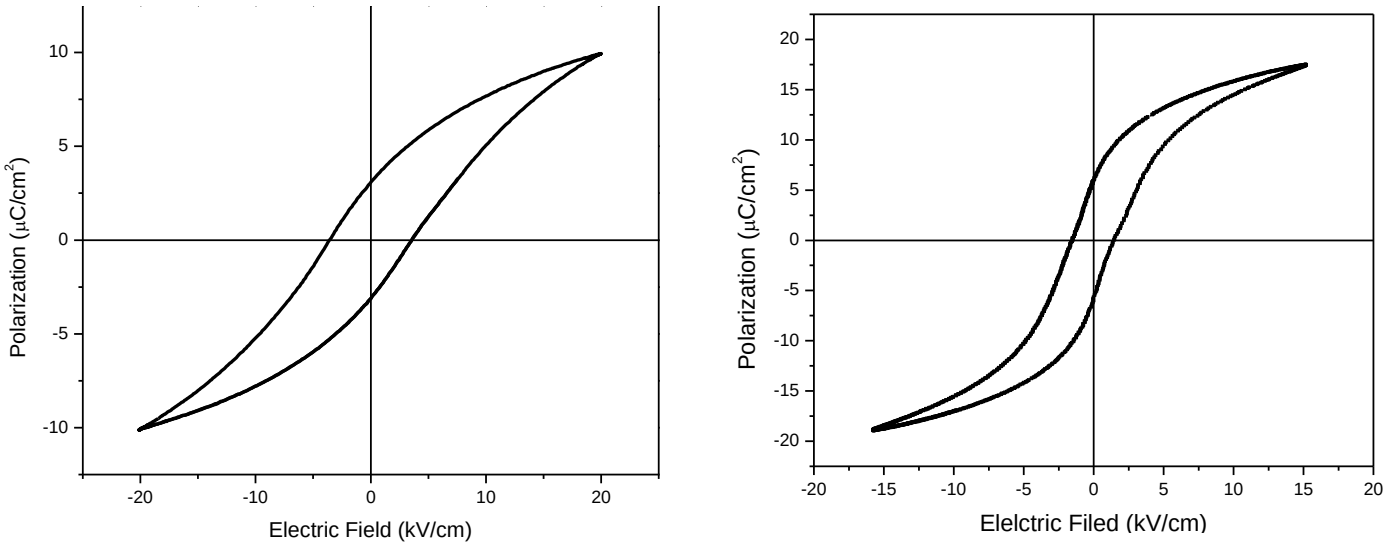

(a) **(b)**

Fig. 7.19 P-E Hysteresis loops of (a) conventionally & (b) MW sintered BT samples.

Fig. 7.19 (a) & (b) shows the P–E hysteresis loops of BT samples sintered conventionally & by MW processing technique, respectively. Development of P-E hysteresis loops confirms the ferroelectric nature of BT samples. Values of remnant polarization (P_r) and coercive filed (E_c) of BT samples synthesized by SSR route are ~3μC/cm^2 and 3.55kV/cm. Whereas, remnant polarization (P_r) and coercive fields (E_c) of the MW sintered BT samples are ~6μC/cm^2 and 1.45kV/cm, which is higher than the earlier reports on modified BT system processed through SSR route [48]. High value of P_r in the

MW sintered BT samples may be related to the better crystalline, better density and larger tetragonality (c/a ratio) nature [32].

7.5.2 Ferroelectric Properties of MW sintered Ca and La modified BT Systems:

In this section, the polarization versus electric field (P-E) hysteresis loop properties of MW sintered Ca & La modified BT systems has been discussed.

Table 7.5 Variation of Coercive field, E_c (kV/cm), remnant polarization, P_r ($\mu C/cm^2$) & saturated polarization Ps ($\mu C/cm^2$) with different x of MW sintered Ca & La modified BT samples.

	P_r ($\mu C/cm^2$) x				P_s ($\mu C/cm^2$) x				E_c (kV/cm) x			
BCTx	1	2	3	4	1	2	3	4	1	2	3	4
	7.15	6	4.86	4.36	13	12.13	11.7	1178	3.66	2.92	3.47	2.37
BLTx	x				x				x			
	1	2	3	4	1	2	3	4	1	2	3	4
	0.74				7.34				1.12			

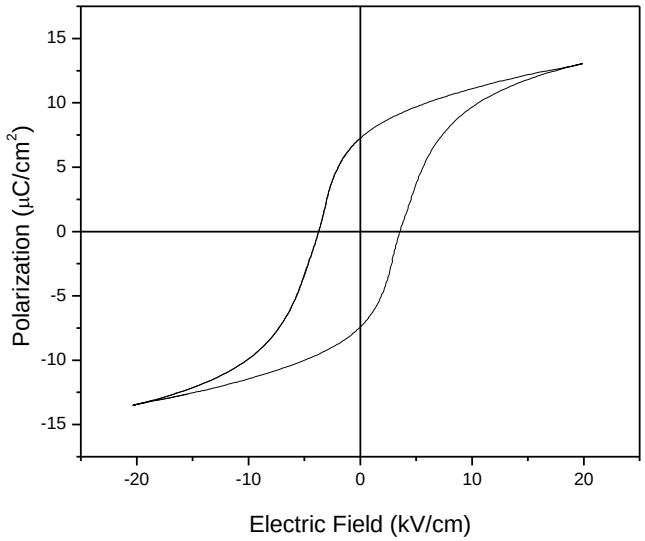

(a)

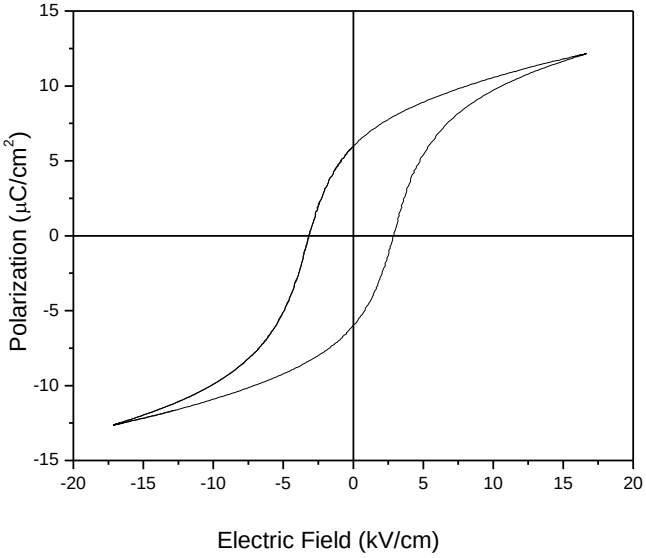

(b)

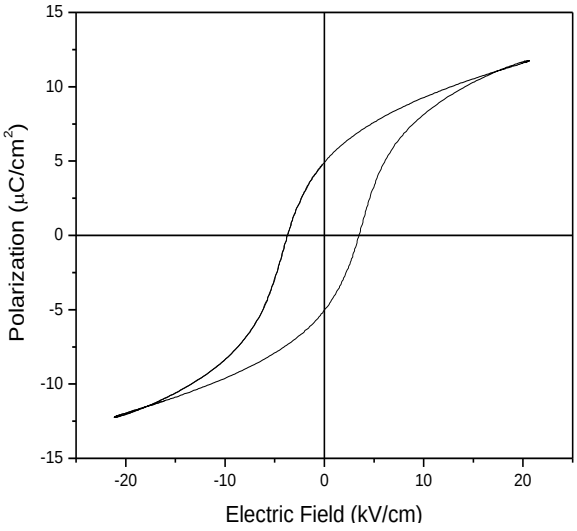

(c)

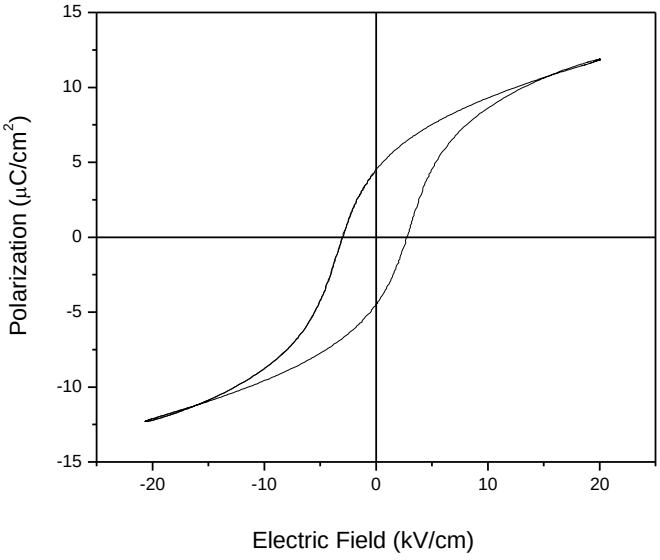

(d)

Fig. 7.20 P-E Hysteresis loops of (a) $Ba_{0.98}Ca_{0.02}TiO_3$ (b) $Ba_{0.96}Ca_{.0.04}TiO_3$ (c) $Ba_{0.94}Ca_{0.06}TiO_3$ & (d) $Ba_{0.92}Ca_{0.08}TiO_3$ samples

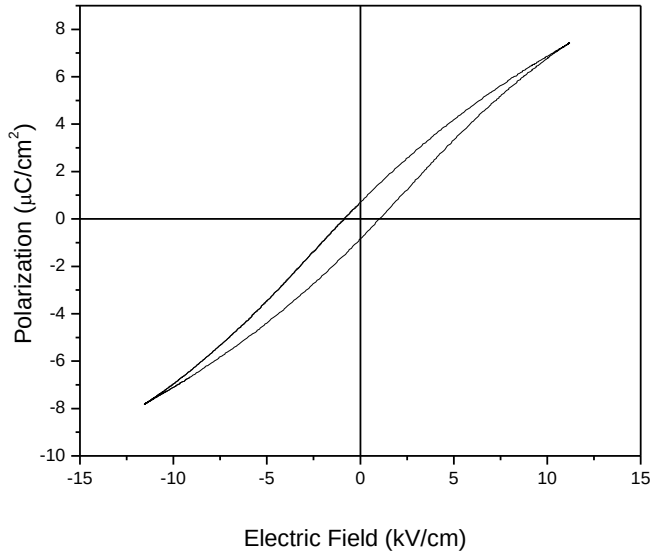

(a)

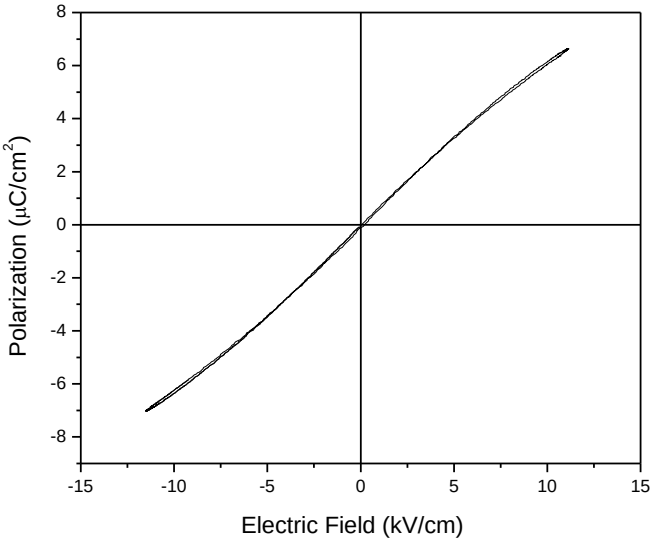

(b)

Fig. 7.21 P-E Hysteresis loops of (a) BLT1 & (b) BLT2 samples.

Fig. 7.20 shows the P–E hysteresis loops of Ca substituted BT samples sintered by microwave processing technique. Development of P-E hysteresis loops confirms the ferroelectric nature of Ca substituted BCT samples. Remnant polarization (P_r) decreases with the increase of Ca substitution concentration in BCT systems. The values of P_r for BCT systems are given in Table 7.6. This decrease in the value of P_r with the increase in Ca substitution concentration in BCT systems may be due to decrease in density, grain size and tetragonality of the BCT systems [49]. The value of P_r is higher than the same system sintered by SSR route [48]**.** There seems no direct correlation between grain size and E_c in the case of MW sintered Ca modified BT samples.

Fig. 7.21 shows the P–E hysteresis loops of La^{3+} ions modified BT ceramic samples sintered by microwave process. Development of P-E hysteresis loops confirms the ferroelectric nature of La^{3+} ions modified BT ceramic samples for BLT1 ceramic samples. Whereas, non occurrence of well saturated P-E hysteresis loops suggest the paraelectric nature of the BLT2, BLT3 and BLT4 ceramic samples at RT. This is as per the XRD and dielectric study.

7.6 Strain induced by Electric Field Behavior of Ca & La modified BT samples

In this section, strain induced by bi-polar electric field behavior of unmodified & modified BT samples synthesized using MW route has been discussed.

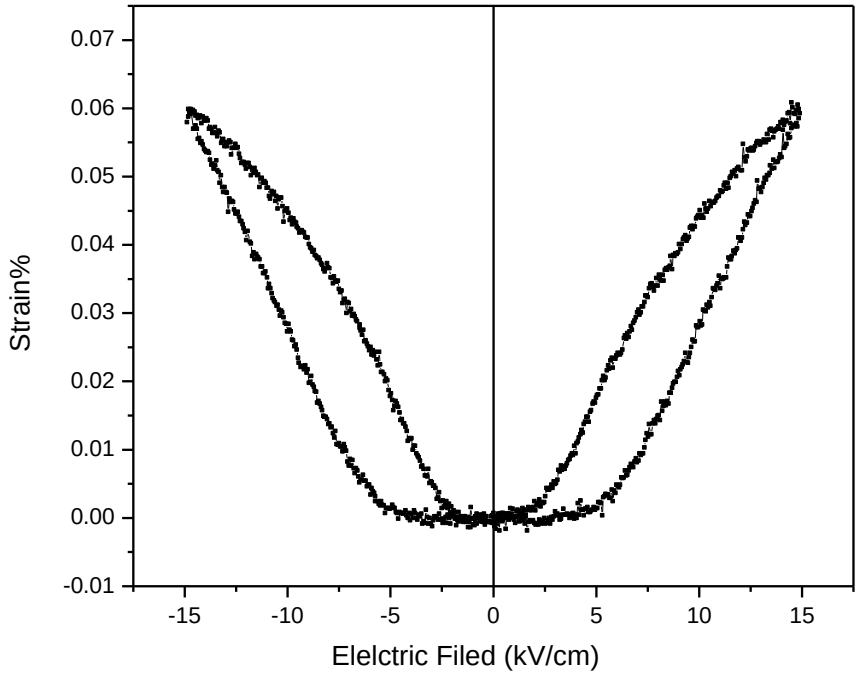

Fig. 7.22 Strain versus bipolar electric field loop of BT samples.

Fig. 7.22 shows the development of S-E butterfly loop with a max. strain `0.06% at 15kV/cm & confirms the piezoelectric nature of the MW sintered BT samples [52-68]. Piezoelectric coefficient, d_{33}, has also been calculated from converse piezoelectric effect, i.e by using the slope of the strain vs. electric field plot in the higher field region, using the relation [69]

$$d_{33} = (\Delta\text{strain\%} / \Delta\text{Electric field at higher side}) \quad \ldots 8.1$$

The d_{33} piezoelectric coefficient calculated from the slope of strain vs. electric field plot is found to be 543pC/N.

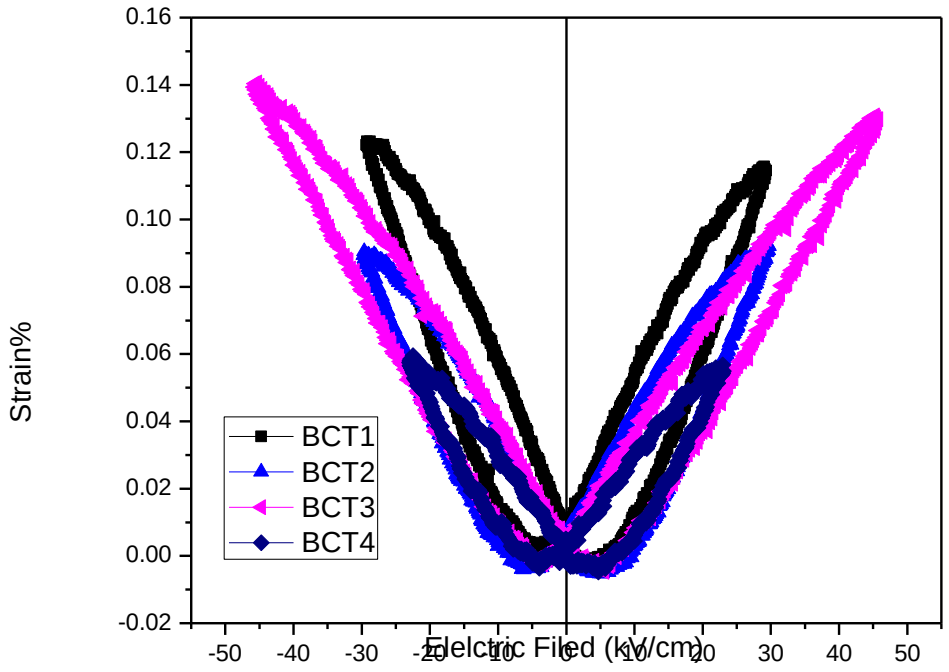

Fig. 7.23 Strain versus bipolar electric field loop of (a) $Ba_{0.98}Ca_{0.02}TiO_3$ (b) $Ba_{0.96}Ca_{.0.04}TiO_3$ (c) $Ba_{0.94}Ca_{0.06}TiO_3$ & (d) $Ba_{0.92}Ca_{0.08}TiO_3$ samples

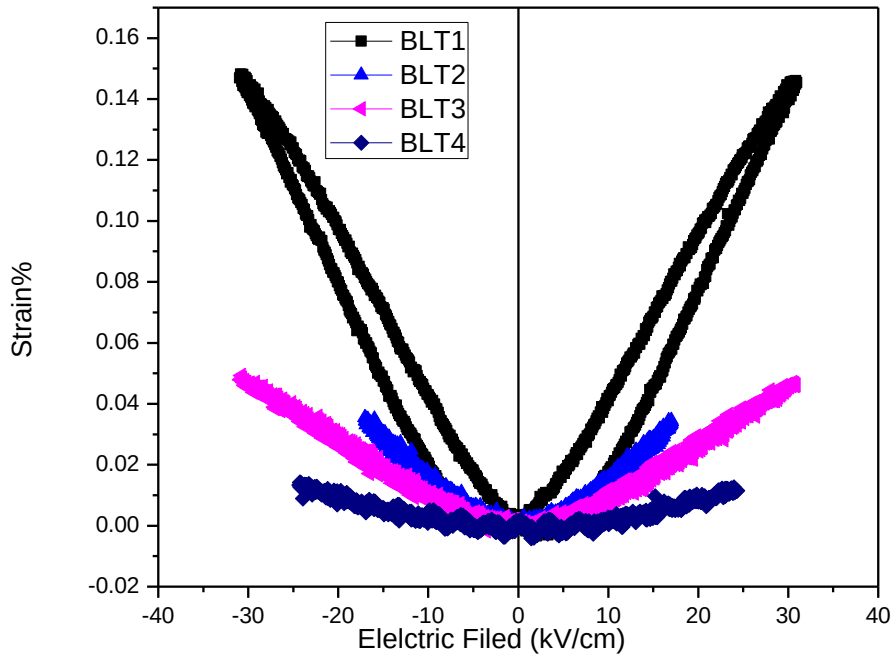

Fig. 7.24 Strain versus bipolar electric field loop of (a) BLT1 (b) BLT2, BLT3 & BLT4 samples.

Figs. 7.23 & 7.24 show the strain vs. electric field loops of the MW sintered Ca and La modified BT systems. Development of butterfly shape loops in the Ca modified BT samples hints towards the piezoelectric nature of these samples [53-69]. A max. strain ~0.15% is found in BCT3 samples, whereas a max. strain ~ 0.15% is found in BLT1 samples. The S-E loops of the MW sintered Ca and La modified BT systems are symmetric in nature. With the increase of La substitution% in BLT systems, max. strain and S-E hysteresis decreases. As, discussed in section 7.3.1 that with the increase of La substitution% in the BLT systems, the structure is changing from non-centrosymmetric to centrosymmetric nature. Here, the S-E hysteresis loop study of MW sintered La modified BT samples also suggest that with the increase of La substitution% in BLT system, the samples are transforming from piezoelectric to electrostrictive nature [53]. Since, in our present study we are relating non-centrosymmetric nature of the crystal structures with the tetragonality of the system [53]. Therefore, decrease in tetragonality hints that we are moving towards centrosymmetric structure (cubic structure in our present study). It is well established that S-E butterfly loop in dielectric materials comes from piezoelectric nature of the materials [53] and for electrostrictive materials (centrosymmetric structure) there is no hysteresis in S-E behaviour [53]. The d_{33} piezoelectric coefficient, calculated from the slope of strain vs. electric field plot at lower electric field is given in Table 7.7. Among MW sintered Ca modified BT samples, a piezoelectric coefficient as high as ~278pC/N is found in BCT1 system whereas among La modified BLT samples a max. piezoelectric coefficient is found to be ~341pC/N in BLT1samples. High value of d_{33} coefficient of BT, BCT1 & BLT1 systems suggests the suitability of these materials for actuator applications [70].

Table 7.6 d_{33} piezoelectric coefficients from S-E study

System	$Ba_{0.98}Ca_{0.02}TiO_3$	$Ba_{0.96}Ca_{0.04}TiO_3$	$Ba_{0.94}Ca_{0.06}TiO_3$	$Ba_{0.92}Ca_{0.08}TiO_3$
d_{33} (pC/N)	**278**	**182**	**270**	**155**
System	BLT1	BLT2	BLT3	BLT4
d_{33} (pC/N)	**341**	**178**	**104**	**39**

References

1. W.D. Kingery, H.K. Bowen, D.R. Uhalmann, Introduction to ceramics, 2nd Edition, John Wiley and sons, New York (1976).
2. N. Setter, J. Euro. Ceram. Soc., **21** (2001) 1279.
3. D.W. Richerson, Modern Ceramic Engineering, Marcel Dekker, New York (1992).
4. J.S.Reed, Principles of Ceramic Processing, John Wiley & Sons, Inc., New York (1995).
5. I.D. Marinescu, H.K. Tonshoff , I. Inasaki, Handbook of Ceramic Grinding and Polishing, Noyes Publications, USA (2002)
6. J. Valasek, Phys. Rev., **17** (1921) 475.
7. C. Kittel, Introduction to Solid State Physics, 7th edition, Wiley Publications (1995).
8. T. R. Shrout and A. Halliyal, Am. Ceram. Soc. Bull., **66** (1987) 704.
9. Yuhuan Xu, Ferroelectric Materials and Their Applications, Elsevier Science Pub. Co. New York, USA (1991).
10. K. Katayama, M. Abe, T. A. Yanagida, J. of Euro. Ceram. Soc., **5** (1989) 183.
11. R. C. Pullar, Y. Zhang, L. Chen, S. Yang, J. R. G. Evans, A. N. Salak, D. A. Kiselev, A.L. Kholkin, V. M. Ferreira, N. M. Alford, J Electroceram., **22** (2009) 245.
12. Finlay D. Morrison, Derek C. Sinclair, Anthony R. West, International Journal of Inorganic Materials, **3** (2001) 1205.
13. R. Zhang, J. F. Li, D. Viehland, J. Am. Ceram. Soc., **87** [5] (2004) 864.

14. Y. Li, Y. Qu, Materials Research Bulletin., **44** (2009) 82.

15. H. Saka, Y. Nishikawa, T. Imura, Philo. Mag. A **57** (1988) 895.

16. P. Yadoji, R. Peelamedu, D. Agrawal, R. Roy, Materials Science and Engineering B **98** (2003) 269.

17. D. Agrawal, Journal of Materials Education, **19** (1999) 49.

18. D.E. Clark, D.C. Folz, J.K. West, Materials Science and Engineering A **287** (2000) 153.

19. C. Leonelli, P. Veronesi, L. Denti, A. Gatto, L. Iuliano, Journal of Materials Processing Technology, **205** (2008) 489.

20. M. Oghbaei, O. Mirzaee, Journal of Alloys and Compounds, **494** (2010) 175.

21. C. T. Hu, *et.al*., Jpn. J. Appl. Phys., **37** (1) (1998) 186.

22. E. T. Thostenson, T. W. Chen, Compos. Part A, **30** (1999) 1055.

23. O.P. Thakur, C. Prakash, D.Agrawal, Int. J. Ceram. Process. Research, **3**(2) (2002) 75.

24. O.P. Thakur, C. Prakash, D. Agrawal, J. Mater. Sci. Engg B, **96** (2002) 221.

25. O.P. Thakur, C. Prakash, D. Agrawal, Mater. Letters, **56** (2002) 970.

26. M. Fu, D. Agrawal, Y. Fang, J. of Microwave Power & Electromagnetic Energy, **40** [3] (2007) 133.

27. C. Y. Fang, C. Wang, A. V. Polotai, D. K. Agrawal, M. T. Lanagan, Materials Letters, **62** (2008) 2551.

28. N. Yoshikawa, T. Kato, J. Phys. D: Appl. Phys., **43** (2010) 425403

29. N. Yoshikawa, Fundamentals and Application of Microwave heating of Metals", Materia, Japan (Bulletin of Japan Inst.Metals), **48** [1] (2009) 3-10.

30. M.M. Vijatovic, B. D. Stojanovic, J. D. Bobic, T. Ramoska, P. Bowen, Ceramics International, **36** (2010) 1817.

31. K. Tkacz-Śmiech, A. Koleżyński, W. S. Ptak, Solid State Communications, **127** (2003) 557.

32. M. E. Lines, A. M. Glass, Principles and Applications of Ferroelectrics and Related Materials, Oxford, Clarendon (1979).

33. A. K. Singh, T. C. Goel, R. G. Mendiratta, O. P. Thakur, C.Prakash, J. Appl. Phys., **91** (2002) 6626.

34. D.J. Griffiths, Introduction to Electrodynamics , 3rd edition, Prentice Hall (1998).

35. B. Jaffe, W.R. Cook, H. Jaffe, Piezoelectric ceramics, Academic Press, London (1971).

36. F. J. Chen, Y. N. Pan, C. Y. Lee, C. S. Lin, J. Electrochem. Soc., **157** [3] (2010) D154.

37. S. Jayanthi, T.R.N. Kutty, Materials Science and Engineering, B **110** (2004) 202.

38. Q. Jia, B. Shen, X. Hao, S.Song, J. Zhai, Materials Letters, **63** (2009) 464.

39. R. Varatharajana, S.B. Samantab, R. Jayavela, C. Subramaniana, A.V. Narlikarb, P. Ramasamy, Materials Characterization, **45** (2000) 89

40. G. Arlt, D. Hennings , J de With, J. Appl. Phys., **58** (1985) 4.

41. M. McNeal, S. Jang, R.E. Newnham, J. Appl. Phys. **83** (1998) 3288.

42. M. Raghavender, G S. Kumar, G Prasad, Indian J. Pure & applied Physics, **44** (2010)

43. S. Jain, A. K. Jha, J. Electroceram., **24** (2010) 58.

44. P. Kumar, S. Sharma, O.P. Thakur, C. Prakash, T.C. Goel, Ceramics

International, **30** (2004) 585.

45. N. Setter , L.E.Cross J. Mat. Sci., **15** (1980) 1573.

46. M. Kuwabara, S. Takahashi, K. Goda, K. Watande, Jpn. J. Appl. Phys., **31** (1992) 3241

47. P. Kumar, S. Singh, J. K.Juneja, C. Prakash, K. K.Raina, Physica B, **404** (2009) 1752.

48. T. M. Shaw, S. T.McKinstry, P. C. McIntyre, Annual Review of Material Sci., **30** (2000) 263.

49. P. Kumar, S. Singh, O. P. Thakur, C. Prakash and T. C. Goel, Japanese Journal of Applied Physics, **43** (4A)(2004)1501

50 Y. Li, Y. Qu, Materials Research Bulletin, **44** [1] (2009) 82.

51. G. H. Heartling, J. Amer. Ceram. Soc., **82** (1999) 797.

52. K. Uchino, Ferroelectric Devices, Marcel Dekker, New York (2000).

53. S. Bashash, N. Jalili, P. Evans, M. J. Dapino, *J.* of Intelligent Material Systems and Structures December, **20** [18] (2009) 2161.

54. S.T. Zhang, A. B. Kounga, E. Aulbach, W. Jo, T. Granzow, H. Ehrenberg, J. Rödel, J. Appl. Phys., **103** (2008)034108

55. A. Hall, M. Allahverdi, E.K. Akdogan, A. Safari, J. European Ceram. Soc., **25[** 12] (2005) 2991.

56. W. Jiang, R Zhang, B Jiang, W. Cao, Ultrasonics, **41**[2] (2003) 55.

57. Z. Feng, H. Luo, Y. Guo, T. He, H. Xu, Solid State Comm., **126** [6] (2003 347.

58. **J**. B. Lim, S. Zhang, T. R. Shrout, Journal of Electroceramics, Online First™, 1 February 2011.

59. D .Damjanovi, The Science of Hysteresis, **3**[4] (2006) 337.

60. W. Wersing, W. Heywang, H. Beige, H. Thomann, Springer Series in Materials Science 114 (2009) 37.

61. M. Ozgul, S. T. Mckinstry, C. A. Randall, J. Electroceram., **20**[3](2008) 133.

62. A. Pathak, R. Chatterjee, C. Prakash, Ceramics International, **36**[8] (2010) 2263.

63. A. Pathak, C. Prakash, R. Chatterjee, Materials Chem. & Phys.,**123**[1](2010) 132.

64. A. Pathak, C. Prakash, R. Chatterjee, Physica B: Condensed Matter, **404** [20] (2009) 3457

65. M. E. Lines, A. M. Glass, Principles and Applications of Ferroelectrics and Related Materials, Clarendon Press, Oxford (1977).

66. J. X. Zhang, G. Sheng, L. Q. Chen, Appl. Phys. Lett., **96** (2010) 132901

67. S. Zhang, L. Lebrun, C. A. Randall, T. R. Shrout, J. Crystal Growth, **267** [1] (2004) 204.

68. S. Zhang, L. Lebrun, S. Rhee, R.E. Eitel, C. A. Randall, T. R. Shrout, J. Crystal Growth, **236**[1] (2002) 210.

69. M. Kondo, K. Kunhara, Key Engineering Materials, **248** (2003) 15.

70. S. W. Choi, T. R. Shrout, S. J. Jang, A. S. Bhalla, Ferroelectrics, **100** (1989) 29.

CHAPTER VIII

CONCLUSIONS AND FUTURE WORKS

8.1 Introduction

Among lead free ferroelectric systems BT system is one of the best systems for MLC applications. But, in multilayer ceramic capacitors (MLCC) applications, the $BaTiO_3$-based compounds must be sintered at a temperature low enough to suppress electrode oxidation for its practical applications in devices. There is also a need to modify BT system for getting higher density, uniform microstructure, higher dielectric constant at room temperature, less dielectric loss, diffuse phase transition nature, stable capacitors with satisfactory operational capacity with increased temperature stability. In the present work iso-valent and off valent modified BT systems have been synthesized with modified solid state reaction (MSSR) & microwave (MW) routes which are economical, energy saver and promises excellent electrical properties at low processing temperatures and time.

In the present study, single perovskite phase formation conditions of iso-valent and off-valent substituted BT systems synthesized by MSSR route are optimized. As, the variation of iso-valent and off-valent substitution% in modified BT system greatly affects the ceramic samples properties, we have studied these substituent variation influence on the perovskite phase evolution, structural, microstructural, dielectric, ferroelectric, strain vs. electric field & piezoelectric properties. Following series are synthesized by MSSR route:

(i) $Ba_{1-x}Ca_xTiO_3$/BCT{y} (ii) $Ba_{1-x}Sr_xTiO_3$/BST{y}

(ii) $Ba_{1-x}Mg_xTiO_3$ (iii) $Ba_{1-x}Sm_xTi_{(1-x/4)}O_3$ /BSmT{y}; **where y=x/0.02**

(iii) $Ba_{1-x}La_xTi_{(1-x/4)}O_3$/BLT {y} samples, **where x=0.02, 0.04. 0.06 & 0.08**

Therefore, in the present work for x=0.02, 0.04. 0.06 & 0.08, we have used BCT1, BCT2, BCT3, BCT4, BST1, BST2, BST3, BST4, BMT1, BMT2, BMT3, BMT4, BSmT1, BSmT2, BSmT3, BSmT4 & BLT1, BLT2, BLT3, BLT4 notations.

BCT & BLT samples synthesized by MSSR route are showing better dielectric properties. Therefore, these two series were also synthesized by MW process. We have studied the MW processing effect on the perovskite phase evolution, structural, density microstructural, dielectric, ferroelectric, strain vs. electric field and piezoelectric properties and compared with the properties of same systems synthesized by conventional sintered route. Conclusions of the present work and recommendation for the future work are listed below:

8.2 Conclusions

8.2.1 Modified BT ceramic samples processed through MSSR route

- Lower calcination (900^oC) and sintering (1300^oC) temperatures compared to conventional processing routes for single perovskite phase formation and better densification of iso-valent and off-valent modified BT samples.
- Low temperature coefficient of capacitance in BCT1, BCT2, BCT3 samples makes these materials useful for MLC applications.
- High value of ε_r ~5826 & 6214 at room temperature in BLT2 & BSmT4 modified BT systems makes these materials useful for MLC & DRAM applications.
- P-E hysteresis loop study reveals the disappearance of ferroelectric nature with the increase of La and Sm substitution% in modified BT systems.
- A max. strain ~0.13% was observed in BT system synthesized by MSSR route.
- Strain vs. electric field behaviour confirms the appearance of centro-symmetric nature with the increase of La & Sm substitution% in modified BT systems.
- MSSR route gives higher dielectric properties & piezoelectric and ferroelectric at significantly cost & lower processing temperatures.

- High value of d_{33} coefficient of BT, BST1, BST2, BST3 & BST4, BLT1 samples synthesized by MSSR route suggests the suitability of these materials for actuator applications.

8.2.2 Modified BT ceramic samples processed through MW route

- ✓ Sintering temperature for dense morphology and higher density was optimized at 1100^oC for 1hr.
- ✓ Nearly theoretical density was observed in BLT2, BLT3 & BLT4 ceramics samples.
- ✓ Better micro-structural and dielectric properties were observed in case of MW samples at lower processing temperature and time.
- ✓ Temperature coefficient of capacitance is negligible from RT temperature to 75^oC for BCT2, BCT3 samples, make these materials useful for MLC applications.
- ✓ High Value of ε_r & low value of $\tan\delta$ at room temperature was observed in BLT2 samples, make this material useful for MLC & DRAM applications.
- ✓ A max. strain ~0.15% was observed in BT system synthesized by MW route.
- ✓ Strain vs. electric field behaviour confirms the appearance of centro-symmetric nature with the increase of La substitution% in modified BT systems.
- ✓ A highest d_{33} piezoelectric coefficient ~ 543pC/N was obtained in BT system synthesized by MW technique.

8.3 Scope for Future Works:

Following recommendations for further extension of present work are made.

- The size effect of nano-size particles on the MW synthesis, dielectric, piezoelectric properties can be studied.
- The MSSR and microwave processing can be combined to further lower the processing time and temperature.
- Calcination of modified BT systems can also be done by microwave processing.
- BST ceramic are good candidate for their application in the field of tunable devices, further reduction of dielectric loss can be achieved by better densification using MW processing technique.

- Various other characterizations such as pyroelectric, resistivity vs. temperature measurements can be carried out and their applications can be explored.
- Strain vs. electric field of poled samples can be done.
- Strain vs. electric field study can be discussed in detail related to domain wall motions and phase transitions.

ABOUT THE AUTHOR

The author was born at Sonipat (Haryana), India, on 18th May 1983. She received her B.Sc. Degree from G.V.M College, Sonipat in 2003 and M.Sc. in Chemistry from M. D. University, Rohtak (Haryana) in 2005. She has secured more than 70% marks throughout her academic career. Since, January 2007, she had been engaged in the research for her Ph.D. degree in Chemistry at National Institute of Technology, Rourkela. Her current research interests are in synthesis & characterizations of functional materials by different techniques.